UNIVERSITAT POLITÈCNICA DE CATALUNYA (UPC)

Programa de doctorat d'Enginyeria Ambiental

Ph. D. thesis

Implementation, development and evaluation of the gas-phase chemistry within the Global/Regional NMMB/BSC Chemical Transport Model (NMMB/BSC-CTM)

Alba Badia i Moragas

Directors:
Dr. Oriol Jorba i Casellas (Dept. of Earth Sciences, Barcelona Supercomputing Center- Centro Nacional de Supercomputación [BSC-CNS], Barcelona)
Dr. Santiago Gassó i Domingo (Projectes d'Enginyeria, Universitat Politècnica de Catalunya [UPC], Barcelona)

Barcelona, October 2014

Per a la Laia

"Essentially, all models are wrong, but some are useful."
- George E.P. Box (1979)

Acknowledgements

Primer de tot m'agradaria agrair el gran esforç del meu director de tesi, el Dr. Oriol Jorba. Sense la seva gran ajuda, consells, paciència i seguiment en tot moment, aquesta tesi no hauria estat possible. Gràcies altra vegada, Oriol, que, des del primer moment, vas confiar amb mi. També vull donar les gràcies a l'altre director de tesi, el Dr. Santiago Gassó, i al cap del departament, el Dr. José Maria Baldasano, per ajudar-me i orientar-me amb tota la documentació i temes logístics necessaris.

També vull dedicar aquesta tesi a la meva família. Sobretot a la Queralt i al Jordi, que sempre heu estat i sou al meu costat quan us necessito, preguntant-me per la tesi, i animant-me en moments difícils. Gràcies, també, a la Marta per les seves explicacions de química, a l'Arnau per alguns consells informàtics i al Marc i la Maria, per ser tant eixerits. També vull agrair a l'Estel, l'Amalia i el Joan el seu suport. Gràcies també a tota la família de la Laia, per preocupar-se per mi i donar-me ànims.

L'amistat és un valor infinit que també vull remarcar aquí. Vull donar les gràcies a la gent que ha mostrat interès i m'ha donat suport durant aquest temps que ha durat la tesis, com les amigues de Callús (Alba, Anna, Laura, Elisabet i Anahí), a la xiqueta valenciana (Carmeta), els matemàtics (Anna, Alberto, Nahikari i Monica), a les cosines bisbalenques (Cecilia i Mireia), i a les amigues de Gràcia. També vull donar les gràcies al meu cosí Quim per la fantàstica correció d'alguna part de la tesi. No em voldria deixar la gent que en algun moment ha passat pel BSC o hi manté alguna relació. N'hi ha que, més que companys de feina, s'han convertit en amics. Sobretot vull donar les gràcies al Michele per fer-me de fratello maggiore en aquesta aventura, al duet Sara i Maria Teresa pels seus consells científics i l'amistat durant aquests anys, a l'Enza per compartir i ensenyar-me de la seva experiència, al Francesco i la Francesca pels seus consells culinàris, també al Luca, a l'Angel, al Karsten, al Simone, al Vincenzo, i a molts més. Ha estat un plaer treballar amb tots vosaltres! It's been a pleasure working with all of you!

I would also like to thank those I had the pleasure and luck to work with/for in my visit at the University of Copenhagen and the Danish Meteorological Institute (DMI). Especially, Dr. Brian Højen-Sørensen and Dr. Roman Nuterman for their help and technical support, and Dr. Alexander Baklanov and Dr. Eigil Kaas for giving me this opportunity and being my supervisors during this visit.

No tothom té la sort de ser remunerat per apendre. Gràcies al Barcelona Supercomputing Center-Centro Nacional de Supercomputación (BSC-CNS) i a la Universitat Politècnica de Catalunya (UPC) per la gran oportunitat que m'han donat i el seu suport econòmic durant aquesta tesi. This work is funded by grants CGL2010-19652, Supercomputación and e-ciencia Project (CSD2007-0050) from the Consolider-Ingenio 2010 program of the Spanish Ministry of Economy and Competitiveness. Further support was provided by the SEV-2011-00067 grant of the Severo Ochoa Program, awarded by the Spanish Government.

I would like to acknowledge the researchers from EMC NCEP Dr. Zavisa Janjic and Tom Black for helping us in the use of the NMMB model and in the implementation of the chemistry processes.

Moreover, this P.h.D was also possible thanks to the collaboration of many scientists. I would like to acknowledge all the co-authors of the publications done in the framework of this thesis. Specially Dr. Monge-Sanz for providing the COPCAT linear model and suggestions on its implementation, and the Dr. Hillbol for providing the SCIAMACHY data and useful feedback on the results.

I ja només em queda agrair-te a tu, Laia, el gran suport, la paciència, l'empenta que m'has donat, i sobretot per ser al meu costat en tot moment. Sense tu, aquesta tesi hauria estat molt més feixuga.

Moltes gràcies! Thank you very much! Mange tak! Muchas gracias! Grazie mille!

Summary (English version)

Air pollution is a serious issue that affects human health, the environment and the climate at levels from local to global scales. The main processes that affect air pollution levels are: emissions, chemistry, transport and deposition. Air quality models (AQMs) are mathematical tools that describe relevant physicochemical processes and quantify concentrations of air pollutants. Therefore, AQMs can be used to develop and detail measures taken to reduce air quality problems.

Several AQMs are currently used and they have undergone a rapid evolution in recent years. Computer capacity has increased during the last decade enabling us to use higher spatial resolutions and more complex parameterizations schemes that resolve more complex atmospheric processes. Moreover, previous research has shown that the feedbacks between meteorology and chemistry are important in the context of many research applications. Therefore, this increase in computing power allows accurately simulate those feedbacks (online modelling). Online models are becoming more used in the atmospheric community.

The NMMB/BSC Chemical Transport Model (NMMB/BSC-CTM) is being developed through an ongoing team effort at the Earth Sciences Department of the Barcelona Supercomputing Center (BSC). The main motivation for this thesis is to contribute in the development of a unified fully coupled chemical weather prediction system able to solve gas-aerosol-meteorology interactions within a wide range of scales on local to global domains that can be used in both operational and research applications. In this sense, the focus in this Ph.D. has been on the development and evaluation of the tropospheric gas-phase chemistry within the online Global / Regional atmospheric model NMMB/BSC-CTM. With the meteorological core NMMB as the starting point, different parameterizations of several atmospheric chemistry processes such as dry deposition, photolysis, wet deposition, gas-phase chemistry, and stratospheric ozone handling have been reviewed, implemented and evaluated during this Ph.D. thesis.

A complete spatial, temporal and vertical model evaluation of the relevant chemical species using different observational data has been performed in this Ph.D. thesis. Observational data has included ground-monitoring stations, ozonesondes, satellite data, climatologies and, aircraft campaigns. This is the first time that the gas-phase chemistry of the NMMB/BSC-CTM has been evaluated on a regional and global scales over a full year. Concerning the model evaluation in the regional scale, we had the opportunity to participate in the Air Quality Model Evaluation Inter-

national Initiative (AQMEII) Phase2 which aims to intercompare online coupled regional-scale models over North America and Europe. In this sense, we were participating in this initiative in the European runs with NMMB/BSC-CTM model. The model evaluations have shown a good agreement with observations. Overall, the model performance corresponds to state-of-the-art regional and global AQMs.

Resum (Catalan version)

La contaminació de l'aire és un problema greu que afecta la salut humana i el medi ambient, tant a escala local com global. Els principals processos que concerneixen els nivells de contaminació de l'aire són les emissions, la química, el transport i la deposició. Els Models de Qualitat de l'Aire (AQMS) són eines matemàtiques que descriuen aquests processos fisicoquímics i quantifiquen les concentracions de contaminants de l'aire. Per tant, els AQMS es poden utilitzar per desenvolupar i detallar les mesures preses per reduir la mala qualitat de l'aire.

Actualment, es fan servir diversos AQMS i aquests darrers anys han evolucionat molt ràpidament. La capacitat de la computació ha augmentat durant l'última dècada, i això ha fet possible una resolució espacial més bona i uns esquemes de parametritzacions més complexos que resolen més processos atmosfèrics. D'una altra banda, la investigació ha demostrat que els feedbacks entre la meteorologia i la química són certament importants en moltes aplicacions de recerca. Per tant, l'augment de la potència de càlcul permet simular acuradament aquests feedbacks (modelització online). Els models online són cada vegada més utilitzats en la comunitat atmosfèrica.

El NMMB/BSC Chemical Transport Model (NMMB/BSC-CTM) es desenvolupa gràcies a un esforç d'equip al Departament de Ciències de la Terra del Barcelona Supercomputing Center (BSC). La principal motivació d'aquesta tesi és contribuir al desenvolupament i a l'avaluació d'un sistema de predicció unificat que sigui capaç de resoldre les interaccions gas-aerosol-meteorologia dins un ampli rang d'escales, des de dominis locals a globals, i que pugui ser utilitzat tant en aplicacions operatives com d'investigació. En aquest sentit, el principal objectiu d'aquesta tesi doctoral és el desenvolupament i l'avaluació de la química troposfèrica en fase gasosa del model online global/regional NMMB/BSC-CTM. Utilitzant el nucli meteorològic NMMB com a punt de partida, diverses parametritzacions de processos químics atmosfèrics com ara la deposició seca, la fotòlisi, la química dels núvol, la química en fase gasosa i l'intercanvi d'ozó entre estratosfera i troposfera han estat revisats, implementats i avaluats durant aquesta tesi doctoral.

S'ha dut a terme una avaluació completa a nivell espacial, temporal i vertical de les espècies químiques més rellevants mitjançant diverses observacions a escala global i regional. Aquestes observacions inclouen estacions a nivell de superfície, ozonosondes, dades de satèl·lit, climatologies i campanyes d'aeronaus. És la primera vegada que la química en fase gasosa

de l'NMMB/BSC-CTM s'avalua a escala global i regional durant un any complet. Respecte l'evaluació del model a nivell regional, vam tenir l'oportunitat de participar en el projecte de l'Air Quality Model Evaluation International Initiative (AQMEII) Phase2. L'objectiu principal d'aquest projecte és la intercomparació de models online a escala regional sobre l'Amèrica del Nord i Europa. El nostre grup va participar en aquesta iniciativa sobre el domini europeu utilitzant el model NMMB/BSC-CTM. L'avaluació del model mostra una bona avinença amb les observacions. En general, els resultats del model es corresponen amb l'estat de l'art dels AQMS a escala regional i global.

Publications derived from this Thesis

International Journals Included in the Science Citation Index (SCI)

A. Badia and, O. Jorba. Gas-phase evaluation of the online NMMB/BSC-CTM model over Europe for 2010 in the framework of the AQMEII-Phase2 project. Atmospheric Environment. DOI:http://dx.doi.org/10.1016/j.atmosenv.2014.05.055, 2014 (In Press, Accepted Manuscript)

U. Im, R. Bianconi, E. Solazzo, I. Kioutsioukis, **A. Badia**, A. Balzarini, R. Baró, R. Bellasio, D. Brunner, C. Chemel, G. Curci, J. Flemming, R. Forkel, L. Giordano, P. Jiménez-Guerrero, M. Hirtl, A. Hodzic, L. Honzak, O. Jorba, C. Knote, J.J.P. Kuenen, P. A. Makar, A. Manders-Groot, L. Neal, J. L. Pérez, G, Pirovano, G. Pouliot, R. San Jose, N. Savage, W. Schroder, R. S. Sokhi, D. Syrakov, A. Torian, P. Tuccella, J. Werhahn, R. Wolke, K. Yahya, R. Zabkar, Y. Zhang, J. Zhang, C. Hogrefe, S. Galmarini. Evaluation of operational online-coupled regional air quality models over Europe and North America in the context of AQMEII phase 2. Part I: Ozone, Atmospheric Environment. DOI:http://dx.doi.org/10.1016/j.atmosenv.2014.09.042. (In Press, Accepted Manuscript)

U. Im, R. Bianconi, E. Solazzo, I. Kioutsioukis, **A. Badia**, A. Balzarini, R. Baró, R. Bellasio, D. Brunner, C. Chemel, G. Curci, J. Flemming, R. Forkel, L. Giordano, P. Jiménez-Guerrero, M. Hirtl, A. Hodzic, L. Honzak, O. Jorba, C. Knote, J.J.P. Kuenen, P. A. Makar, A. Manders-Groot, L. Neal, J. L. Pérez, G, Pirovano, G. Pouliot, R. San Jose, N. Savage, W. Schroder, R. S. Sokhi, D. Syrakov, A. Torian, P. Tuccella, J. Werhahn, R. Wolke, K. Yahya, R. Zabkar, Y. Zhang, J. Zhang, C. Hogrefe, S. Galmarini. Evaluation of operational online-coupled regional air quality models over Europe and North America in the context of AQMEII phase 2. Part II: Particulate Matter, Atmospheric Environment. DOI:http://dx.doi.org/10.1016/j.atmosenv.2014.08.072. (In Press, Accepted Manuscript)

I. Kioutsioukis, U. Im, R. Bianconi, E. Solazzo, **A. Badia**, A. Balzarini, R. Baró, R. Bellasio, D. Brunner, C. Chemel, G. Curci, J. Flemming, R. Forkel, L. Giordano, P. Jiménez-Guerrero, M. Hirtl, A. Hodzic, L. Honzak, O. Jorba, C. Knote, J.J.P. Kuenen, P. A. Makar, A. Manders-Groot, L. Neal, J. L. Pérez, G, Pirovano, G. Pouliot, R. San Jose, N. Savage, W. Schroder, R. S. Sokhi, D. Syrakov, A. Torian, P. Tuccella, J. Werhahn, R. Wolke, K. Yahya, R. Zabkar, Y. Zhang, J. Zhang, C. Hogrefe, S. Galmarini. Challenges in the deterministic skill of air quality ensembles. Atmospheric Environment (submitted)

I. Kioutsioukis, U. Im, R. Bianconi, E. Solazzo, **A. Badia**, A. Balzarini, R. Baró, R. Bellasio, D. Brunner, C. Chemel, G. Curci, J. Flemming, R. Forkel, L. Giordano, P. Jiménez-Guerrero, M. Hirtl, A. Hodzic, L. Honzak, O. Jorba, C. Knote, J.J.P. Kuenen, P. A. Makar, A. Manders-Groot, L. Neal, J. L. Pérez, G, Pirovano, G. Pouliot, R. San Jose, N. Savage, W. Schroder, R. S. Sokhi, D. Syrakov, A. Torian, P. Tuccella, J. Werhahn, R. Wolke, K. Yahya, R. Zabkar, Y. Zhang, J. Zhang, C. Hogrefe, S. Galmarini. Online versus offline simulations: an indirect comparison from the ensemble-based deterministic forecasting perspective. Atmospheric Environment (submitted)

D. Brunner, B. Eder, O. Jorba, N. Savage, P. A. Makar, L. Giordano, **A. Badia**, A. Balzarini, R. Baró, R. Bellasio, C. Chemel, G. Curci, J. Flemming, R. Forkel, P. Jiménez-Guerrero, M. Hirtl, A. Hodzic, L. Honzak, C. Knote, J.J.P. Kuenen, A. Manders-Groot, L. Neal, J. L. Pérez, G, Pirovano, G. Pouliot, R. San Jose, W. Schroder, R. S. Sokhi, D. Syrakov, A. Torian, P. Tuccella, J. Werhahn, R. Wolke, K. Yahya, R. Zabkar, Y. Zhang, J. Zhang, C. Hogrefe, S. Galmarini. Evaluation of the meteorological performance of coupled chemistry-meteorology models in phase 2 of the Air Quality Model Evaluation International Initiative. Atmospheric Environment (submitted).

L. Giordano, J. Brunner, Flemming, D., U. Im, C. Hogrefe, B. Bianconi, **A. Badia**, A. Balzarini, R. Baró, C. Chemel, G. Curci, R. Forkel, P. Jiménez-Guerrero, M. Hirtl, A. Hodzic, L. Honzak, O. Jorba, C. Knote, J. Kuenen, P. Makar, A. Manders-Groot, L. Neal, J. Pérez, G. Pirovano, R. Pouliot, G. San Jose, N. Savage, W. Schroder, R. Sokhi, D. Syrakov, A. Torian, R. Tuccella, J. Werhahn, R. Wolke, K. Yahya, R. Zabkar, Y. Zhang, and S. Galmarini. Assessment of the MACC/IFS-MOZART model and its influence as chemical boundary conditions in AQMEII phase 2. Atmospheric Environment (submitted).

O. Jorba, D. Dabdub, C. Boxe, C. Pérez, Z. Janjic, J.M. Baldasano, M. Spada, **A. Badia** and M. Gonçalves. Impact of Photoexcited NO2 on Global Air Quality with the NMMB/BSC Chemical Transport Model. Journal of Geophysical Research, DOI: 10.1029/2012JD017730, 2012

Conference contributions:

A. Badia and O. Jorba. Evaluation of the on-line NMMB/BSC-CTM model gas-phase results on the European domain for 2010 in the framework of the AQMEII-PHASE2 Initiate. Air Quality 2014 - Science and Application. Garmisch-Partenkirchen, 24 - 28 March 2014, Oral Presentation

O. Jorba, **A. Badia**, M. Spada, C. Pérez,, S. Basart, J.M. Baldasano, Z. Janjic and D. Dabdub. Multiscale Air Quality Modelling with the NMMB/BSC Chemical Transport model. XVIII Jornades de Meteorologia Eduard Fontserè. Barcelona, Spain, 22 - 24 November 2013, Poster.

A. Badia, O. Jorba, R. Nuterman, A. Baklanov and J.M. Baldasano. Model inter-comparison study between NMMB/BSC-CTM and Enviro-HIRLAM on-line systems contributing to the

AQMEII-Phase2 initiative. 33rd International Technical Meeting on Air Pollution Modeling and its Application. Miami, Florida USA, 26 - 30 August, 2013, Oral Presentation

O. Jorba, C. Pérez, **A. Badia**, M. Spada, Z. Janjic, J. M. Baldasano, D. Dabdub. The NMMB/BSC Chemical Transport model air quality results form global to regional scales. 4th International Meeting on Meteorology and Climatology of the Mediterranean. Banyuls, Roussillon, France, 27 February - 1 March, 2013, Poster

A. Badia and O. Jorba. Evaluation of gas-phase results of the online NMMB/BSC-CTM model at regional and global scales. 24th ACCENT/GLOREAM Workshop. Barcelona, Spain, 17 - 19 October 2012, Oral presentation

A. Badia, O. Jorba and A. Voulgarakis. Intercomparison of the impact of stratospheric ozone handling on tropospheric composition using the global NMMB/BSC-CTM model in summer 2004. European Geosciences Union General Assembly 2012 (EGU), Vienna, Austria, 22 - 27 April 2012, Poster.

O. Jorba, C. Pérez, K. Haustein, Z. Janjic, J. M. Baldasano, D. Dabdub, **A. Badia**, and M. Spada. The NMMB/BSC-CTM: a multiscale online chemical weather prediction system. 14th Conference on Harmonisation within Atmospheric Dispersion Modeling for Regulatory Purposes, Kos, Greece, 02 - 06 October 2011, Oral presentation

A. Badia and O. Jorba. Evaluation of the NMMB/BSC-CHEM gas-phase results at global scale for summer 2004. European Geosciences Union General Assembly 2011 (EGU), Vienna, Austria, 03 - 08 April 2011, Poster

O. Jorba , D. Dabdub , J. M. Baldasano, M. Spada, and **A. Badia**. Assessing the impact of NO2 photo-excitation at global scale. European Geosciences Union General Assembly 2011 (EGU), Vienna, Austria, 03 - 08 April 2011, Poster

P. Jiménez-Guerrero, O. Jorba, and **A. Badia** . Global chemical regimes for ozone formation in a global on-line chemical weather prediction model (NMMB/BSC-CHEM). European Geosciences Union General Assembly 2011 (EGU), Vienna, Austria, 03 - 08 April 2011, Poster

O. Jorba , C. Pérez , K. Haustein , Z. Janjic, D. Dabdub, J. M. Baldasano , **A. Badia**, and M. Spada. Status of development and firsts results at global scale of NMMB/BSC-CHEM: an online multiscale air quality model. European Geosciences Union General Assembly 2010 (EGU), Vienna, Austria, 02 - 07 May 2010, Poster

Publications under preparation

Inter-comparison of two ozone stratospheric linear models within a global Chemical Transport Modeling, will be submitted to the Atmospheric Environment journal

The NMMB/BSC Chemical Transport Model: model description and gas-phase evaluation at global scale, will be submitted to Geoscientific Model Development journal.

Contents

List of Tables

List of Figures

List of Symbols

F actinic fluxs. 67, 68

F_c flux density. 69

H Henry's Law coefficient. 73

I radiance. 68

$J - values$ photolysis rates. 66, 67

K_h eddy diffusion coefficients for energy. 44

K_m eddy diffusion coefficients for momentum. 44

L chemical loss. 66

N_e number of sources and sinks. 44, 45

P chemical production. 66

P_r precipitation rate. 74

Q_n diabatic energy sources and sinks. 44

R universal gas constant. 44, 53, 74

$R_{aerosol}$ rate of aerosols production. 45

$R_{deposition}$ rate of dry or wet deposition. 45

$R_{emission}$ rate of surface or elevated emissions. 45

R_n external sources and sinks. 45

$R_{reaction}$ rate of photochemical production or loss. 45

S solar flux. 68

T temperature. 53, 74

T_a temperature of air. 44

T_v virtual temperature. 44

V_a volume of air. 44

W_T total water content. 74

Ω angular velocity vector. 44

Φ geopotential vector. 44, 53

Φ_S geopotential of the Earth's surface. 53

Σ cross section. 68

α_i scavenging coefficient for the gas specie. 73

χ potential velocity. 54

ε central point of the extended nonhydrostatic dynamics. 53

η_A dynamic viscosity of air. 44

λ wavelength. 68

μ cosine of zenith angle. 68

μ_0 cosine of solar zenith angle. 68

$\overline{\omega}$ single scattering albedo. 68

ϕ azimuth angle. 68

ϕ_0 solar azimuth angle. 68

π hydrostatic pressure. 52

π_s hydrostatic pressure at the base. 52

π_t hydrostatic pressure at the top. 52

ψ stream function. 54

ρ air density. 44

σ vertical coordinate. 52, 55

τ optical depth level. 68

τ_{cld} cloud timescale. 73, 74

$\tau_{washout}$ washout time. 74

θ zenith angle. 68

θ_v potential virtual temperature. 44

ϑ quantum yield for photodissociation. 68

c concentration vector. 66

$c_{p,d}$ specific heat of dry air at constant pressure. 44

c_q concentration of gas q. 45, 69

m difference in hydrostatic pressure between the base and top. 52

n_a number of air moles. 44

p nonhydrostatic pressure. 53

p_a partial pressure of air. 44

pt top pressure. 55

$ptsgm$ pressure that separate the two vertical regions. 55

$q_{I,i}$ moist-air mass mixing ratio of ice. 45

$q_{L,i}$ moist-air mass mixing ratio of liquid water. 45

q_v specific humidity of water vapor. 45

r Correlation coefficient. 138

r_{ac} transfer resistance for processes that depend only on canopy height and density. 71

r_a aerodynamic resistance. 70, 71

r_b quasilaminar sublayer resistance. 70, 71

r_{cl} lower canopy resistance. 71

r_c canopy (or surface) resistance. 70, 71

r_{dc} resistance of gas-phase transfer affected by buoyant convection in canopy. 71

r_{gs} resistance of soil, leaf litter, and other ground material. 71

r_{lu} resistance of outer surface of leaves in the upper canopy. 71

r_m mesophyll resistance. 71

r_s leaf stomata resistance. 71

v_d deposition velocity. 69, 70

z height. 69

$C_{i_{cld}}$ gas concentration within the cloud. 73, 74

$\mathbf{v}$ horizontal wind vector. 44, 53, 54

List of Acronyms

ACCMIP Atmospheric Chemistry and Climate Model Intercomparison Project. 48, 77, 78, 100, 101, 131

AirBase The European air quality database. 137

AQ Air Quality. 35

AQM Air Quality Model. 38, 39, 41, 44, 47, 48, 56, 74, 76, 77, 98, 99, 103, 106, 107, 134, 159, 162, 163

AQMEII Air Quality Model Evaluation International Initiative. 99, 134–137, 151, 153, 158, 163

BC Boundary Condition. 47, 76, 146, 158, 163

CASTNET Clean Air Status and Trends Network. 102, 125, 156

CB04 Carbon-Bond IV. 47, 56

CB05 Carbon Bond 2005. 47, 48, 56, 57, 69, 73, 79

CMAQ Community Multi-scale Air Quality Model. 74

CMD Climate Monitoring and Diagnostics Laboratory. 156

CRM Cloud Resolving Model. 39

CTM Chemical Transport Model. 40, 41, 66, 82, 83, 96, 161

EANET Acid Deposition Monitoring Network in East Asia. 102, 119, 125

EBI Euler Backward Iterative. 56, 66

ECMWF European Centre for Medium-Range Weather Forecasts. 83

EF Emission Factor. 77

EMEP European Monitoring and Evaluation Programme. 102, 119, 125, 137, 156

EPA US Environmental Protection Agency. 56

FNL Final Analysis. 84, 100, 136

GCM General Circulation Model. 39

GMD Global Monitoring Division. 85, 91, 96, 103

HALOE Halogen Occultation Experiment. 83, 85, 91, 93, 96, 155

IC Initial Conditions. 76

IFS Integrated Forecast System. 98, 136, 139

IVP Initial Value Problem. 65, 66

MACC Monitoring Atmospheric Composition and Climate. 77, 79, 88, 98, 117, 136, 138, 139, 163

MB Mean Bias. 138

MEGAN Model of Emissions of Gases and Aerosols from Nature version. 77–79, 101, 131, 136, 162

MetM Meteorological model. 40, 98, 134

MFB Mean Fractional Bias. 138

MFE Mean Fractional Error. 138

MNBE Mean Normalized Bias Error. 138

MNGE Mean Normalized Gross Error. 138

MOPITT Measurement of Pollution in the Troposphere. 106, 107, 114, 131, 138, 147, 153, 156–159, 162

MOZAIC Measurement of Ozone, Water Vapor, Carbon Monoxide, Nitrogen Oxide by Airbus In-Service Aircraft. 102, 103, 107, 112, 156, 162

MOZART Model for OZone And Related chemical Tracers. 74, 84, 98, 100, 109, 110, 112, 124, 125, 136, 139, 162

MYJ Mellor-Yamada-Janjic. 51

NADP National Atmospheric Deposition Program. 102

NAM North American Mesoscale. 51

NCEP National Centers for Environmental Prediction. 50–52, 74, 84, 99, 100, 136

NMB Normalized Mean Bias. 138

NMM Non-hydrostatic Mesoscale Model. 51, 52, 54

NMMB Non-hydrostatic Multiscale Model on the B grid. 47, 50–52, 54, 56, 154

NMMB/BSC-CTM NMMB/BSC Chemical Transport Model. 46, 47, 49, 50, 56, 73, 74, 79, 83, 84, 88, 96, 99, 107, 110, 117, 124, 125, 130–132, 134, 136, 139, 150, 151, 153–156, 158–160, 162–164

NWP Numerical Weather Predicition. 40, 41, 51, 52, 82, 83

ODE Ordinary Differential Equation. 65, 66

OMI Ozone Monitoring Instrument. 137, 138, 147, 151, 153, 158, 159

PBL Planetary Boundary Layer. 51, 52, 76, 101, 114, 149, 150, 153, 157–159

PFT Plant Functional Type. 77

POET Precursors of Ozone and their Effect on the Troposphere. 78, 100

RADM Regional Acid Deposition Model. 74

RMSE Root Mean Square Error. 138

SCIAMACHY SCanning Imaging Absorption spectroMeter for Atmospheric CHartographY. 83–85, 87, 91, 96, 104–107, 117, 123, 131, 132, 155, 156

SHADOZ Southern Hemisphere Additional Ozonesondes. 85, 91, 96, 103, 156

SNAP Selected Nomenclature for sources of Air Pollution. 136

STE Stratosphere-Troposphere Exchange. 47, 82, 83, 95, 96, 98, 125, 132, 154, 156

TNO The Netherlands Organisation for Applied Scientific Research. 48, 77, 79, 136

TOA Top Of the Atmosphere. 69

TWF total water fraction. 74

VTC Vertical Tropospheric Columns. 35, 123, 132, 137, 147, 148, 151, 153, 158, 159

WDCGG World Data Centre for Greenhouse Gases. 102, 110, 125, 156

WHO World Health Organization. 37

WOUDC World Ozone and Ultraviolet Radiation Data Center. 85, 91, 96, 103, 137, 153, 156

WRF Weather Research and Forecasting. 51, 52, 54

Chapter 1

Introduction

1.1 Air pollution

The atmosphere is a thin layer of gases and aerosols surrounding the planet Earth. Earth's atmosphere is mainly composed of nitrogen (N) and oxygen (O), and with small amounts of other trace gases such as water vapor (H_2O), carbon dioxide (CO), nitrogen oxides (NO_x), ozone (O_3) and methane (CH_4) (Finlayson-Pitts and Pitts, 2000).

Many environmentally important trace gases are removed from the atmosphere mainly by oxidation chemistry avoiding any substantial accumulation of pollutants. This capacity of self-cleansing process is called the oxidation capacity of the atmosphere. Oxidation in the troposphere is of key importance, without this process, atmospheric composition and climate would be very different. The hydroxyl radical (OH) is the most important oxidant in the troposphere which reacts with several pollutants controlling their atmospheric abundance and lifetime. Complex series of chemical reactions involving tropospheric O_3, CH_4, CO, NMVOCs, NO_x, solar radiation and humidity, determine the tropospheric concentration of OH (Logan et al., 1981; Thompson, 1992; Voulgarakis et al., 2013).

Air pollution occurs when some of these aerosols and gases in the air are found at concentrations higher than their normal levels and can pose a danger to the environment and human health. The substances that cause air pollution are called pollutants. Air Quality (AQ) is a measure of the concentration of pollutants (Seinfeld and Pandis, 1998; Jacobson, 1999; Vallero, 2007). Nowadays, air pollution is a serious problem in many cities of the world (WHO, 2014). OMI satellite image of NO_2 Vertical Tropospheric Columns (VTC) in Figure 1.1 clearly shows that the problem of air pollution is affecting developed areas such as North America, Europe, China, and also other developing countries such as South Africa, Chile, Cairo and India.

Transboundary pollution is the pollution that is originated in one country but, due to long distance transport, affects other countries. One of the main problems with transboundary pollution is that the pollution is moved away from high emission sources and deposited onto regions with comparatively low emissions.

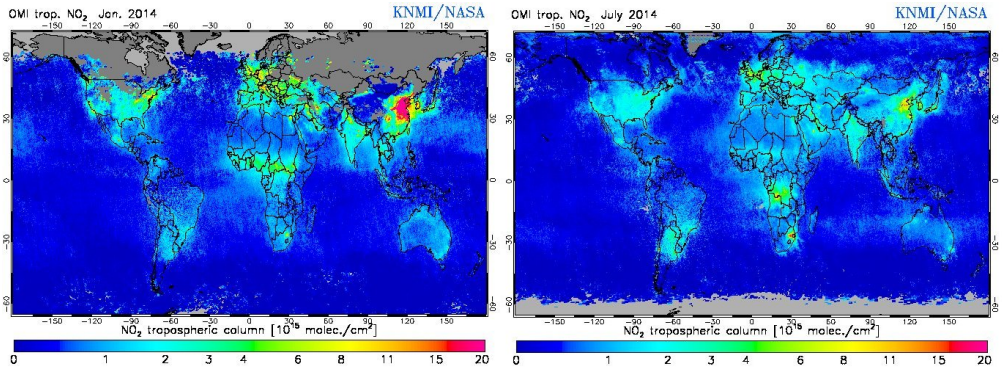

Figure 1.1: Global monthly mean NO_2 vertical tropospheric columns for January and July 2014 in $1e^{15}$molec/cm^2 measured by the OMI satellite instrument (source: `http://www.temis.nl/airpollution/`)

Air pollutants that are emitted directly into the atmosphere from sources are called primary pollutants. The conversion of primary pollutants by a complex series of chemical reactions in the atmosphere leads to the formation of secondary pollutants, many of which are even more harmful than their precursors (e.g., tropospheric O_3). The major air pollutants include sulphur dioxide (SO_2), NO_x, tropospheric O_3, ammonia (NH_3), a number of volatile organic compounds (VOCs) and particulate matter (PM). Some of the air pollution problems include photochemical smog, acid deposition, Antarctic ozone depletion, and global climate change. Figure 1.2 shows the most relevant air pollutants in Europe and their impact on human health, ecosystems and the climate.

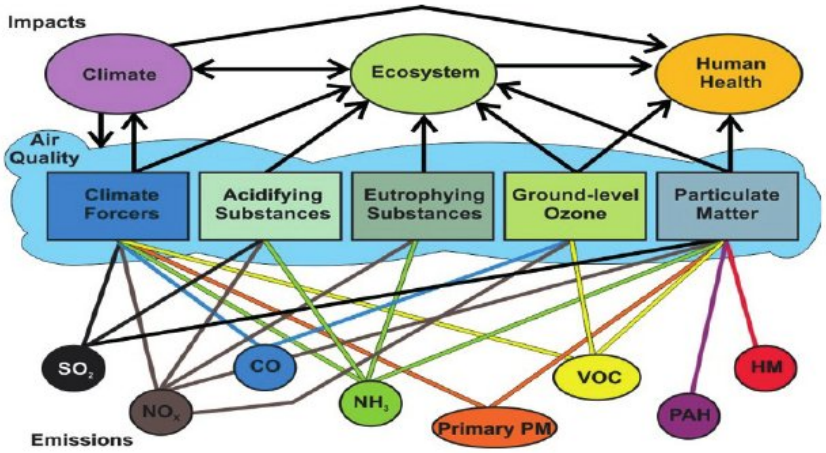

Figure 1.2: Relevant air pollutants in Europe, clustered according to impacts on human health, ecosystems and the climate (source: EEA (2011))

Ground-level O_3, one of the major constituents of photochemical smog, is harmful to human health and ecosystems. A common human health impact of tropospheric O_3 is on the respiratory track, aggravating chronic diseases and affecting children's lung development. Tropospheric O_3 formation is driven by the oxidation of VOCs (emitted by vehicles, solvents, industry and plants) in the presence of NO_x (from vehicle and industry emissions) and sunlight (Atkinson, 2000). What is more, some of the NO_2 can react with the VOCs to produce toxic chemicals such as the peroxyacyl nitrates (PAN). The formation of O_3 involving NO_x is showed in Figure 1.3 in the presence of VOCs. Therefore, O_3 plays an important role in the tropospheric chemistry and it is considered as a main indicator of air quality, reaching unhealthy levels at high concentrations. Several European studies have reported that the daily mortality rate in Europe increases by 0.3% and that of heart diseases by 0.4% , per 10 μg/ m^3 increase in O_3 exposure (WHO, 2014). For the protection of human health, the current global (based on the World Health Organization (WHO) 2005 Air Quality Guidelines) and European (based on the Directive 2008/50/EC) target values for O_3 concentrations are 100 and 120 μg/m^3 8-hour means, respectively.

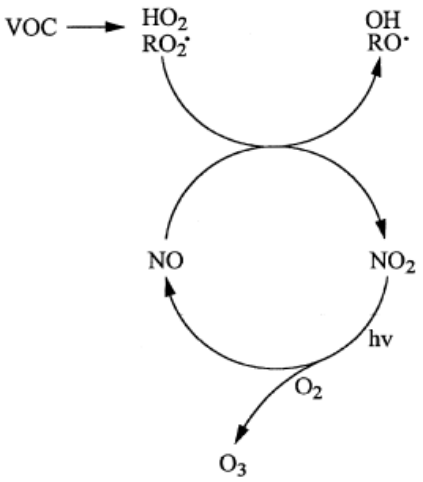

Figure 1.3: Schematics of the reactions of the NO-NO_2-O_3 systems in the presence of VOCs (adapted from Atkinson (2000)

Another important pollutant is SO_2 which is mainly formed during the burning of fuels containing sulphur. SO_2 can affect the respiratory system and the functions of the lungs, and causes irritation of the eyes. Moreover, when SO_2 combines with water, it forms sulfuric acid (H_2SO_4), the main component of acid rain, which is also toxic to plants and causes deforestation. H_2SO_4 is also formed of the sulphate aerosol and can have seriously detrimental effects on the human health.

Since the pre-industrial era, anthropogenic emissions have changed, modifying the regional and

global distribution and concentrations of tropospheric trace gases (Lamarque et al., 2013). The links between emissions and concentrations of air pollutants can only become well-understood by means of air quality modelling. In addition, the development of detailed computer models that solve reactions occurring in the atmosphere is required to evaluate the impacts and consequences of different emission scenarios on atmospheric composition.

1.2 Air quality models

Air Quality Models (AQMs) can be defined as a mathematical representation of the relevant physico-chemical processes occurring in the atmosphere, which are solved using numerical algorithms to simulate the transport and emissions of air pollutants from their sources, chemical reactions, physical transformation, and depositions (Tonnesen et al., 1998b; Jacobson, 1999).

AQMs mathematically represent different processes such as the gas-phase chemistry, the aerosol chemistry, the aqueous chemistry, the wet and dry deposition, and the transport of pollutants. Based on inputs such as meteorological data (solar radiation, wind, temperature, precipitation, etc.), and source information (emissions, initial and boundary concentrations of chemical species), these models are designed to describe primary pollutants as well as secondary pollutants.

AQMs are essential tools to evaluate control strategies aimed at reducing air pollution and, therefore, can strongly contribute to air pollution health studies. These models are important to air quality management because they are broadly used by agencies devoted to air pollution control to both identify source contributions to air quality problems and help in the design of effective strategies to reduce air pollution. Some applications of AQMs are, for example, to make sure that a new source will not surpass the limit of ambient air quality or to decide on appropriate additional control requirements. AQMs are also used to calculate pollutant forecast concentrations from multiple sources after the implementation of a new regulatory programme, in order to estimate the efficiency of the programme in reducing harmful exposures to humans and the environment. AQMs are also used for emissions scenarios to assess the effects of climate policies on air pollution, and to estimate emission reduction potentials and costs (EPA, 2011). Furthermore, research applications use AQMs to understand the complex physico-chemical processes occurring in the atmosphere.

EPA (2011) groups AQMs in several different ways depending on: the required model inputs (i.e., meteorological data); the spatial scale (global; regional-to-continental; local-to-regional; local); the temporal scale (short-term - 1-3 days, midterm - seasonal, long-term - climate models); the treatment of the transport equations (Lagrangian or Eulerian models); the treatment of different physicochemical processes (chemistry, photolysis, wet and dry deposition, aqueous chemistry, stratosphere-troposphere exchange); and the complexity of the approach. The selection of a model depends on the available data, the needs of the researcher and the computational resources.

1.2.1 Urban/Regional/Global/Multiscale Eulerian Air quality - Meteorological Models

Since the late 1940s, scientists have used computational models to simulate the weather, climate and air quality, on a wide range of temporal and spatial scales. Due to the limited computer capacity available to the early models, many approximations were made to their governing equations and coarse resolution where used in the simulations (Randell et al., 2007). Nowadays, the AQMs contain more complex chemical mechanisms and aerosols physics and use sub-grid scales to treat atmospheric turbulence and other processes. Moreover, computing power has increased dramatically and, consequently, regional models are expanding their domain and global models are increasing their resolution to converge in a common dynamic and physical framework. High-resolution modelling systems are increasingly being considered as a necessary step for improving the monitoring and predictions of air quality (Shrestha et al., 2009).

A multiscale model is designed to simulate atmospheric processes over a wide range of scales, from the global scale down to the meso-gamma scale within a single modelling system (Tonnesen et al., 1998b; Janjic and Black, 2005; Arakawa et al., 2011). Multiscale modelling involves two families of atmospheric models (Figure 1.4): one is the General Circulation Models (GCMs) and the other is the Cloud Resolving Models (CRMs). In this figure, the x-axis is the horizontal resolution and the y-axis is a measure for the degree of parametrization. These two families of models have developed different parametrizations to run over different horizontal resolution. The main idea is that GCMs and CRMs converge to a common single modelling system able to solve both scales.

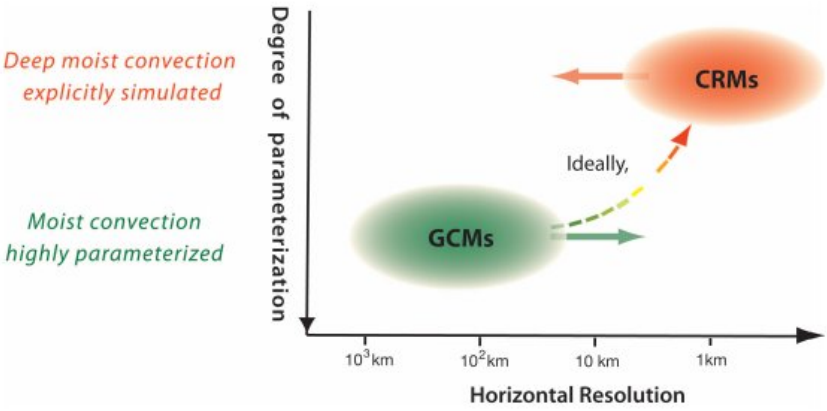

Figure 1.4: Multiscale modelling involving two families of atmospheric models with different parametrizations to resolve the physics: General Circulation Models (GCMs) and Cloud Resolving Models (CRMs) (source: Arakawa et al. (2011))

1.3 Overview of regional and global online and offline meteorological and chemical transport modelling

Weather is known to strongly influence air quality, and atmospheric composition can influence both weather and climate (Forster et al., 2007). Modelling techniques are a valuable approach to study such processes.

The development of Chemical Transport Models (CTMs) and Numerical Weather Predicitions (NWPs) have traditionally proceeded in separate fields due to the scientific complexities and the limitations in computational resources. This idea was plausible in the previous decades when the resolution of NWPs was too low for the meso-scale air pollution forecasting (Baklanov and Korsholm, 2007). Nowadays, due to a general increase in computing capacity this situation has changed, leading to a different types of coupling the NWPs with atmospheric CTM.

There are two types of coupling the NWP with atmospheric CTM: online and offline. Different studies discuss the main characteristics of online and offine approaches (Peters et al., 1995; Baklanov et al., 2014; Baklanov and Korsholm, 2007; Zhang, 2008; Zhang et al., 2012a,b). According to Baklanov and Korsholm (2007) various levels of NWPs and CTMs coupling/integration can be considered:

- **Offline**:
    1. Separate CTMs driven by meteorological input data from meteo-preprocessors, measurements or diagnostic models.
    2. Separate CTMs driven by analysed or forecasted meteodata from NWPs archives or datasets.
    3. Separate CTMs reading output-files from operational NWPs models or specific Meteorological model (MetM) with a limited period of time.
- **Online**:
    1. Online access models, when meteodata is available at each time-step.
    2. Online integration of CTMs into NWPs, where feedbacks are considered, defined as **online coupled/integrated modelling**.

Both offline and online models are actively used in current regional and global models. Figure 1.5 shows the structures of the offline and online air quality modelling systems, respectively, normally used nowadays. Offline modelling has the advantage that the CTMs simulations only need a single meteorological dataset to generate many chemical simulations. Although this approach requires lower computational capacity, it can cause a loss of essential information about some atmospheric processes (e.g., cloud formation and precipitation) that have a time scale smaller than the output time of the meteorological model (Grell et al., 2005; Zhang, 2008; Baklanov et al., 2014). On the other hand, these feedbacks can be simulated in fully-coupled online models, without space and time interpolation of meteorological fields but normally with higher

computational costs. Over recent years, due to advances in computing power, online coupled meteorology-chemistry global and regional-scale models have been developed and used by science communities that recognize online models more realistic than offline models (Baklanov et al., 2014).

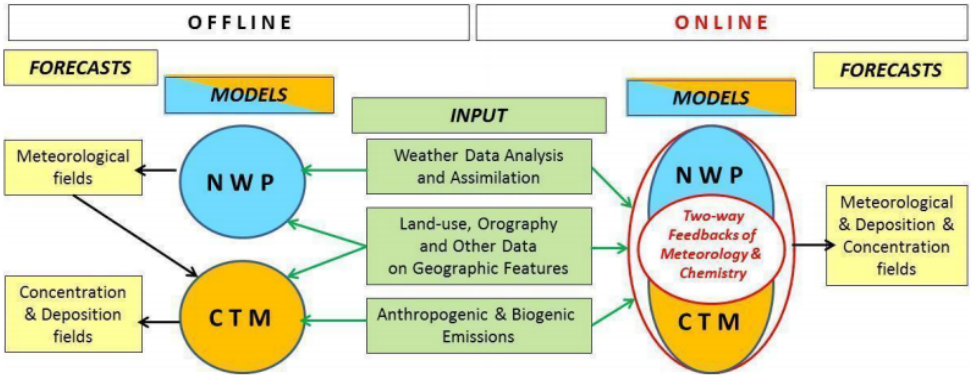

Figure 1.5: Schematic diagram of offline and online coupled NWP and CTM modelling systems (from Baklanov et al. (2014))

Both offline and online approaches are useful in different applications. Offline models are usually used in ensembles and operational forecasting, inverse/adjoint modelling, and sensitivity simulations, while online models are used for applications in which the feedbacks between the meteorology and chemistry are important, the local scale wind and the circulation system changes quickly, and the coupled meteorology-air quality modelling is required for accurate model simulations (Zhang, 2008). An overview on current offline models is discussed in Kukkonen et al. (2012).

Online coupling was first applied at the Novosibirsk scientific school (Marchuk, 1986; Penenko and Aloyan, 1985; Baklanov, 1988), during the 1980's, for modelling active artificial/ anthropogenic impacts on atmospheric processes. During the 1990 the first online coupled (with two-way feedback) regional air quality meteorological model worldwide, the GATOR-MMTD model (Jacobson et al., 1996; Jacobson, 1997b,a), was developed in the USA and it still remains the most advanced online coupled model, in terms of the complexity of the coupling. Since then, American, Canadian and Europe institutions have been developing and using online coupled models for air quality forecasting and for research.

Significant differences between the AQMs include those related to the horizontal and vertical resolutions, the chemical mechanism, the photolysis scheme, the meteorological fields, the deposition parametrization or the stratospheric chemistry scheme. An overview of regional and global online and offline models currently used in the atmospheric communities are summarised in Table 1.1 and Table 1.2, respectively.

Table 1.1: Online models and their applications

Model	Reference/ Model Type	Chemical Mechanism	Photolysis scheme	Dry deposition	Wet deposition	Stratospheric model	Meteorological core	Applications
Online models (with feedbacks)								
GATOR-MMTD	Jacobson et al. (1996)/ regional	Jacobson (1994)	Yes	McRae et al. (1982); Russell et al. (1993a)	Jacobson (1997c)		MMTD Lu and Turco (1995)	USA
GATOR-GCMM	Jacobson (2001b,c)/ regional	Jacobson (1999)	Yes (27 photolysis reactions)	Wesely (1989); Walmsley and Wesely (1996)	Yes		GCMM Jacobson (2001b,c)	USA
BOLCHEM	Mircea et al. (2008)/ regional	SAPRC-90 (Carter, 1990), CB04 (Gery et al., 1989)	From a look-up table (Carter, 1990)	Wesely (1989)	EMEP (2003)		BOLAM (Buzzi et al., 1994)	Europe, Italy
ENVIRO-HIRLAM	Baklanov et al. (2008)/ regional	NWP-Chem (Korsholm et al.), CBMZ (Zaveri and Peters, 1999)	Madronich (1987)	Wesely (1989)	Washout, Seinfeld and Pandis (1998); Baklanov and Sørensen (2001)		HIRLAM (Unden et al., 2002)	Europe, Denmark
WRF-CMAQ	Mathur et al. (2010)/ urban and regional	CB05 (Yarwood et al., 2005), RADM2 (Stockwell et al., 1990), SAPRC99 (Carter, 2000)	δ- Eddington (Joseph et al., 1976); Madronich (1987), Fast-TUV	Byun et al. (1990)	Roselle and Binkowski (1999)		WRF-ARW, WRF-NMM (Skamarock et al., 2008)	USA, Europe
WRF- Chem	Grell et al. (2005)/ regional	RADM2 (Stockwell et al., 1990), CBMZ (Zaveri and Peters, 1999)	Madronich (1987), Fast-J (Wild et al., 2000)	Wesely (1989)	Fahey and Pandis (2001); Easter et al. (2004)	Yes	WRF-ARW, WRF-NMM (Skamarock et al., 2008)	USA, Europe, Germany, UK, Spain, Italy, etc.
COSMO-ART	Vogel et al. (2009)/ regional	Extended RADM2 (Stockwell et al., 1990)	GRAALS radiation (Ritter and GELEYN, 1992)	Binkowski and Shankar (1995)	Rinke (2008)		COSMO (Steppeler et al., 2003)	Europe, Germany
ECHAM5-MESSy	Jöckel et al. (2005)/ multiscale	MECCA (Sander et al., 2005)	JVAL (Landgraf and Crutzen, 1998)	Wesely (1989); Kerkweg et al. (2006)	Jöckel et al. (2006)	Steil et al. (1998)	ECHAM5 (Roeckner et al., Retrieved January 2009)	Europe, Germany
MC2-AQ	Plummer (1999); Plummer et al. (2001)/ regional	ADOM-II Lurmann et al. (1986)	Tabulated values (correction of the clear-sky photolysis rates by RADM)	Wesely (1989)	Simplified scheme based on constant scavenging coefficient		MC2 (Benoit et al.)	Europe, Poland
GEM-AQ	Kaminski et al. (2007)/ multiscale	Extended ADOM-II Lurmann et al. (1986)	δ − 2 stream (Landgraf and Crutzen, 1998; Jöckel et al., 2006)	Wesely (1989)	SimpliïňĄed scheme: only below-cloud scavenging of gas phase species	Climatological values	GEM (Côté et al., 1998)	Canada
NMMB/BSC-CTM	Jorba et al. (2012); Badia and Jorba (2014); Pérez et al. (2011); Spada et al. (2013)/ multiscale	CB05 (Yarwood et al., 2005)	Fast-J (Wild et al., 2000) and Fast-JX (Barnard et al., 2004)	Wesely (1989)	Grid and sub-grid scale from Foley et al. (2010)	COPCAT (Monge-Sanz et al., 2011) or Cariolle v2 (Cariolle and Teyssèdre, 2007) for O_3 and climatological values for other gases	NMMB (Janjic and Black, 2005; Janjic and Gall, 2012)	Europe, Global

Table 1.2: Offline models and their applications

Model	Reference/ Model Type	Chemical Mechanism	Photolysis scheme	Dry deposition	Wet deposition	Stratospheric model	Meteorological core	Applications
Offline models (no feedbacks)								
MM5-CHIMERE	Vautard et al. (2003)/ urban to regional	MELCHIOR2 (Lattuati, 1997)	TUV module, Madronich and Flocke (1999)	Seinfeld and Pandis (1998)	Loosmore and Cederwall (2004); Guelle et al. (1998)		MM5 (Grell et al., 1994)	Europe, France, Portugal
MOCAGE	(Peuch et al., 1999)/ multiscale	RACM (Stockwell et al., 1997)	Madronich (1987)	Wesely (1989); Noilhan and Planton (1989)	Giorgi and Chameides (1986)	REPROBUS (Lefevre et al., 1994); Cariolle v2 (Cariolle and Teyssèdre, 2007)	ECMWF/IFS http://www.ecmwf.int/research/ifsdocs	Europe, France
SILAM	Sofiev et al. (2006)/ regional	DMAT (Sofiev, 2000), CB04 (Gery et al., 1989)	Yes	Wesely (1989); Hicks et al. (1987); Lindfors et al. (1993)	Sofiev (2000)		HIRLAM (Unden et al., 2002)	Europe, Finland
EURAD-RIU	(Hass, 1991; Hass et al., 1993)/ regional	RADM2 (Stockwell et al., 1990), RACM (Stockwell et al., 1997), Euro-RADM	δ- Eddington (Joseph et al., 1976);; Madronich (1987)	Walcek et al. (1986)	Roselle and Binkowski (1999)	Yes	MM5 (Grell et al., 1994)	Europe, Germany
FARM	(Silibello and Calori, 2003)/ regional	SAPRC-90 (Carter, 1990), SAPRC99 (Carter, 2000)	Madronich (1987)	Walcek et al. (1986); Wesely (1989)	EMEP (2003); Maul (1980)		MM5 (Grell et al., 1994), WRF (Skamarock et al., 2008)	Europe, Italy
MOZART-4	(Brasseur et al., 1998; Emmons et al., 2010)/ global	Emmons et al. (2010) for global; CBMZ (Zaveri and Peters, 1999) for regional	Fast-TUV (Tie et al., 2003)	Wesely (1989); Walmsley and Wesely (1996); Wesely and Hicks (2000)	Brasseur et al. (1998)	SYNOZ (McLinden et al., 2000)	ECMWF/IFS http://www.ecmwf.int/research/ifsdocs	USA, Europe
GEOS-Chem	(Bey et al., 2001a)/ multiscale	Horowitz et al. (1998); DeMore et al. (2000)	Fast-J (Wild et al., 2000)	Wesely (1989); Wang et al. (1998)	Liu et al. (2001a)	SYNOZ (McLinden et al., 2000)	GEOS http://gmao.gsfc.nasa.gov/GEOS/	USA, Europe
TM5	(Krol et al., 2005; Huijnen et al., 2010)/ multiscale	Modified CB04 (Houweling et al., 1998)	Lookup table (Landgraf and Crutzen, 1998; Williams et al., 2006)	Wesely (1989); Ganzeveld et al. (1998)	Roelofs and Lelieveld (1995); Guelle et al. (1998)	ST-TM5; Cariolle v2 (Cariolle and Teyssèdre, 2007)	ECMWF/IFS http://www.ecmwf.int/research/ifsdocs	Global
LOTOS-EUROS	Schaap et al. (2008)/ regional	CB04 (Gery et al., 1989)		Erisman et al. (1994)	EMEP (2003)		ECMWF/IFS http://www.ecmwf.int/research/ifsdocs	Europe and the Netherlands
MM5-CAMx	Halenka et al. (2007)/ urban to regional	CB04 (Gery et al., 1989)		Wesely (1989)	Seinfeld and Pandis (1998)		MM5 (Grell et al., 1994)	Europe, NA,Greece
EMEP	Jonson et al. (1998)/ regional and global	EMEP (Simpson et al., 1993)	DeMore et al. (1985); Kylling et al. (1998)	Wesely (1989)	EMEP (2003)		HIRLAM (Unden et al., 2002)	Europe, Norway

1.3.1 Governing equations

The main objective of the AQM is to reproduce the concentration of pollutants, temperature, moisture, pressure, and wind components. To provide a fundamental view of the atmospheric modelling, a robust and fully compressible governing set of equations for the atmosphere is introduced. The **meteorological governing equations** are based in laws of conservation of mass, energy, momentum, and the ideal gas law. Moreover, AQMs include **chemical governing equations** for atmospheric trace gases. The governing equations and computational algorithms need to be consistent and compatible with each component of the modelling system.

Following the formulation and nomenclature from Jacobson (1999) the basic physical equations used in meteorological models and AQMs are:

A) Meteorological equations

1. **Equation of motion** (prognostic equation)

$$\frac{\partial v}{\partial t} + (v \cdot \nabla)v = -2\Omega \times v\nabla\Phi - \frac{1}{\rho_a}\nabla p_a + \frac{\eta_a}{\rho_a}\nabla^2 v + \frac{1}{\rho_a}(\nabla \cdot \rho_a K_m \nabla)v \tag{1.1}$$

   where **v** is the velocity vector, Ω is the angular velocity vector, Φ is the geopotential vector, ρ is the air density, p_a is the partial pressure of air, η_A is the dynamic viscosity of air and K_m is the eddy diffusion coefficients for momentum.

2. **Ideal gas equation** (a diagnostic relation).

$$p_a = \frac{n_a R T_a}{V_a} \tag{1.2}$$

   where n_a is the number of air moles, R is the universal gas constant, T_a is the temperature of air and V_a is the volume of air.

3. **Thermodynamic energy equation** (prognostic equation)

$$\frac{\partial \theta_v}{\partial t} + (v \cdot \nabla)\theta_v = \frac{1}{\rho_a}(\nabla \cdot \rho_a K_h \nabla)\theta_v + \frac{\theta_v}{c_{p,d} T_v}\sum_{n=1}^{N_e}\frac{dQ_n}{dt} \tag{1.3}$$

   where θ_v is the potential virtual temperature, K_h is the eddy diffusion coefficients for energy, T_v is the virtual temperature, $c_{p,d}$ is the specific heat of dry air at constant pressure, Q_n diabatic energy sources and sinks and N_e is the number of these sources and sinks.

4. **Continuity equation for mass of air** (prognostic equation)

$$\frac{\partial \rho_a}{\partial t} + (v \cdot \nabla)\rho_a = 0 \tag{1.4}$$

An aspect worth pointing out on this equation is that external sources and sinks (R_n) are relatively small and, consequently, are ignored.

5. **Continuity equations for water** in its three phases: solid, liquid, and vapor (prognostic equation)

$$\frac{\partial q_v}{\partial t} + (\mathbf{v} \cdot \nabla)q_v = \frac{1}{\rho_a}(\nabla \rho_a \mathbf{K}_h \nabla)q_v + \sum_{n=1}^{N_e} R_n \tag{1.5}$$

$$\frac{\partial q_{L,i}}{\partial t} + (\mathbf{v} \cdot \nabla)q_{L,i} = \frac{1}{\rho_a}(\nabla \rho_a \mathbf{K}_h \nabla)q_{L,i} + \sum_{n=1}^{N_e} R_n \tag{1.6}$$

$$\frac{\partial q_{I,i}}{\partial t} + (\mathbf{v} \cdot \nabla)q_{I,i} = \frac{1}{\rho_a}(\nabla \rho_a \mathbf{K}_h \nabla)q_{I,i} + \sum_{n=1}^{N_e} R_n \tag{1.7}$$

where q_v is the specific humidity of water vapor, $q_{L,i}$ is the moist-air mass mixing ratio of liquid water in a size bin and $q_{I,i}$ is the moist-air mass mixing ratio of ice in a size bin, R_n are the external sources and sinks processes affecting the specie and N_e is the number of these external processes. In a model the total water content is estimate as: $q_T = q_v + \sum_{i=1}^{N_e}(q_{L,i} + q_{I,i})$.

B) Chemical equations

1. **Atmospheric trace gases continuity equation** (prognostic equation):

$$\frac{\partial c_q}{\partial t} + (v \cdot \nabla)c_q = (\nabla \cdot \mathbf{K}_h \nabla)c_q + \sum_{n=1}^{N_{e,t}} R_{emission} + R_{deposition} + R_{reaction} + R_{aerosol} \tag{1.8}$$

where c_q is the concentration gas q, $R_{emission}$ is the rate of surface or elevated emissions, $R_{deposition}$ is the rate of dry or wet deposition, $R_{reaction}$ is the rate of photochemical production or loss, and the $R_{aerosol}$ is the rate of aerosols production.

If one takes meteorology equations 1.1-1.7 and chemistry equations 1.8 separately, it may find an uncoupled (or offline) approach, computationally very attractive. Nevertheless, this approach cannot capture the climate-chemistry-aerosol-cloud-radiation feedbacks; consequently, important information about atmospheric characteristics are lost. Online models solve not only the chemical equation 1.8, but also contain a coupled meteorological model solving, some or all, meteorological equations 1.1-1.7.

1.4 Motivation

The Earth Sciences Department of the Barcelona Supercomputing Center - Centro Nacional de Supercomputación develops and maintains the state-of-the-art air quality forecasting systems. Since 2008, the group works in the development of a fully online unified global/regional air quality and meteorological model, the NMMB/BSC-CTM. The new modelling system is intended to be a powerful tool for research and to provide efficient global and regional chemical weather simulations at sub-synoptic and mesoscale resolutions. The new model is developed within the framework of three national research projects: (1) "Improvement of the Dust REgional Atmospheric Model (DREAM) for prediction of Saharan dust events in the Mediterranean and the Canary Islands" (CGL2006-11879/CLI) in which a mineral dust module was developed and implemented "online" into the NMMB atmosperic global/regional atmospheric model; (2) "Coupling of a Fully Online Chemical Mechanism Within the Atmosperic Global-Regional UMO/DREAM Model" (CGL2008-02818/CLI) in which a gas-phase chemical module was implemented "online" into the NMMB atmospheric model; and (3) "Coupling of a fully online multi-component aerosol module within the atmosperic global-regional NMMB model" (CGL2010-19652), in which a multicomponent aerosol module for global relevant aerosols in the troposphere was developed. Furthermore, the system is extended nowadays to higher resolution within the framework of the BSC Severo-Ochoa project (SEV-2011-00067) of the Severo Ochoa Program, awarded by the Spanish Government.

Currently the system is providing mineral dust forecasts to the World Meteorological Organization (WMO) Sand and Dust Storm Warning Advisory and Assessment System (SDS-WAS) Northern Africa-Middle East-Europe (NA-ME-E) Regional Center managed by a consortium of AEMET and BSC. Furthermore, the model has been selected as the reference mineral dust model for the recently created First WMO Regional Meteorological Center specialized on Atmospheric Sand and Dust Forecast, the Barcelona Dust Forecast Center.

The present Ph.D. thesis work is part of the project "Coupling of a Fully Online Chemical Mechanism Within the Atmosperic Global-Regional UMO/DREAM Model" (CGL2008-02818/CLI) and the BSC Severo-Ochoa project, and has undertaken both implementation and evaluation works of the gas-phase chemistry within the new modelling system NMMB/BSC-CTM.

1.5 Objectives of the Thesis

The main objective of this Ph.D. thesis is the **implementation and evaluation of the tropospheric oxidant gas-phase chemistry within the online multiscale atmospheric model NMMB/BSC Chemical Transport Model (NMMB/BSC-CTM) to provide a basis for computer modelling studies of O_3, PM, visibility, acid deposition and air toxics and further extend the range of applicability to study interactions between the meteorological and the chemical processes occurring in the atmosphere**. This main goal is divided into three main specific objectives:

1. **Contribute to the development of a new state-of-the-art online model implementing**

the oxidant gas-phase chemistry of the troposphere.

2. **Design the configuration of the modelling system and prepare the required input information to run the model at regional and global scales.**

3. **Evaluate the tropospheric gas-phase chemistry using a wide range of observational datasets for a regional and a global model scenarios.**

1.5.1 Model development

This Ph.D. thesis has contributed to the development of the new online global/regional atmospheric model NMMB/BSC-CTM. The model developments are focused on the processes occurring in the troposphere that involve the oxidant gas-phase chemistry.

One of the major aims is to review and implement the main physical and chemical processes that affect pollutants in the atmosphere into the meteorological core, Non-hydrostatic Multiscale Model on the B grid (NMMB), using a modular approach. The strategy followed is:

1. Review several state-of-the-art photochemical mechanisms (e.g., CB04, CB05, RADM, RADM2, SAPRC07) that describe the chemical reactions, product yields and kinetics data and select a computational efficient scheme to be implemented into the model.

2. Review the most used and extended state-of-the-art photolysis schemes (e.g., Fast-J, Fast-JX, FAST-TUV, Madronich) and check which improvements can be introduced in Fast-J, already implemented in the NMMB/BSC-CTM model. We focus in implement further CB05 photolysis reactions and update their different cross sections and quantum yield tables.

3. Extend the Wesely dry deposition scheme to all the gas-species considered by the CB05 chemical mechanism. The complex part of this scheme is to compute the canopy resistance, R_c. However, other parameters used in these parameterizations need to be updated (i.e., Effective Henry's law coefficient, reactivity factors, diffusion coefficients). These parameters describe soil type, vegetation and friction gas resistances.

4. Evaluate the cloud chemistry scheme, already implemented within the NMMB/BSC-CTM.

5. Implement a simplified linear stratospheric ozone scheme to model the Stratosphere-Troposphere O_3 exchange properly with low computational cost. Since we are focused in the tropospheric chemistry, we are not interested in including a detailed stratospheric chemistry. Hence, simple parameterizations of stratospheric O_3 are evaluated as an upper boundary condition to model the O_3 Stratosphere-Troposphere Exchange (STE).

The importance of lateral Boundary Conditions (BCs) in the regional AQMs is well recognized by in the atmospheric community. For that reason, one of the specific technical implementations related to the BC is to design an algorithm that read, adapt and prepare the BCs for the regional configuration using the output data from a global or regional model.

1.5.2 Experiment design

A second major aim of this Ph.D. thesis is the definition of the model configuration for runs at different scales. Hence, it is important to set up the domain, the horizontal and vertical resolutions, the meteorological model parameterizations, and all the required input data to execute the model properly. In this sense, two main domains of study are defined:

1. Global annual simulation with a horizontal grid spacing of 1.4°x1° and 64 vertical layers up to 1 hPa (Global run).
2. Regional annual simulation over Europe with a horizontal resolution of 0.2°x0.2°. To test the sensitivity of the results to the vertical grid discretization, two different vertical configurations are defined: 1) 24 vertical layers up to 50 hPa, and 2) 48 vertical layers up to 50 hPa (Regional run).

A critical part in an atmospheric chemistry model simulation is the required model inputs (i.e., meteorological initial and boundary conditions, geomorphological characterisation, chemistry emissions). The main critial inputs to computed are the emission fluxes of the primary gases under study. For that, emission inventories available in the community are used. Different emission sources (e.g. human activity, sea, soil, vegetation, biomass burning, etc.) have a relative contribution to the modelled final concentrations of the relevant pollutants. For that reason, two main tasks are done:

1. Review and select different emissions inventories currently implemented in the AQMs (ACCMIP and TNO).
2. Prepare emission inventory data as input to the regional and global modelling system (conservative remapping to the model grid, temporal disaggregation, speciation into the CB05 chemical mechanism, and pre-process the files into the model format).

1.5.3 Model evaluation

The third objective of this Ph.D. thesis is to perform a reference model evaluation in terms of the relevant air pollutants in order to determine and quantify the model's performance capabilities and weaknesses. Therefore, the specific goals are:

1. Review the present air quality modelling evaluation studies in order to decide which statistical metrics and observational data are used for gas-phase species and which relevant air pollutants are analysed.
2. Perform a complete model evaluation over a full year period for both Global and Regional runs. This evaluation consists of several qualitative and quantitative comparisons of the model results with the observational dataset selected (surface air quality monitoring stations, ozonesondes, satellite, climatology studies, and aircraft campaigns).

1.6 Outline of this thesis

This thesis is structured in six chapters each containing extracts or full-length journal publications as indicated in the beginning of each sub-chapter (where reference is given to the relevant publication). For chapters that contain model results (3, 4, and 5) a short introduction and conclusion are provided.

A full description of the NMMB/BSC-CTM, including the meteorological driver and the gas-phase chemistry module is given in Chapter 2. Chapter 3 describes the implementation of a simplified chemical mechanism for the stratospheric ozone as an upper boundary condition to model the Stratosphere-Troposphere ozone exchange at the global scale. Model evaluation results for a global and a regional runs are given in Chapters 4 and 5, respectively. Chapter 6 summarises the main findings and conclusions of this Ph.D. thesis with an outlook on ongoing work and recommendations for future research.

Chapter 2

Model description: NMMB/BSC Chemical Transport Model

TheNMMB/BSC-CTM is a fully online multiscale chemical transport model for mesoscale to global-scale applications (Jorba et al., 2012). The system is based on the meteorological Nonhydrostatic Multiscale Model on the B grid (NMMB; Janjic and Gall, 2012), developed at the Environmental Modeling Center of National Centers for Environmental Prediction (NCEP), which has been applied operationally as the North American Mesoscale model at NCEP since October 2011. The model couples online the meteorological driver with the gas-phase and aerosol continuity equations to solve the atmospheric chemistry processes with detail. Due to its fully online coupling approach, the model can take into account the feedback processes of gases, aerosol particles and radiation. In particular, it considers the radiative effect of aerosols while presently ignoring cloud-aerosol interactions. Table 2.1 summarises the model characteristics.

As stated previously, this Ph.D. thesis is focused on the gas-phase chemistry, therefore only the gas-phase module is presented here. No interaction between gas-phase and aerosol-phase is considered in all the works presented in this thesis. However, an aerosol module for primary and secondary aerosols is being developed within the NMMB/BSC-CTM. Then, a proper representation of the gaseous species is a fundamental step for the correct formation of secondary aerosols .

In this chapter, a description of the model developments undertaken within the present thesis is presented starting with a general overview of the meteorological core of the system NMMB.

2.1 The atmospheric driver

We have decided to use the Non-hydrostatic Multiscale Model on the B grid (NMMB; Janjic and Black, 2005; Janjic and Gall, 2012) as the meteorological core. The main reasons behind this decision are: (1) it was conceived for short- and medium-range forecasting over a wide range of spatial and temporal scales from local (1 km^2) to global simulations, (2) its unified non-

Table 2.1: Model characteristics

	Meteorology
Dynamics	nonhydrostatic NMMB (Janjic and Gall, 2012)
Physics	Ferrier microphysics (Ferrier et al., 2002)
	BMJ cumulus scheme (Betts and Miller, 1986)
	MYJ PBL scheme (Janjic et al., 2001)
	LISS land surface model (Vukovic et al., 2010)
	RRTMG radiation and GFDL (Mlawer et al., 1997; Fels and Schwarzkopf, 1975)
	Chemistry
Chemical mechanism	Carbond Bond 05 (Yarwood et al., 2005)
Chemical solver	EBI (Hertel et al., 1993)
Photolysis scheme	online Fast-J photolysis scheme (Wild et al., 2000)
Dry deposition	Wesley resistance approach from Wesely (1989)
Wet deposition	Grid and sub-grid scale from Foley et al. (2010)
Ozone tropospheric upper boundary condition	COPCAT (Monge-Sanz et al., 2011) or Cariolle v2a (Cariolle and Teyssèdre, 2007) linear stratospheric scheme
Biogenic emissions	online MEGAN v2.04 (Guenther et al., 2006)

hydrostatic dynamical core allows regional and global simulations, (3) NMMB evolves from the experience of previous mesoscale NWP models Eta and Weather Research and Forecasting (WRF)-Non-hydrostatic Mesoscale Model (NMM) (Janjic et al., 2001; Janjic, 2003), (4) the regional NMMB is the operational regional North American Mesoscale (NAM) model at NCEP since October 2011, (5) its code is freely available, and (6) previous modelling systems used in our department were based in the meteorological predecesors of NMMB (i.e., Eta model used in BSC/DREAM8b).

The numerical schemes used in the NMMB were designed following the principles set up in Janjic (1977, 1979, 1984, 2003). Isotropic horizontal finite volume differencing is employed so a variety of basic and derived dynamical and quadratic quantities are conserved. Among these, the conservation of energy and entropy (Arakawa, 1966) improves the accuracy of the nonlinear dynamics. The hybrid pressure-sigma coordinate (Laprise, 1992) is used in the vertical and the Arakawa B-grid is applied in the horizontal. The global model on the latitude-longitude grid with polar filtering was developed as the reference version. The non-hydrostatic component of the model dynamics is introduced through an add-on module that can be turned on or off, depending on the resolution. The physical package includes: (1) the Mellor-Yamada-Janjic (MYJ) level 2.5 turbulence closure for the treatment of turbulence in the Planetary Boundary Layer (PBL) and in the free atmosphere (Janjic et al., 2001), (2) the surface layer scheme based on the Monin-Obukhov similarity theory (Monin and Obukhov, 1954) with introduced viscous sublayer over land and water (Zilitinkevich, 1965; Janjic, 1994), (3) the NCEP NOAH (Ek et al., 2003) or the LISS land surface model (Vukovic et al., 2010) for the computation of the heat and moisture surface fluxes, (4) the GFDL or RRTMG long-wave and shortwave radiation package (Mlawer et al., 1997; Fels and Schwarzkopf, 1975), (5) the Ferrier gridscale clouds and microphysics (Ferrier et al., 2002), and (6) the Betts-Miller-Janjic convective parametrization (Betts, 1986; Betts and Miller, 1986; Janjic, 1994, 2000). Vertical diffusion is handled by the surface

layer scheme and by the PBL scheme. Lateral diffusion is formulated following the Smagorinsky non-linear approach (Janjic, 1990).

2.1.1 The Unified Global/Regional Nonhydrostatic Multiscale Model NMMB

Historically, hydrostatic NWP models have been developed using the hydrostatic equation which simplifies and stabilizes primary equations. Hydrostatic NWP models have achieved a high level of reliability and accuracy. The majority of NWP and climate models use hydrostatic pressure, or mass-based vertical coordinates, that guarantee the mass conservation. However, hydrostatic approximation is not sufficient in the present weather forecasting models that have reached finer horizontal resolutions. For that reason, many meteorological services and research institutions consider a matter of priority the formulation and/or implementation of nonhydrostatic NWP (Janjic et al., 2001). Efforts to use hydrostatic pressure as the vertical coordinates in nonhydrostatic models have been made (Laprise, 1992; Bubnová et al., 1995).

The NCEP-ETA weather forecast model (Janjic, 1990, 1994), in operational application at NCEP since late 80ies until 2006, was replaced by a state-of-the-art regional model with improved dynamics and physics, the Nonhydrostatic Mesoscale Model WRF-NMMe (Janjic et al., 2001; Janjic, 2003). WRF-NMMe became the next-generation NCEP mesoscale model for operational weather forecasting in 2006. WRF-NMMe was built on an evolutionary approach based on the NWP experience by using the mass-based σ vertical coordinate and an add-on module that includes the nonhydrostatic motions, preserving the favorable features of the hydrostatic formulation (Janjic et al., 2001; Janjic, 2003). Later on, an evolution to an unified system was developed at NCEP, theUnified Global/Regional Nonhydrostatic Multiscale Model on the B grid NMMB (Janjic and Ferrier, 2006; Janjic, 2007; Janjic and Gall, 2012). The NMMB represents the second generation of nonhydrostatic models developed at NCEP. NMMB has the same capabilities that WRF-NMMe, however, is faster and presents a better computational efficiency (Janjic and Gall, 2012). The NMMB model is intended for wide range of spatial and temporal scales (from meso to global). With just a simple switch, NMMB can achieve regional or global domains solving the hydrostatic or nonhydrostatic equations. Recently, the system has been enhanced with the implementation of telescoping nest capabilities (one-way, two-way and moving nests).

Here, we present a brief description of the model formulation. NMMB model uses the sigma (σ) vertical coordinate (Laprise, 1992) that is mass conservative

$$\sigma = \frac{\pi - \pi_t}{m} \tag{2.1}$$

where π is the hydrostatic pressure, and m represents the difference in hydrostatic pressure between the base (π_s) and top (π_t) of the model column, i. e.,

$$m = \pi_s - \pi_t \tag{2.2}$$

The model equations governing a dry, inviscid and adiabatic nonhydrostatic atmosphere are (Janjic et al., 2001; Janjic, 2003; Janjic and Gall, 2012)

$$\frac{\partial m}{\partial t} = -\int_0^1 \nabla_{\sigma'} \cdot (m\mathbf{v}) d\sigma', \tag{2.3}$$

$$p\alpha = RT, \tag{2.4}$$

$$\Phi = \Phi_s + m\int_\sigma^1 \frac{RT}{p} d\sigma', \tag{2.5}$$

$$\frac{dv}{dt} = -(1+\varepsilon)\nabla_\alpha \Phi - \alpha \nabla_\alpha p + f\mathbf{k}\times\mathbf{v}, \tag{2.6}$$

$$\frac{\partial T}{\partial t} = -\mathbf{v}\cdot\nabla_\sigma T - \dot{\sigma}\frac{\partial T}{\partial \sigma} + \frac{\alpha}{c_p}\left[\mathbf{v}\cdot\nabla_\sigma p - (1+\varepsilon)\int_0^\sigma \nabla_{\sigma'}\cdot(m\mathbf{v})d\sigma'\right] + \frac{\alpha}{c_p}\left[\frac{\partial p}{\partial t} - (1+\varepsilon)\frac{\partial \phi}{\partial t}\right], \tag{2.7}$$

$$\frac{\partial p}{\partial \pi} = 1+\varepsilon, \tag{2.8}$$

$$w = \frac{1}{g}\frac{d\Phi}{dt} = \frac{1}{g}\left(\frac{\partial \Phi}{\partial t} + \mathbf{v}\dot{\nabla}_\sigma \Phi + \dot{\sigma}\frac{\partial \Phi}{\partial \alpha}\right), \tag{2.9}$$

$$\varepsilon = \frac{1}{g}\frac{dw}{dt} = \frac{1}{g}\left(\frac{\partial w}{\partial t} + \mathbf{v}\dot{\nabla}_\sigma w + \dot{\sigma}\frac{\partial w}{\partial \sigma}\right) \tag{2.10}$$

where $\mathbf{v}$ is the horizontal wind vector, p is the actual, nonhydrostatic pressure, R is the gas constant from dry air, T is the temperature, Φ is geopotential and Φ_S is the geopotential of the Earth's surface.

Equation 2.3 gives the tendency of the hydrostatic surface pressure, 2.4 is the equation of state, 2.5 is the hydrostatic pressure, equation 2.6 defines the horizontal part of the wind, 2.7 is the basic equation of the thermodynamics, 2.8 is the vertical equation of motion, 2.9 is the nonhydrostatic continuity equation. Equation 2.10 refers to the definition of the parameter ε which is the central point of the extended nonhydrostatic dynamics. As can be readily verified, if ε is zero, 2.3-2.7 reduce to the hydrostatic equations. Thus, the nonhydrostatic module can be turned on and off. Using this approach, useful features of hydrostatic models are preserved, however, it is possible to extend these kind of models to nonhydrostatic applications.

In addition, a conservative, positive definite and monotone Eulerian scheme for the tracers is applied (Janjic and Gall, 2012). The positive definitness is guaranteed by advecting the square root of the tracer (c.f. e.g., Schneider (1984)). The conservation is achieved due to conservation of quadratic quantities by the advection scheme. However, a forced conservative a posteriori monotonization is used to prevent creation of new extrema (Janjic et al., 2009; Janjic, 2009).

2.1.2 Horizontal discretization: the Arakawa B grid

Basic discretization of any continuous system, using numerical analysis, needs to conserve important properties of the continuous system (Janjic, 2007). NMMB conserves the following properties :

1. Energy and entropy

2. First order and quadratic quantities

3. Properties of differential operators

Winninghoff (1968), and Arakawa et al. (1977) examined the frequencies of gravity-inertia waves obtained using second-order centered differences on various types of rectangular horizontal grids. These studies concluded that, in general, staggered grid C, and semi-staggered grid B (or E) obtained higher accuracy of the exact frequencies quantities. NMMB uses Arakawa B grid in contrast to the model WRF-NMM that uses E grid (see Figure 2.1).

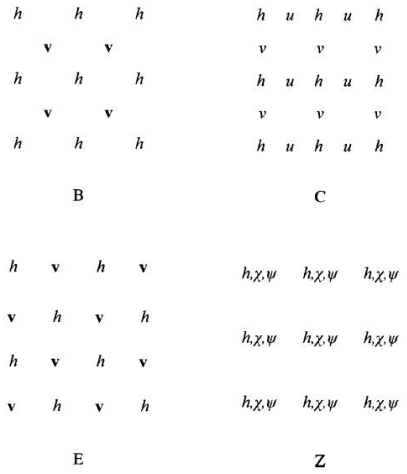

Figure 2.1: The staggered grid C and the semi-stagged grids B, E and Z from Janjic (2003)

Here, the points denoted by *h* carry surface pressure, temperature, specific humidity, cloud water, vertical velocity, turbulent kinetic energy as well as passive substances. The **v** points are horizontal velocity vectors and carry *u* and υ components of the horizontal wind. In grid *Z* is represented the velocity potential by χ and the stream function by ψ.

2.1.3 The NMMB hybrid vertical coordinate

The model uses a hybrid vertical coordinate, merging more than one type of vertical coordinate. The hybrid coordinate is specified as non-dimensional (from 1 to 0) interface values which define the model layers and their relative depths:

pt = 1 hPa
ptsgm = 300 hPa
eta levels = 1.000, 0.994, 0.982, 0.968, 0.950, 0.930, 0.908, 0.882, 0.853, 0.821, 0.788, 0.752, 0.715, 0.677, 0.637, 0.597, 0.557, 0.517, 0.477, 0.438, 0.401, 0.365, 0.330, 0.298, 0.268, 0.240, 0.214, 0.188, 0.162, 0.137, 0.114, 0.091, 0.068, 0.045, 0.022, 0.000

where *pt* is the top pressure, *ptsgm* is the pressure that separate the two vertical regions (isobaric and sigma) and *eta levels* are the sigma values (σ) defining the hybrid vertical coordinate.

The pre-processing to generate the model grid uses these values to define two vertical regions:

- terrain-following sigma layers near the ground (sigma realm)
- a relaxation with increasing altitude from terrain following to isobaric (isobaric realm), thus, purely isobaric layers from *ptsgm* value to the model top are defined (see Figure 2.2).

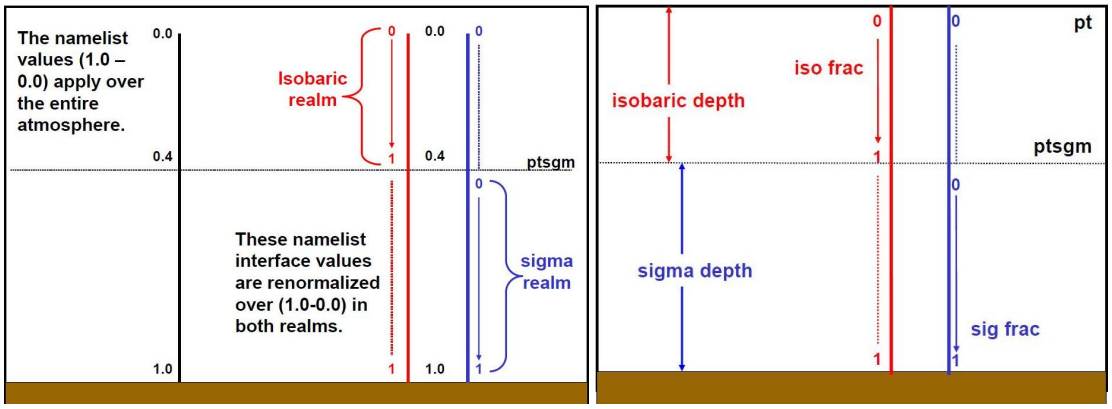

Figure 2.2: Hybrid vertical coordinate distribution (Janjic, 2007)

Then the pressure is defined as, p, where:

$$p = (isobaric\ depth) * (iso\ frac) + (sigma\ depth) * (sig\ frac) + pt \tag{2.11}$$

With the hybrid coordinate, the coordinate surfaces are flat above and away from the mountains (see Figure 2.3).

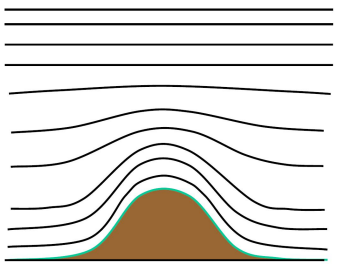

Figure 2.3: Example of hybrid vertical coordinate distribution applied in a mountain from Janjic (2007)

2.2 Gas-phase chemistry module

A gas-phase module is implemented within NMMB/BSC-CTM to properly simulate the tropospheric gas-phase chemistry of the NO_x-VOCs-SO_x. Different chemistry processes are implemented in the model, which uses a modular approach to solve the advection, diffusion, chemistry reactions, dry and wet deposition, and emission processes.

The Carbon Bond 2005 (CB05) (Yarwood et al., 2005) chemical mechanism is implemented. The chemical solver used to solve the chemical reactions is the Euler Backward Iterative (EBI) solver (Hertel et al., 1993) and the chemical time step employed is typically four times the fundamental dynamical timestep. The photolysis scheme is based on the Fast-J scheme (Wild et al., 2000) , which has been coupled with the physics of each model layer (e.g., clouds, absorbers as ozone), and it considers grid-scale clouds from the atmospheric driver. The Fast-J scheme has been updated with CB05 photolytic reactions. The Wesely scheme (Wesely, 1989) is implemented using a resistance analogy to compute the dry deposition velocities of CB05 gases. The cloud chemistry scheme of Foley et al. (2010) has been implemented to model the wet deposition. The processes included are: grid-scale scavenging and wet deposition, subgrid-scale vertical mixing, scavenging, and wet deposition for precipitating and non-precipitating clouds. Only incloud scavenging is considered in the current implementation. The transport of gases follows the same numerical schemes of NMMB for passive species. Advection is Eulerian, positive definite and monotonic (Janjic and Gall, 2012). It is important to note that the inter-phase chemistry is not considered in the present version of the model and important sinks of reactive gases may be underestimated. The following sections describe in more detail the different schemes implemented in the gas-phase chemistry module.

2.2.1 Chemical Mechanism

The photochemical mechanism is the main component of an AQM. Species considered in a photochemical gas-phase mechanism are classified into two groups: **inorganic** compounds, such as NO_x, O_x, HO_x and SO_x; and **organic** compounds, essentially volatile organic compounds (VOCs). There are two types of atmospheric reactions included in photochemical mechanisms: (1) thermal reactions in which the collision of molecules or the vibrations of molecules causes a reaction (e.g., thermal decomposition of PAN) or, (2) photochemical reactions in which the absorption of a photon provides energy for reaction (e.g., photodissociation of O_3 or NO_2).

A fully explicit chemical mechanism for representing gas-phase atmospheric chemistry would include around 20,000 reactions and thousands of species (Atkinson, 2000). Due to computational limitations, this would mean too many reactions and species to incorporate into a three-dimensional photochemical model.

For the present study, the CB05 (Yarwood et al., 2005) is used. It is an updated version of the Carbon-Bond IV (CB04) Gery et al. (1988). CB05 was developed in 2005 for use in US Environmental Protection Agency (EPA) atmospheric modelling studies. Yarwood et al. (2005) described CB05 as a condensed mechanism of atmospheric oxidant chemistry that provides a ba-

sis for computer modelling studies of ozone, particulate matter (PM), visibility, acid deposition and air toxic issues. CB05 core mechanism has 51 chemical species and solves 156 reactions. It extends inorganic reactions from urban to remote tropospheric conditions. The rate constants are updated based on evaluations of Atkinson et al. (2004) and Sander et al. (2006). A full list of all gas-phase species and reactions are provided in Table 2.2 and Table 2.3 , respectively.

Table 2.2: The chemical trace species of the CB05 chemical mechanism implemented in the gas-phase tropospheric chemistry of NMMB/BSC-CTM.

Species	Description	Species	Description
NO	Nitric oxide	SO_2	Sulfur dioxide
NO_2	Nitrogen dioxide	MEO_2	Methylperoxy radical
O_3	Ozone	MEOH	Methanol
O	Oxygen atom in the $O^3(P)$ electronic state	MEPX	Methylhydroperoxide
O^1D	Oxygen atom in the $O^1(D)$ electronic state	FACD	Formic acid
OH	Hydroxyl radical	ETHA	Ethane
HO_2	Hydroperoxy radical	ROOH	Higher organic peroxide
H_2O_2	Hydrogen peroxide	AACD	Acetic and higher carboxylic acids
NO_3	Nitrate radical	PACD	Peroxyacetic and higher peroxycarboxylic acids
N_2O_5	Dinitrogen pentoxide	PAR	Paraffin carbon bond (C-C)
HONO	Nitrous acid	ROR	Secondary alkoxy radical
HNO_3	Nitric acid	ETH	Ethene
PNA	Peroxynitric acid (HNO_4)	OLE	Terminal olefin carbon bond (R-C=C)
CO	Carbon monoxide	IOLE	Internal olefin carbon bond (R-C=C-R)
FORM	Formaldehyde	ISOP	Isoprene
ALD2	Acetaldehyde	ISPD	Isoprene product (lumped methacrolein, methyl vinyl ketone, etc.)
C_2O_3	Acetylperoxy radical		
PAN	Peroxyacetyl nitrate	TERP	Terpene
ALDX	Propionaldehyde and higher aldehydes	TOL	Toluene and other monoalkyl aromatics
CXO_3	C3 and higher acylperoxy radicals	XYL	Xylene and other polyalkyl aromatics
PANX	C3 and higher peroxyacyl nitrates	CRES	Cresol and higher molecular weight phenols
XO_2	NO to NO_2 conversion from alkylperoxy (RO_2) radical	TO_2	Toluene-hydroxyl radical adduct
XO_2N	NO to organic nitrate conversion from alkylperoxy (RO_2) radical	OPEN	Aromatic ring opening product
NTR	Organic nitrate (RNO_3)	CRO	Methylphenoxy radical
ETOH	Ethanol	MGLY	Methylglyoxal and other aromatic products
SULF	Sulfuric acid (gaseous)		

Table 2.3: The gas-phase CB05 chemical mechanism reactions applied in the NMMB/BSC-CTM.

Reactants		**Products**	**Rate expression**
$O + O_2 + M$	$\rightarrow$	$O_3 + M$	$6.0E\text{-}34*(300/T)^{2.4}$
$O_3 + NO$	$\rightarrow$	NO_2	$3.0E\text{-}12*\exp(T/1500)$
$O + NO_2$	$\rightarrow$	NO	$5.6E\text{-}12*\exp(180/T)$
$O + NO_2$	$\rightarrow$	NO_3	$K_0= 2.5E\text{-}31*\exp(300/T)^{1.8}$ $K_\infty=2.2E\text{-}11*\exp(300/T)^{0.7}$
$O + NO$	$\rightarrow$	NO_2	$K_0=9.0E\text{-}32*\exp(300/T)^{1.5}$ $K_\infty=3.0E\text{-}11$
$NO_2 + O_3$	$\rightarrow$	NO_3	$1.2E\text{-}13*\exp(T/2450)$
$O(^1)D + M$	$\rightarrow$	$O + M$	$2.1E\text{-}11*\exp(102/T)$
$O(^1)D + H_2O$	$\rightarrow$	$2.000*OH$	$2.2E\text{-}10$
$O_3 + OH$	$\rightarrow$	HO_2	$1.7E\text{-}12*\exp(T/940)$
$O_3 + HO_2$	$\rightarrow$	OH	$1.0E\text{-}14*\exp(T/490)$
$NO_3 + NO$	$\rightarrow$	$2.000*NO_2$	$1.5E\text{-}11*\exp(170/T)$
$NO_3 + NO_2$	$\rightarrow$	$NO + NO_2$	$4.5E\text{-}14*\exp(T/1260)$
$NO_3 + NO_2$	$\rightarrow$	$N2O_5$	$K_0= 2.0E\text{-}30 *(300/T)^{4.4}$ $K_\infty= 1.4E\text{-}12*(300/T)^{0.7}$
$N_2O_5 + H_2O$	$\rightarrow$	$2.000*HNO_3$	$2.5E\text{-}22$
$N_2O_5 + H_2O + H_2O$	$\rightarrow$	$2.000*HNO_3$	$1.8E\text{-}39$
N_2O_5	$\rightarrow$	$NO_3 + NO_2$	$K_0= 1.0E\text{-}03*\exp(11000/T)^{3.5}$ $K_\infty= 9.7E+14*\exp(T/11080)^{0.1}$ $F_c= 0.45$ $n= 1.0$
$NO + NO + O_2$	$\rightarrow$	$2.000*NO_2$	$3.3E\text{-}39*\exp(530/T)$
$NO + NO_2 + H_2O$	$\rightarrow$	$2.000*HONO$	$5.0E\text{-}40$
$NO + OH$	$\rightarrow$	$HONO$	$7.0E\text{-}31*\exp(300/T)^{2.6}$ $3.6E\text{-}11*\exp(300/T)^{-0.1}$
$OH + HONO$	$\rightarrow$	NO_2	$1.8E\text{-}11*\exp(T/390)$
$HONO + HONO$	$\rightarrow$	$NO + NO_2$	$1.0E\text{-}20$
$NO_2 + OH$	$\rightarrow$	HNO_3	$K_0=2.0E\text{-}30*\exp(300/T)^{3.0}$ $K_\infty=2.5E\text{-}11$
$OH+ HNO_3$	$\rightarrow$	NO_3	$K_0=2.4E\text{-}14*\exp(460/T)$ $K_2= 2.7E\text{-}17*\exp(2199/T)$ $K_3= 6.5E\text{-}34*\exp(1335/T)$
$HO_2 + NO$	$\rightarrow$	$OH + NO_2$	$K_0=3.5E\text{-}12*\exp(250/T)$

Table 2.3 Continued from previous page

Reactants		Products	Rate expression
HO_2 + NO_2	→	PNA	K_0=1.8E-31*exp(300/T)$^{3.2}$ K_∞=4.7E-12 F_c=0.6
PNA	→	HO_2+NO_2	K_0=4.1E-5*exp(T/10650) K_∞=4.8E15*exp(T/11170) F_c=0.6
OH + PNA	→	NO_2	1.3E-12*exp(380/T)
HO_2 + HO_2	→	H_2O_2	K_1=2.3E-13*exp(600/T) K_2=1.7E-33*exp(1000/T)
HO_2+HO_2+H_2O	→	H_2O_2	K_1=3.22E-34*exp(2800/T) K_2=2.38E-54*exp(3200/T)
OH + H_2O_2	→	HO_2	2.9E-12*exp(T/160)
O^1D + H_2	→	OH + HO_2	1.1E-10
OH + H_2	→	HO_2	5.5E-12*exp(T/2000)
OH + O	→	HO_2	2.2E-11*exp(120/T)
OH + OH	→	O	4.2E-12*exp(T/240)
OH + OH	→	H_2O_2	K_0=6.9E-31*exp(300/T)$^{1.0}$ K_∞=2.6E-11
OH + HO_2	→		4.8E-11*exp(250/T)
HO_2 + O	→	OH	3.0E-11*exp(200/T)
H_2O_2 + O	→	OH + HO_2	1.4E-12*exp(-2000/T)
NO_3 + O	→	NO_2	1.0E-11
NO_3 + OH	→	HO_2+ NO_2	2.2E-11
NO_3 + HO_2	→	HNO_3	3.5E-12
NO_3 + O_3	→	NO_2	1.0E-17
NO_3 + NO_3	→	2.000*NO_2	8.5E-13*exp(T/2450)
XO_2 + NO	→	NO_2	2.6E-12*exp(365/T)
XO_2N + NO	→	NTR	2.6E-12*exp(365/T)
XO_2 + HO_2	→	ROOH	7.5E-13*exp(700/T)
XO_2N + HO_2	→	ROOH	7.5E-13*exp(700/T)
XO_2 + XO_2	→		6.8E-14
XO_2N + XO_2N	→		6.8E-14
XO_2 + XO_2N	→		6.8E-14
NTR + OH	→	HNO_3+ HO_2 + 0.330*FORM+ 0.330*ALD2+ 0.330*ALDX- 0.660*PAR	5.9E-13*exp(360/T)
ROOH + OH	→	XO_2+ 0.500*ALD2 + 0.500*ALDX	3.01E-12*exp(190/T)

Table 2.3 Continued from previous page

Reactants		Products	Rate expression
OH + CO	→	HO_2	K_1= 1.44E-13 K_2=3.43E-33
OH + CH4	→	MEO_2	2.45E-12*exp(T/1775)
MEO_2 + NO	→	FORM + HO_2+ NO_2	2.8E-12*exp(300/T)
MEO_2 + HO_2	→	MEPX	4.1E-13*exp(750/T)
MEO_2 + MEO_2	→	1.370*FORM+ 0.740*HO_2+ 0.630*MEOH	9.5E-14*exp(390/T)
MEPX + OH	→	0.700*MEO_2+ 0.300*XO_2+ 0.300*HO_2	3.8E-12*exp(200/T)
MEOH + OH	→	FORM + HO_2	7.3E-12*exp(T/620)
FORM + OH	→	HO_2 + CO	9.0E-12
FORM + O	→	OH + HO_2 + CO	3.4E-11*exp(T/1600)
FORM + NO_3	→	HNO_3+HO_2+ CO	5.8E-16
FORM + HO_2	→	HCO_3	9.7E-15*exp(625/T)
HCO_3	→	FORM + HO_2	2.4E+12*exp(T/7000)
HCO_3 + NO	→	FACD+ NO_2 + HO_2	5.6E-12
HCO_3 + HO_2	→	MEPX	5.6E-15*exp(2300/T)
FACD + OH	→	HO_2	4.0E-13
ALD2 + O	→	C_2O_3 + OH	1.8E-11*exp(T/1100)
ALD2 + OH	→	C_2O_3	5.6E-12*exp(270/T)
ALD2 + NO_3	→	C_2O_3+ HNO_3	1.4E-12*exp(T/1900)
C_2O_3 + NO	→	MEO_2 + NO_2	8.1E-12*exp(270/T)
PAN	→	C_2O_3 + NO_2	K_0= 4.9E-3*exp(12100/T) K_∞= 5.4E16*exp(T/13830) F_c=0.3
C_2O_3 + HO_2	→	0.800*PACD+ 0.200*AACD+ 0.200*O_3	4.3E-13*exp(1040/T)
C_2O_3 + MEO_2	→	0.900*MEO_2+ 0.900*HO_2+ FORM+ 0.100*AACD	2.0E-12*exp(500/T)
C_2O_3 + XO_2	→	0.900*MEO_2+ 0.100*AACD	4.4E-13*exp(1070/T)
C_2O_3 + C_2O_3	→	2.000*MEO_2	2.9E-12*exp(500/T)
PACD + OH	→	C_2O_3	4.0E-13*exp(200/T)
AACD + OH	→	MEO_2	4.0E-13*exp(200/T)
ALDX + O	→	CXO_3 + OH	1.3E-11*exp(T/870)
ALDX + OH	→	CXO_3	5.1E-12*exp(405/T)
ALDX + NO_3	→	CXO_3 + HNO_3	6.5E-15
CXO_3 + NO	→	ALD2+ NO_2+ HO_2+XO_2	6.7E-12*exp(340/T)
CXO_3 + NO_2	→	PANX	K_0=2.7E-28*exp(300/T)$^{7.1}$ K_∞=1.2E-11*exp(300/T)$^{0.9}$

Table 2.3 Continued from previous page

Reactants		Products	Rate expression
			F_c=0.3
PANX	→	CXO_3 + NO_2	
PANX + OH	→	ALD2 + NO_2	3.0E-13
CXO_3 + HO_2	→	0.800*PACD+ 0.200*AACD+ 0.200*O_3	4.3E-13*exp(1040/T)
CXO_3 + MEO_2	→	0.900*ALD2+ 0.900*XO_2+ HO_2+ 0.100*AACD+ 0.100*FORM	2.0E-12*exp(500/T)
CXO_3 + XO_2	→	0.900*ALD2+ 0.100*AACD	4.4E-13*exp(1070/T)
CXO_3 + CXO_3	→	2.000*ALD2 + 2.000*XO_2+ 2.000*HO_2	2.9E-12*exp(500/T)
CXO_3 + C_2O_3	→	MEO_2+ XO_2+ HO_2+ ALD2	2.9E-12*exp(500/T)
PAR + OH	→	0.870*XO_2+ 0.130*XO_2N+ 0.110*HO_2+ 0.060*ALD2- 0.110*PAR+ 0.760*ROR+ 0.050*ALDX	8.1E-13
ROR	→	0.960*XO_2+ 0.600*ALD2+ 0.940*HO_2- 2.100*PAR+ 0.040*XO_2N+ 0.020*ROR+ 0.500*ALDX	1.E+15*exp(T/8000)
ROR	→	HO_2	1.6E+3
ROR + NO_2	→	NTR	1.5E-11
O + OLE	→	0.200*ALD2+ 0.300*ALDX+ 0.300*HO_2+ 0.200*XO_2+ 0.200*CO+ 0.200*FORM+ 0.010*XO_2N+ 0.200*PAR+ 0.100*OH	1.E-11*exp(T/280)
OH + OLE	→	0.800*FORM+ 0.330*ALD2+ 0.620*ALDX + 0.800*XO_2+ 0.950*HO_2- 0.700*PAR	3.2E-11
O_3 + OLE	→	0.180*ALD2+ 0.740*FORM+ 0.320*ALDX+ 0.220*XO_2+ 0.100*OH+ 0.330*CO+ 0.440*HO_2 - 1.000*PAR	6.5E-15*exp(T/1900)
NO_3 + OLE	→	NO_2+ FORM+ 0.910*XO_2+ 0.090*XO_2N+ 0.560*ALDX+ 0.350*ALD2- 1.000*PAR	7.0E-13*exp(T/2160)

Table 2.3 Continued from previous page

Reactants		Products	Rate expression
O + ETH	→	FORM+ 1.700*HO_2+ CO+ 0.700*XO_2+ 0.300*OH	1.04E-11*exp(T/792)
OH + ETH	→	XO_2+ 1.560*FORM+ 0.220*ALDX+ HO_2	K_0=1.0E-28*exp(300/T)$^{0.8}$ K_∞=8.8E-12
O_3 + ETH	→	FORM+ 0.630*CO+ 0.130*HO_2+ 0.130*OH+ 0.370*FACD	1.2E-14*exp(T/2630)
NO_3 + ETH	→	NO_2+ XO_2+ 2.0*FORM	3.3E-12*exp(T/2880)
IOLE + O	→	1.240*ALD2+ 0.660*ALDX+ 0.100*HO_2+ 0.100*XO_2+ 0.100*CO+ 0.100*PAR	2.3E-11
IOLE + OH	→	1.300*ALD2 + 0.700*ALDX + HO_2 + XO_2	1.0E-11*exp(550/T)
IOLE + O_3	→	0.650*ALD2 + 0.350*ALDX + 0.250*FORM + 0.250*CO + 0.500*O + 0.500*OH + 0.500*HO_2	8.4E-15*exp(T/1100)
IOLE + NO_3	→	1.180*ALD2 + 0.640*ALDX + HO_2 + NO_2	9.6E-13*exp(T/270)
TOL + OH	→	0.440*HO_2 + 0.080*XO_2 + 0.360*CRES + 0.560*TO_2 + 0.765*$TOLRO_2$	1.8E-12*exp(355/T)
TO_2 + NO	→	0.900*NO_2 + 0.900*HO_2 + 0.900*OPEN + 0.100*NTR	8.1E-12
TO_2	→	CRES + HO_2	4.2
OH + CRES	→	0.400*CRO + 0.600*XO_2 + 0.600*HO_2 + 0.300*OPEN	4.1E-11
CRES + NO_3	→	CRO + HNO_3	2.2E-11
CRO + NO_2	→	NTR	1.4E-11
CRO + HO_2	→	CRES	5.5E-12
OPEN + OH	→	XO_2 + 2.000*CO + 2.000*HO_2 + C_2O_3 + FORM	3.0E-11
OPEN + O_3	→	0.030*ALDX + 0.620*C_2O_3 + 0.700*FORM + 0.030*XO_2 + 0.690*CO + 0.080*OH + 0.760*HO_2 + 0.200*MGLY	5.4E-17*exp(T/500)

Table 2.3 Continued from previous page

Reactants		Products	Rate expression
OH + XYL	→	0.700*HO_2 + 0.500*XO_2 + 0.200*CRES + 0.800*MGLY + 1.100*PAR + 0.300*TO_2 + 0.804*$XYLRO_2$	1.7E-11*exp(116/T)
OH + MGLY	→	XO_2 + C_2O_3	1.8E-11
O + ISOP	→	0.750*ISPD + 0.500*FORM + 0.250*XO_2 + 0.250*HO_2 + 0.250*CXO_3 + 0.250*PAR	3.6E-11
OH + ISOP	→	0.912*ISPD + 0.629*FORM + 0.991*XO_2 + 0.912*HO_2 + 0.088*XO_2N + ISOPRXN	2.54E-11*exp(407.6/T)
O_3 + ISOP	→	0.650*ISPD + 0.600*FORM + 0.200*XO_2 + 0.066*HO_2 + 0.266*OH + 0.200*CXO_3 + 0.150*ALDX + 0.350*PAR + 0.066*CO	7.86E-15*exp(T/1912)
NO_3 + ISOP	→	0.200*ISPD + 0.800*NTR + XO_2 + 0.800*HO_2 + 0.200*NO_2 + 0.800*ALDX + 2.400*PAR	3.03E-12*exp(T/448)
OH + ISPD	→	1.565*PAR + 0.167*FORM + 0.713*XO_2 + 0.503*HO_2 + 0.334*CO + 0.168*MGLY + 0.252*ALD2 + 0.210*C_2O_3 + 0.250*CXO_3 + 0.120*ALDX	3.36E-11
O_3 + ISPD	→	0.114*C_2O_3 + 0.150*FORM + 0.850*MGLY + 0.154*HO_2 + 0.268*OH + 0.064*XO_2 + 0.020*ALD2 + 0.360*PAR + 0.225*CO	7.1E-18
NO_3 + ISPD	→	0.357*ALDX + 0.282*FORM + 1.282*PAR + 0.925*HO_2 + 0.643*CO + 0.850*NTR + 0.075*CXO_3 + 0.075*XO_2 + 0.150*HNO_3	1.0E-15
TERP + O	→	0.150*ALDX + 5.12*PAR + TRPRXN	3.6E-11
TERP + OH	→	0.750*HO_2 + 1.250*XO_2 + 0.250*XO_2N + 0.280*FORM + 1.66* PAR + 0.470*ALDX + TRPRXN	1.5E-11*exp(449/T)

Table 2.3 Continued from previous page

Reactants		Products	Rate expression
TERP + O_3	$\rightarrow$	0.570*OH + 0.070*HO_2 + 0.760*XO_2 + 0.180*XO_2N + 0.240*FORM + 0.001*CO + 7.000*PAR + 0.210*ALDX + 0.390*CXO_3 + TRPRXN	1.2E-15*exp(T/821)
TERP + NO_3	$\rightarrow$	0.470*NO_2 + 0.280*HO_2 + 1.030*XO_2 + 0.250*XO_2N + 0.470*ALDX + 0.530*NTR + TRPRXN	3.7E-12*exp(175/T)
SO_2 + OH	$\rightarrow$	SULF + HO_2 + SULRXN	K_0= 3.0E-31*exp(300/T)$^{3.3}$ K_∞= 1.5E-12
OH + ETOH	$\rightarrow$	HO_2 + 0.900*ALD2 + 0.050*ALDX + 0.100*FORM + 0.100*XO_2	6.9E-12*exp(T/230)
OH + ETHA	$\rightarrow$	0.991*ALD2 + 0.991*XO_2 + 0.009*XO_2N + HO_2	8.7E-12*exp(T/1070)
NO_2 + ISOP	$\rightarrow$	0.200*ISPD + 0.800*NTR + XO_2 + 0.800*HO_2 + 0.200*NO + 0.800*ALDX + 2.400*PAR	1.5E-19

Numerical Method to solve chemical reactions

Computation of a full transport-chemistry system involves a huge number of stiff Ordinary Differential Equation (ODE) integrations. For their numerical solution, commonly the operator splitting approach is followed. A major computational task is, then, the numerical integration of the stiff ODE system describing the chemical transformations. The main idea of stiffness is that the equation includes some terms that can lead to rapid variation in the solution.

ODEs are differential equations with one independent variable, such as time. We consider solving the Initial Value Problem (IVP) of first order ODEs

$$\frac{du(t)}{dt} = f(t, \mathbf{u}(t)), \qquad given \;\; u(0) = u_0 \tag{2.12}$$

for $\mathbf{u}(t) \in \Re^N$, $0 \leq t \leq T$.

An example of stiff ODE systems describing the kinetics of a chemical system, called *Production-Loss ODE*, can be written as:

$$\frac{dc(t)}{dt} = f(t, c(t)) = P(t, c(t)) - L(t, c(t))c(t) \tag{2.13}$$

or for every concentration of the ith chemical as:

$$\frac{dc_i(t)}{dt} = P_i(t, c(t)) - L_i(t, c(t))c_i(t) \tag{2.14}$$

where c(t)= $(c_1(t), ..., c_m(t))^T$ is the concentration vector and each c_i corresponds to the concentration of the ith chemical compound, m is the number of compounds, and P and L (diagonal matrix) are the chemical production and loss terms, respectively. Note that both P_i and L_i are in general functions of other concentrations, and, consequently, equations 2.13 and 2.14 constitute a system of coupled ODEs.

The aim of the numerical method is to approximate solutions of the ODE systems by numerically solving the IVP (equation 2.12) using discretization of the interval into mesh points. This gives approximations:

$$u^n \approx u(t^n) \quad n = 1, 2, ..., N$$

with step size

$$\Delta t = t^{n+1} - t^n$$

Sometimes it is taken a constant step size to make easier the calculations so that: $t^n = n\Delta t$, $t^0 = 0$, $t^1 = N\Delta t = T$.

The EBI is used for solving the chemical equations. The corresponding scheme is the following:

$$u^{n+1} = u^n + \Delta t f(t^{n+1}, u^{n+1}), \qquad n = 0, 1, 2, ... \tag{2.15}$$

As a result, if the EBI is applied to production-loss ODEs (see equation 2.14) the approximation scheme is written as:

$$c_i^{n+1} = c_i^n + \Delta t(P_i^{n+1} - L_i c_i^{n+1}) \tag{2.16}$$

The EBI is widely used in the CTM and due to the linear nature of equation 2.15, the chemical mass balance is preserved exactly.

2.2.2 Photolysis Scheme

The chemistry of the atmosphere is strongly driven by sunlight by dissociating certain key molecules into fragments which are frequently highly reactive. The splitting or decomposition of a chemical compound by means of light energy or photons is called photolysis (or photodissociation). Photolysis reactions are of major importance to the atmospheric chemistry determining tropospheric composition. Photolysis is responsible for the majority of the smog buildup detrimental to humans, animals, plant life and materials. In order to accurately predict and model the effects of air pollution, accurate $J - values$ must be estimated. Hence, in CTMs is essential the simulation of the enhanced photochemical rates above and in the upper levels of clouds as well as the reduced rates below optically thick clouds and absorbing aerosols (Logan et al., 1981).

Table 2.4: Photolysis reactions applied in the NMMB/BSC-CTM

Reactants		**Products**	**Cross section reference**
NO_2 +hv	$\rightarrow$	NO + O	Carter (January, 2000)
O_3 +hv	$\rightarrow$	O	Atkinson et al. (2004)
O_3 +hv	$\rightarrow$	O^1D	Atkinson et al. (2004)
NO_3 +hv	$\rightarrow$	NO_2 + O	Carter (January, 2000)
NO_3 +hv	$\rightarrow$	NO	Carter (January, 2000)
HONO +hv	$\rightarrow$	NO + OH	Atkinson et al. (2004)
H_2O_2 +hv	$\rightarrow$	2.000*OH	Carter (January, 2000)
PNA +hv	$\rightarrow$	0.610*HO_2 + 0.610*NO_2 + 0.390*OH+ 0.390*NO_3	Atkinson et al. (2004)
HNO_3 +hv	$\rightarrow$	OH + NO_2	Atkinson et al. (2004)
N2O5 +hv	$\rightarrow$	NO_2+ NO_3	Atkinson et al. (2004)
NTR +hv	$\rightarrow$	NO_2+ HO_2+ 0.330*FORM+ 0.330*ALD2+ 0.330*ALDX- 0.660*PAR	(Atkinson et al., 2004)
FORM +hv	$\rightarrow$	2.000*HO_2 + CO	Carter (January, 2000)
FORM +hv	$\rightarrow$	CO	Carter (January, 2000)
ALD2 +hv	$\rightarrow$	MEO_2 + CO + HO_2	Barnard et al. (2004)
PAN +hv	$\rightarrow$	C_2O_3 + NO_2	Atkinson et al. (2004)
PANX +hv	$\rightarrow$	CXO_3 + NO_2	Atkinson et al. (2004)
PACD +hv	$\rightarrow$	MEO_2 + OH	Yarwood et al. (2005)
ALDX +hv	$\rightarrow$	MEO_2 + CO+ HO_2	Carter (January, 2000)

The light available to a molecule in air for absorption and photodissociation including direct, scattered and reflected radiation coming from all directions is called actinic flux (Finlayson-Pitts and Pitts, 2000). The calculation of the actinic flux, which is the quantity needed for $J-values$ calculations, begins with the solar radiation incident at the top of the atmosphere and must take into account absorption and scattering of the light in the atmosphere (by gas molecules, cloud droplets and aerosols particles) and at the ground surface. As a result, clouds and aerosols can both modify, reducing and enhancing, the actinic flux depending on their optical properties, solar zenith angle, and the position of the layer of interest relative to the observation point.

The rate of photodissociation of a molecule, A, upon light absorption,

$$A + hv \rightarrow B + C \tag{2.17}$$

can be described as a first-order process with a rate constant, J, called photolysis rate constant or $J-values$:

$$\frac{d[A]}{dt} = -J[A] \tag{2.18}$$

An expression for photolysis rate constant J, measured in s^{-1}, is

$$J = \int_{\lambda} \overbrace{\vartheta(\lambda)}^{\mathbf{c}} \overbrace{\Sigma(\lambda)}^{\mathbf{b}} \overbrace{F(\lambda)d\lambda}^{\mathbf{a}} \tag{2.19}$$

where J depends on three terms:

1. intensity of available light that the molecule can absorb, called actinic flux F (**a**).

2. the intrinsic strength of light absorption in that region by A, called absorption cross section Σ (**b**).

3. the quantum yield for photodissociation, ϑ (**c**).

As in the majority of photolysis schemes, the solar spectrum is divided up into a number of wavelength bins, then, the actinic flux is calculated for each bin, and, finally, the contribution to the total photolysis rate is summed, given the mean absorption cross-section for each species over each bin (see equation (2.20)). Thus equation (2.19) becomes:

$$J_i = \sum_{\lambda}^{\lambda_i} \vartheta_{av}(\lambda)\Sigma_{av}(\lambda)F_{av}(\lambda) \tag{2.20}$$

where λ is the wavelength, ϑ_{av} is the primary quantum yield for the photolysis of the molecules averaged over the wavelength interval $\Delta\lambda$, centered at λ, Σ_{av} is the absorption cross section, base e, averaged over the wavelength interval $\Delta\lambda$, centered at λ, and F_{av} is the actinic flux in photons summed over the wavelength interval $\Delta\lambda$, centered at λ. Actinic flux, $F(\lambda)$, is given by:

$$F(\lambda) = \int_{\phi}\int_{\theta} I(\lambda,\theta,\phi)sin(\theta)d\theta d\phi \tag{2.21}$$

where I is the radiance or intensity, and θ and ϕ represents zenith and azimuth angles, respectively. The radiance is defined as the intensity of the incoming light at angle θ (see Figure 2.4). Hence, actinic flux depends on many factors, such as geographical location, time, season, presence or absence of clouds, and the total amount of O_3 and particles in the air which scatter light as it passes through the atmosphere.

Following Chandrasekhar (1960) the basic equation of radiative transfer for a scattering atmosphere with an incoming solar beam is defined as

$$\mu\frac{dI(\tau,\mu,\phi)}{d\tau} = I(\tau,\mu,\phi) - \frac{\overline{\omega}(\tau)}{4\pi}\int_{-1}^{+1} d\mu' \int_{0}^{2\pi} d\phi' p(\tau,\mu,\phi,\mu',\phi') - \frac{\overline{\omega}(\tau)}{4} p(\tau,\mu,\phi,-\mu_0,\phi_0)Se^{-\tau/\phi_0} \tag{2.22}$$

where ϕ and ϕ_0 are, respectively the azimuth angle and the solar azimuth angle, μ and μ_0 are, respectively, the cosine of zenith angle and the cosine of solar zenith angle and $\overline{\omega}$ is the single scattering albedo at optical depth level τ, and S is the solar flux.

Table 2.4 shows the photolysis reactions considered. To compute the photolysis rates, we have implemented the Fast-J (Wild et al., 2000) online photolysis scheme. Fast-J has been coupled with the physics of each model layer (e.g., clouds, absorbers as ozone). The optical depths of grid-scale clouds from the atmospheric driver are considered by using the fractional cloudiness based on relative humidity (Fast et al., 2006). The main advantages of Fast-J are the optimization of the phase function (equation 2.22) expansion into Legendre polynomials and the optimization of the integration over wavelength (Wild et al., 2000). The Fast-J scheme has been upgraded

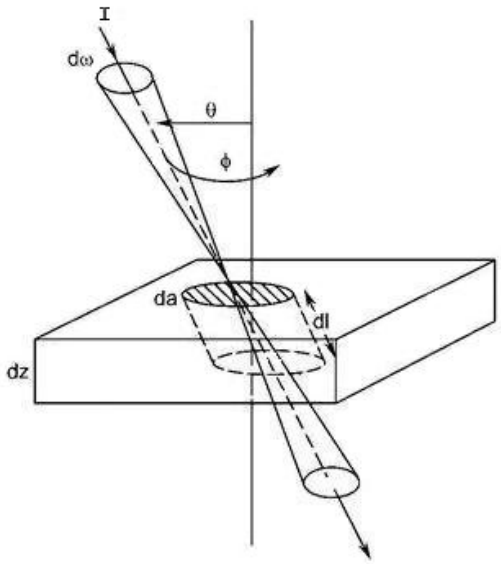

Figure 2.4: Typical light ray striking a thin layer of air in the atmosphere (from Finlayson-Pitts and Pitts (2000))

with the CB05 photolytic reactions. The quantum yields and cross section for the CB05 photolysis reactions have been revised and updated following the recommendations of Atkinson et al. (2004), Sander et al. (2006) and Barnard et al. (2004). The Fast-J scheme uses 7 different wavelength bins appropriate for the troposphere to calculates the actinic flux covering from 289 to 850 nm (see Table VIII from (Wild et al., 2000)). Figure 2.5 displays the photolysis rates for the NO_2 (top panel) and PAN (bottom panel) used in this model at the surface (left panel) and the Top Of the Atmosphere (TOA) (right panel) for the first of July 2004 at 12 UTC.

2.2.3 Dry deposition

In general terms, dry deposition is defined as the transport of particulate and gaseous pollutants from the atmosphere onto surfaces in the absence of precipitation. Dry deposition of gases and particles is a basic process that removes air pollutants from the atmosphere. As a consequence of this process, the deposition of pollutants onto the ground can damage the ecosystem.
Usually, the parameter used to model the deposition rate is the deposition velocity v_d whose product with the concentration at a specified height (z) results in the mass flux density as:

$$v_d = -\frac{F_c}{c_z} \tag{2.23}$$

where F_c is the flux density and c_{qz} is the concentration at height z.

Approximation of deposition velocities (v_d) represents the main output of the dry deposition

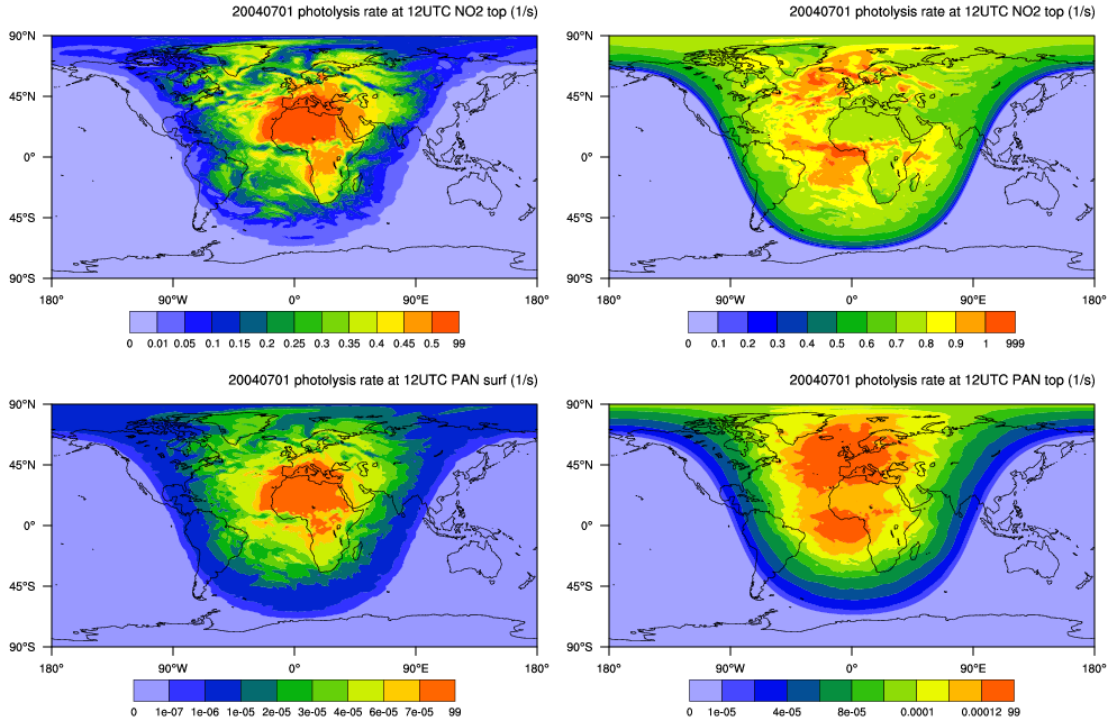

Figure 2.5: Photolysis rate used in the NMMB/BSC-CTM for the NO_2 (top panel) and PAN (bottom panel) for the first of July 2004 (12 UTC) at the surface (left panel) and the TOA (right panel).

models which, for gases, is computed from a formula comparable to Ohm's law in electrical circuits (Wesely, 1989).

An online implementation is used to characterize the dry-deposition of several atmospheric species based on the Wesely (1989) scheme. Wesely (1989) developed a methodology for the parametrizations of surface resistances to gaseous dry deposition in regional-scale modelling over a variety of species, land-use types and season, thus, replacing the previous systems which presented simple look-up tables or bulk surface resistances.

The magnitude of v_d is the following:

$$|v_d| = (r_a + r_b + r_c)^{-1} \tag{2.24}$$

Equation above is composed by three resistances: r_a is the *aerodynamic resistance* (the same to all species), r_b is the *quasilaminar sublayer resistance* (depends on the landuse specific friction velocity and molecular characteristics of gases), and r_c is the *canopy (surface) resistance* (depends on surface properties such as moisture level, pH of the surface solubility and reactivity of the gas) (Baldocchi et al., 1987; Wesely, 1989; Wesely and Hicks, 1997; Garland, 1977).

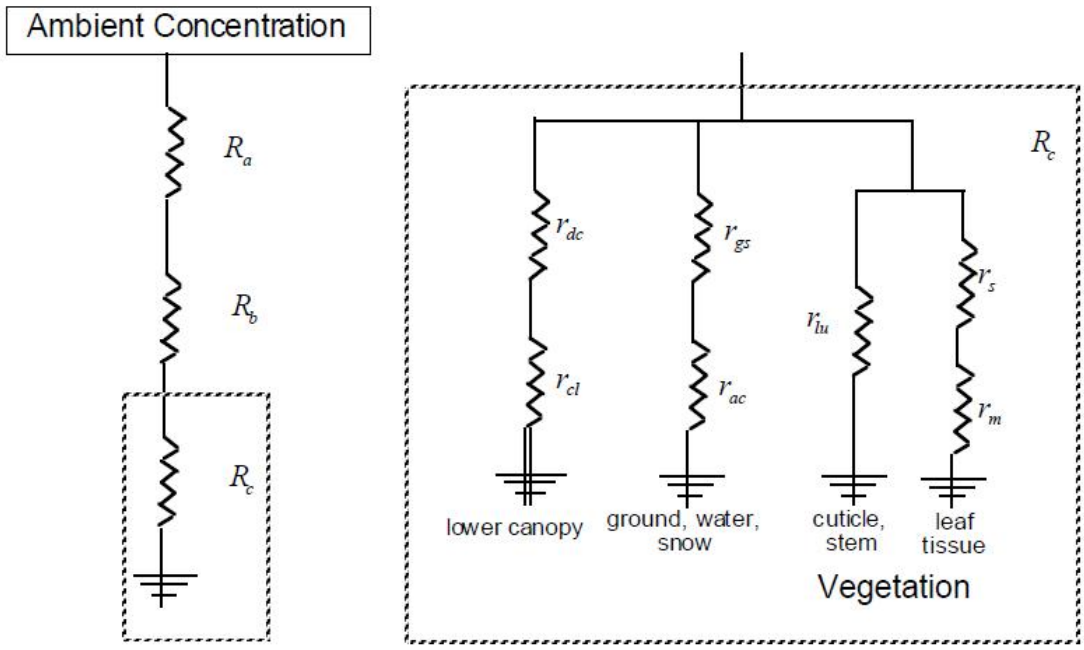

Figure 2.6: Scheme of pathway resistances used in Equation 2.25 (from Byun et al. (1990)).

Generally, the canopy resistance r_c is the most difficult of the three flux resistances to evaluate theoretically. Under ideal conditions, r_c could be related to the surface conditions, time of the day and season.

Wesely (1989) assumed that r_a and r_b were evaluated using existing techniques and suggested a method to estimate r_c for the five seasonal categories and 11 landuse types employed with the module. Analogously to Ohm's law in electrical circuits, r_c is divided into various resistances:

$$r_c = \left[\frac{1}{r_s + r_m} + \frac{1}{r_{lu}} + \frac{1}{r_{dc} + r_{cl}} + \frac{1}{r_{ac} + r_{gs}} \right]^{-1} \tag{2.25}$$

where

r_s= leaf stomata resistance;
r_m= mesophyll resistance;
r_{lu}= resistance of outer surface of leaves in the upper canopy ;
r_{dc}= resistance of gas-phase transfer affected by buoyant convection in canopy ;
r_{cl}= lower canopy resistance (uptake pathways at the leaves, twigs, bark, etc.);
r_{ac}= transfer resistance for processes that depend only on canopy height and density; and
r_{gs}= a resistance of soil, leaf litter, and other ground material.

These resistances are illustrated in Figure 2.6. The tabulated values of seven components of baseline resistances :

$$(r_j, r_{lu}, r_{ac}, r_{gsS}, r_{gsO}, r_{clS}, r_{clO})$$

for five categories of seasons and for eleven land-use types are listed in Table 1 of the Wesely (1989) work. On these tables both SO_2 and O_3 (respectively subscripts S and O of the tabulated values) are taken as base species, meaning that estimated resistance of other gases are calculated by scaling according to several chemical properties, such as measures of aqueous solubility and oxidizing capacity of SO_2 and O_3.

Figure 2.7 shows the ozone dry mean velocity for the first day of July 2004.

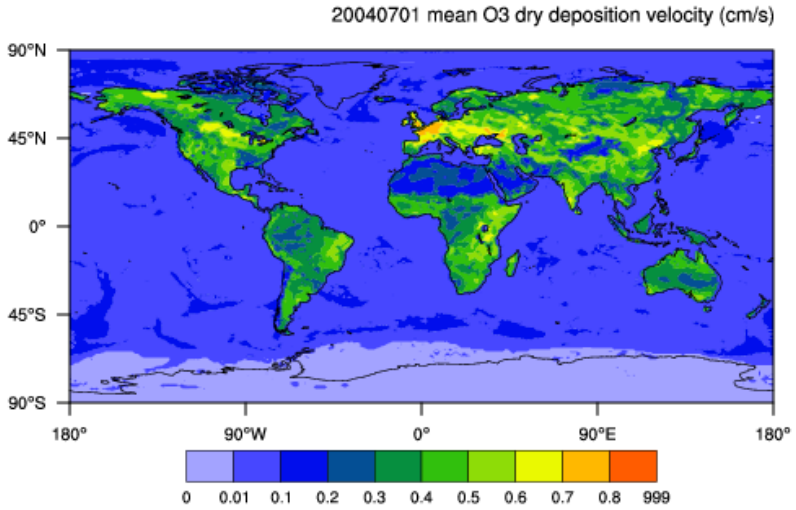

Figure 2.7: Ozone dry mean velocity (cm/s) for the first of July 2004.

2.2.4 Wet deposition

Clouds play an important role in the boundary layer meteorology and air quality. Gases and aerosol particles can go inside cloud droplets through absorption/condensation (of soluble gases) and activation and impact scavenging (of aerosol particles) (Flossmann et al., 1985; Pruppacher and Klett, 1997). Once inside the cloud or rain water, some compounds can dissociate into ions and/or react through aqueous chemistry (Seinfeld and Pandis, 1998). Cloud chemistry contributes to the chemical processing of NO_x, SO_2, and NH_3 and ultimately to wet deposition of N and S onto the ground. Hence, wet deposition removes several air pollutants from the atmosphere but at the same time the deposition of air pollutants onto the ground may lead to ecosystem damage (e.g. acidification). Clouds and fog droplets also affect gas-phase species concentrations by attenuating solar radiation below the cloud base which has a significant impact on the photolysis reactions, or by scavenging species from the gas-phase and mediating the formation of secondary products in the heterogeneous reactions (Jacob, 2000).

Pollutant concentrations are affected by several processes (vertical-convective mixing, scavenging, aqueous chemistry, and removal by wet deposition) occurring in clouds. The overall wet flux of the species is the sum of the transfer of the species from clouds to rain plus the transfer effect due below-cloud scavenging. Cloud's processes are summarised on Figure 2.8.

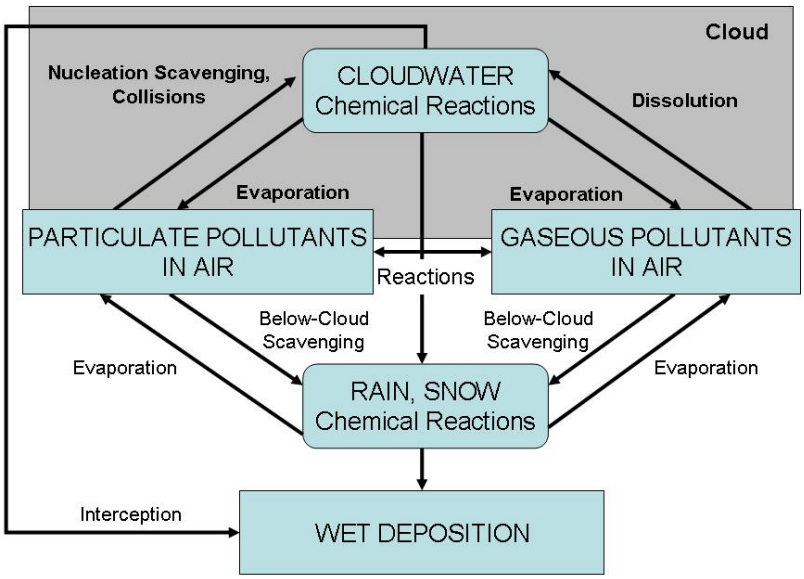

Figure 2.8: Conceptial framework of cloud chemistry processes

The cloud chemistry scheme of Byun and Ching (1999) and Foley et al. (2010) has been implemented within NMMB/BSC-CTM in order to resolve the cloud processes affecting the concentration of air pollutants. The wet deposition of 36 gases from the CB05 chemical mechanism are considered here. The processes included are grid-scale scavenging and wet deposition, subgrid-scale vertical mixing, scavenging and wet deposition for precipitating and non-precipitating clouds. Only incloud scavenging is considered in the current implementation. The incloud scavenging process is computed using the Henry's Law equilibrium equation. The rate of change for incloud pollutant concentration is given by:

$$\frac{\partial C_{icld}}{\partial t} = C_{icld}\frac{e^{-a_i\tau_{cld}}-1}{\tau_{cld}} \tag{2.26}$$

$$\alpha_i = \frac{1}{\tau_{washout}(1+\frac{TWF}{H_i})}, \tag{2.27}$$

where C_{icld} is the gas concentration within the cloud [ppm], τ_{cld} is the cloud timescale [s], α_i is the scavenging coefficient for the gas specie, H_i is the Henry's Law coefficient for the gas

specie [M/atm], total water fraction (TWF)=$\rho_{H_2O}/(W_T RT)$ is the total water fraction (where W_T is the total mean water content) [kg/m^3], R is the Universal gas constant, and T is the incloud air temperature [K]), and $\tau_{washout}$ is the washout time [s] representing the amount of time required to remove all of the water from the cloud volume at a specified precipitation rate [m/s]. The washout time is given by:

$$\tau_{washout} = \frac{W_T \triangle z_{cld}}{\rho_{H_2O} P_r} \tag{2.28}$$

where $\triangle z_{cld}$ is the cloud thickness [m] and P_r is the specified precipitation rate [m/s]. Both grid-scale and subgrid-scale scavenging are computed with equation 2.26, where τ_{cld} is 1 hour for subgrid-scale clouds, and the chemistry timestep for grid-scale clouds. Wet deposition is computed following the algorithm of Chang et al. (1987), which depends upon P_r and C_{icld}. Thus, the wet deposition is given by:

$$wdep_i = \int_0^{\tau_{cld}} C_{icld} P_r dt \tag{2.29}$$

The sub-grid cloud scheme implemented solves the convective mixing, scavenging and wet deposition of a representative cloud within the grid cell following the Community Multi-scale Air Quality Model (CMAQ) and Regional Acid Deposition Model (RADM)v2.6 models schemes (Byun and Ching, 1999; Chang et al., 1987). Precipitating and non-precipitating sub-grid clouds are considered. The latter are categorized as pure fair weather clouds and non-precipitating clouds and may coexists with precipitating clouds (Byun and Ching, 1999; Foley et al., 2010).

2.2.5 Tropospheric upper boundary condition

In applications focused on the troposphere, such as AQMs, the stratospheric chemistry may be solved in a simplified approach avoiding complex stratospheric chemistry schemes.

Mixing rations of several species (NO, NO_2, N_2O_5, HNO_3, and CO) are initialised each day from a climatology of a global chemical model Model for OZone And Related chemical Tracers (MOZART)-4/NCEP (Emmons et al., 2010). These mixing rations are implemented above 100hPa.

Ozone is an important reactive gas with complex chemistry in the stratosphere, therefore, needs a better representation there. Two different linear ozone stratospheric scheme, Cariolle v2a (Cariolle and Teyssèdre, 2007) and COPCAT (Monge-Sanz et al., 2011), are implemented in the current version of the model in handling stratospheric ozone as an upper boundary condition within the model NMMB/BSC-CTM. These two linear photochemical ozone models are also implemented above 100hPa.

Linear stratospheric schemes

Cariolle and Déqué (1986) where the first to include a linearized ozone stratospheric scheme,

namely Cariolle v1.0, in a three-dimensional CTM model. The change in ozone with time due to the local chemistry is given by:

$$C = \frac{d\chi}{dt} = (P-L)[\chi, T, \Phi] \tag{2.30}$$

where $(P-L)$ represents the ozone tendency, the square brackets denote a functional dependence on χ the ozone mixing ratio ($kgkg^{-1}$), the air temperature T(K), and Φ the column of ozone above the point under consideration ($kg\,m^{-2}$) where :

$$\Phi = 1/g \int_{TOA}^{l} \chi \, dp \tag{2.31}$$

The integral runs over all pressure levels from the top of the atmosphere (TOA) down to level l, where l is the level under consideration.

Equation (2.30) is expanded to the first order Taylor series

$$C = \frac{d\chi}{dt} = (P-L)_0 + \overbrace{\left.\frac{\partial(P-L)}{\partial\chi}\right|_0 (\chi-\chi_0)}^{\mathbf{a}} + \overbrace{\left.\frac{\partial(P-L)}{\partial T}\right|_0 (T-T_0)}^{\mathbf{b}} + \overbrace{\left.\frac{\partial(P-L)}{\partial\Phi}\right|_0 (\Phi-\Phi_0)}^{\mathbf{c}} \tag{2.32}$$

The second term in the expansion accounts for the variations in the local ozone amount (**a**), the third term for the temperature (**b**) and the last term, called radiation term, accounts for the influence of non-local ozone on the amount of solar radiation reaching the considered level(**c**). Specific terms in this equation are coefficients applicable at the equilibrium state (represented with the subscript 0) which can be either climatological values or have been pre-calculated with a complete photochemical model. In Cariolle v2a (Cariolle and Teyssèdre, 2007), these coefficients are obtained at equilibrium from the MOBIDIC 2-D photochemical model (Cariolle and Teyssèdre, 2007). These terms are presented as functions of latitude, model level and month.

Heterogeneous processes describing the polar stratospheric chemistry are non-linear and depend on the three-dimensional structure of the atmosphere. The original Cariolle v1.0 considered only gas-phase, hence, no heterogeneous chemistry was included. The reason was that the ozone hole chemistry was not well known when this scheme was first developed. Later, Cariolle v2a incorporates an additional ozone destruction term (-$K_{het}\chi$) on the equation 2.32 to compensate for that lack of heterogenous chemistry. This term describes an specific ozone destruction process when conditions for polar stratospheric cloud (PSC) formation are reached, consequently, it must be used only if temperature is less than 195 K and during daytime (for solar zenith angles lower than 87°) at high latitude (over 45° latitude).

The new approach COPCAT (Monge-Sanz et al., 2011), based on the Cariolle v1.0 linear approach, uses the TOMCAT/SLIMCAT full-chemistry CTM (Chipperfield, 2006) to calculate the coefficients of the equation 2.32. In COPCAT no additional heterogeneous term is required because this new scheme has been calculated considering complete heterogeneous and gas-phase chemistry. Then, it considers heterogeneous and gas-phase chemistry to be consistent when are applied in this linear ozone parametrization. This kind of parametrization is in better agreement with the current state of knowledge of stratospheric heterogeneous chemistry than previous schemes (Monge-Sanz et al., 2011).

2.3 Initial and Boundary Conditions

Before starting a simulation, it is necessary to determine the initial concentration of the chemical species used in the model, called the Initial Conditions (IC). In addition, when using a regional configuration it is also necessary to determine concentrations of all model species at the boundaries of the domain, called the BC. Appropriate IC and BC are required in order to solve the set of stiff differential equations included in AQMs.

In principle, observational data would be preferred for providing chemical IC and BC. However, such high-resolution observations are generally not available and other approaches are used. The methods applied for setting the IC and BC into the model range from the use of 1) default background values predefined by the user, 2) previous run outputs, and 3) the output from a regional or global AQM.

Numerous studies show the influence of IC and BC in the concentration results. Berge et al. (2001) suggests that running an appropriate spin-up prior to the simulation could minimized the influence of IC considering that the influences of IC basically depend on species lifetime. Liu et al. (2001b) presents that the influence of BC decreases during the downwind transport, and is significant to a specific region where the arrival time of the boundary condition is short and the species lifetime is long. Hence, influences of BC are more important for regions near the domain boundaries. Jiménez et al. (2007) focuses on the conditions within the PBL in the northeastern Iberian Peninsula, and proves that using a 48-h spin-up is sufficient to reduce the impact factor of IC to 10% or less for O_3 concentrations since the influence of pervasive local emissions.

For the global domain, a spin-up of one year 2004 is applied to achieve the chemical equilibrium before the actual simulation is performed. On the other hand, the regional configuration applies a spin-up of 10 days starting from ideal background concentrations.

2.4 Emissions

Emission inventories are one of the main critical parts of an AQMs due to their uncertainties (Zhao et al., 2011; Guenther et al., 2006; Smith et al., 2011). Emissions can be divided into:

anthropogenic (influenced by humans or human-induced activities) and natural. Anthropogenic sources include: industrial activities, power generation, on-road traffic, ports, airports, agriculture, etc. Although many natural emissions are from biogenic origin, i.e., produced by living organisms, there are other natural sources such as soil, biomass burning, volcanoes and lightning that need to be taken into account. Natural emissions depend strongly on meteorological fields (e.g., temperature, solar radiation, precipitation) and vegetation cover (e.g., leaf area index, land use, vegetation cover) and are considered the most uncertain source of total emissions (Zhang, 2008). Most pollutants are emitted both by natural and by anthropogenic sources.

Emissions estimates are developed using emissions models combining descriptions of various processes (EEA, 2013; IPCC, Japan, 2013; Olivier et al., 1999). These models combine estimates of process rates and Emission Factors (EFs) to produce an estimate of the emissions from a particular source (e.g., industrial facility, road traffic, biogenic emission). In models, such as Model of Emissions of Gases and Aerosols from Nature version (MEGAN) (Guenther et al., 2006), biogenic emissions are calculated for each Plant Functional Type (PFT) and are a function of sunlight and temperature. The processing of emissions is an important step that prepares the emission files to be used by the AQMs later on. The emission module converts point, area, and mobile source emissions to hourly emissions of the model species in each grid cell. Therefore, emissions inputs are built to be well-matched with the chemical mechanisms used in the model, and with the model resolution. This conversion method consists in a sequence of steps called temporization, speciation, and gridding. These files, normally, consist of hourly, spatially gridded estimates of the emissions of primary pollutants such as CO, NO, NO_2, SO_2, HNO_2 and of the various primary VOCs that treated in the chemical mechanism.

The quality of the available emission inventories varies from high quality inventories to less available or reliable emissions information in other regions, especially in developing countries due to lack of test based in EFs (Klimont and Streets, 2007). The resulting uncertainty leads to a range of possible emission outcomes for a given source. Hence, emissions are one of the most uncertain inputs into AQMs (Tonnesen et al., 1998a; Pierson et al., 1990; Geron et al., 1994; Simpson, 1995; Smith et al., 2011).

Several emission inventories have been developed (`http://accent.aero.jussieu.fr`). These emission sources covers different domains: POET (Granier et al., 2005), RETRO (Schultz et al., 2007), EDGAR-FT2000 (Olivier et al., 1996), ACCMIP Lamarque et al. (2013), GAINS (Janusz Cofala and Markus Amann and Zbigniew Klimont and Kaarle Kupiainen and Lena Höglund-Isaksson, 2007) or GEIA (GEIA/ACCENT, 2005) are examples for the global domain, EPA-2006 (`http://www.epa.gov/airtrends/`) for United States, EMEP (EEA, 2007; Vestreng and Støren, 2000) and TNO-MACC (Kuenen et al., 2014) for Europe, REAS (Ohara et al., 2007) for Asia, TRACE-P (Streets et al., 2006) for China, and HERMESv2.0 (Guevara et al., 2013) for Iberian Peninsula and Canary Islands are examples for regional domain inventories.

Pollutant emission fluxes significantly vary between emission inventories. The case of CO emissions is highlighted in Table 2.5 . Table 2.5 presents regional and global anthropogenic and

biomass burning emissions for CO (Tg CO) for the year 2000. This table comes from Lamarque et al. (2013).

Table 2.5: Regional and global anthropogenic and biomass burning emission inventories for CO (Tg CO) for the year 2000 (Lamarque et al., 2013). In addition, TNO-MACC (Kuenen et al., 2014) for the year 2009 is also added to this comparison.

Anthro.	**EDGAR-FT2000**	**RETRO**	**GAINS**	**EPA-2006**	**EMEP-2004**	**TRACE-P**	**ACCMIP**	**TNO-MACC**
Global	548	476	542	-	-	-	611	-
US	74	56	75	102	-	-	93	-
Europe	30	19	38	-	31	-	31	38.2
China	98	95	128	-	-	100	121	-

Bio. burn.	**GFED-v2**	**GICC**	**ACCMIP**
Global	427	467	459

In this Ph.D. thesis, the global run experiment uses anthropogenic and biomass burning emissions based on the Atmospheric Chemistry and Climate Model Intercomparison Project (ACCMIP) inventory Lamarque et al. (2013), and soil and ocean emissions based on Precursors of Ozone and their Effect on the Troposphere (POET) inventory (Granier et al., 2005). These emissions are described in Section 4.2.1. Biogenic emissions are computed online with the MEGANv2.04 (Guenther et al., 2006), described in Section 2.4.1. Global anthropogenic emissions of NO for January and July 2004 used in the global model simulation are displayed in Figure 2.9.

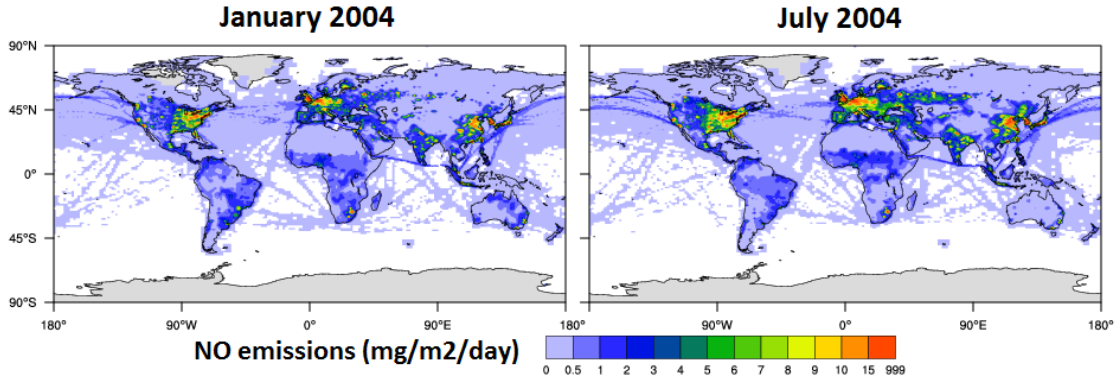

Figure 2.9: Anthropogenic emissions of NO (mg/m2/day), from ACCMIP inventory Lamarque et al. (2013) , for January (left) and July (right) 2004 used in this model simulation

For the regional experiments, the anthropogenic emissions are based on the The Netherlands Organisation for Applied Scientific Research (TNO)-Monitoring Atmospheric Composition and Climate (MACC) database (Kuenen et al., 2011, 2014; Pouliot et al., 2012), described in Section 5.2.1. Concerning to natural online emissions, only biogenic emissions are considered as a natural source in the regional scale and are computed with the MEGANv2.04 model.

2.4.1 Online biogenic emissions

In the NMMB/BSC-CTM, biogenic emissions are computed online with the MEGANv2.04 (Guenther et al., 2006). MEGAN is a modelling system for estimating the net emission rate of gases and aerosols from terrestrial ecosystems into the above-canopy atmosphere at specific location and time. Driving variables include landcover and weather. Weather driving variables considered are temperature at 2m and short wave radiation. MEGAN canopy-scale emission factor differs from most other biogenic emissions models, which use a leaf-scale emission factor. The emission-factor maps used in MEGAN are updated periodically and the algorithms are refined. MEGAN can be applied at regional or global scale with a horizontal resolution up to 1 km^2. MEGAN estimates the emission of more than 130 non-methane volatile organic compounds (NMVOCs). All the MEGAN NMVOCs are speciated, following the CB05 chemical mechanism; thus, emissions for isoprene, lumped terpenes, methanol, nitrogen monoxide, acetaldehyde, ethanol, formaldehyde, higher aldehydes, toluene, carbon monoxide, ethane, ethene, paraffin carbon bond, and olefin carbon bond are considered within the chemical processes of the NMMB/BSC-CTM model. Biogenic emissions are computed every hour in order to account for evolving meteorological changes in solar radiation, surface temperature, moisture and precipitation. Figure 2.10 (upper and bottom panels) shows the emission of isoprenes and terpenes (Tg/year) for January (left) and July (right) 2004 used in this model simulation.

Land cover, emission factors, and meteorological parameters are important driving variables of MEGAN, and the uncertainties of estimated biogenic volatile organic compounds (BVOCs) emissions and their impacts on surface ozone are hence associated with uncertainties in these inputs. Ashworth et al. (2010) evaluates the effect of varying the temporal resolution of the weather input data on isoprene emission estimates generated by the MEGAN. This study suggest that using daily or monthly data instead of hourly data a reduction of 3% and 7% is obtained. Moreover, the impact on a local scale can be more significant with reductions of up to 55% at some locations when using monthly average data compared with using hourly data. Another study, Marais et al. (2014), performs several sensitivity model runs to study the impact of different model input and model settings on isoprene estimates and resulted in differences of up to $\pm$ 17% of the reference isoprene total. In our study, weather inputs are based on previous day 24h averages and data of the hour of interest.

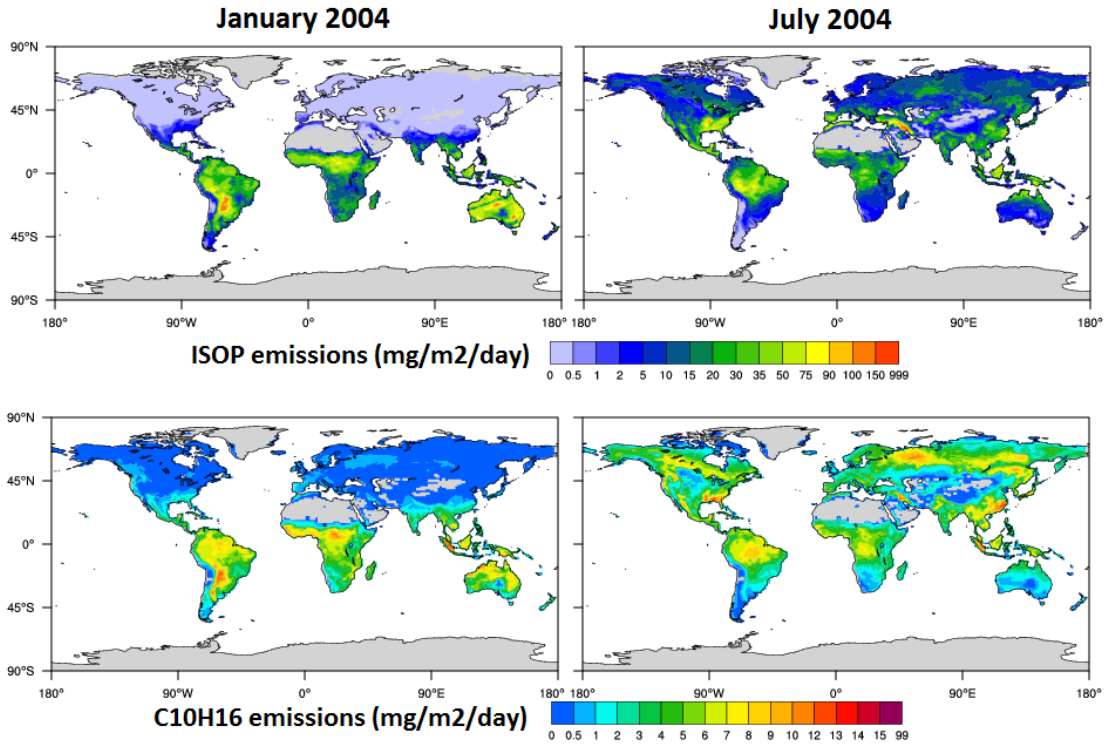

Figure 2.10: Biogenic emissions of isoprene (upper panel) and monoterpene (bottom panel), from the online model MEGANv2.04 for January (first column) and July (second column) 2004 used in this model simulation

Chapter 3

Inter-comparison of two ozone stratospheric linear models within the online global model

3.1 Introduction

Ozone is one of the dominant chemical species in the stratosphere. The majority of the ozone in the atmosphere, around 85 - 90%, is found in the stratosphere (Holton et al., 1995). The distribution of ozone in the stratosphere is a combination of chemical, dynamical and radiative processes. Ozone budgets in the upper troposphere and lower stratosphere (UTLS) are also controlled by Stratosphere-Troposphere Exchange (STE). Anthropogenic pollution increases in relation to STE events (Santer et al., 2003; Holton et al., 1995). Some regional air quality modelling results have shown a strong impact on ozone boundary conditions (obtained from global Chemical Transport Model (CTM)) in background ozone concentrations with the troposphere (Im et al., 2014a; Giordano et al., 2014). In this sense, proper STE treatment is demanded from global CTMs to properly model the ozone budget in the atmosphere.

A detailed description of the photochemistry of the ozone involves hundreds of chemical species and reactions. This significantly increases the complexity of numerical models a requiring large amount of computer time. In applications such as NWP or CTMs, with focus on the tropospheric chemistry, it is not feasible to implement full ozone photochemistry throughout the whole atmosphere. Consequently, a simple and faster ozone photochemistry approach for the stratosphere is preferable.

In the last two decades, a new generation of linear stratospheric photochemistry schemes and ozone distributions were developed using coefficients derived from a photochemical model with more detailed chemistry (Cariolle and Déqué, 1986; Cariolle and Teyssèdre, 2007; McLinden et al., 2000; McCormack et al., 2004, 2006; Monge-Sanz et al., 2011). These schemes are based on Cariolle and Déqué (1986), Cariolle v1.0, which uses a linear parameterization depending

only on temperature and ozone amount in their coefficients. Cariolle v1.0 model lacks a heterogeneous term to treat the ozone polar loss, however, in the later versions a heterogeneous term is included in the parametrization since the coefficients included only gas-phase chemistry (Cariolle and Teyssèdre, 2007). However, a new linear ozone scheme COPCAT (Monge-Sanz et al., 2011) incorporates implicitly heterogeneous chemistry in their four coefficients and, hence, does not need an extra term accounting for the heterogeneous chemistry on its parametrization. Thus, both gas- phase and heterogeneous processes are included in a consistent way in the COPCAT linear approach providing a better representation of the stratospheric ozone in comparison with the current knowledge than in previous schemes (Monge-Sanz et al., 2011). Linear stratospheric photochemistry schemes have been implemented in many models (climate, CTM, NWP). The Cariolle and Déqué (1986) model has been introduced in the ARPEGE-Climate General Circulation Model and the European Centre for Medium-Range Weather Forecasts (ECMWF) model (Andersson et al. (2003)) for operational forecasts. It has also been used within 3D SLIMCAT stratospheric CTM for the study of ozone trends (Hadjinicolaou et al. (2005)). Parameterizations from Cariolle and Teyssèdre (2007) have been implemented within the MOCAGE CTM (Josse et al., 2004) and a 5 year simulation, 2000-2004, has been run with wind and temperature fields from the ECMWF operational analyses. Monge-Sanz et al. (2011) compare the new O_3 scheme, COPCAT, within the same CTM used to calculate it, the TOMCAT/SLIMCAT (Chipperfield, 2006). COPCAT agrees mainly with TOMCAT/SLIMCAT full-chemistry. In addition, COPCAT is compared with the current ECMWF scheme based on Cariolle and Teyssèdre (2007) for stratospheric O_3 and it is observed that COPCAT performs better the Antarctic ozone hole and also at northern high latitudes (Monge-Sanz et al., 2011).

The principal motivation of this specific study is that a simple linear stratospheric ozone scheme is a good option to model the STE and gives a valuable alternative to the introduction of complex and computationally costly chemical schemes into a CTM that mainly focuses on tropospheric chemistry.

In this Ph.D. thesis, we implement and evaluate two different linear parameterisations for the stratospheric ozone within the global CTM model NMMB/BSC Chemical Transport Model (NMMB/BSC-CTM). The two linear schemes evaluated are the last version of CD86, Cariolle v2a (Cariolle and Teyssèdre, 2007) and the COPCAT scheme (Monge-Sanz et al., 2011). The ozone vertical structure is evaluated with ozonesondes, and Halogen Occultation Experiment (HALOE) and SCanning Imaging Absorption spectroMeter for Atmospheric CHartographY (SCIAMACHY) satellite retrievals. Both, the ozone vertical profile and the total ozone column are analysed. Special analysis on the stratosphere-troposphere ozone transition is presented.

Chapter 2 summarises the main characteristics of the modelling system applied (NMMB/BSC-CTM), including a description of the ozone linear stratospheric models implemented (see Section 2.2.5). The model setup is described in Section 3.2. Observations used to evaluate the model are briefly described in Section 3.3. Results and conclusions of this work are given in Sections 3.4 and 3.5.

3.2 Model setup

For the present work, the model NMMB/BSC-CTM is configured as global. It solves the chemistry of the troposphere and the stratospheric ozone with the linear scheme. The global domain is configured with a horizontal grid spacing of 1.4° x1° and 64 vertical layers. The top of the atmosphere is set at 1 hPa. The atmospheric model fundamental time step is set to 180s and the chemistry processes are solved every 4 fundamental time steps. NCEP/Final Analysis (FNL) is used as initial conditions for the meteorological driver. The meteorology is reinitialised every 24 h. To initialise the chemistry on the first day of simulation, initial conditions from the global atmospheric model MOZART-4/NCEP (Emmons et al., 2010) are used and a spin-up of 1 year is then run. After this spin-up, one year simulation is used for the model evaluation. Above 100hPa, two different model configurations are defined to establish the most suitable scheme for the performance of the stratospheric ozone: (1) the NMMB/BSC-CTM coupled with the Cariolle v2a linear model (hereinafter referred to as CAR experiment), and (2) the NMMB/BSC-CTM model coupled with the COPCAT linear model (hereinafter referred to as COP experiment). The year of simulation is 2004. Table 3.1 shows the main configuration of the model and the experiment set-up.

Table 3.1: Model characteristics and experiment configuration

Chemistry	
Tropospheric ozone (below 100hPa)	Chemical mechanism CB05 (Yarwood et al., 2005)
Stratospheric ozone (above 100hPa)	Experiment 1: Cariolle v2a (Cariolle and Teyssèdre, 2007)
	Experiment 2: COPCAT (Monge-Sanz et al., 2011)
Resolution and Initial conditions	
Horizontal resolution	1.4° x 1°
Vertical layers	64
Top of the atmosphere	1 hPa
Chemical Initial condition	MOZART-4 (Emmons et al., 2010)
Meteorological Initial condition	Final Analysis (FNL) NCEP
Spin-up	1 year

3.3 Ozone observational data

3.3.1 SCIAMACHY data

Total O_3 columns are compared with SCIAMACHY (`http://www.sciamachy.org/`) satellite data and used in this model evaluation to provide some insight into the spatial distribution of the model. SCIAMACHY (on board ENVISAT that was operational from March 2002 to April 2012) is a passive remote sensing spectrometer measuring backscattered, reflected, transmitted or emitted radiation from the atmosphere and the Earth's surface with a wavelength range between 240-2380 nm. The SCIAMACHY instrument has a typical spatial resolution of 60 x 30 km^2. The SCIAMACHY Level-2 data product, used here, provides retrieved daily total ozone columns (Lerot et al., 2014). Total O_3 error is generally less than 0.5% at moderate solar zenith angle (SZAs) and may reach 2% at SZAs larger than 80° (Weber, M., 2014). Moreover, Borchi

and Pommereau (2007) present a validation of several satellites, including SCIAMACHY, in comparison with several series of profiles obtained by long duration balloon measurements during 2003 and 2004. The ozone relative biases reach +5.5% for the SCIAMACHY satellite product.

3.3.2 HALOE data

The vertical structure of stratospheric O_3 is compared against available HALOE data. HALOE recorded data is at almost every sunrise (SR) and sunset (SS) event of middle atmosphere composition and temperature on board the Upper Atmosphere Research Satellite (UARS). The observed coverage is from 11th of October 1991 until 21st of November 2005 with a few observations for some individual months. HALOE uses solar occultation to measure simultaneous vertical profiles of ozone with a very high vertical resolution (2 km) (see Russell et al. (1993b) for further details of the experiment). Brühl et al. (1996) successfully intercompare HALOE vertical profiles of ozone with 400 profiles of other sounders including ozonesonde, lidars, ballons, rocketsondes and other satellites with coverage of almost all seasons and all latitudes. From this intercomparison, Brühl et al. (1996) conclude that the quality of HALOE ozone data is excellent throughout the whole stratosphere. Bhatt et al. (1999) find an agreement, after averaging HALOE data, to within 10% of their corresponding ozonesonde measurements down to 100 hPa at tropical/subtropical latitudes and to 200 hPa at extratropical latitudes. Several studies estimate uncertainties of single profile HALOE retrievals and state that its accuracy decreases near the tropopause (Eyring et al., 2006; Brühl et al., 1996; Harries et al., 1996; Park et al., 1996; Russell III et al., 1996). In Remsberg (2008) 14 years (1991-2005) of ozone-versus-pressure profiles from the HALOE are analysed and concluded that the solar occultation technique of HALOE provided adequate sampling and enough vertical resolution for obtaining the solar cycle response in stratospheric ozone. HALOE Version 19 daily data for SR and SS experiments during the complete year of 2004 has been used in this study with different geolocation by latitude and longitude displayed in initialis 3.1.

3.3.3 Ozonesondes: WOUDC, GMC and SHADOZ

Available ozonosondes of the World Ozone and Ultraviolet Radiation Data Center ozonosonde network (WOUDC;`http://www.woudc.org/`), the Global Monitoring Division (GMD; `ftp://ftp.cmdl.noaa.gov/ozwv/ozone/`) and the Southern Hemisphere Additional Ozonesondes (SHADOZ; `http://croc.gsfc.nasa.gov/shadoz/`; Thompson et al., 2003a,b) are used in this model evaluation to complement the vertical ozone analysis. Most of the ozonesonde stations provide between 4 to 12 profiles per month each year with a precision of $\pm$ 3-8 % in the troposphere (Tilmes et al., 2012). A total of 23 ozonesonde stations, following the study of Tilmes et al. (2012) are selected for the present evaluation. Figure 3.1 displays the location of these selected ozonosondes. Following a similar criteria as Tilmes et al. (2012), regional aggregates are formed in combining stations with similar O_3 characteristics.

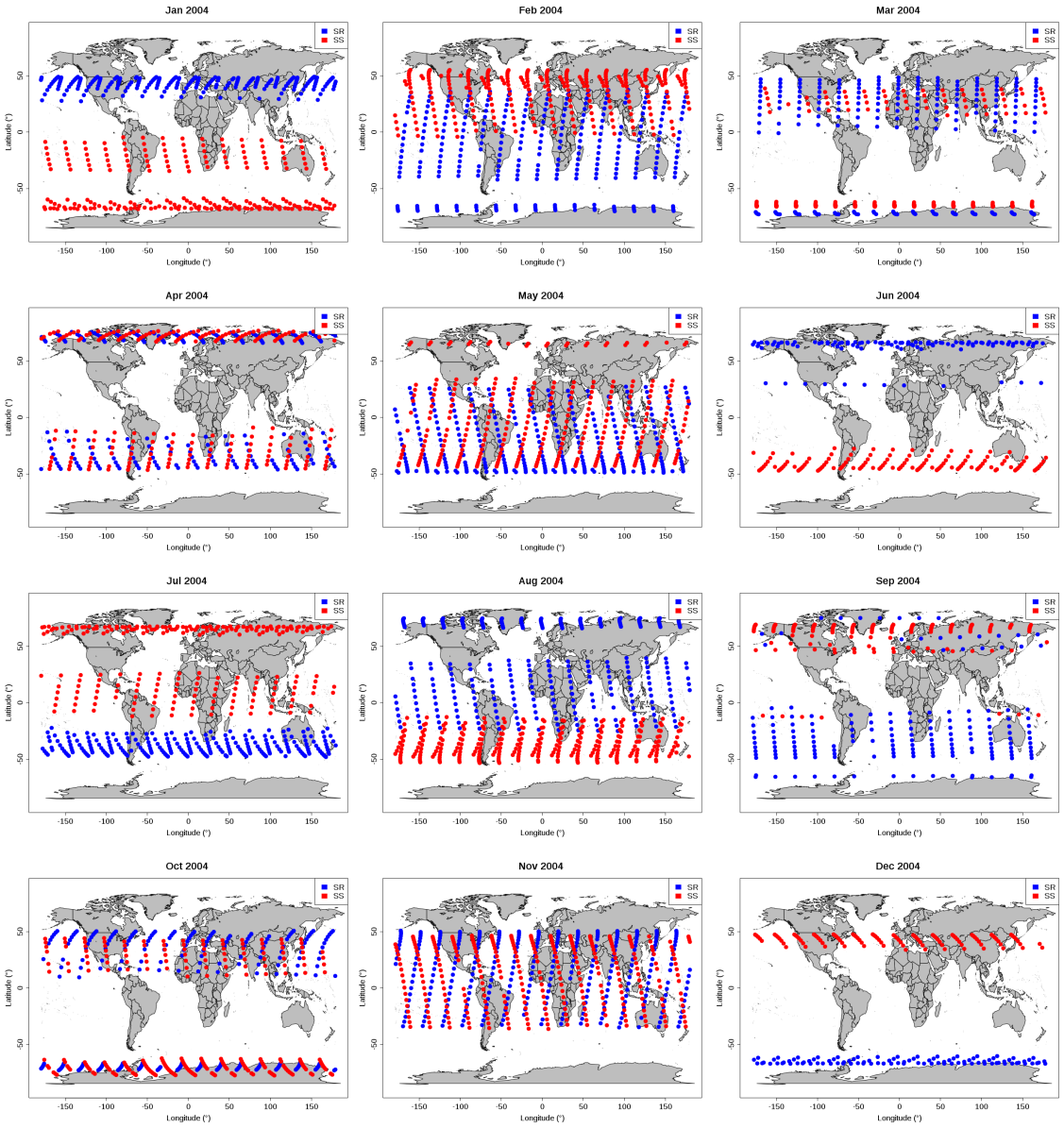

Figure 3.1: Monthly HALOE locations used in this model evaluation

3.4 Results

3.4.1 Total ozone column

To know the capability of two linear schemes to simulate stratospheric ozone in time and space, the monthly zonal mean total column of ozone in Dobson Units (DU) from the two model sim-

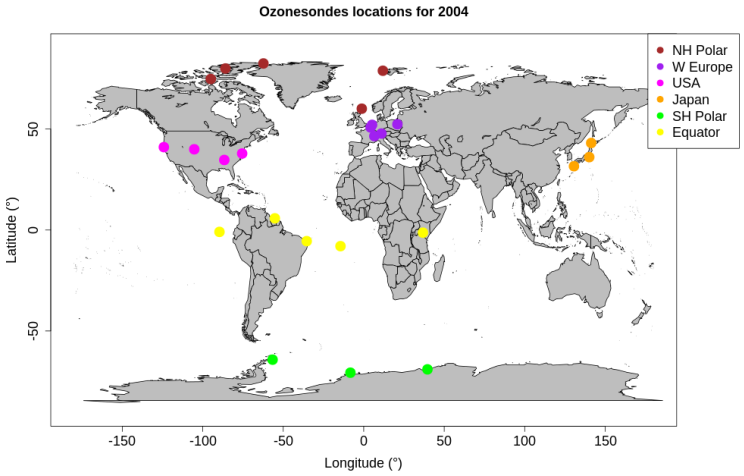

Figure 3.2: Ozonesondes locations used in this model evaluation

ulations are compared with the SCIAMACHY observations. CAR (first column), COP (second column) and, SCIAMACHY satellite retrievals (third column) for January to June are displayed in Figure 3.3, and July to December 2004 in Figure 3.4. To make a proper comparison, data from the model simulation is compared only when satellite data is available at each time and location of each overpass.

In general, both COP and CAR simulations show a realistic seasonal cycle, where: (1) in the NH extratropics, ozone values are highest during spring and lower during Sept-Oct, due to the poleward and downward transport of the ozone by the large-scale Brewer-Dobson circulation (Brewer, 1949; Dobson, 1956; Weber et al., 2011), (2) in the tropics, where there is slow large-scale ascent, the ozone columns are lower mostly during Nov-Jan when the upwelling branch of the Brewer-Dobson circulation is strongest, (3) in the south pole, low values of the Antarctic ozone hole are seen during the Antarctic spring, (4) over the circum-Antarctic belt the highest ozone concentrations are seen during Sep-Nov when ozone rich air is brought down by a large-scale descendent.

Figure 3.3 shows that during the first part of the year (January-April), both simulations result in low column values over northern high latitudes with respect to the satellite data. This underestimation is particularly large for the COP simulation (50 DU less). During late spring and the beginning of summer, a reduction in ozone concentrations is observed in northern high latitudes. COP is able to capture this ozone descendent with similar values, and CAR has higher values in comparison with the satellite data. Moreover, COP modelled ozone values are in agreement with the satellite data over the north hemisphere during autumn and summer. Larger biases between April and November are noticeable through CAR simulation ($\sim$ 25-100 DU). Over the Equator latitudes (-5° to 5°) both simulations have positive bias throughout the year, except in

November-January, and is more significant in February-March and July-August of the order of 25-50 DU. Total column differences (DU) with respect to TOMS satellite data for SLIMCAT runs using the COPCAT and the Cariolle v2a are presented in Monge-Sanz et al. (2011). Results from this comparison show a clear underestimation: from -30 to -20 DU for COPCAT and less than 10 DU in the case of Cariolle v2a over the Equator latitudes. These results are different from what we see in our model simulation suggesting a possible limitation in the parameterization of the radiation scheme (underestimation of the aerosol attenuation) in our model over this area. Having said that, the positive O_3 bias over the tropics requires further investigation. Lower concentrations over the tropics are observed during December-February when the Brewer-Dobson circulation is strongest. Over the north tropical Pacific, both simulations underestimate ozone concentrations during the year, more significantly in late autumn and winter seasons. From December to May, CAR and COP simulations have a tendency to overestimate concentrations over southern mid and high latitudes. Higher values are particularly large by 50 DU in these latitudes for the COP simulation during December-February. Moreover, Figure 3.4 shows that from June-August CAR simulation has a tendency to overestimate O_3 at southern high latitudes by 25 DU.

The Antartic ozone hole is most commonly defined as the region at high southern latitudes enclosed by the 220 DU of ozone (Newman et al., 2004). Figure 3.4 shows that over the Antarctic, the ozone hole during September-October is well-simulated by COP capturing its extension and magnitude. On the other hand, CAR captures the ozone decrease during the Antarctic spring but clearly overestimates ozone concentrations by 25 DU compared to satellite data. This result may be due to the different heterogeneous chemistry treatment adopted in each scheme. Note that, both simulations have a shorter duration of the ozone hole in comparison to the satellite data that has lower concentrations during November. In addition, higher values in the belt above the Antarctic are well-simulated by both CAR and COP models with significant overestimation by CAR during Sept-Nov, and also by COP only during November.

Total column ozone field is also computed in previous studies such as Inness et al. (2013) using the MACC reanalysis. The MACC reanalysis system assimilates ozone satellite retrievals from several satellite sensors. Over the NH, the MACC reanalysis is able to simulate higher values ($>$ 400 DU) during winter and spring; lower values are seen in CAR (only for winter) and COP in comparison with the MACC reanalysis. Similar values between the NMMB/BSC-CTM simulations and MACC reanalysis are seen from -45° to 45° latitudes throughout the year, with the exception of the positive bias already observed in the Equator for February-March and July-August. Over the SH, the MACC reanalysis has lower values in comparison to COP and CAR from December-May, but it is in agreement with COP successfully simulating the Antarctic ozone hole during the months of September-October.

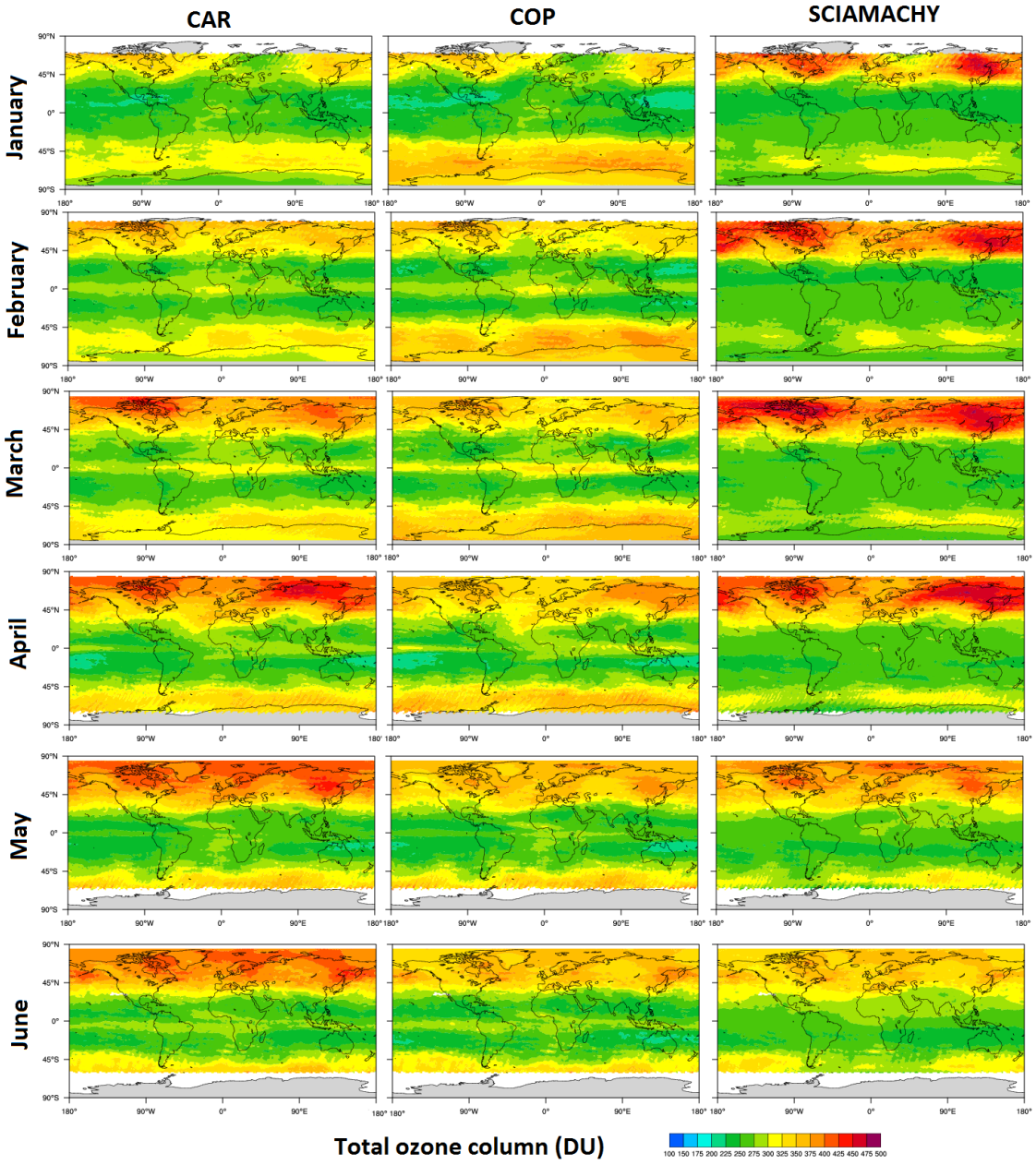

Figure 3.3: Total O_3 (DU) between the two simulations, CAR (first column) and COP (second column), and the SCIAMACHY satellite data (third column) for the months of January to June (from the first row to the last, respectively) .

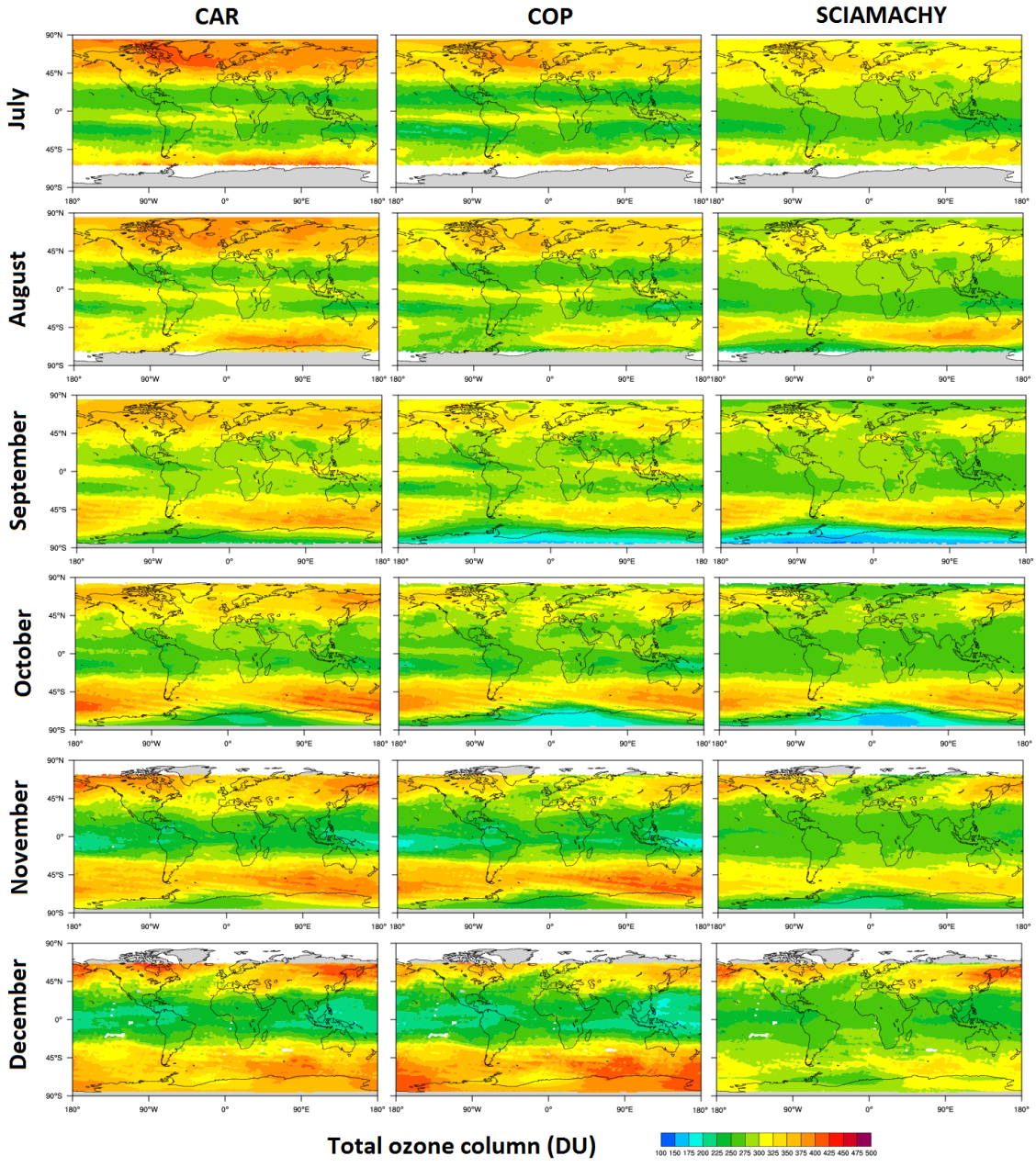

Figure 3.4: Total O_3 (DU) between the two simulations, CAR (first column) and COP (second column), and the SCIAMACHY satellite data (third column) for the months of July to December (from the first row to the last, respectively) .

3.4.2 Stratosphere vertical structure

Total ozone columns are complemented with the stratospheric ozone vertical profiles from the HALOE retrievals and upper tropospheric ozone vertical profiles from WOUDC, GMD and SHADOZ ozonesondes in order to assess the vertical distribution of ozone in the stratosphere-upper troposphere. Upper tropospheric vertical profiles are discussed in the next section. The comparison is made only when HALOE retrievals are available; thus, only the same data from the model and the observations is compared.

Figure 3.5 shows the seasonal average (DJF for December, January and February, MAM for March, April and May, JJA for June, July and August, and SON for September, October and November) simulated vertical profiles of ozone for the model simulations, CAR and COP, and HALOE observations. Results in Figure3.5 are displayed by latitude bands of 50N-90N, 20N-50N, 20S-20N, 50S-20S, 90S-50S (from top to bottom rows). The number of observations available is added on the top of each sub-figure. Measurements are represented by the solid red line and the model results COP by the solid black line, and CAR by a solid blue line. To know the variability of data, standard deviation is plotted in each vertical layer for both models (black and blue for COP and CAR, respectively) and observations (red) in horizontal lines.

As in all previous studies using linear ozone schemes, major features are well captured by both simulations. These major features include: (1) the maximum stratospheric ozone concentration is seen around 6-10hPa, (2) higher ozone values are observed in the tropics (20N-20S) and lower in the mid-high latitudes (90N-50N and 50S-90S) and, (3) the ozone concentration decrease from the maximum to the tropopause is well-captured.

These results show that CAR has a tendency to overestimate the maximum stratospheric ozone concentration during the whole year, which is more significant in the tropical and north extratropical regions. This result is consistent with the higher total ozone values by the CAR simulation seen in Figs. 3.3 and 3.4. On the other hand, COP underestimates the ozone maximum between 50N-20S latitudes. In addition, COP has a tendency to underestimate the ozone above 10 hPa. The underestimation of the maximum stratospheric ozone and the ozone concentrations above 10hpa is consistent and already seen in the study by Monge-Sanz et al. (2011), which compares the annual average from the year 2000 ozone profiles between the COPCAT parameterization and the HALOE measurements in the tropics (4 $^\circ$ N). However, CAR has a positive bias above 10 hPa in most of the latitudes compared with the COP, of the order of 2ppm, and HALOE observations, of the order of $\sim$ 1-2ppm. The ozone is well-captured in the mid/low stratosphere between 50N-50S for both simulations. Nonetheless, both simulations underestimate the ozone in the low stratosphere between 90N-50N during DJF and MAM. This result is consistent with the comparison against the ozone total columns from SCIAMACHY seen for this latitudes at this period. During MAM, JJA and SON CAR there is a significant positive bias at 90N-50N latitudes. Over high southern latitudes, we have seen in Figure 3.4 that COP tends to overestimate O_3 concentrations during (the months of) DJF and MAM. With the results of the ozone vertical profiles, we see that this overestimation is located in the mid/low stratosphere below 20 hPa. During the JJA, the same results are seen for both simulations, that underestimate ozone in

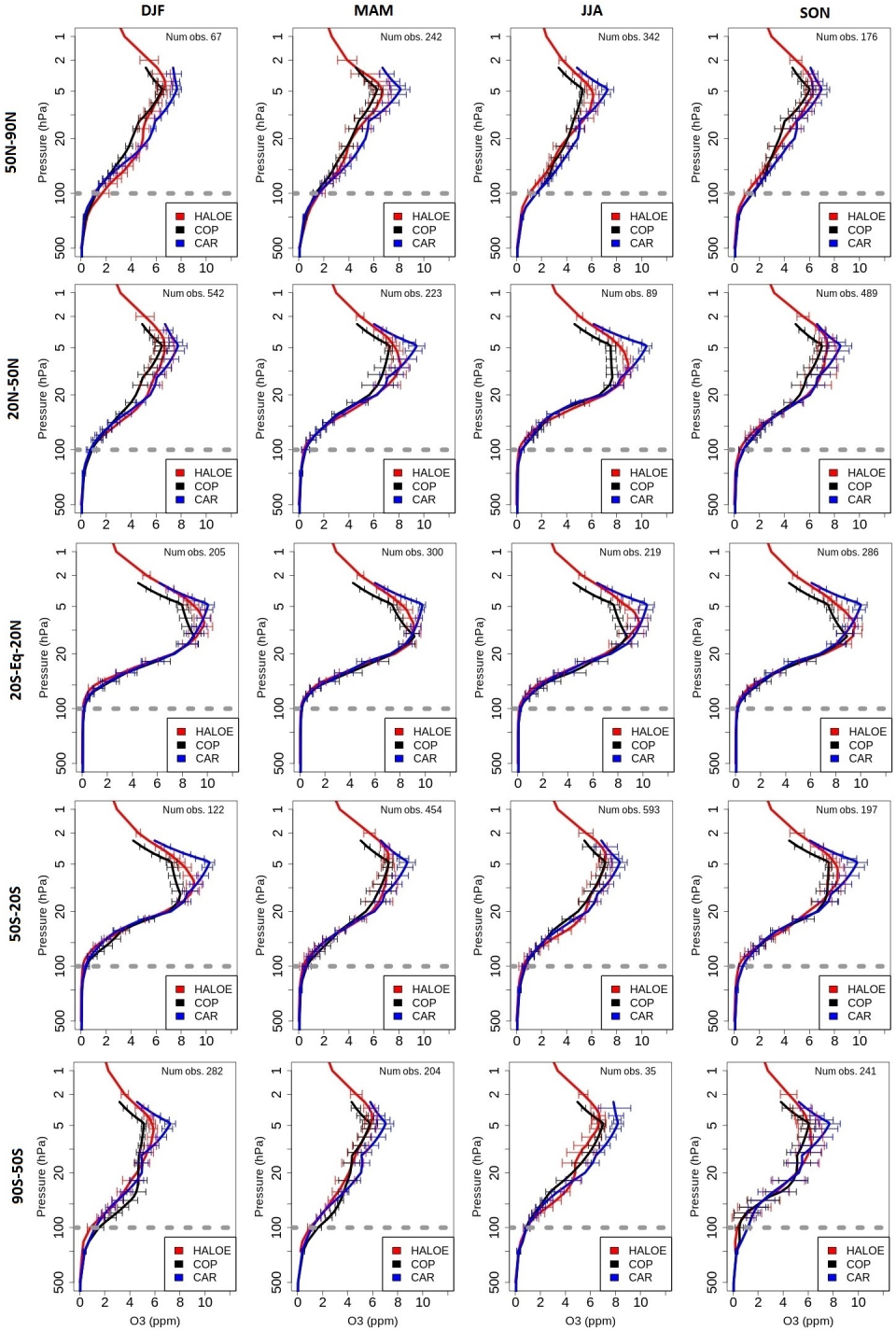

Figure 3.5: O_3 (ppb) comparison of HALOE measurements (red lines) and simulated (black lines) seasonal vertical profiles and standard deviations (horizontal lines) for the latitude bands of 30N-90N (top row), 30S-30N (middle row) and 90S-30S (bottom row). To emphasize that the parametrizations were implemented above 100 hPa, an horizontal grey line was added in this pressure level.

the lower stratosphere especially in latitudes between 90S-50S. In spring, the vertical profile of ozone at high northern latitudes is well-captured by COP. Furthermore, the ozone hole in the south pole during autumn is successfully simulated, by the COP simulation. This result is consistent with the previous analysis of the ozone tropospheric columns (see Figure 3.4).

3.4.3 Upper troposphere vertical structure

Since the main purpose of this study is to evaluate two different simple parameterizations for the stratospheric ozone as an upper boundary condition to model the tropospheric ozone chemistry, we are interested in evaluating in more detail the model performance around and below 100 hPa, where the transition between the linear schemes and the comprehensive tropospheric chemical mechanism is located. For that reason, the vertical structure of the upper troposphere is assessed with ozonesonde observations. Hence, the model results are compared with available ozonesondes that have a better accuracy near the tropopause level than the HALOE measurements. Figure 3.6 compares the seasonal average mean simulated vertical profiles of ozone for both the model simulations and observations. Figure 3.6 shows (from left to right) four panels: DJF, MAM, JJA and SON for each region. The location and the number of profiles of the ozonesondes is depicted in Figure 3.6. The ozonesonde profiles are averaged by regions following Tilmes et al. (2012): USA, W. Europe, Equator and Japan. Measurements are represented by the solid red line, the COP model results by the solid black line, and CAR model results by the solid blue line. To know the variability of data, standard deviation is plotted in each vertical layer for both model (black for COP and blue for CAR) and observations (red) in horizontal lines.

To summarise, both simulations well-captured the ozone around the tropopause level. The agreement for the O_3 vertical profiles over USA, W. Europe, Equator and Japan, is very good for both simulations in particular during MAM. Over Europe, a slight ozone underestimation ($<$10ppb) during winter is seen by CAR simulation. In the summer, the ozone concentrations are overestimated in most of the stations, in particular over Japan and W. Europe ($<$300ppb). Higher differences between the two simulations are seen over the polar stations. Over the N. Polar stations, CAR has higher concentrations throughout the whole year with a better performance during the spring than COP below 100 hPa. On the other hand, the ozone inflection in the tropopause level is better-simulated by COP during DJF and MAM. Significant overestimation ($<$1ppm) is seen in the S. Polar stations for the COP simulation during DJF and MAM. On the other hand, COP shows a better performance, with lower concentrations, during JJA and SON in the south polar stations. As it has been shown in Sections 3.4.1 and 3.4.2, the ozone reduction during SON in the south polar stations by the COP simulation, is in good agreement with the observations; CAR, on the other hand, overestimates ($<$1ppm) the intensity/duration of the ozone hole. Part of the ozone bias in the troposphere might be attributed to the net influx of ozone around 100hPa. Thus, ozone concentrations in the upper troposphere need to be well-captured by the model simulations.

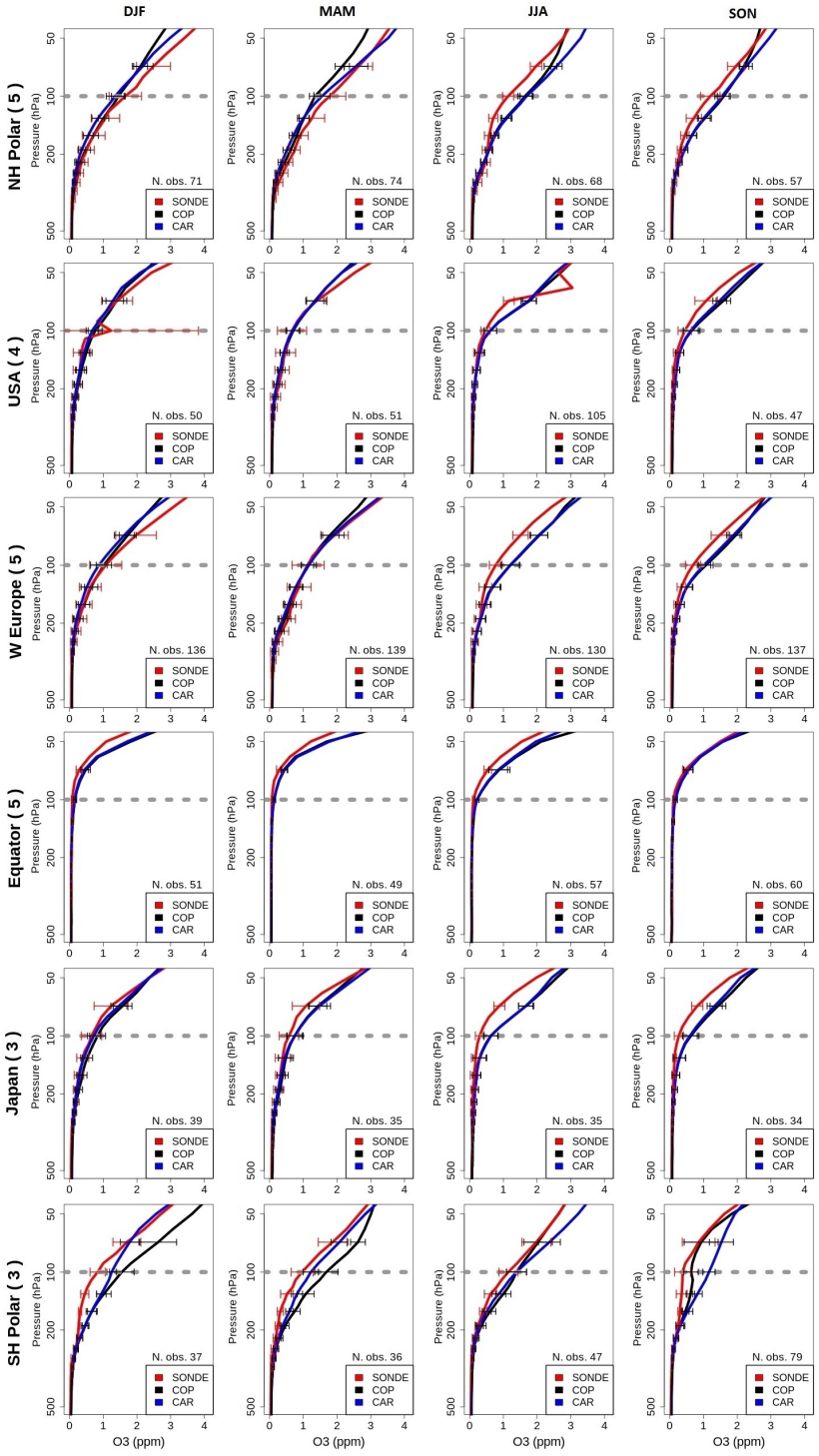

Figure 3.6: Comparison of ozonesonde measurements (red lines) and simulated COP (black lines) and CAR (blue lines) seasonal vertical profiles of O_3 (ppb) and standard deviations (horizontal lines). The region name and the number of stations, using brackets, are given above each plot. To emphasize that the parametrizations were implemented above 100 hPa, an horizontal grey line was added in this pressure level.

3.4.4 Stratospheric inflow

The different treatment of the stratospheric ozone in the model results in a different stratospheric ozone inflow in the troposphere. The stratospheric inflow of ozone at 100 hPa is shown in table 3.2 for the two experiments. It is calculated as an approximation of the stratosphere-troposphere ozone exchange flux, as the annual balance of the ozone mass crossing the 100 hPa height. The stratospheric inflow is computed on the global, Northern Hemisphere, Southern Hemisphere, Northern Extratropics and Southern Extratropics domains, and annual and seasonal budgets are provided.

Common features are seen in both simulations: (1) there is a hemispheric asymmetry in the stratosphere-troposphere exchange of ozone where most of the net influx of ozone occurs in the northern hemisphere, (2) higher stratospheric influx happens during DJF, and less during JJA, (3) over the tropics the STE balance is positive, thus, ozone flux mainly goes from the troposphere to the stratosphere especially during JJA. In general, COP (-383.87 Tg) has higher stratospheric inflow than CAR (-358.35 Tg). Over the NH, this higher inflow occurs in DJF, JJA and SON, and over the SH from December to May. Over the tropics, the ozone flux from the troposphere to the stratosphere is higher in CAR than COP. Significant differences are seen in the N. Extratopics where higher stratospheric influx occurs during winter with the COP simulation. In addition, over the S. Extratropics higher influx is seen in CAR during SON. These results are consistent with Figure 3.6, where, during the winter months, stations that are located in the N. Extratopics (NH Polar, USA, Europe and Japan) have higher concentrations in COP. On the other hand, stations that are located in the S. Extratropics (Equator and SH Polar) have higher concentrations in CAR simulation during spring around 100 hPa.

Several previous studies that calculate the global stratospheric inflow of ozone include: Huijnen et al. (2010) with -421 Tg O_3, Folberth et al. (2006) with -715 Tg O_3, Horowitz et al. (2003) with -343 Tg O_3 , and Stevenson et al. (2006) with -552 $\pm$ 168 Tg O_3. Both simulations results are in good agreement with these studies, although they exhibit a lower range value of the model estimates of STE.

Table 3.2: Stratospheric inflow of ozone mass (Tg O_3) at 100 hPa for season and whole 2004 year for simulations COP and CAR.

	Period	Global	NH	SH	Trop.	N. Extratrop.	S. Extratrop.
COP	DJF	-135.83	-86.04	-49.79	-1.31	-73.16	-61.35
	MAM	-111.34	- 58.40	-52.94	5.22	-63.95	-52.61
	JJA	-60.15	-36.58	-24.23	14.47	-52.82	-22.47
	SON	-75.96	-49.22	-26.61	4.32	-37.28	-42.87
	Annual	-383.87	-230.46	-153.41	22.77	-227.36	-179.28
CAR	DJF	-114.14	-75.19	-38.95	0.72	-64.23	-50.63
	MAM	-101.22	-60.11	-41.11	5.16	-65.42	-40.96
	JJA	-62.42	-33.37	-29.04	15.80	-50.51	-27.71
	SON	-80.59	-45.86	-34.73	5.91	-34.52	-51.99
	Annual	-358.35	-214.80	-143.55	27.66	-214.86	-171.15

3.5 Conclusions

Two simplified treatments of the stratospheric ozone have been evaluated with the global chemical transport model NMMB/BSC-CTM: the Cariolle v2a linear scheme (CAR experiment) and the COPCAT linear scheme (COP experiment). Both model simulations are compared to the total ozone columns retrieved from the SCIAMACHY satellite, ozone vertical profiles from the WOUDC, SHADOZ and GMD ozonesondes (upper troposphere), and HALOE profiles satellite retrievals (stratosphere).

Both simulations reproduce realistic total ozone columns in comparison with the SCIAMACHY satellite data, capturing the main seasonal cycle features. In NH, higher ozone values are seen in spring and in the SH, the very low values of the Antarctic ozone hole are well-captured by both simulations. Both simulations result in the column values being too low in the northern higher latitudes with respect to the satellite data during the first half of the year. Ozone concentrations tend to be higher in the CAR simulation. The main limitation of COP is the higher ozone values over the south polar region from December to May. The main limitations of CAR are the higher values in the north hemisphere during summer and autumn and also, in the south pole during the spring season. The treatment in the heterogeneous chemistry adopted by COP provides a more realistic ozone hole performance during September-October over the Antarctic. CAR, on the contrary, overestimates the ozone hole concentrations values. Both simulations perform a shorter duration of the ozone hole in comparison with the satellite data.

Concerning the vertical structure of O_3 in the stratosphere and upper troposphere, COP and CAR simulations well-captured the maximum stratospheric ozone around 6-10hPa, the higher ozone values in the Equator and the lower values in the poles and the ozone decrease in the tropopause level. In general, CAR has a tendency to overestimate the maximum stratospheric ozone during the whole year and COP underestimates the ozone in the upper stratosphere. The ozone destruction is well-captured in spring at high northern latitudes and in high southern latitudes by the COP simulation. In addition, both parametrizations well-captured the ozone in the tropopause level. Good results are seen over USA, W. Europe, Equator and Japan stations by both models, particularly during spring time. The main differences between simulations are seen in the polar ozonesonde stations, where COP overestimates the S. Polar stations during DJF and MAM and CAR overestimate during SON.

Both simulations exhibit a hemispheric asymmetry in stratosphere-troposphere exchange of ozone where most of the stratospheric influx of ozone occurs in the northern hemisphere. Over the tropics the STE balance is positive. Higher stratospheric inflow is seen in the COP simulation (-383.87 Tg O_3) than CAR (-358.35 Tg O_3) and both results are within the lower range of the STE model estimates.

Overall, this study has shown that a simple ozone stratospheric scheme can capture the main characteristics of the stratospheric ozone with reasonably dynamic performance. Hence, these simplified parameterizations are a good option to be implemented in the tropospheric CTMs

providing a realistic ozone upper boundary condition with a very low computational cost. COP well-simulated stratospheric ozone from August to October and well-captured the ozone hole during the Antarctic spring; on the other hand, CAR has a good agreement throughout the whole year with the observations, however, presents significant limitations over the SH.

Chapter 4

Global run evaluation

4.1 Introduction

Ozone plays an important role in global tropospheric chemistry. In the lower troposphere, it is one of the main indicators of air quality, reaching unhealthy levels at high concentrations, however, in the free troposphere and the stratosphere, it is as an important greenhouse gas. In the presence of nitrogen oxides (NO_x), it is produced during the photochemical oxidation of methane (CH_4), carbon monoxide (CO) and non-methane volatile organic compounds (NMVOC) (Crutzen, 1974; Derwent et al., 1996). Since the pre-industrial era, emissions of ozone precursors from anthropogenic and biomass burning sources have changed, modifying the distribution of tropospheric ozone concentrations and other trace gases (Lamarque et al., 2013). Stratosphere-Troposphere Exchange (STE) events contributing to the influx of stratospheric O_3 into the troposphere are also an important source of the tropospheric ozone (Stohl et al., 2003; Hsu and Prather, 2009).

The development of AQMs and MetM have traditionally evolved as separate fields (offline approach) due to the scientific complexities and limitations in computer resources. Although, the offline approach requires lower computational capacity, it can cause a loss of essential information about some atmospheric processes that have a time-scale smaller than the output time of the meteorological model (Baklanov et al., 2014). However, nowadays, due to a general increase in computer capacity, online coupled meteorology-chemistry models have been developed and used by the science community that recognizes the online approach more realistic than offline (Byun, 1990). Overviews of online AQM-MetM models are available in the literature (Zhang, 2008; Baklanov et al., 2014).

Several global AQMs have been developed during the last decades, e.g., : online multiscale GEM-AQ (1.5° x 1.5°) (Gong et al., 2012), offline TM5-chem-v3.0 (3° x 2°) (Huijnen et al., 2010), online LMDZ-INCA (3.8° x 2.5°) (Folberth et al., 2006), online GATOR-GCMM (4° x 5°) (Jacobson, 2001a), Integrated Forecast System (IFS)-MOZART used in MACC reanalysis project (horizontal resolution of about 80 km) (Inness et al., 2013) and the offline MOZART-4 (2.8° x 2.8°) (Emmons et al., 2010). Most of these models have been applied at coarse resolu-

tions. Currently, the systems are being updated and prepared for higher resolution applications.

The model presented in this study is the NMMB/BSC Chemical Transport Model (NMMB/BSC-CTM; Pérez et al., 2011; Jorba et al., 2012; Spada et al., 2013; Badia and Jorba, 2014). It is a fully online multiscale chemical transport model for mesoscale to global-scale applications, developed at the Barcelona Supercomputing Center in collaboration with NCEP, NASA-Goddard Institute for Space Studies and University of California Irvine research groups. This is the first time that the NMMB/BSC-CTM gas-phase chemistry results are evaluated over a full one-year period for the global domain with a horizontal resolution of 1° x 1.4°, higher than most of the existing global AQMs. The NMMB/BSC-CTM model, configured as a limited area model, has recently participated in the Air Quality Model Evaluation International Initiative (AQMEII)-Phase2 intercomparison exercise. A spatial, temporal and vertical evaluation of the chemical model results for the year 2010 on a regional scale are presented in Badia and Jorba (2014). Moreover, a comparison between other modelling systems currently applied in Europe and North America in the context of AQMEII phase 2 is presented in Im et al. (2014a). Other previous evaluations of the model include the dust implementation, presented in Pérez et al. (2011) and Haustein et al. (2012), and the sea-salt aerosol module, described and evaluated on a global scale in Spada et al. (2013). The aerosol module for other relevant global aerosols (natural, anthropogenic and secondary) is currently under development within the NMMB/BSC-CTM. This is an ongoing project and the final objective is to develop a fully coupled chemical multiscale (global/regional) weather prediction system able to resolve gas-aerosol-meteorology interactions and to provide chemical initial and boundary conditions for high resolution air quality forecasts with a unified dynamics-physics-chemistry environment. The aim of this chapter is to evaluate the NMMB/BSC-CTM applied at global scale in terms of the spatial distribution and seasonal variations for ozone and its precursors. This is the first time that the NMMB/BSC-CTM gas-phase chemistry results are evaluated over a full one-year period (year 2004) for the global domain with a horizontal resolution of 1° x 1.4°, higher than most of the existing global AQMs.

A full description of the NMMB/BSC-CTM concerning the atmospheric driver, the gas-phase chemistry module, the model configuration including online biogenic emissions and initial conditions is presented in Chapter 2. In Section 4.2, we present an overview of the model setup, describing the chemical and meteorological initial conditions, and the anthropogenic and natural emissions implemented in this experiment. To illustrate the capability of the NMMB/BSC-CTM to reproduce the main reactions occurring in the atmosphere, the model is evaluated with available ground-based monitoring stations, ozonesondes, aircraft data, climatology vertical profiles and satellite retrievals described in Section 4.3. The results of the model performance are discussed in Section 4.5 for an annual simulation of the year 2004. The last section is devoted to the conclusions.

Table 4.1: Model characteristics and experiment configuration

Emissions	
Biogenic emissions	MEGANv2.04 (Guenther et al., 2006)
Anthropogenic and other natural emissions	ACCMIP (Lamarque et al., 2010) and POET (Granier et al., 2005)
Resolution and Initial conditions	
Horizontal resolution	1.4° x 1°
Vertical layers	64
Top of the atmosphere	1 hPa
Chemical initial condition	MOZART4 (Emmons et al., 2010)
Meteorological initial condition	FNL/NCEP (`http://rda.ucar.edu/datasets/ds083.2/`)
Ozone tropospheric upper boundary condition	COPCAT (Monge-Sanz et al., 2011) linear stratospheric scheme
Spin up	1 year

4.2 Model setup

For the present work, the model is set up as global. The global domain is configured with a horizontal grid spacing of $1.4°x1°$ and 64 vertical layers. The top of the atmosphere is set at 1 hPa. The atmospheric model's fundamental time step is set to 180s and the chemistry processes are solved every 4 fundamental time steps. The radiation, photolysis scheme and biogenic emissions are computed every hour. NCEP/FNL are used as initial conditions for the meteorological driver. The meteorology is reinitialised every 24 h. To initialise the chemistry on the first day of simulation, initial conditions from the global atmospheric model MOZART-4 Emmons et al. (2010) are used and a spin-up of 1 year is then performed. After this spin-up, one year simulation is used for the model evaluation. Table 4.1 shows the main configuration of the model. Specifically the stratospheric ozone is solve using the COPCAT (Monge-Sanz et al., 2011) linear stratospheric scheme discussed in Chaper 3. The interaction of chemistry and meteorology is not considered in this study.

4.2.1 Emissions

Global emissions applied in the present study are based on the Atmospheric Chemistry and Climate Model Intercomparison Project (ACCMIP; Lamarque et al., 2013) emissions database for anthropogenic and biomass burning, and on the Precursors of Ozone and their Effect on the Troposphere inventory (POET; Granier et al., 2005) for soil and ocean emissions. ACCMIP anthropogenic and biomass burning emissions with $0.5°x0.5°$ horizontal resolution are described in Lamarque et al. (2010). This emission inventory is a combination of several existing regional and global inventories available. Note that specific events occurring during 2004 (e.g., large summer wildfires in Alaska and Canada) are not described in the emissions inventory, as the 2004 emissions come from a linear interpolation of 2000 and 2010 values. Two historical available emissions inventories, namely RETRO (1960-2000; Schultz and Rast (2007)) and EDGAR-HYDE (1890-1990; Van Aardenne et al. (2005)), are used in the case of surface anthropogenic emissions. Monthly variations for biomass burning, soil NO_x, ship and aircraft emissions are provided. Land-based anthropogenic have constant values for all the whole year. Lamarque et al. (2010) presents a comparison of the annual total CO anthropogenic and biomass

burning emissions (Tg(CO)/year) for different regional and global emission inventories for the year 2000 (see Table 5). Note that ACCMIP global CO anthropogenic emissions are significantly higher (610.5 Tg CO/year) than other emissions inventories (e.g. RETRO with 476 Tg CO/year, EDGAR-HYDE with 548 Tg CO/year, and GAINS with 542 Tg CO/year). NO_x lightning emissions are not included in this simulation. Emissions of NO for January and July used in this model simulation are shown in Figure 2.10 (top panel). Yearly total for anthropogenic and biomass burning are summarised in Table 4.2.

Biogenic emissions are computed online with the Model of Emissions of Gases and Aerosols from Nature version version 2.04 (MEGANv2; Guenther et al., 2006) (see Chapter 2). Isoprene biogenic emissions used in this study amount to 683.16 Tg/year. Some others global models uses lower isoprene biogenic emissions (Huijnen et al., 2010; Horowitz et al., 2003; Emmons et al., 2010). However, the annual global isoprene emissions estimated with MEGAN ranges from about 500 to 750 Tg isoprene (Guenther et al., 2006), implying that there is sizeable uncertainty.

Table 4.2: Emissions totals by category for 2004 in Tg(species)/year. Anthropogenic and biomass burning applied in this study are based on Lamarque et al. (2013). Ocean and soil natural emissions are based on the POET (Granier et al., 2005) global inventory. Biogenic emissions are computed online from the MEGAN (Guenther et al., 2006).

Species	Anthrop.	Bio. burning	Biogenic	Soil	Ocean
CO	610.5	459.6	148.13	-	19.85
NO	85.8	5.4	16.54	11.7	-
SO_2	92.96	3.84	-	-	-
Isoprene (C_5H_8)	-	0.15	683.16	-	-
Terpene ($C_{10}H_6$)	-	0.03	120.85	-	-
Xylenes (C_8H_{10})	1.05	0.16	1.36	-	-
Methanol (CH_3OH)	-	-	159.91	-	-
Ethanol (C_2H_6O)	4.28	3.7	17.06	-	-
Formaldehyde (HCHO)	4.24	0.35	9.58	-	-
Aldehyde (R-CHO)	-	-	5.06	-	-
Toluene (C_7H_8)	0.66	0.19	0.79	-	-
Ethane (C_2H_6)	1.27	0.57	0.48	-	-
Ethylene (C_2H_4)	3.32	2.71	32.03	-	-

To account for the sub-grid scale vertical diffusion within the PBL all the land-based anthropogenic emissions are emitted in the first 500 meters of the model, biomass burning emissions from forests in the first 1300 meters, biomass burning emissions from grass in the first 200 meters, ocean emissions on the first 30 meters and shipping emissions on the first 500 meters.

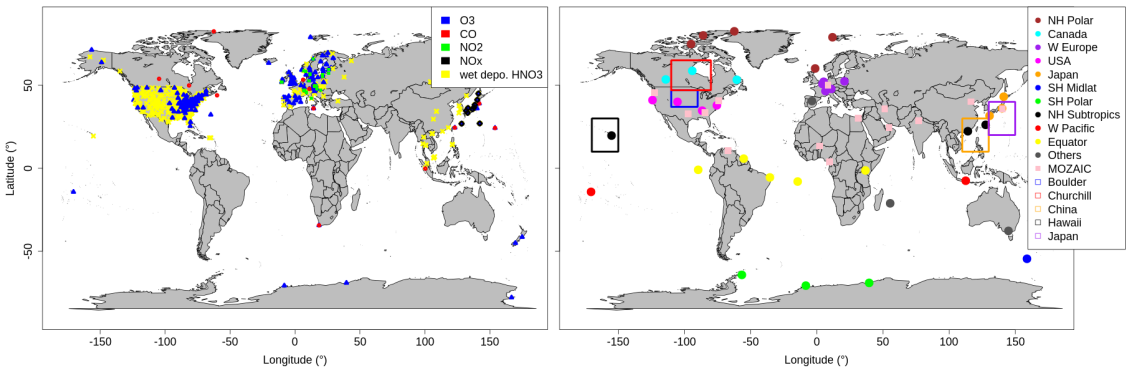

Figure 4.1: Stations used for the evaluation of the NMMB/BSC-CTM model. On the left, surface-monitoring rural stations of O_3 (blue triangle), CO (red circle), NO_2 (green square cross) and NO_X (black diamond) are shown. Moreover wet deposition HNO_3 (yellow cross) measurement locations are also presented. On the right, locations of the different ozonesondes used (O_3 vertical profiles) are shown. Ozonesonde are grouped by the following regions: NH Polar (brown circle), Canada (cyan circle), W. Europe (purple circle), USA (pink circle), Japan (orange circle), SH Midlat (blue circle), SH Polar (green circle), NH Subtropics (black circle), W. Pacific (red circle), Equator (yellow circle) and Others (grey circle). In addition, CO vertical profiles from the aircraft campaign Measurement of Ozone, Water Vapor, Carbon Monoxide, Nitrogen Oxide by Airbus In-Service Aircraft (MOZAIC) (pink square) is also presented. Finally, large rectangles show areas for the climatology analysis (NO_x, PAN and HNO_3) of Boulder (blue), Churchill (red), China (orange), Hawaii (black) and Japan (purple).

4.3 Observational data

4.3.1 Ground observations

Background stations from the World Data Centre for Greenhouse Gases database (WDCGG; `http://gaw.kishou.go.jp/wdcgg/`), the European Monitoring and Evaluation Programme (EMEP; `http://www.emep.int/`), the Clean Air Status and Trends Network in USA (CASTNET; `http://java.epa.gov/castnet/`) and the Acid Deposition Monitoring Network in East Asia (EANET; `http://www.eanet.asia/`) with available hourly data are selected for the evaluation of surface gases. O_3 data from 41 WDCGG, 52 EMEP, 64 CASTNET and 11 EANET stations having a good coverage in EU and, US, and more limited in east Asia, are used to evaluate the model. Moreover, NO_2 data from 21 EMEP and NO_x data from 10 EANET stations and CO data from 14 WDCGG stations are selected (see Figure 4.1, left panel, for the coverage maps).

HNO_3 wet deposition from the model is compared against nitrate (HNO_3 and aerosol nitrate) wet deposition observations. In this evaluation study we have selected 260 deposition measurements from the National Atmospheric Deposition Program (NADP; `http://nadp.sws.uiuc.edu/`) network in North America, 51 from the EMEP network in Europe and 28 from EANET in East Asia for the year 2004 (see Figure 4.1, left panel, for the coverage maps).

4.3.2 Vertical structure: ozonesondes and MOZAIC

The surface evaluation is complemented with an assessment of the ozone vertical structure. The model vertical structure of O_3 is compared with available ozonosondes of the World Ozone and Ultraviolet Radiation Data Center ozonosonde network (WOUDC;http://www.woudc.org/), the Global Monitoring Division (GMD; ftp://ftp.cmdl.noaa.gov/ozwv/ozone/) and the Southern Hemisphere Additional Ozonesondes (SHADOZ; http://croc.gsfc.nasa.gov/shadoz/; Thompson et al., 2003a,b).

Most of the ozonesonde stations provide between 4 to 12 profiles per month each year with a precision of $\pm$ 3-8 % in the troposphere (Tilmes et al., 2012). A total of 39 ozonesonde stations, following the study of Tilmes et al. (2012) are selected for the present evaluation. Table 4.3 summarises the main information of these ozonesondes with available profiles while the location is displayed in Figure 4.1 (right panel). Following a similar criteria as Tilmes et al. (2012), regional aggregates are formed in combining stations with similar O_3 characteristics (see Table 4.3 fifth column).

Additional observations considered in this study are vertical profiles from Measurement of Ozone, Water Vapor, Carbon Monoxide, Nitrogen Oxide by Airbus In-Service Aircraft (MOZAIC; http://http://www.iagos.fr). The modelled vertical structure of CO is compared against available MOZAIC data. These measurements are geo-localized in latitude, longitude and pressure, and come with meteorological observations. Based on the availability of data, 14 airports (shown in right panel of Figure 4.1) are selected covering different regions of the world during the whole of 2004. The number of vertical profiles available are indicated by season in Table 4.4.

In addition, we use nitric oxide (NO_x), peroxyacetyl nitrate (PAN) and acid nitric (HNO_3) vertical profiles from two different measurement campaigns: TOPSE (Atlas et al., 2003; Emmons et al., 2003) and TRACE-P (Jacob et al., 2003). Tropospheric data from these two previous campaigns together with other aircraft campaigns were gridded onto global maps with resolution 5°x5° x1km, forming data composites of important chemical species in order to provide a picture of the global distributions (Emmons et al., 2000).

When running an AQM model, it is preferable to compare the model output with an observational database from the same year as the model simulation. Nevertheless, in our case, there are insufficient global observations to achieve this goal for any full year. Hence, in this model evaluation, all the observations are for 2004, except for the vertical profiles obtained from measurement campaigns. Hence, model output from selected regions are compared with this campaign from the same regions regardless of the year of the measurements. In addition, it is valuable to compare the same regions for different species which can allow to identify systematic differences between the model results and observations (Emmons et al., 2000). Details of these campaigns describing their geographical region and period are described in Table 4.5, and the location displayed in Figure 4.1 (right panel).

Table 4.3: Ozonesondes main information used in this model evaluation for the year 2004. Location of these ozonesondes is displayed on the third and fourth column. Columns 6-9 display the number of available measurements for each season (DJF for December-January-February, MAM for March-April-May, JJA for June-July-August and SON for September-October-November).

Station	Country	Lat.	Lon.	Region	DJF	MAM	JJA	SON
Kagoshima	Japan	31.6N	130.6E	Japan	13	12	11	12
Saporo	Japan	43.1N	141.3E	Japan	12	10	12	10
Tsukubay	Japan	36.1N	140.1E	Japan	14	13	12	12
Alert	Canada	82.5N	62.3W	NH Polar	11	10	13	9
Edmonton	Canada	53.5N	114.1W	Canada	7	12	10	10
Resolute	Canada	74.8N	95.0W	NH Polar	9	10	8	6
Macquarie Island	Australia	54.5S	158.9E	SH Midlat	6	15	12	9
Lerwick	Great Britain	60.1N	1.2W	W Europe	9	13	13	12
Uccle	Belgium	50.8N	4.3E	W Europe	35	37	36	36
Goose Bay	Canada	53.3N	60.4W	Canada	12	13	13	12
Churchill	Canada	58.7N	94.1W	Canada	7	6	4	8
NyAlesund	Norway	78.9N	11.9E	NH Polar	25	24	23	17
Hohenpeissenberg	Deutschland	47.8N	Europe	11.0E	34	34	26	31
Syowa	Antarctica	69.0S	39.6E	SH Polar	16	16	19	26
Wallops Island	USA	37.9N	75.5W	USA	11	15	17	7
Hilo	USA	19.7N	155.1W	NH Subtropic	13	18	14	12
Payerne	Switzerland	46.5N	6.6E	Europe	38	40	38	40
Nairobi	Kenya	1.3S	36.8E	Equador	11	13	13	13
Naha	Japan	26.17N	127.7E	NH Subtropics	9	12	8	10
Samoa	Samoa	14.2S	170.6W	W Pacific	9	11	8	9
Legionowo	Poland	52.4N	20.9E	Europe	16	18	16	18
Marambio	Antarctica	64.2S	56.6W	SH Polar	10	7	15	22
Lauder	New Zealand	45.0S	169.7E	SH Midlat	11	13	13	9
Madrid	Spain	40.5N	3.6W	Others	11	9	8	12
Eureka	Canada	80.0N	85.9W	NH Polar	17	17	11	13
De Bilt	Nederland	52.1N	5.2E	Europe	13	10	14	12
Neumayer	Antarctica	70.7S	8.3W	SH Polar	11	13	13	31
Hong Kong	China	22.3N	114.2E	NH Subtropics	12	26	11	13
Broad Meadows	Australia	37.7S	144.9E	Others	6	7	7	11
Huntsville	USA	34.7N	86.6W	USA	14	13	23	13
Parambio	Surinam	5.8N	55.2W	Equador	11	8	9	9
Reunion Island	France	21.1S	55.5E	Others	9	14	9	6
Watukosek	Indonesia	7.5S	112.6E	W Pacific	7	11	10	6
Natal	Brasil	5.5S	35.41W	Equador	10	12	13	7
Ascencion Island	Great Britain	7.98S	Equador	14.42W	12	12	12	18
San Cristobal	Galapagos	0.92S	89.6W	Equador	7	4	10	13
Boulder	USA	40.0N	105.26W	USA	12	11	17	16
Trinidad Head	USA	40.8N	124.2W	USA	4	7	5	8
Suva	Fiji	18.13S	178.4E	W Pacific	13	12	48	11

4.3.3 Satellite data

Modelled tropospheric NO_2 and HCHO columns are compared with SCanning Imaging Absorption spectroMeter for Atmospheric CHartographY (SCIAMACHY, `http://www.sciamachy.org/`) satellite data and used in the model evaluation to provide some insights on the spa-

Table 4.4: MOZAIC aircraft information used in this model evaluation for the year 2004. Location of the MOZAIC measurements is displayed on the third and fourth column. Columns 5-8 display the number of available measurements for each season (DJF for December-January-February, MAM for March-April-May, JJA for June-July-August and SON for September-October-November).

Station	Country	Latitude	Longitude	DJF	MAM	JJA	SON
Abu Dhabi	United Arab Emirates	24.44N	54.65E	11	17	58	20
Atlanta	USA	33.63N	84.44W	24	130	168	66
Beijing	China	40.09N	116.6E	5	12	23	17
Cairo	Egypt	30.11N	31.41E	19	16	2	8
Caracas	Venezuela	10.6N	67W	21	9	9	21
Dallas	USA	32.9N	97.03W	8	24	24	10
Douala	Cameroon	4.01N	9.72E	7	0	10	6
Frankfurt	Germany	50.02N	8.53E	169	295	286	192
New Delhi	India	28.56N	77.1E	30	24	72	38
New York	USA	40.7N	74.16W	79	23	41	16
Niamey	Niger	13.48N	2.18E	4	0	12	12
Portland	USA	45.59N	122.6W	5	8	5	4
Tehran	Iran	35.69N	51.32E	8	11	31	18
Tokyo	Japan	35.76N	140.38E	38	50	56	34

Table 4.5: Description of additional aircraft campaign data. Location of the measurements campaigns is displayed on the third and fourth column. Fifth column lists the date of these campaigns.

Region Name	Expedition	Latitude	Longitude	Date
Boulder	TOPSE	37-47N	110-90W	5 February to 23 May 2000
Churchill	TOPSE	47-65 N	110-80W	5 February to 23 May 2000
China	TRACE-P	10-30N	110-130E	24 February to 10 April 2001
Hawaii	TRACE-P	10-30N	170-150W	24 February to 10 April 2001
Japan	TRACE-P	20-40N	130-150E	24 February to 10 April 2001

tial distribution of the model. SCIAMACHY (on board ENVISAT that was operational from March 2002 to April 2012) is a passive remote sensing spectrometer measuring backscattered, reflected, transmitted or emitted radiation from the atmosphere and Earth's surface with a wavelength range between 240-2380 nm. The SCIAMACHY instrument has a spatial resolution of typically 60 x 30 km^2. SCIAMACHY has three different viewing geometries: nadir, limb, and sun/moon occultation. Alternating nadir and limb views, global coverage is achieved in six days.

NO_2 daily satellite data was taken from the Institute of Environmental Physics, the University of Bremen (`http://www.iup.uni-bremen.de/doas/scia_no2_data_tropos.htm`), based on Version 3.0 data product (Hilboll et al., 2013). This dataset is an improved extension of the data presented in Richter et al. (2005). Validation of the data product used in this study has been performed in, e.g., Petritoli et al. (2004) and Heue et al. (2005). Several daily satellite overpasses of tropospheric slant column densities (SCDtrop NO_2) from SCIAMACHY radiances using the limb/nadir matching approach, are available and used in this study (Hilboll et al., 2013). The total uncertainty of these tropospheric column data is estimated to vary between 35-60% in heavily polluted cases and $>$100% in clean scenarios (see Boersma et al. (2004)).

Daily satellite retrievals from SCIAMACHY tropospheric HCHO columns are provided by the BIRA/KNMI retrieval (De Smedt et al., 2008). Level 2 data file, available on the TEMIS webpage (`www.temis.nl`), is used in this model evaluation. SCIAMACHY HCHO validation are found in the literature (Dufour et al., 2009; De Smedt et al., 2008). Total errors of the monthly mean HCHO observations from SCIAMACHY are estimated to range between 20-40%, but individual can have much larger errors (De Smedt et al., 2008). These range of errors need to be considered when evaluating the model HCHO results.

Additionally, CO mixing ratios at 800 and 500 hPa are evaluated with the Measurement of Pollution in the Troposphere (MOPITT: `http://www2.acd.ucar.edu/mopitt`) instrument retrievals. The MOPITT, aboard the NASA EOS-Terra satellite, is a gas filter radiometer and measures thermal infrared (near 4.7 μm) and near-infrared (near 2.3 μm) radiation, only during clear-sky conditions, with a ground footprint of about 22 km x 22 km. The MOPITT satellite overpasses cover the whole day. The MOPITT Version 5 (V5) Level 2 data product, which was used here, provides daily surface CO mixing ratios. MOPITT CO mixing ratios have been validated with in situ CO profiles measured from numerous NOAA/ESRL aircraft profiles in Deeter et al. (2013), and they were found to be positive biased by about 1% and r = 0.98 at the surface level.

4.4 Statistical Measures

There are several metrics that are used by the modelling community to evaluate performances of AQMs (U.S.EPA, 1991; Cox and Tikvart, 1990; Russell and Dennis, 2000). The statistical indicators selected in this study are: Correlation coefficient (r: Eq. 5.1) , Mean Bias (MB: Eq. 5.2) and Root Mean Square Error (RMSE: Eq.5.3).

$$r = \frac{1}{N} \frac{\sum_{i=1}^{N} (O_i - \overline{O})(P_i - \overline{P})}{\sigma_O \sigma_P} \tag{4.1}$$

$$MB = \frac{\sum_{i=1}^{N} (P_i - O_i)}{N} \tag{4.2}$$

$$RMSE = \sqrt{\frac{1}{N} \sum_{i=1}^{N} (P_i - O_i)^2} \tag{4.3}$$

where σ is the standard deviation and P and O denote the vector of model output and the vector observations, respectively. No threshold has been applied in the computation of the statistics.

4.5 Model evaluation

This section presents the evaluation of relevant trace gases from the NMMB/BSC-CTM and compares them with different sets of observations described in the previous section. Concerning the surface-level comparison, three-hourly averages from the observations and model are used to compute daily ozone averages and calculate some statistical measures defined previously in Section 4.4. Ground-monitoring stations were selected with a maximum altitude of 1000 meters. In the case of ozonesondes and MOZAIC the comparison is made only when vertical profiles observations are available; thus, the data from the model and the observations are collocated/simultaneous. Similar criteria is used in the case of MOPITT and SCIAMACHY, though for HCHO, and NO_2. Moreover, averaging kernels for CO are taken into account to represent the observational sensitivity at different pressure levels. When computing the modelled tropospheric columns of NO_2 and HCHO, the tropopause was assumed to be fixed at 100 hPa in the tropics and 250 hPa in the extratropics. Similarly, when comparing model data with data composite from aircraft campaigns the same period of the year at the same location is selected and mapped into the same grid resolution, 5° x 5° x 1km, before the comparison is made. For some species, the model evaluation is given per seasons: DJF for December-January-February, MAM for March-April-May, JJA for June-July-August and SON for September-October-November.

4.5.1 Hydroxyl Radical (OH)

One of the means of characterizing the general properties of an AQM is through its ability to simulate OH oxidation. The OH is the main oxidant in the troposphere and is responsible for the removal of many compounds from the atmosphere, thereby controlling their atmospheric abundance and lifetime. OH is mostly found in the tropical lower and mid troposphere with a strong dependence in high levels of ultraviolet radiation and water vapour. The tropospheric OH formation is mainly due to O_3 photolysis, dominated by the tropics. On the other way, OH is directly connected to the chemistry of O_3 production since the initial reactions of O_3 formation (VOC+OH and CO+OH) are driven by OH. Hence, the O_3 production rates depend on the sources and sinks of odd hydrogen radicals. Primary OH formation also includes the photolysis of HCHO and secondary VOC.

The tropospheric mean (air mass weighted) OH derived by the model is 11.5 molec 10^5 cm^{-3}. This value was estimated assuming a troposphere domain from 200 hPa to the surface. Previous studies suggest that the differences between this estimate do not depends on the definition of the tropopause (Voulgarakis et al., 2013). Our tropospheric mean OH is in good agreement with other studies, such as Voulgarakis et al. (2013) where the global multimodel (14 models) mean OH concentration for 2000 is estimated as 11.1 ± 1.8 10^5 molec cm^{-3}, Spivakovsky et al. (2000) with 11.6 10^5 molec cm^{-3}, and Prinn et al. (2001) that estimates this value by 9.4 ± 0.13 10^5 molec cm^{-3}.

The zonal mean OH concentrations calculated for January, April, July and October 2004 are shown in Fig 4.2. Seasonal differences are seen reflecting the impact of high concentrations of water vapor and low stratospheric ozone column, meaning higher incident ultraviolet (UV)

radiation (Spivakovsky et al., 2000; Lelieveld et al., 2002). Highest concentrations of OH arise in the tropics throughout the year. In northern midlatitudes, the highest OH concentrations are found during summer in the lower to middle troposphere. The latitude and seasonal variation in the modelled OH concentrations are comparable to the climatological mean computed by Spivakovsky et al. (2000). Lower values in the extratropics are well captured by the model. However, the model peak concentrations are slightly larger in comparison with this climatology and also with other studies (e.g., Horowitz et al., 2003; Huijnen et al., 2010). During January and October these peaks are seen in the southern tropics between 700-1000 hPa and 800-1000 hPa, respectively. The peak for April and July is found in the northern tropics between 800-1000 hPa and 700-1000 hPa, respectively. The implied OH overestimates could be explained by the lack of aerosols in the simulation of photolysis, leading to an atmosphere with excessive oxidising capacity, especially, below the aerosol layers (boundary layer of polluted regions).

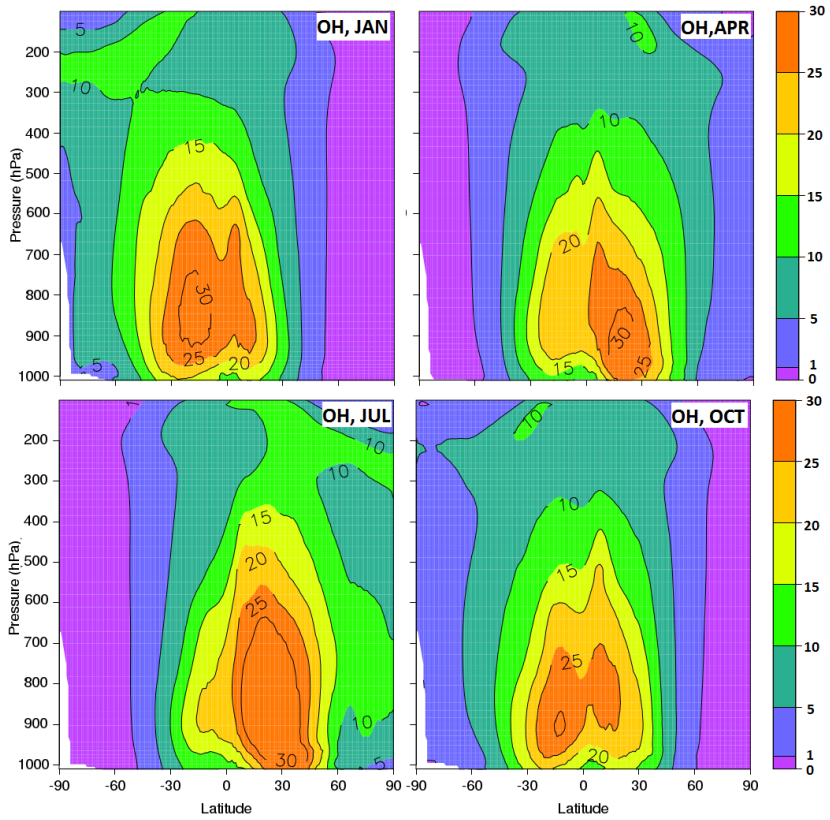

Figure 4.2: Zonally monthly mean OH concentrations (10^5 molecules / cm^3) for January, April, July and October by the NMMB/BSC-CTM model

4.5.2 Carbon monoxide (CO)

Carbon monoxide (CO) exerts a high influence on the concentrations of oxidants such as the hydroxyl radical (OH) and ozone (O_3); thus, CO is one of the most important trace gases in the troposphere (Wotawa et al., 2001). Main sources of CO in the troposphere is by photochemical production from the hydrocarbons oxidation and by direct emissions, mainly fossil fuel combustion, biomass burning and biogenic. CO main loss in the troposphere is by the reaction with OH, occurring primarily in the tropics but also in the extratropics. In the northern extratropics, CO concentrations are dominated by high anthropogenic emissions and precursor hydrocarbons, leading to a net CO export to the tropics (Shindell et al., 2006; Bergamaschi et al., 2000). Although most biomass burning occurs in the tropics, gases and aerosols emitted from large wildfires can be transported to the southern extratropics, where emissions and chemical production are lower. Moreover, due to the strong convection, enhanced by forest fire activity, emissions can reach the upper troposphere and lower stratosphere layers (Jost et al., 2004; Cammas et al., 2009). CO has chemical lifetime of a few months (1$\sim$ 3), and therefore it can be a very useful tracer for transport processes. Thus, comparing modelled CO with observations might be a useful diagnostic of both transport and emissions in the model. Before we start this evaluation, it is important to keep in mind that despite the Alaskan and Canadian wildfires that occurred during the summer, globally the year 2004 had lower CO concentrations in comparison with other years (Elguindi et al., 2010).

An analysis of the CO burden in different regions is given in Table 4.6. The global and annual mean burden of CO for 2004 is 399.03 Tg, with higher abundances in the tropics (229.43 Tg CO), followed by the concentration in the Northern Extratropics (101.71 Tg CO), and the concentration in the Southern Extratropics (67.88 Tg CO). Other model studies of the CO burden have also been performed by Horowitz et al. (2003) (MOZART-2) and Huijnen et al. (2010) (TM5), which are also shown in Table 4.6. Our model CO burden is higher ($\sim$ 46-48 Tg CO) in comparison with these studies in all regions. The largest absolute difference is in the tropics where our model has $\sim$ 30-40 Tg CO more than these studies, even though OH is also overestimated. The main sources of CO in the tropics are from biomass burning, biogenic emissions and anthropogenic direct emissions of CO. For instance, preliminary tests have been done comparing the annual mean burden of tropospheric CO with and without biomass burning emissions in the model simulation. We have detected that in the simulation without biomass burning emissions only 7% of the tropospheric CO annual mean burden is reduced. Hence, other factors also have an influence on this higher CO burden. On the other hand, as we explain in section 2.4.1, biogenic emissions are computed online every hour in order to account for evolving meteorological changes, such as solar radiation and surface temperature. Note that the model does not have implemented the attenuation of radiation due to aerosols (e.g. from big fires). This limitation implies that the radiation is higher than has to be and consequently VOCs biogenic emissionsare higher too, and CO production from biogenic VOCs may be overestimated. In addition, the CO anthropogenic emissions used in this study (610.5 Tg/year) are higher in comparison with other inventories (see 4.2.1). Then, part of this CO overestimation might be due to higher anthropogenic or biogenic emissions in the tropical area. Having said that, the higher CO burden over the tropics requires further investigation.

Table 4.6: Annual mean burden of tropospheric CO (Tg CO) in NMMB/BSC-CTM, MOZART-2 and TM5 global models

Model	Reference
NMMB/BSC-CTM	This study
MOZART-2	Horowitz et al. (2003)
TM5	Huijnen et al. (2010)

Model	Burden						Dry depo.
	Global	NH	SH	Trop.	N. Extra.	S. Extra.	
NMMB/BSC-CTM	399	221	177	229	101	67	24
MOZART-2	351	210	142	199	102	50	2
TM5	353	-	-	188	106	59	184

Dry deposition of CO at the surface seems to be significantly weaker in the NMMB/BSC-CTM (24 Tg CO) than the global model TM5 (184 Tg CO) and the study of Bergamaschi et al. (2000) (292-308 Tg CO) (see Table 4.6). By contrast, other global models such as MOZART-2 has significantly lower dry deposition (2 Tg CO) and the study of Wesely and Hicks (2000) suggests that CO and other relatively inert substances are deposited very slowly. Clearly, there are major uncertainties in the sources and sinks of CO that could be responsible of our modelled CO biases.

Fig 4.3 shows the time series of CO daily mean concentration over 14 ground-monitoring stations from the WDCGG database (primarily in the northern mid-latitudes, but with a few of them in the tropics and southern mid-latitudes). The solid red line and the solid black line represent, respectively, the average of observations and model simulation. Bars show the 25th-75th quartile interval of all observations (orange) and model simulation (grey). The model is in good agreement with the CO field in the surface layer. However, the model is not able to fully capture the seasonal CO variability, with a slight underestimation during cold months and overestimation during warm months. Such a model limitation could be explained by the fact that most of the stations are closer to anthropogenic polluted areas, where its concentration is primarily determined by local emissions, and the CO land-based anthropogenic emissions inventory does not have any seasonal variation in this study (see Section 4.2.1).

Figure 4.4 shows the CO mean bias (MB), correlation and root mean square error at all rural WDCGG stations. The model has a negative MB over stations in Europe and Japan and a positive bias in stations in Canada and Africa, where the correlations are low. The negative bias for several of the northern mid-latitude stations indicates that the higher CO burden found in our model compared to other models in these areas is a feature mainly driven by free tropospheric abundances. Higher correlations are found in northern regions of Europe, South Africa and East Asian countries. Correlation in Canadian stations is between 0.3-0.5. In most of the stations, RMSE is found to be less than 60-40 $\mu g\ m^{-3}$; only 4 stations have an RMSE higher than 60 $\mu g\ m^{-3}$.

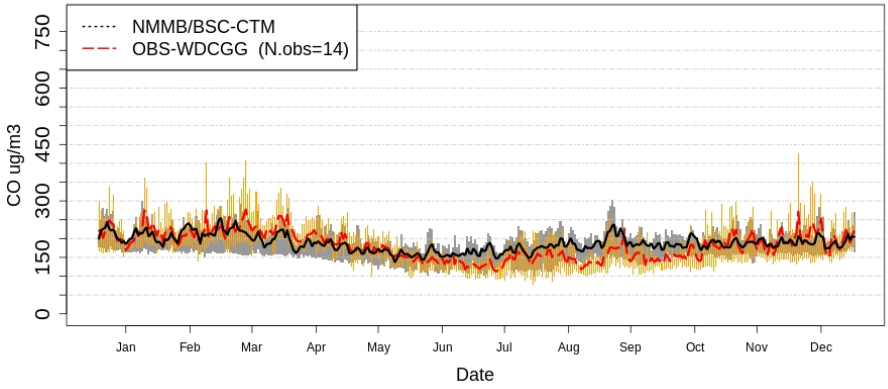

Figure 4.3: Time series of CO daily mean concentration in $\mu g\ m^{-3}$, averaged over all the rural WDCGG stations used. Observations are in a solid red line and model data in a solid black line. Bars show the 25th-75th quartile interval for observations (orange bars) and for model simulation (grey bars).

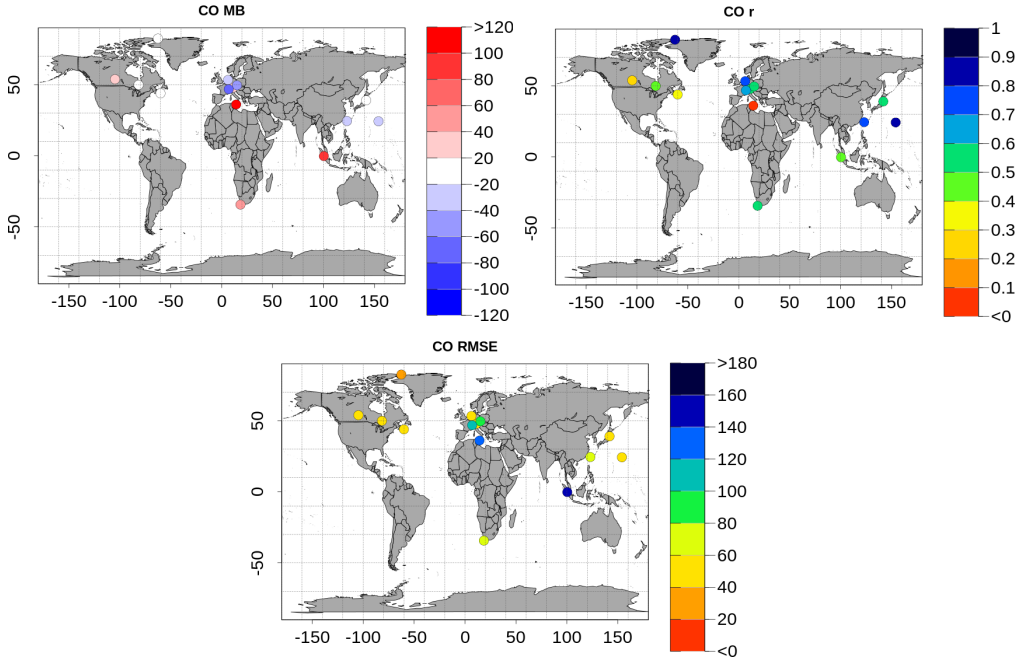

Figure 4.4: CO spatial distribution of mean bias (MB, %) (top left panel) , correlation (r) (top right panel) and root mean square error (RMSE,$\mu g\ m^{-3}$) (bottom panel) at all rural WDCGG stations used.

Additionally, the model has been compared with the seasonally averaged vertical profiles of CO from MOZAIC aircraft observations for 2004 in Figure 4.5 from selected airports: Frankfurt, Beijing, Atlanta, Portland, Abu Zabi and Niamey (from top to bottom). The comparison is made only when observations are available; thus, the same data from the model and the observations are used. Measurements are represented by the solid red line and the model simulation by the solid black line. To understand the variability of data, standard deviation is plotted in each vertical layer for both model and observations. It is important to note that the number of flights is significantly different between the different airports; therefore, not all comparisons are statistically robust. In addition, note that the scale for Beijing is different (0-1000 ppb) from the others stations (0-400 ppb). The model captures well the first part of the year, with higher biases during the warm months. Generally it overestimates CO from middle to the upper troposphere in most of the stations throughout the year. Over Frankfurt, the model is in good agreement with the observation during the whole year, despite a slight underestimation during MAM and overestimation during SON in the middle troposphere. For Beijing, one of the most polluted cities in the world, the model shows a clear tendency to underestimate CO in the lower atmosphere (below 600hPa). Probably due to an underestimation in the CO anthropogenic emissions. Most of the CTMs seem to be unable to capture the extreme growth of anthropogenic emissions in China (Akimoto, 2003; Turquety et al., 2008). Over Atlanta, the model performs much better during the winter and spring along the troposphere but positive biases ($\sim$ 20-25 ppb) are seen during the summer and autumn. Regions with biomass burning and biogenic influence, such as Abu Dhabi and Niamey, show a significant overestimation during warm months throughout the tropospheric column.

During winter, CO vertical profiles underestimation in airports located in the NH is also seen in Stein et al. (2014), where the global model MOZART-3 is compared against monthly averaged CO profiles from MOZAIC in Frankfurt and North America airports.

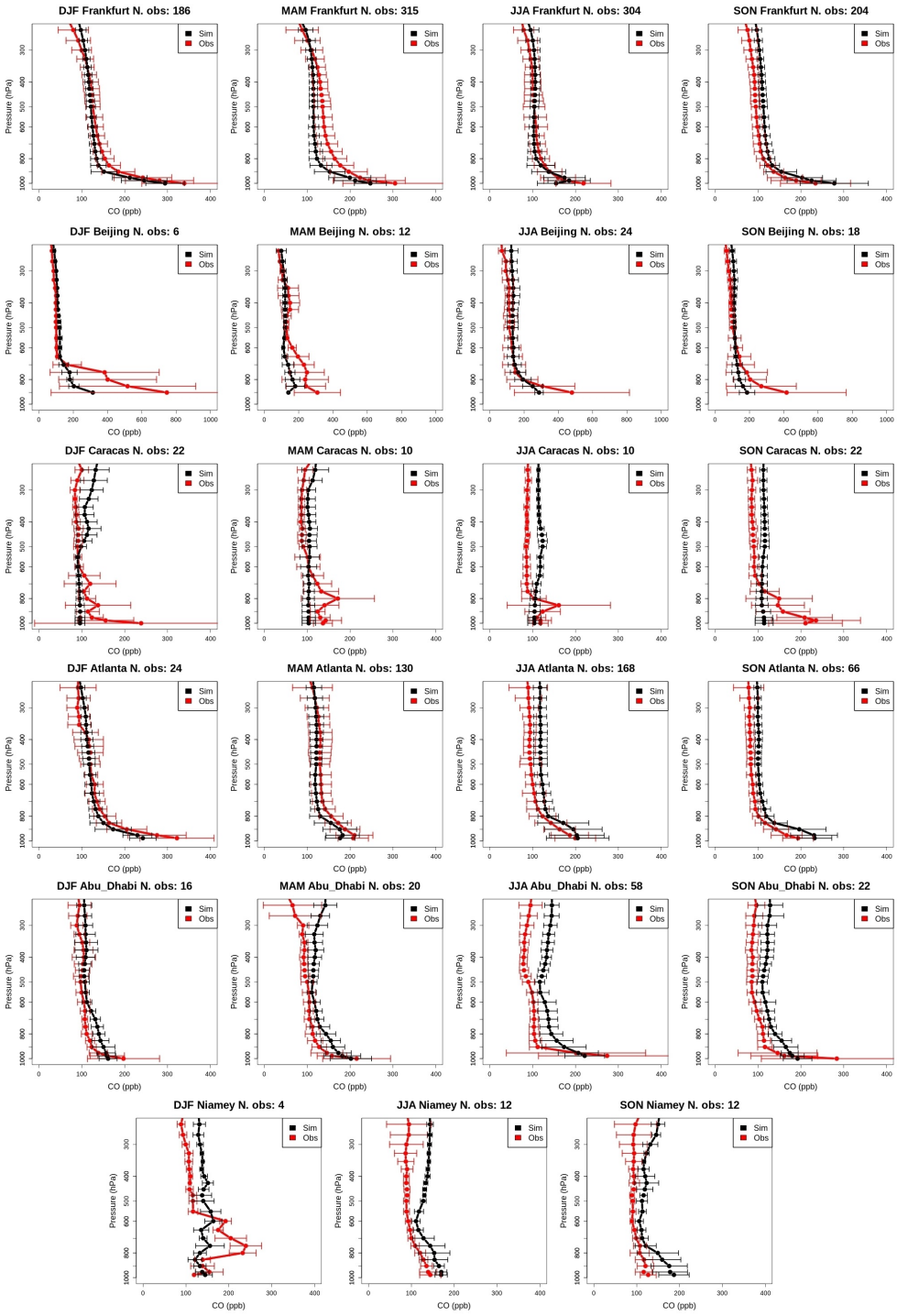

Figure 4.5: CO vertical profile seasonal averages over Frankfurt, Beijing, Atlanta, Portland, Abu Zabi and Niamey (from top to bottom) for the whole year 2004. Observations are in a solid red line and model data in a solid black line. The number of observations flights is given on the top of each plot.

To complete this CO model evaluation, we compare seasonal averaged model results with data from the MOPITT instrument at 800hPa and 500hPa in Figs. 4.6 and 4.7, respectively. At 800hpa, largest differences are seen during winter and spring, where the model clearly overestimates in the tropics and underestimate in the north extratropics and north of Africa. The negative bias in winter ($\sim$ 10-35 ppb) in the NH could further be explained by the lack of a seasonal cycle in anthropogenic emissions. However, the underestimation during NH winter is seen by most state-of-the-art CTMs and can be originated from an underestimation of CO sources (Stein et al., 2014).

Significantly positive biases are seen over west-central Africa and also over western South America, Indonesia and surrounding Pacific and Indian oceans during the dry season. Sources of CO over west-central Africa are mainly from biomass burning and biogenic emissions. Uncertainties in the emission inventories have probably contributed to the CO overestimation for these regions. Due to the long-range transport of CO, higher CO concentrations are seen during all the year over the tropics and are extended over some parts of the extratropics from June to November. Hence, during JJA and SON the model overestimates in most of the places including south and central of EU and USA ($\sim$ 10-25 ppb). At 500hPa, the model presents similar results as 800 hPa, with a clear underestimation in the north extratropics and overestimation in the tropics and southern latitudes. Higher emissions in Africa or Asia above the PBL can lead to this positive bias in the middle of the troposphere due to the transport of CO from the lower to the higher levels.

Naik et al. (2013) presents an annual average bias of multi-model (17 global models) mean CO for 2000 against average 2000-2006 MOPITT CO at 500 hPa. These models used the same anthropogenic and biomass burning emissions as our study, and a priori and averaging kernels are taken into account for each model before computing biases. Similar biases are seen in the tropics and extra tropics as in our model results. Hence, these biases might possibly be related to discrepancies in anthropogenic and biomass burning emissions inventories, where the magnitude, and perhaps location of emission is not completely understood or correctly modelled. In Naik et al. (2013), the authors also discuss too high OH concentrations possibly leading to the northern mid-latitude underestimates of CO, which is also a possibility in our case, given the high OH concentrations that our model shows compared to other models. Numerous studies show the variability in simulated CO among CTMs is large, and uncertainties are diverse including emission's inventories and injection height (Elguindi et al., 2010; Shindell et al., 2006; Prather et al., 2001). A detailed evaluation of MOPITT V4 CO retrievals between 2002-2007 with in situ measurements show bias of about -6% at 400 hPa (Deeter et al., 2010). However, this bias is not able to explain the model biases that vary in sign and magnitude between different regions of the globe. Stein et al. (2014) suggests that the persistent negative bias in northern mid-latitude CO in models is most likely due to a combination of too low road traffic emissions and due to dry deposition errors.

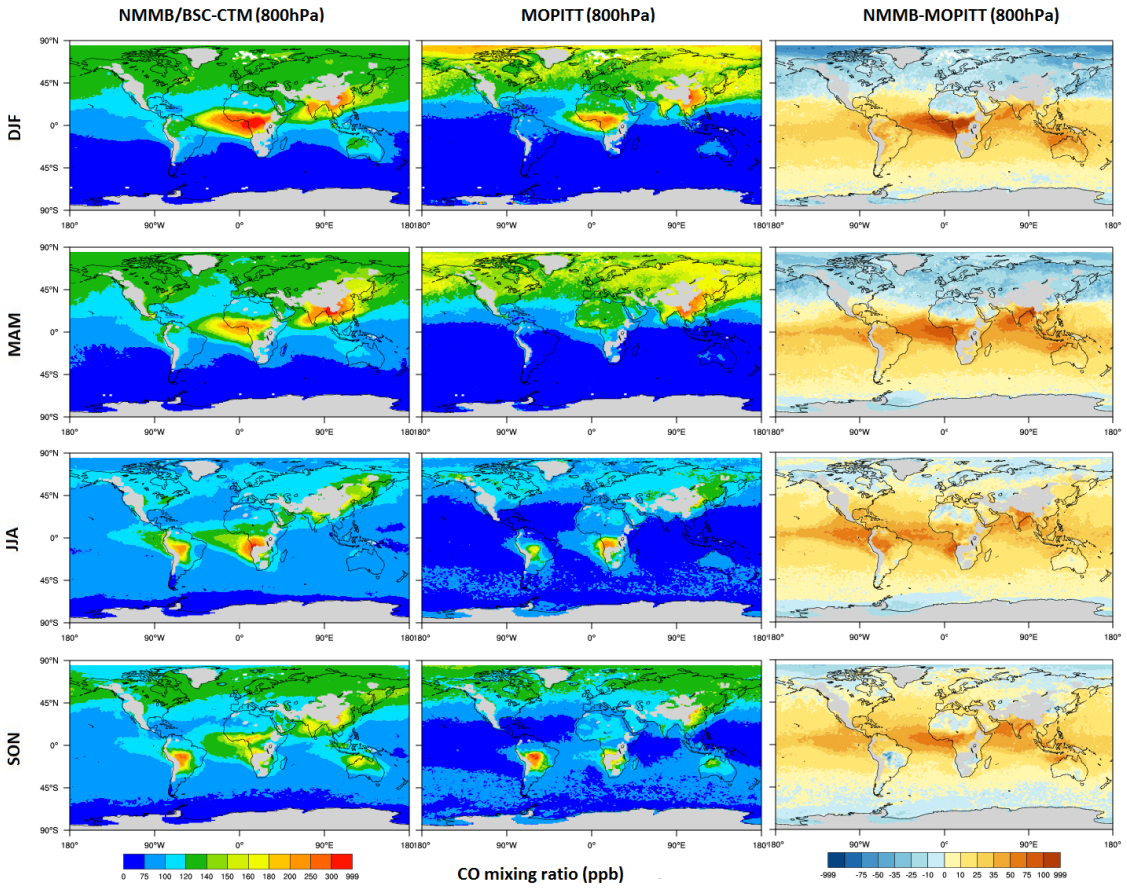

Figure 4.6: Comparison of modelled NMMB/BSC-CTM CO mixing ratio at 800hPa against satellite data (MOPITT) for (from top) (DJF for December-January-February, MAM for March-April-May, JJA for June-July-August and SON for September-October-November) for the whole year 2004 in ppb. NMMB/BSC-CTM data is displayed in the left panel, MOPITT data in the middle panel and the bias in the right panel.

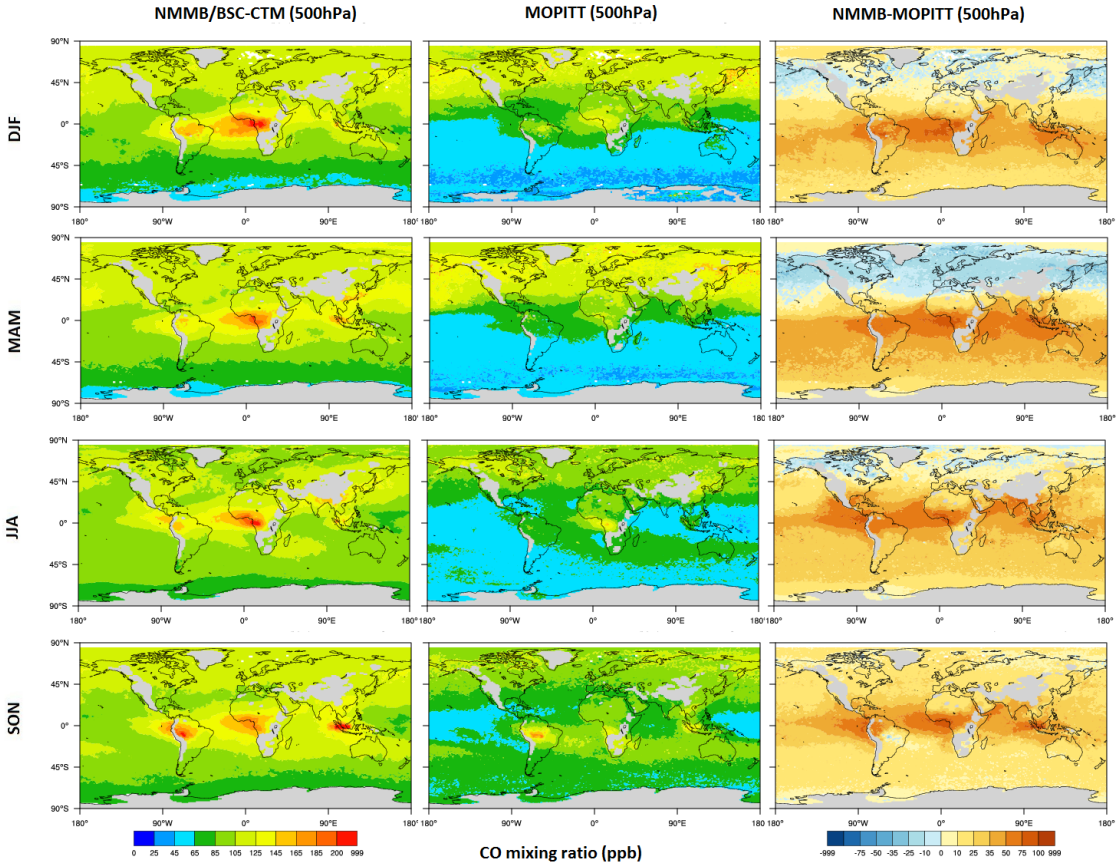

Figure 4.7: Comparison of modelled NMMB/BSC-CTM CO mixing ratio at 500hPa against satellite data (MOPITT) for (from top) DJF, MAM, JJA, and SON for the whole year 2004 in ppb. NMMB/BSC-CTM data is displayed in the left panel, MOPITT data in the middle panel and the bias in the right panel.

4.5.3 Formaldehyde (HCHO)

Formaldehyde (HCHO) is one of the most abundant hydrocarbons in the atmosphere with a lifetime of typically a few hours (Arlander et al., 1995). It is an important indicator of NMVOC emissions and photochemical activity (Chance et al., 2000). HCHO is a primary emission product from biomass burning (Carlier et al., 1986), fossil fuel combustion (Anderson et al., 1996) and biogenic emissions. However, the main source of HCHO in the atmosphere is by photochemical oxidation of methane and non-methane hydrocarbons. The principal removal processes during daytime are by the photolysis reactions and OH radicals oxidations. HCHO is photodissociated to form HCO, which reacts with oxygen producing CO, precursor of CO_2. HCHO photolysis and its oxidation by OH radicals generate hydroperoxy radical (HO_2) which react with NO to form NO_2, a precursor of O_3. An important removal process during the night is by wet and dry deposition (Altshuller, 1993).

Figure 4.8 shows the comparison between seasonal mean SCIAMACHY total columns and the corresponding NMMB/BSC-CTM seasonal average (no averaging kernel application) HCHO tropospheric columns. Note that, as we explain in Section 4.3.3, generally monthly mean HCHO satellite retrievals have a total error of 20-40%; hence the quality of the satellite measurement is not sufficient for a quantitative comparison. The satellite HCHO observations provides information about the localization of biomass burning, NMVOCs biogenic emissions, and the anthropogenic activities, and thus allow for evaluating the modelled geographical distribution.

The largest HCHO concentrations are present in the tropics around regions exhibiting high biogenic VOC emissions and biomass burning. For that reason, higher concentrations are found during the main fire season. In the northern extratropics, higher concentrations are found during the summer and are indicative of the oxidation of the isoprene emitted during the growing season (see Figure 2.10 for isoprene emissions). In central Africa and Southeast Asia maximum values are seen during DJF. Over South America, South of the equator and Europe, the maximum HCHO values are found in JJA. HCHO concentrations in the region of Indonesia are always high, with a minimum observed during SON. Over northern Australia, HCHO concentrations are largest during DJF and SON. The model is able to capture the spatial and seasonal variation in HCHO tropospheric columns as observed by SCIAMACHY. Although, positive model biases over central Africa, Australia and Southeast Asia in March and the Amazon and eastern United States in August point to uncertainties in the biogenic and biomass burning emissions. Over the ocean, the model is in good agreement with the observations with similar HCHO concentrations.

Comparing with other studies, Inness et al. (2013) also presents a seasonal mean tropospheric HCHO columns using the MACC reanalysis global model. Our HCHO results are in good agreement with the MACC reanalysis, though slightly higher mainly in Australia, central Africa and Southern Asia during DJF, were biogenic emissions are higher. The too high HCHO concentrations in the tropics may be partly contributing to the CO biases found there (photolysis of HCHO produces CO), though we expect this effect to be minor compared to other factors (e.g. errors in CO emissions).

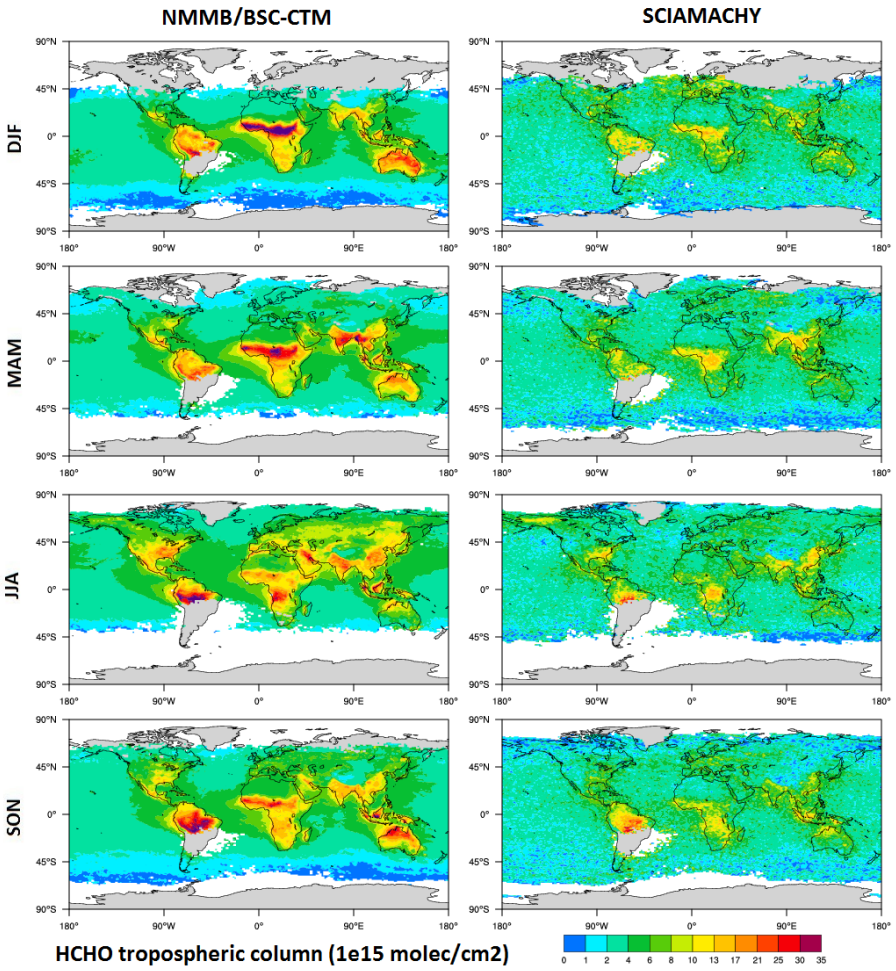

Figure 4.8: Seasonal mean tropospheric HCHO columns from NMMB/BSC-CTM vs SCIAMACHY total column retrieval

4.5.4 Nitrogen compounds

The NO_x(= NO_2 + NO) family is one of the key players in the formation of the O_3 in the troposphere, and during pollution episodes causes photochemical smog and contributes to acid rain. It has a relatively short lifetime; consequently, it is generally restricted to emission sources, both natural and anthropogenic (mainly fossil fuel combustion). The seasonal cycle of NO_x near the surface is controlled by the seasonality of anthropogenic emissions (especially in the North hemisphere) and biomass emissions (especially in the South Hemisphere). As a result, NO_x is more sensitive to errors in emissions than other pollutants, and errors in NO_x emissions can change NO_x concentrations even more drastically (Miyazaki et al., 2012).

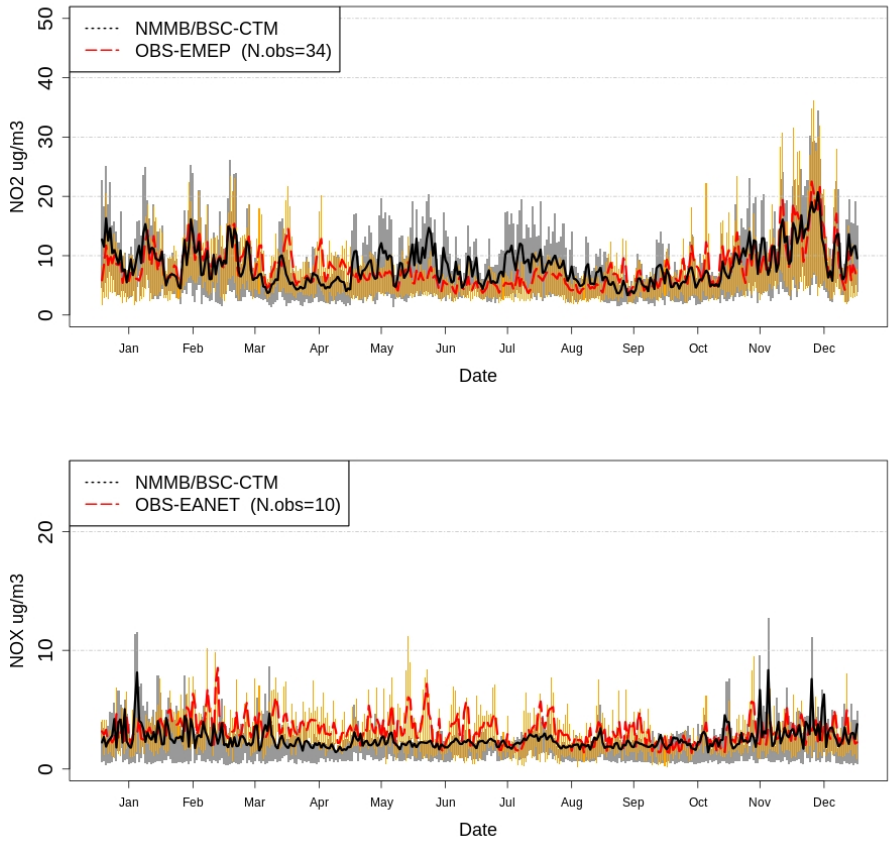

Figure 4.9: Time series of NO_2 (top) and NO_x (bottom) daily mean concentration averaged over all the rural EMEP and EANET stations, respectively, used in $\mu g\ m^{-3}$. Observations are in a solid red line and model data in a solid black line. Bars show the 25th-75th quartile interval for observations (orange bars) and for model simulation (grey bars).

Figure 4.9 shows the time series of NO_2 and NO_x daily mean concentrations over 21 and 10 ground-monitoring stations from the EMEP and EANET network, respectively. In both cases, the model is able to successfully reproduce the seasonal cycle of NO_2 and NO_x. However, a positive bias is found during the summertime for NO_2 in Europe (Figure 4.9 top panel). Such a result could be explained by the limitation on the anthropogenic emissions that are constant during the whole year. Because of that, the model cannot reproduce the decrease on anthropogenic emissions during the summertime leading to higher concentrations. Daily profiles show that the model tends to be too high at nighttime (not shown). This result may be due to the lack of the heterogeneous formation of HNO_3 through N_2O_5 hydrolysis, an important sink of NO_2 at night (Badia and Jorba, 2014). In addition, the current model does not consider secondary aerosol formation for the present exercise, which might result in an atmosphere that is too oxidising (overestimation of OH radicals), and in combination with the nocturnal chemistry this may lead

to an accumulation of NO_2 in the surface layers. However, a slight underestimation is observed between 9-18 UTC. Looking at the annual time series of NO_x in the Asian network (Figure 4.9 bottom), we observed that the model is not able to reproduce NO_x values, with a sizeable negative bias during the summer. This underestimation could be attributed to an underestimation in the emissions inventories which do not capture the extreme increase of anthropogenic emissions over Asia during the last decade (Akimoto, 2003; Richter et al., 2005), as was the case for CO.

Concerning the spatial statistics (see Figure 4.10), the model's skills are lower in some regions such as Iberian Peninsula and most of the stations in Japan, with poor correlations. Best performance is seen in central EU and Japan stations that are not in the main island. In general there is a negative bias in most of the stations for these two regions.

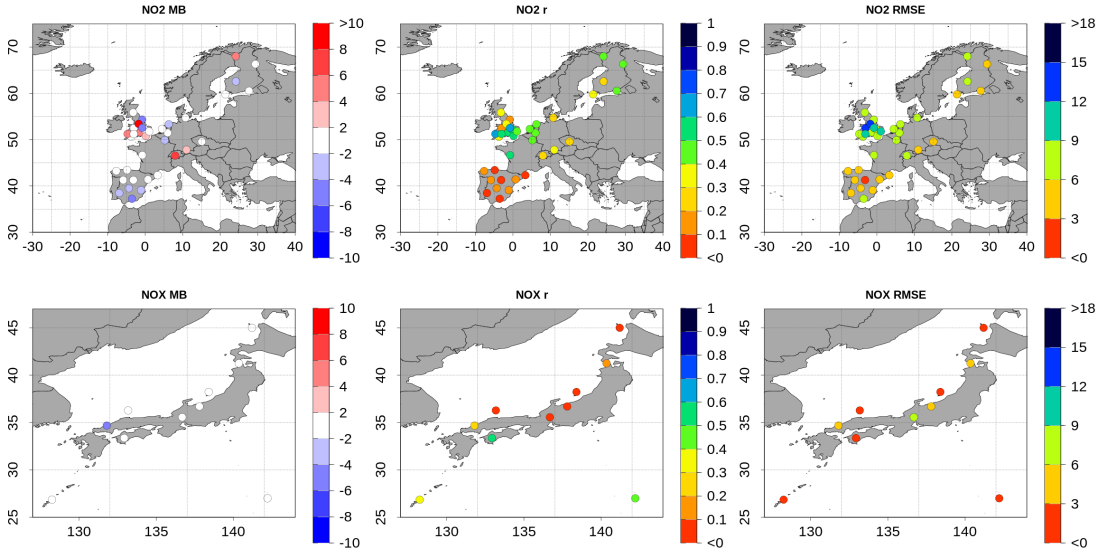

Figure 4.10: NO_2 (top) NO_x (bottom) and spatial distribution of mean bias (MB, %) (left panel) , correlation (r) (middle panel) and root mean square error (RMSE, $\mu g\ m^{-3}$) (right panel) at all rural EMEP and EANET, respectively, stations used

Comparison of modelled and observed vertical profiles of NO_X, HNO_3 and PAN are presented in Figure 4.11 for several regions over US, China, Hawaii and Japan (see Table 4.5 for more detail). As we explain in Section 4.3.2, these observational vertical profiles are not from the same year as the model simulation (see Table 4.5 for more detail), however, the qualitative patterns may provide insights on the model skills to reproduce the chemistry involved. Figure 4.11 (first column) shows that vertical profiles of NO_X are in a very good agreement with the observed values. The model has a tendency to overestimate values near the surface, it is likely that NO_X emissions used in this study are higher than the real emissions during these campaigns period. Another reason for these higher values over island locations (Japan and Hawaii) could be that emissions in the surface are spread throughout the entire model grid box while the measure-

ments might measure in the clean marine boundary layer. In the middle and upper troposphere the model well reproduces the concentrations with a slight of underestimation in most of the locations. Note that NO_x lightning emissions are not included in this simulation, explaining part of this underestimation especially in the upper troposphere.

PAN is the principal tropospheric reservoir species for NO_x with important implications for the tropospheric O_3 production and of the main atmospheric oxidant, OH (Singh and Hanst, 1981). PAN is mainly formed in the boundary layer by oxidation of non-methane volatile organic compounds (NMVOCs) in the presence of NO_x. NMVOCs and NO_x have both natural and anthropogenic sources. Rapid convection can transport PAN to middle and upper troposphere and enables the long-range transport of NO_x away from the urban and polluted areas, where it can produce O_3 and OH remotely. Some features of vertical profiles are well-captured by the model, although the model largely overpredicts PAN concentrations (see Figure 4.11, second column). Higher concentrations at the surface to middle atmosphere are found in Japan, China, Boulder and Churchill, which present a high positive bias in the vertical profile, possibly explained by an overestimation in biogenic and anthropogenic NO_x emissions in this area at the surface-level. Another possibility for this overestimation of the modelled PAN might be attributed by a too long lifetime of calculated PAN. At most sites, PAN model concentrations tend to increase with altitude, reaching its maximum mixing ratios around 6km, and above that level it starts to decrease. This behaviour explains the long thermal decomposition time of PAN (lifetime of approximately a month) and the slow loss by photolysis in the cold middle-upper troposphere. Fischer et al. (2014), presents a sensitivity of PAN to different emission types. It shows that most of the northern hemisphere and Japan is more sensitive to anthropogenic emissions and south hemisphere and the west coast of the USA to biogenic emissions, both contributing to 70-90% PAN concentrations.

HNO_3 is mainly produced by the reactions of NO_2 with OH and by the hydrolysis of N_2O_5 on aerosols (we do not account for this reaction in this simulation), and then it is removed by wet and dry deposition. HNO_3 is the main sink of NO_x chemistry. In general, the modelled and observed nitric acid concentrations are in good agreement throughout the troposphere, although the model reveals a tendency to overestimate HNO_3 concentrations, which is more pronounced in USA regions. In the regions of Hawaii, Japan and China the model overestimates HNO_3 in the lower-middle troposphere (up to 5km) and underestimates it in the upper troposphere (above 6km). Overestimation of HNO_3 in the troposphere is a common problem in global models (Hauglustaine et al., 1998; Bey et al., 2001b; Park et al., 2004; Folberth et al., 2006). One possible reason for this overestimation is that the scavenging from the convective precipitation is underestimated. Hence, HNO_3 concentrations are highly sensitive to the parameterization of wet deposition.

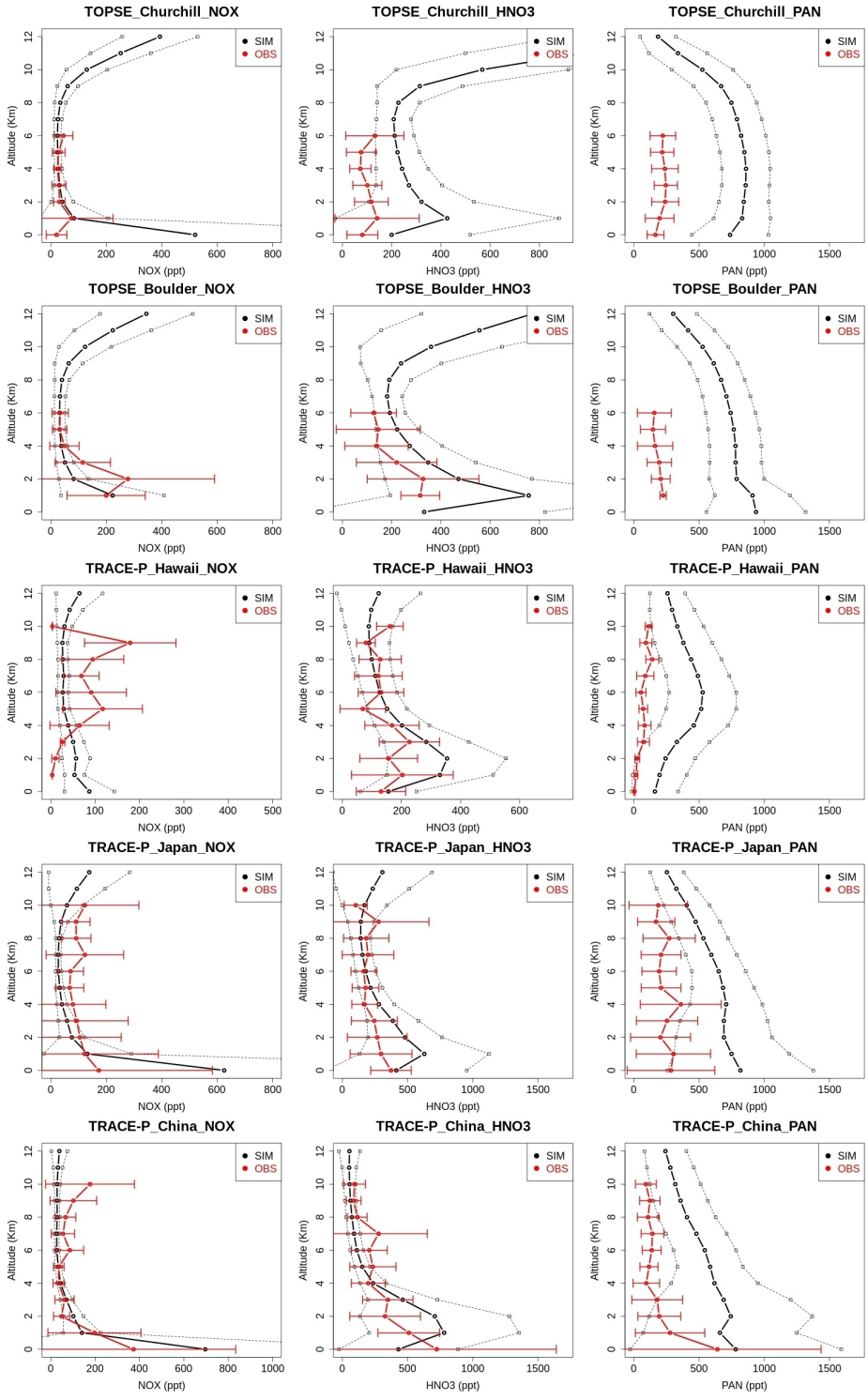

Figure 4.11: Comparison of modelled (black lines) and observed (red lines) vertical profiles of NO_X (first column), HNO_3 (second column) and PAN (third column) for several regions over US, China, Hawaii and Japan.

Figure 4.12 presents the wet deposition fluxes of HNO_3 in comparison with nitrate observations for three different networks located in Europe, USA and Asia. Satisfactory agreement is found in the HNO_3 wet deposition with correlations 0.63 in Europe, 0.80 in USA and 0.52 in Asia. There is a tendency to underestimate in most of the stations, principally in Asia and Europe. Part of this underestimation is because we are comparing nitric acid (gas) with nitrate (nitric acid + particulate nitrate) concentrations. However, this tendency to underestimate is consistent with the higher values of HNO_3 seen at lower and middle troposphere.

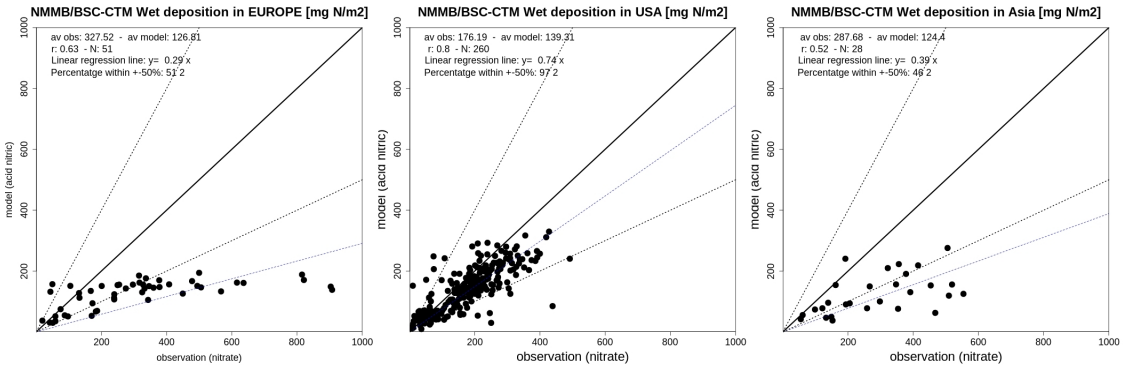

Figure 4.12: Scatter plots of the simulated HNO_3 versus nitrate measurements for three networks: Europe (left panel), USA (middle panel) and Asia (right panel). Dashed lines have slopes equal to 2 resp. 0.5. The dotted line is the result of the linear regression fitting through the origin.

Seasonally modelled VTC of NO_2 ((no averaging kernel application) are calculated here and compared with SCIAMACHY satellite data in Figure 4.13. The model is in good agreement with the observations, capturing higher NO_2 over the most polluted regions, such as Europe, USA and Eastern Asia. The phase in the seasonal cycle of the NO_2 columns is well-performed by the model. During the whole year, the model tends to underestimate NO_2 VTCs in big cities, especially during the colder months, and overestimate them in rural regions. The largest differences are seen for eastern China suggesting an underestimation in the emission inventory for this area. Biomass burning cycle is captured remarkably well by the model, with higher NO_2 VTC in central Africa during DJF and NO_2 VTC in South America in the JJA. Over the sea, the model concentrations are in very good agreement, with only small differences ($\pm$ 0.5 1e^{15} molec/cm^2).

4.5.5 Ozone (O_3)

Ozone is one of the central species that drive tropospheric chemistry, and for that reason it is essential that a model reproduces spatial and temporal concentrations of the ozone well, both at the surface and also across the troposphere and stratosphere. The ozone found in the troposphere is originated from in situ photochemical production and from intrusions of ozone from the stratosphere. Ozone photochemical production in the troposphere involves oxidation of CO

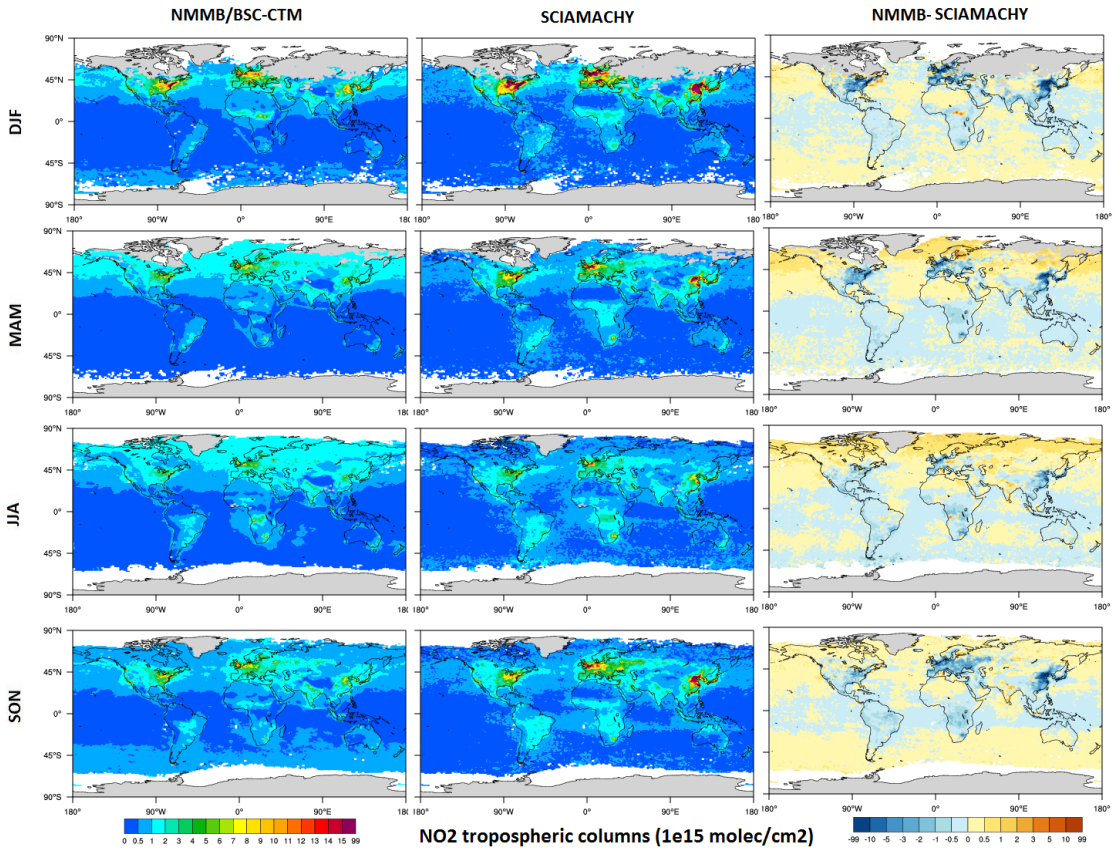

Figure 4.13: Comparison of modelled NMMB/BSC-CTM NO_2 vertical tropospheric columns against satellite data (SCIAMACHY) for (from top) DJF, MAM, JJA, and SON for the whole year 2004 in $1e^{15}$molec/cm^2 . NMMB/BSC-CTM data is displayed in the left panel, SCIAMACHY data in the middle panel and the bias in the right panel.

and hydrocarbons in the presence of NO_x and sunlight. In rural areas, CO and CH_4 are the most important species being oxidised in the O_3 formation. However, in polluted areas, short-lived NMHCs (e.g. HCHO) are present in high concentrations and are the most important species.

The global burden of tropospheric O_3 in NMMB/BSC-CTM is show in 4.7. In the troposphere, the O_3 chemical sources and sinks are dominated by the tropics, where higher abundances are found (171.60 Tg O_3). Lowe abundances are obtained in the northern extratropics (101.56 Tg O_3) and especially the Southern Extratropics (75.41 Tg O_3), where precursors are not present in high amounts. Similar results are found from the others global models, such as MOZART-2 (Horowitz et al., 2003) and TM5 (Huijnen et al., 2010). In general, MOZART-2 has higher and TM5 lower annual mean burden of ozone than the NMMB/BSC-CTM. Our annual mean ozone burden in the southern extratropics is higher (10-14 Tg O_3) than the other two models. Higher CO concentrations in the southern hemisphere (see Table 4.6) might lead to exces-

Table 4.7: Annual mean burden and dry deposition of tropospheric O_3 and stratospheric inflow (Tg O_3) for the NMMB/BSC-CTM, MOZART-2, TM5 and LMDz-INCA global models, and two different Multimodel ensembles (25 and 15 global models).

Model	Reference
NMMB/BSC-CTM	This study
MOZART-2	Horowitz et al. (2003)
TM5	Huijnen et al. (2010)
LMDz-INCA	Folberth et al. (2006)
Multimodel	Stevenson et al. (2006)
Multimodel	Young et al. (2013)

Model	Burden						Dry depo	Strato. inflow
	Global	NH	SH	Trop.	N. Extra.	S. Extra.		
NMMB/BSC-CTM	348	189	158	171	101	75	1201	384
MOZART-2	362	203	159	203	99	60	857	343
TM5	312	-	-	165	84	63	829	421
LMDz-INCA	303	178	125	-	-	-	1261	715
Multimodel	344 ± 39	-	-	-	-	-	1003 ± 200	552 ± 168
Multimodel	337 ± 23	-	-	-	-	-	-	-

sive production of ozone in this area. In addition, the global tropospheric ozone burden of the NMMB/BSC-CTM is in good agreement with the two multimodel ensemble mean of 25 and 15 state-of-the-art atmospheric chemistry global models presented in Stevenson et al. (2006) and Young et al. (2013), respectively. According to the calculations with the NMMB/BSC-CTM, 1209 Tg O_3 are removed from the troposphere by dry deposition at the surface. This quantity is higher in comparison with the global models TM5 (829 Tg O_3) and MOZART-2 (857 Tg O_3), even so, is in good agreement with the global model LMDz-INCA (1261 Tg O_3) and with the multimodel ensemble study Stevenson et al. (2006) (1003 ± 200). The net stratospheric input (STE) annual rate of the model (384 Tg O3) is also showed in the Table 4.7. STE of the model is in good agreement with other modelling studies, especially with the multimodel ensemble Stevenson et al. (2006) (552 ± 168).

Figure 4.14 shows the time series of O_3 daily mean concentration averaged over all available monitoring sites, (from top to bottom, WDCGG, CASTNET, EMEP and EANET) in the entire period of simulation. The solid red line, solid black line represent, respectively, the average of observations and model simulation. Bars show the 25th-75th quartile interval of all observations (orange) and model simulation (grey). As illustrated in Figure 4.14, there is an overall good performance, concerning the O_3 time series concentrations, with significant positive bias from May to October in regions of USA and Japan. The seasonal cycle of ozone from the model agrees well with the observations, with the highest concentrations during July-August and the lowest concentrations during Nov-Dec over all stations. Although, the model captures the inter-seasonal O_3 variability along this period, there is a tendency to overestimate concentrations during warmer months, i.e. May-September. This positive bias is significantly higher in the USA, where the overestimation is occurring during all the day (10-20 $\mu g\, m^{-3}$). Over Europe, the overestimate of O_3 levels during summer is lower than in the other regions. Over East Asia the model captures

reasonably well the peaks in April and May, however a positive bias is seen during the rest of the year. In this area, concentrations during cold months are overestimated, different form Europe where the model concentrations agree with the observations. Overall the observational networks observe a reduction of O_3 concentrations from May-June, but the model has a tendency to simulate an annual cycle with higher concentrations until July. Further investigation is required to understand model behaviour during this period.

The spatial statistics of the model for O_3 are displayed in Figure 4.15 over all in-situ monitoring sites, using daily mean data. Areas with no emissions influence, such as the south pole and isolated islands in tropics, has small mean biases and errors and good correlations (>0.80). When we move to polluted areas, we can observe a good performance in the USA midlands, and parts of central and southern Europe (0.60< r<0.80 and RMSE <20 $\mu g\, m^{-3}$). Large errors are seen in northwestern and southern USA and Northern Europe. Although, large errors are seen in all the stations over Japan, the two stations further from the main Island show high correlation (r> 0.7).

In order to assess the vertical distribution of ozone, the model results are compared with available ozonesondes. The seasonal average mean simulated vertical profiles of ozone for both the model and observations are compared in Figure 4.16 for the period of study (see Table 4.3 and Figure 4.1 for more details). The comparison is made only when ozonesonde observations are available. Figure 4.16 shows (from top to bottom) four panels: DJF, MAM, JJA and SON for each region. Measurements are represented by the solid red line and the model results by the solid black line. To know the variability of data, standard deviation is plotted in each vertical layer for both model (black) and observations (red) in horizontal lines.

The simulated magnitude, and vertical gradient of ozone are in good agreement with the observations. However, the model shows a positive bias of $\sim$ 5-20 ppb along the troposphere in most of the regions during the whole year. We have seen in Section 4.5.2 a significant overestimation of CO especially in the free troposphere for some regions; this could be a reason for the positive ozone biases (stronger ozone production due to too abundant CO), although CO overestimation is mostly in the tropics where the bias in ozone is not so significant. Another reason for this result could be that anthropogenic aerosols and secondary aerosol formation are not included in this simulation, leading to a higher O_3 formation in regions with more precursors. However, this would have more localised effects so it cannot completelly explain the biases throughout the troposphere. The vertical variability of model and observational data are in good agreement, with ozone increasing from lower to higher tropospheric layers. In the lower-middle troposphere the model overestimates ozone in regions with high emissions (Japan, Canada, USA and W.Europe), a feature that is more significant in the DJF. In Western Europe and the USA this bias is reduced in the surface-level. At tropical areas (Equator, NH.tropical and W. Pacific) the model captures the observed concentration and vertical structure of ozone well in the lower to middle troposphere. However, the model tends to overestimate the ozone in the vicinity of the tropopause layer in these regions. At polar regions (NH and SH Polar) the model also presents this tendency to overestimate the vertical structure of ozone. Moreover ozone in the the tropopause layer is underestimated in the NH Polar case, and overestimated in SH Polar case.

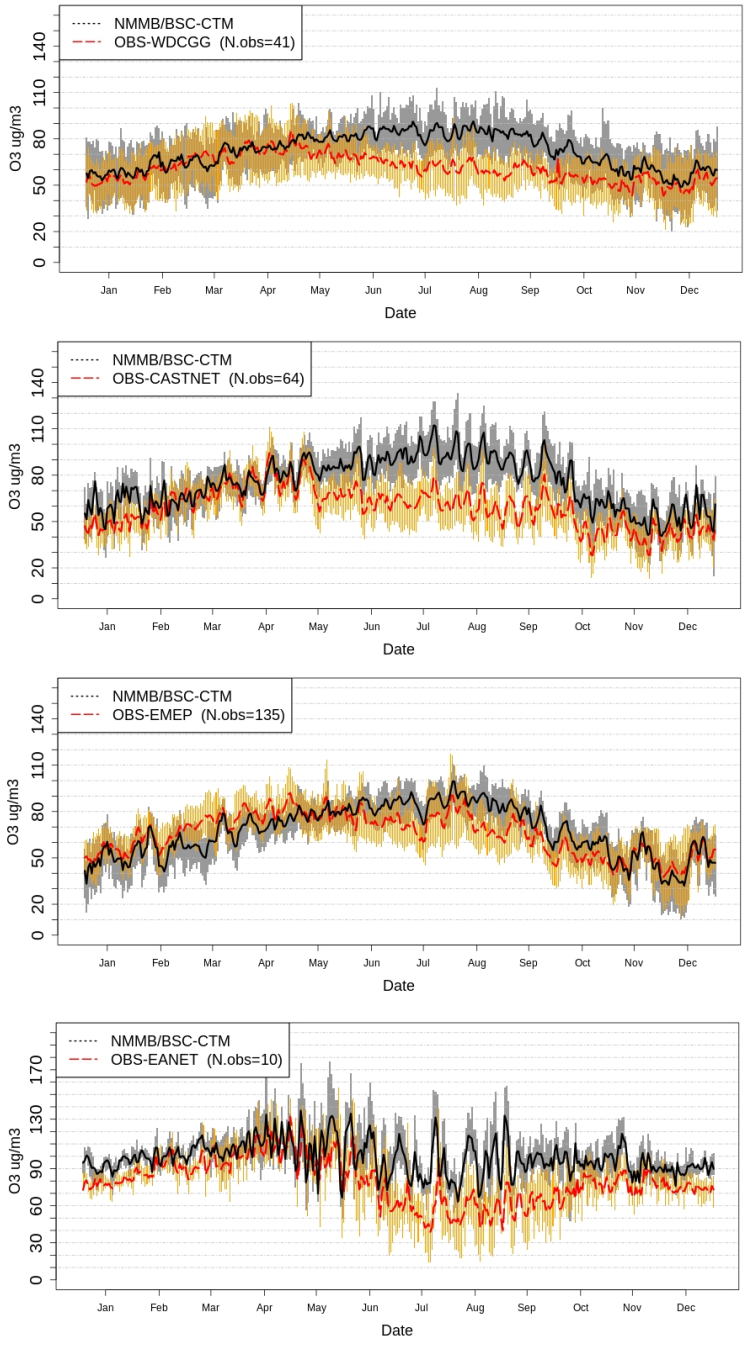

Figure 4.14: Time series of O_3 daily mean concentration averaged over all the rural WDCGG, CASTNET, EMEP and EANET stations (from top to bottom) used in $\mu g\ m^{-3}$. Observations are in a solid red line and model data in a solid black line. Bars show the 25th-75th quartile interval for observations (orange bars) and for model simulation (grey bars).

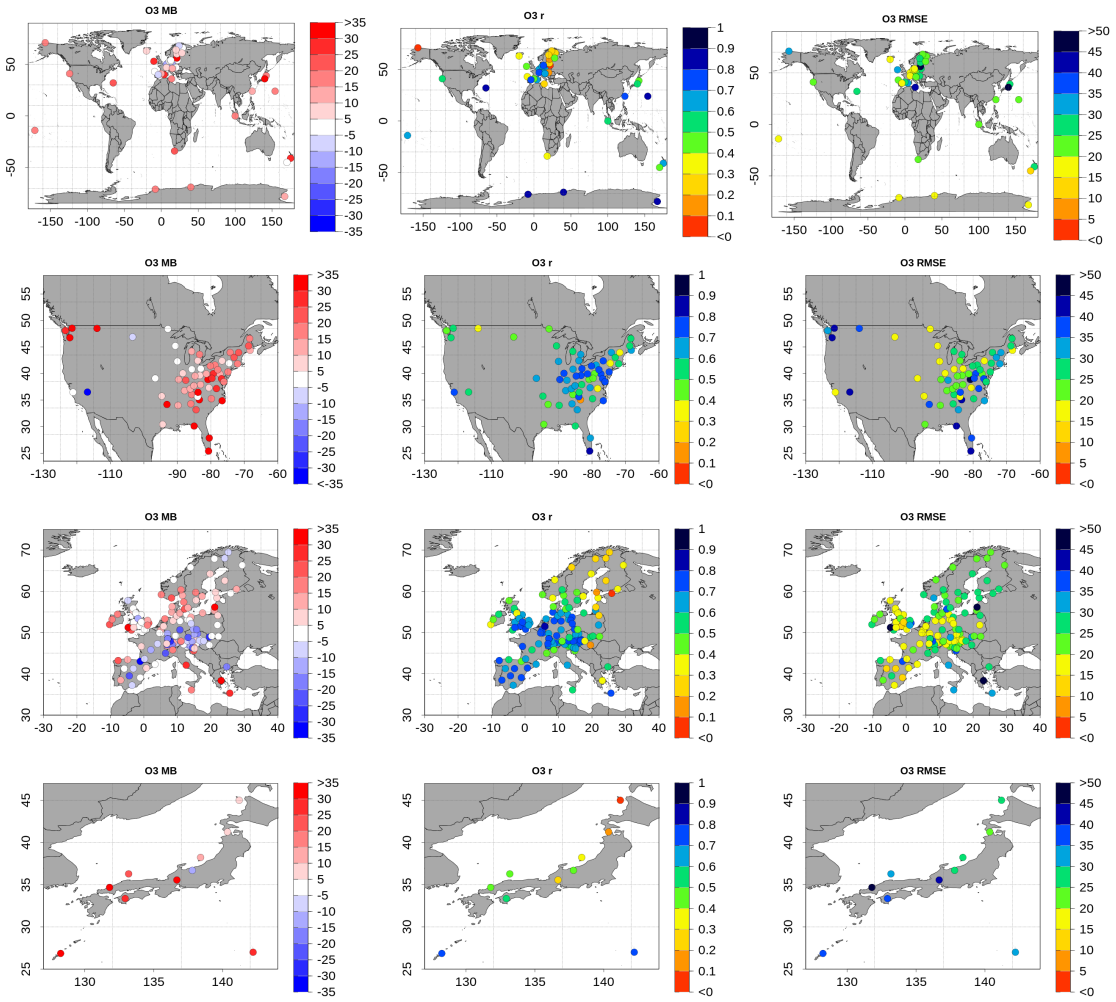

Figure 4.15: O_3 spatial distribution of mean bias (MB, %) (left panel) , correlation (r) (middle panel) and root mean square error (RMSE, $\mu g\, m^{-3}$) (right panel) at all rural WDCGG, CASTNET, EMEP and EANET (from top to bottom) stations used.

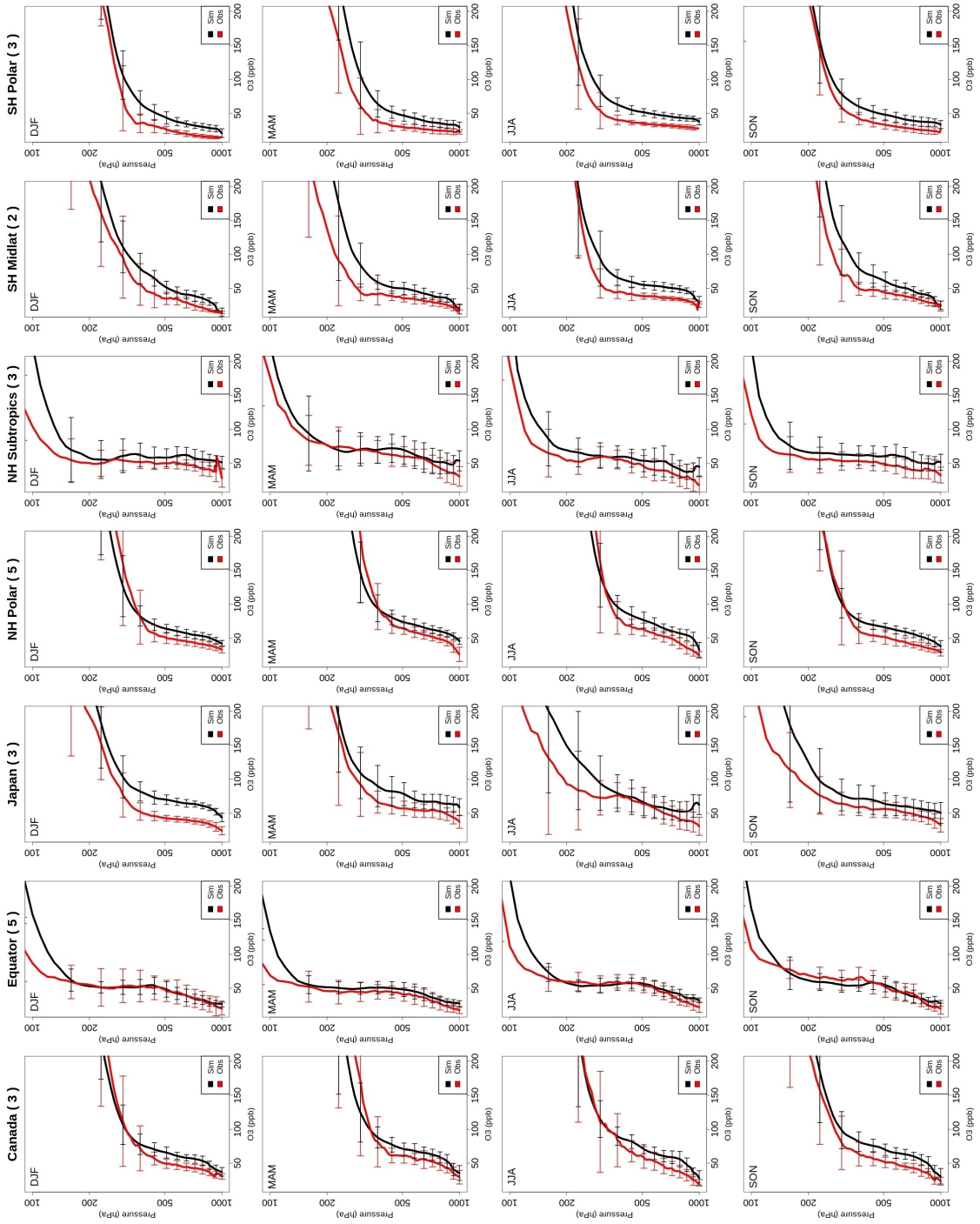

Figure 4.16: Comparison of ozonesonde measurements (red lines) and simulated (black lines) seasonal vertical profiles of O_3 (ppb) and standard deviations (horizontal lines). The region name and the number of stations, using brackets, are given above each plot.

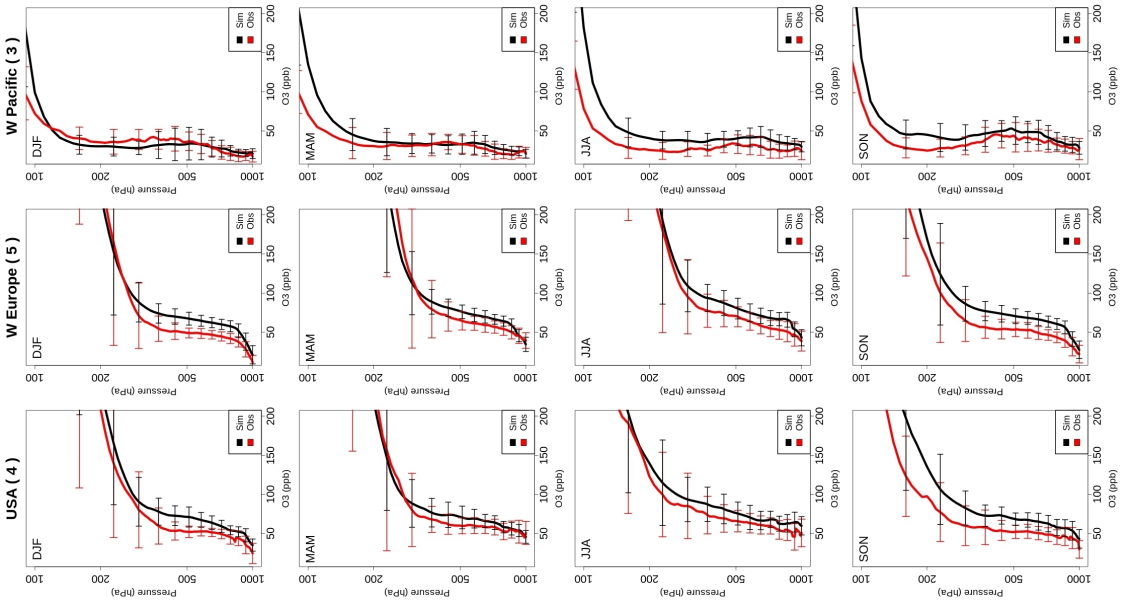

Figure 4.16: Continued

Finally, statistics are computed for the ozone vertical profiles and ozonesondes to identify those areas where the errors are more important. Figure 4.17, shows the mean ozone bias (left), correlation (middle) and RMSE (right) of NMMB/BSC-CTM with respect to ozonesondes, respectively; data is averaged between 400 and 1000 hPa over the year 2004. As we have shown, mean bias is positive for most stations (MB<30%). Large RMSE are seen in northern high latitudes (<50 $\mu g\ m^{-3}$) and also two stations from USA. Europe and Japan present a RMSE around 30$\mu g\ m^{-3}$ and tropics and subtropics are the regions with lower error, i.e. RMSE below 30$\mu g\ m^{-3}$. The highest correlations are seen in polar regions.

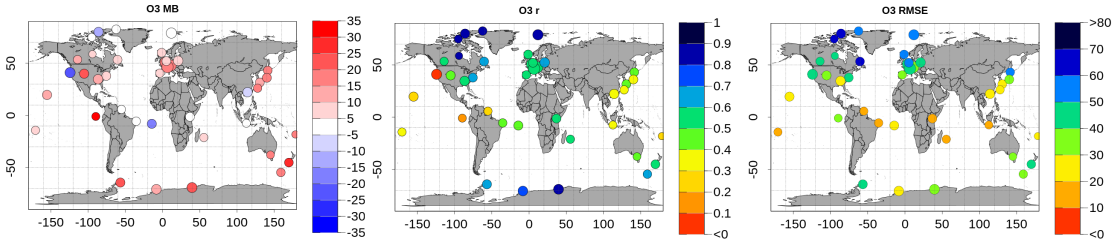

Figure 4.17: Mean tropospheric ozone bias spatial distribution of NMMB/BSC-CTM minus ozonesondes (MB, %) (left panel), root mean square error (RMSE, $\mu g\ m^{-3}$) (middle panel) and correlation (right panel) for the whole 2004, averaged between 400-1000 hPa. The diameter of the circles indicates the number of profiles over the respective stations.

4.6 Conclusions

We have presented a new global chemical transport model, NMMB/BSC-CTM. A comprehensive description has been given for the different components of the gas-phase chemical module coupled online within the NMMB atmospheric driver. This model , which is comprised of 51 chemical species and solves 156 reactions simulates the global distributions of ozone and its precursors, including CO, NO_x, and VOCs. The model simulation presented here is configured with a horizontal resolution of 1° x 1.4°, with 64 vertical layers and a top of the atmosphere at 1hPa. Emissions from ACCMIP (Lamarque et al., 2010) are considered and include fossil fuel combustion, biofuel, biomass burning, soil and oceanic emissions. Biogenic emissions are calculated online with the MEGANv2.04 model (Guenther et al., 2006). In this simulation, aerosols are neglected, thus, no interaction between gas-phase and aerosol-phase is considered. Modelled tropospheric ozone and related tracers have been evaluated for the year 2004 and compared with surface-monitoring stations, ozonesondes, satellite and aircraft campaigns.

The evaluation of OH concentrations shows a good agreement with previous studies Spivakovsky et al. (2000); Voulgarakis et al. (2013). Peaks concentrations of OH seen in April and July at northern latitudes are slightly higher in comparison with the climatological mean computed by (Spivakovsky et al., 2000). Part of this positive bias is possibly explained by the fact that anthropogenic aerosols and secondary aerosol formation are not considered in this simulation; hence, higher oxidised atmosphere is obtained due to higher photolysis when aerosols are not present. However, the widespread positive ozone biases identified in the model seems to be the responsible for this higher OH concentrations.

The global and annual mean burden of CO (399 Tg) is higher in comparison with other studies with larger concentrations located in the tropics (229.43 Tg CO). The model is in relatively good agreement with CO observations at the surface with negative biases at stations over Europe and Japan and positive biases in Canada and Africa. The north European, South African and East Asian countries present higher correlations with observations. Concerning the vertical structure of CO, the model presents a good performance during the DJF and MAM, and positive biases are seen during JJA for most of the stations. In general, the model overestimates CO from the middle to the upper troposphere in most of the stations throughout the year. Significant underestimation of CO is seen in Beijing below 600hPa. This result is similar to other evaluation studies that indicates the emission inventories are not able to capture the extreme growth of anthropogenic emissions in China. The phase and amplitude of the seasonal cycles of CO at 800 and 500 hPa in NMMB/BSC-CTM and MOPITT are very similar. Overestimations of CO are mainly located over west-central Africa, western South America, Indonesia and surrounding Pacific and Indian oceans during the dry season. At 800hPa, a significant negative bias is observed over the northern latitudes during the winter. These results are most likely related to possible errors in anthropogenic and biomass burning emission inventories, where the magnitude or the location of emission is not correctly modelled.

The modelled HCHO tropospheric columns are compared with the SCIAMACHY satellite data.

The spatial and seasonal variation in formaldehyde tropospheric columns are well-captured by the model. Positive model biases over Central Africa, Australia and Southeast Asia are seen during DJF and MAM, and, over the Amazon region and the eastern United States in JJA and SON. These results are most likely related to uncertainties in the magnitude and the location of the biogenic and biomass burning emissions.

Nitrogen oxide abundances are well-simulated in almost all locations. Looking at the annual time series of NO_2 in Europe, the model is capturing higher peaks during winter, however, a positive bias is observed during summertime. Nitrogen compounds are more sensitive to errors in emissions than other pollutants. Note that the emission inventory has no seasonal cycle variation for land-based anthropogenic emissions; hence, the potential reduction of NO_X emissions during the summer is not considered. Over Asia, a negative bias of NO_x from March to August is observed, probably because of underestimated emissions in this area. Vertical profiles of NO_X are in good agreement with the observed values, though with some tendency for underestimation in the upper troposphere, possibly due to the lack of lightning NO_x emissions. Vertical profiles of PAN and HNO_3 were also compared with observations. Some agreement is seen in these vertical profiles, although the model has a tendency to over-predict PAN and HNO_3 concentrations. HNO_3 wet deposition are better captured in the USA compared to Europe and Asia, with a tendency for the model to underpredict the observed values. The comparison with observed NO_2 VTC from SCIAMACHY shows that the model reproduces the seasonality and the spatial variability reasonably well, capturing higher NO_2 over the most polluted regions. However, the results show a tendency to underestimate NO_2 VTC in big cities, especially during DJF and SON. The biomass burning cycle is well captured by the model with higher NO_2 VTC in central Africa during DJF and NO_2 VTC in South America in the JJA.

The ozone burden is in good agreement with other state-of-the-art global atmospheric chemistry model burdens. Ozone burden in the southern extratropics is higher in our model, suggesting that higher CO concentrations in the south hemisphere might lead to excessive production of ozone in this area. It seems unlikely that the positive ozone biases are caused by too much STE. STE is in good agreement with other evaluation studies. In addition, STE has stronger effects in the upper troposphere, hence, the ozone biases would be expected to increase with height, and this is not the case in the present model results. The surface O_3 results show a reasonable agreement with the observations, with significant positive bias from May to October in regions of USA and Japan. Surface O_3 concentrations are very sensitive to the emissions; consequently, the variability of ozone concentrations can potentially be enhanced by improving the spatio-temporal distribution of the ozone precursor emissions. The model captures the spatial and seasonal variation in observed background tropospheric O_3 profiles with a positive bias of $\sim$ 5-20ppb along the troposphere in most of the regions during the whole year. The significant overestimation of CO especially in the free troposphere could be the reason for this positive ozone bias.

In summary, NMMB/BSC-CTM provides a good overall simulation of the main species involved in tropospheric chemistry, though with some caveats that we have highlighted here. Future versions of the model will aim to address problems identified in this study and include the effect

aerosols on the system.

Chapter 5

Regional run evaluation

The work of this chapter has been published as Badia and Jorba (2014)

5.1 Introduction

The COST Action ES1004 European framework for online integrated air quality and meteorology modelling (EuMetChem - http://eumetchem.info) aims to develop a European strategy for online integrated AQM-MetM modelling (Baklanov et al., 2014). A model intercomparison effort is defined within the COST Action ES1004, in coordination with the AQMEII-Phase2 (Rao et al., 2011; Im et al., 2014a,b). AQMEII-Phase2 focuses on intercomparing online coupled regional-scale AQM-MetM models. The main objective is to understand feedback processes of aerosol, radiation, and cloud interactions. To that end, several groups from Europe and North America are participating in the second phase. As in Phase 1, model outputs have been interpolated to a common lat/lon grid and uploaded to the web-distributed system ENSEMBLE: `http://ensemble.jrc.ec.europa.eu` (Bianconi et al., 2004; Galmarini et al., 2012). While online models may vary from group to group, these models are driven by the same inputs: chemical boundary conditions, anthropogenic emissions, forest fire emissions, and domain configuration. Thus, the uncertainties related to using different inputs are minimized, and the intercomparisons provide useful information about different model processes.

The Earth Sciences Department of the Barcelona Supercomputing Center is participating in AQMEII-Phase2 through the use of the NMMB/BSC-CTM (Pérez et al., 2011; Haustein et al., 2012; Jorba et al., 2012; Spada et al., 2013). In this study, we evaluate the NMMB/BSC-CTM online model by simulating the main gaseous pollutant concentrations over Europe for the year 2010. Model results are evaluated with ground-based observations, ozonesondes and satellite retrievals.

The modelling experiment is presented in Section 5.2. Section 5.3 describes the observational dataset and the statistical metrics used to evaluate the model. The results are discussed in Section 5.4 and are compared to other modelling studies in Section 5.4.5. The last section is devoted to

the conclusions of the work.

5.2 Model setup

Following the AQMEII-Phase2 specifications, the model is configured for a regional domain covering Europe from 30W-60E and 25N-70N. Figure 5.1 displays the domain of study and the location of the ground-level monitoring and ozonesondes stations used in this evaluation analysis. The rotated lat-lon projection is used, with a regular horizontal grid spacing of $0.2°x0.2°$, and the top of the atmosphere is set at 50 hPa. To test the sensitivity of the results to vertical grid discretization, two vertical configurations are defined: 1) run with 24 vertical layers, and 2) run with 48 vertical layers. The year of simulation is 2010.

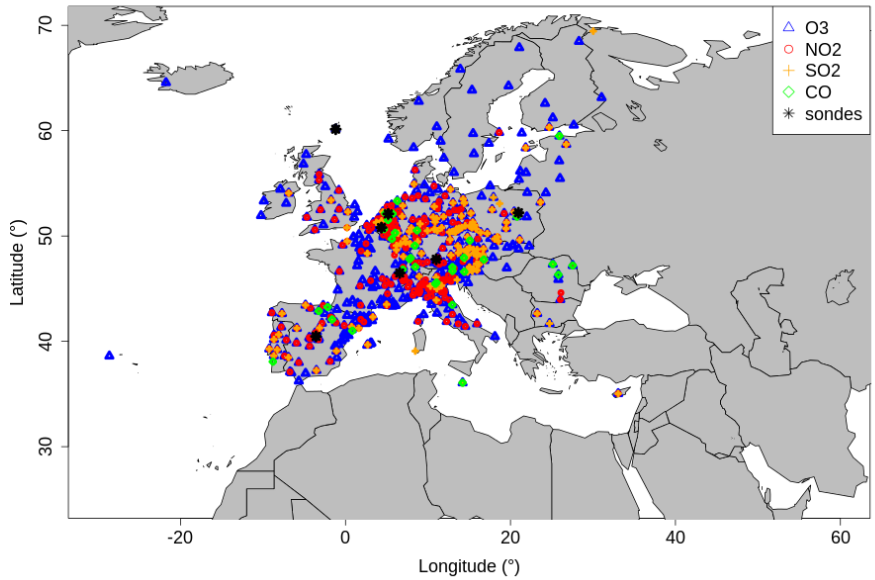

Figure 5.1: AQMEII-Phase2 domain of study. The symbols and colours denote the positions of the rural ground-level O_3 (blue triangle), NO_2 (red circle), SO_2 (orange cross), CO (green diamond) and ozonesondes (black asterisk) stations, all of which were used in this evaluation analysis.

The annual simulation is executed with 48hours model run cycles. Each 48h run requires a 6h spinup for the meteorology, during which the chemistry component is switched off. After that, the meteorology and the chemistry are solved online for the next 48hours. A cold start of 10 days is run to initialise the chemistry for the 1-year simulation. The results from the year 2010 were used in the evaluation. Table 5.1 summarises the configuration of the model experiment.

Table 5.1: Model characteristics and experiment configuration

Emissions	
Anthropogenic	TNO-MACC database (Kuenen et al., 2014)
Biogenic emissions	MEGANv2.04 (Guenther et al., 2006)
Experiment configuration	
Regional domain	30W- 60E, 25N-70N
Horizontal resolution	0.2° x 0.2°
Vertical layers	24/48
Top of the atmosphere	50 hPa
Chemistry	only gas-phase considered, no aerosol chemistry
Meteorological boundary condition	FNL/NCEP (`http://rda.ucar.edu/datasets/ds083.2/`)
Chemical boundary conditions	MACC (IFS-MOZART) (1.125°x1.125°)
Spin up	10 days

5.2.1 Anthropogenic and natural emissions

The applied anthropogenic emissions are based on the TNO-MACC database (Kuenen et al., 2011, 2014; Pouliot et al., 2012) for the year 2009. The dataset consists of the European total annual anthropogenic emissions, provided by Selected Nomenclature for sources of Air Pollution (SNAP) sector and disaggregated per grid cell at a 1/16 by 1/8 degree lat-lon resolution (7x7 km). Species provided are: CO, NO_x, SO_x, NMVOC. Annual emission data was prepared for input to NMMB/BSC-CTM using temporal factors (from year to month, day of the week, and finally hour) and vertical layer distribution provided by AQMEII-Phase2 (Pouliot et al., 2012). Total annual anthropogenic emissions are 38.2 Tg of CO, 18.2 Tg of NO_x, 12.9 Tg of NMVOC and 13.2 Tg of SO_2.

Concerning natural emissions, only biogenic emissions are considered as a natural source. Biogenic emissions are computed online from the MEGANv2.04 (Guenther et al., 2006). For more information see Section 2.4.1. No biomass burning, aircraft and NO_x lightning emissions are considered in this simulation.

5.2.2 Boundary conditions

Meteorological initial and boundary conditions were obtained from the FNL of the NCEP global model for 2010 at a$1^\circ x 1^\circ$ horizontal resolution. Meteorological boundary conditions are provided every 6 hours.

Concerning the chemistry boundary conditions, those are provided from the MACC re-analysis data produced by the IFS-MOZART global chemical model for the year 2010. Horizontal resolution of the chemistry boundaries are $1.125^\circ x 1.125^\circ$, and are updated every 24 hours. The pollutants involved in the boundary conditions are O_3, NO, NO_2, HNO_3, OH, H_2O_2, CO, PAN, SO_2 and CH_2O.

5.3 Observational dataset

5.3.1 Ground observations

Surface data from different European observational networks (AirBase, EMEP) for the year 2010 (available from the AQMEII-Phase2 database (Galmarini et al., 2012)) was used to evaluate the model (see Figure 5.1). This evaluation used only rural stations below an altitude of 1000m with minimum data availability of 75%. Four species were targeted for the evaluation: O_3, NO_2, CO, SO_2. Due to the dubious quality of some observations the measurement dataset was filtered. Concerning NO_2, CO and SO_2, most stations from Spain were removed, as well as some from Italy, France, UK and Portugal, which reduced the final coverage of the dataset. In summary, the total number of monitoring stations used in the evaluation was 498 for O_3, 332 for NO_2, 33 for CO and 153 for SO_2.

5.3.2 Ozone vertical structure: ozonesondes

The surface evaluation was complemented with an analysis of the ozone vertical structure. Model vertical profiles were evaluated with 7 available ozonesondes (Lerwick, Uccle, Hohenpeissenberg, Payerne, Barajas, De Bilt and Legionowo, see Figure 5.1) from the World Ozone and Ultraviolet Radiation Data Center (WOUDC; `http://www.woudc.org/`) for 2010. The approximate launch time was around 11-12 UTC for all the ozonesondes, except for Hohenpeissenberg, which was at 7 UTC. The number of datasets for most of the stations was between 12-40 per season. Table 5.2 summarises the information of the selected ozonesondes.

Table 5.2: Ozonesondes used in the evaluation

Station name	Country	Lat	Lon	Height (m)	Approx launch time (UTC)	Number of available obs.			
						DJF	MAM	JJA	SON
Lerwick	Great Britain	60.1	-1.2	80	11	13	13	13	10
Uccle	Belgium	50.8	4.4	100	11	34	37	40	37
Hohenpeissenberg	Germany	47.8	11.0	976	7	35	42	26	30
Payerne	Switzerland	46.5	6.6	491	11	38	39	40	39
Barajas	Spain	40.5	-3.6	631	11	13	13	12	13
De Bilt	Netherlands	52.1	5.2	4	12	12	15	11	13
Legionowo	Poland	52.2	20.9	96	12	10	12	9	7
TOTAL						155	171	151	149

5.3.3 Satellite observations

Modelled NO_2 VTC and CO mixing ratio at surface layer were evaluated using satellite retrievals. To make a proper comparison, model data were extracted only when satellite data were available at each time and location of each overpass.

Tropospheric NO_2 columns from the were used in the model evaluation to provide some insights into the spatial distribution of modelled NO_2. Ozone Monitoring Instrument (OMI) used ultra-

violet and visible radiation to produce daily global coverage with the nadir pixel size of 24x13 km^2. Daily satellite data was taken from the MACC project: http://www.temis.nl/macc/, based on the Dutch OMI (DOMINO) version 2 data product (Boersma et al., 2011). Several daily satellite overpasses were available (approx. between 9-15 UTC) and they were filtered with nearly cloud-free conditions (cloud radiance fraction <50%). The DOMINO product was validated in several studies (Boersma et al., 2008, 2009; Brinksma et al., 2008).

Additionally, surface CO mixing ratio was evaluated with the Measurement of Pollution in the Troposphere (MOPITT: http://www2.acd.ucar.edu/mopitt) instrument retrievals. The MOPITT, aboard the NASA EOS-Terra satellite, is a gas filter radiometer and measures thermal infrared (near 4.7 μm) and near-infrared (near 2.3 μm) radiation, only during clear-sky conditions, with a ground footprint of about 22 km x 22 km. The MOPITT satellite overpasses cover the whole day. The MOPITT Version 5 (V5) Level 2 data product, which was used here, provides daily near-surface CO mixing ratios. MOPITT CO mixing ratios have been validated with in situ CO profiles measured from numerous NOAA/ESRL aircraft profiles in Deeter et al. (2013), and they were found to be positive biased by about 1% and r = 0.98 at the surface level.

5.3.4 Statistical Metrics

There are several metrics that are used by the modelling community to evaluate performances of AQMs (U.S.EPA, 1991; Cox and Tikvart, 1990; Russell and Dennis, 2000). The statistical indicators selected in this study are: Correlation coefficient (r: Equation 5.1) , Mean Bias (MB: Equation 5.2), Root Mean Square Error (RMSE: Equation 5.3),Mean Normalized Bias Error (MNBE: Equation 5.4), Mean Normalized Gross Error (MNGE: Equation 5.5),Mean Fractional Bias (MFB: Equation 5.6), Mean Fractional Error (MFE: Equation 5.7) and Normalized Mean Bias (NMB: Equation 5.8).

$$r = \frac{1}{N}\sum_{i=1}^{N}\frac{(O_i-\overline{O})(P_i-\overline{P})}{\sigma_O\sigma_P} \tag{5.1}$$

$$MB = \frac{\sum_{i=1}^{N}(P_i-O_i)}{N} \tag{5.2}$$

$$RMSE = \sqrt{\frac{1}{N}\sum_{i=1}^{N}(P_i-O_i)^2} \tag{5.3}$$

$$MNBE = \frac{1}{N}\sum_{i=1}^{N}\frac{P_i-O_i}{O_i} \tag{5.4}$$

$$MNGE = \frac{1}{N}\sum_{i=1}^{N}\frac{|P_i-O_i|}{O_i} \tag{5.5}$$

$$MFB = \frac{2}{N}\sum_{i=1}^{N}\frac{P_i-O_i}{P_i+O_i}\times 100 \tag{5.6}$$

$$MFE = \frac{2}{N}\sum_{i=1}^{N}\frac{|P_i - O_i|}{P_i + O_i} \times 100 \tag{5.7}$$

$$NMB = \frac{\sum_{i=1}^{N} P_i - O_i}{\sum_{i=1}^{N} O_i} \times 100 \tag{5.8}$$

where P and O denote the vector of model output and the vector observations, respectively.

A cut-off threshold (of 1.5 μg m^{-3} for NO_2, 0.2 μg m^{-3} for SO_2, and 11.45 μg m^{-3} for CO) was applied to the measurements and model results to avoid numerical problems, which may arise from low values in the data-set when normalized errors are calculated (Pay et al., 2010; Pirovano et al., 2012; Nopmongcol et al., 2012). Moreover, in order to quantify the model's ability to simulate high ozone concentration, a cut-off threshold of 80 μg m^{-3} (according to the recommendations of the U.S.EPA (1991) and Russell and Dennis (2000)) was applied in the yearly hourly values (yhv) results. If not explicitly specified, metrics are calculated without any threshold.

5.4 Results and discussion

In this section, we discuss the evaluation of the gas-phase results of the NMMB/BSC-CTM model using the 24-vertical-layer configuration (hereinafter referred to as NMMB24). The model results were evaluated with ground-based observations, ozonesondes and satellite retrievals. In the last subsection we compare the results of the NMMB24 run with the 48-vertical-layer run (hereinafter referred to as NMMB48). These two runs show the impact of vertical resolution on the chemistry.

5.4.1 Model evaluation with surface measurements: O_3, NO_2, SO_2 and CO

In the evaluation, we used yearly daily averaged (yda) values and yearly hourly values (yhv) to keep the spread of data during the diurnal cycle in the model comparison (Solazzo et al., 2012). Due to the limitation in the ozone boundary conditions extracted from the MACC reanalysis (significant negative bias of ozone during winter in IFS-MOZART, not shown), O_3 is evaluated only from May to November. Besides ozone, the other pollutants were evaluated for the whole year 2010. Seasonal statistics were computed for winter (January, February and December), spring (March, April and May), summer (June, July and August) and autumn (September, October and November).

Ozone

Figure5.2 (first row) shows the time series of daily (left panel) and diurnal cycle plots (right panel) for O_3, NO_2, SO_2 and CO over all monitoring sites in the entire period of simulation. The solid red line, solid black line and dashed blue line represent, respectively, the average of observations, NMMB24 simulation, and NMMB48 simulation. Bars show the 25th-75th quartile

interval of all observations (orange) and NMMB24 simulation (grey).

As illustrated in Figure 5.2 (left panel), there is an overall good performance concerning the O_3 time series concentrations (r = 0.61 (yhv) / 0.68 (yda)). The model reproduces reasonably well the seasonal cycle during the period of study, with the highest concentrations during May-June and the lowest concentrations during Sept-Oct. Moreover, the model captures the inter-seasonal O_3 variability along this period but significantly overestimates concentrations in the summer months (MB= 8.84 $\mu g\ m^{-3}$). During this period photochemical production of O_3 is higher.

As can be observed in Figure 5.2 (right panel), despite the overestimation of O_3 mainly in daytime (7-15 UTC), the daily profiles show the maximum values of both observed and modelled O_3 concentrations occurring at 14-15 UTC, and minimum concentrations at 7-8 UTC. Moreover, the model demonstrates a good ability to capture the daily variability of observed O_3 concentrations.

The time series of daily maximum O_3 concentrations is shown in Figure 5.3. Red points represent the observations and black and blue the NMMB24 and NMMB48 simulations, respectively. The model captured the seasonal cycle of daily maximum O_3 concentrations well, reproducing most of the higher O_3 peaks taking place between May-July and the lower O_3 peaks between Sept-Oct (r= 0.75 and RMSE= 22 $\mu g\ m^{-3}$). However, the model slightly overestimates the O_3 peaks in the summer months (MB= 3.84 $\mu g\ m^{-3}$, see Table5.3).
The spatial statistics of the model for O_3, NO_2, SO_2 and CO are displayed in Figure 5.4 (first row) over EU stations using hourly data. The best performance for O_3 is observed in Central EU and the Iberian Peninsula, with correlation values ranging from 0.7 to 0.9, and low RMSE and MB values. However, r drops to values lower than 0.4 in the UK, East and North EU. The model tends to overestimate over EU, with higher RMSE and positive MB around East EU and the Po River Valley up to the Alpine area. Positive biases are also observed in the Mediterranean basin and southern EU, which are affected by intense photochemical production of O_3.

A Taylor diagram (left part of Figure 5.5) and a Soccer-goal (right part of Figure 5.5) summarise the main statistical metrics in simple diagrams (standard deviation, correlation, Normalized RMSE, Normalized Median Error (NME) and Normalized median bias (NMB)). Red, blue, green and black points represent, respectively, O_3, NO_2, CO and SO_2 metrics. The red triangle represents O_3 with threshold.

For O_3 the correlation decreases to 0.45 (Taylor Diagram) and MNBE and MNGE are reduced to 3 and 14.8 (Soccer-goal) when a threshold is applied to the data. Thus, errors are reduced for values above 80 $\mu g\ m^{-3}$, which take place during the daytime.

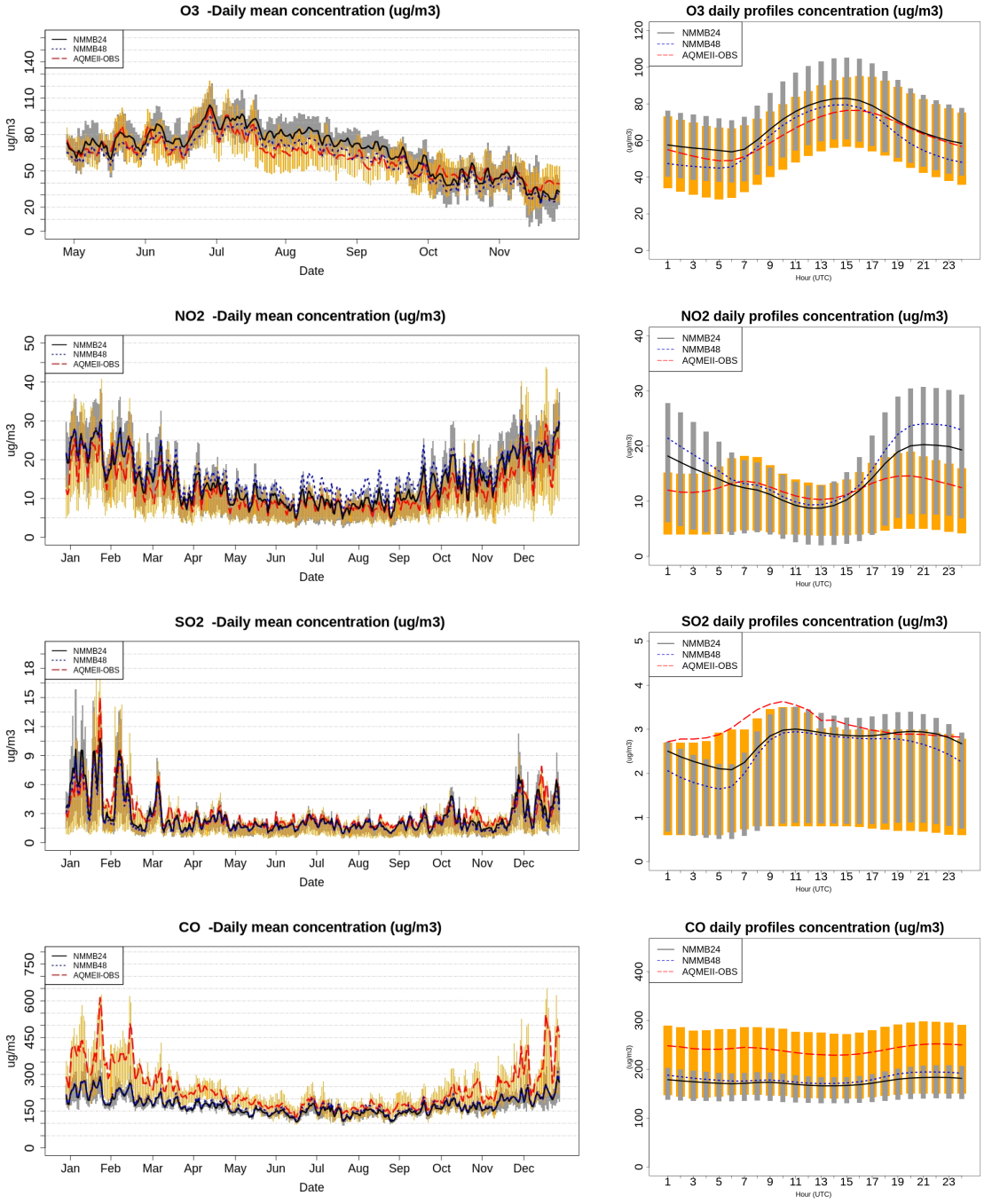

Figure 5.2: Time series of O_3, NO_2, NO, SO_2 (from top to bottom) daily mean concentration (left panels) and daily profiles concentration (right panels) averaged over all the rural stations used in $\mu g\ m^{-3}$. Observations are in a solid red line and model data in a solid black line (NMMB24) and dashed blue line (NMMB48). Bars show the 25th-75th quartile interval for observations (orange bars) and for NMMB24 model simulation (grey bars).

Table 5.3: Statistical evaluation of the model NMMB24 results over Europe for 2010 from observations in hourly basis. (observation mean (ug m-3), model mean (ug m-3), mean bias (MB, $\mu g\ m^{-3}$), correlation (r), root mean squared error (RMSE, $\mu g\ m^{-3}$), mean normalized bias error (MNBE, %), mean normalized gross error (MNGE, %), mean fractional bias (MFB, %) and mean fractional error(MFE,%))

Variable	Period	Type	Data points	Obs mean	Mod mean	MB	r	RMSE	MNBE	MNGE	MFB	MFE
O_3	May-Nov	Hourly	2436039	62.9	67.7	4.8	0.60	27.8	66.5	91.9	6.4	40.9
498 stns	May-Nov	Hourly (thres)	448772	105.2	106.5	1.2	0.45	21.1	3.0	14.8	1.2	14.3
	May-Nov	Daily mean	104995	62.4	67.0	4.6	0.68	21.2	17.1	36.6	5.0	30.0
	May-Nov	Daily max	104995	85.5	89.4	3.8	0.75	22.0	10.1	25.3	3.6	21.9
	Spring	Daily mean	45052	70.9	60.2	-10.8	0.44	24.6	-11.2	31.0	-20.3	34.3
	Summer	Daily mean	44929	73.5	82.3	8.8	0.56	23.0	20.4	30.3	13.2	24.5
	Fall	Daily mean	44320	48.8	50.2	1.4	0.60	19.7	17.2	46.5	-2.0	37.6
NO_2	Annual	Hourly	2733604	12.6	14.5	1.9	0.49	13.4	86.1	125.9	8.8	66.6
332 stns	Annual	Hourly (thres)	2469740	13.6	15.8	2.2	0.46	13.8	66.4	102.2	11.5	62.2
	Annual	Daily mean	118454	12.5	14.5	2.0	0.61	9.7	65.4	92.5	15.8	52.7
	Annual	Daily max	118454	23.4	26.7	3.3	0.48	18.8	63.0	90.9	17.6	55.8
	Winter	Daily mean	29199	19.4	22.0	2.6	0.52	13.1	82.1	104.5	23.6	54.0
	Spring	Daily mean	30042	10.8	12.6	1.8	0.55	8.6	76.2	104.2	14.6	52.8
	Summer	Daily mean	29690	7.9	8.6	0.7	0.47	7.3	39.5	74.9	3.8	52.3
	Fall	Daily mean	29523	12.1	14.8	2.7	0.61	9.0	64.0	86.4	21.3	51.6
SO_2	Annual	Hourly	1180489	3.3	2.8	-0.5	0.41	6.2	103.1	149.8	2.5	72.0
153 stns	Annual	Hourly (thres)	1113282	3.4	2.9	-0.5	0.40	6.4	63.5	110.6	-0.7	68.8
	Annual	Daily mean	54130	3.1	2.7	-0.4	0.55	4.3	162.1	202.0	7.2	64.4
	Annual	Daily max	54130	7.5	4.7	-2.8	0.37	14.2	60.8	111.5	-6.7	68.9
	Winter	Daily mean	13408	5.4	4.7	-0.6	0.58	6.6	253.7	293.7	10.7	68.6
	Spring	Daily mean	13718	2.5	2.2	-0.3	0.42	3.4	147.8	187.6	5.6	61.9
	Summer	Daily mean	13548	2.1	1.8	-0.3	0.39	2.9	153.3	193.3	5.8	62.7
	Fall	Daily mean	113456	2.5	2.2	-0.3	0.37	3.5	94.2	134.2	6.9	64.5
CO	Annual	Hourly	276572	241.6	174.1	-67.5	0.39	195.3	11.1	57.8	-16.2	44.0
33 stns	Annual	Hourly (thres)	275440	242.5	174.2	-68.3	0.39	195.5	5.5	52.4	-17.0	43.4
	Annual	Daily mean	11785	240.8	174.0	-66.7	0.44	179.9	7.2	53.3	-17.3	41.4
	Annual	Daily max	11785	328.3	210.6	-117.7	0.40	285.4	-12.5	41.6	-27.5	43.7
	Winter	Daily mean	2917	364.2	219.8	-144.5	0.28	310.3	-19.2	40.2	-33.4	45.6
	Spring	Daily mean	2979	223.5	168.4	-55.1	0.32	116.7	-0.3	47.3	-18.4	40.8
	Summer	Daily mean	2961	164.2	141.9	-22.3	0.26	81.7	37.9	75.1	-4.9	40.8
	Fall	Daily mean	2928	212.8	166.8	-46.1	0.38	116.9	10.3	50.5	-12.5	38.3

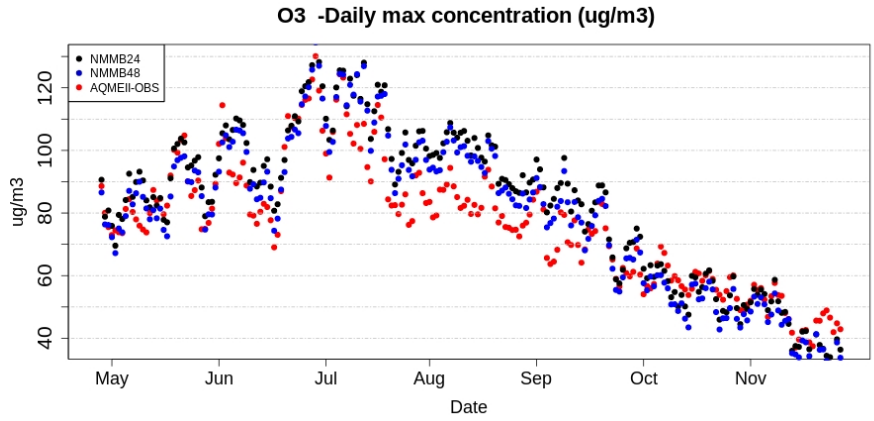

Figure 5.3: Time series of O_3 daily max concentrations averaged over all the rural stations used in $\mu g\ m^{-3}$. Observations are red points and model data are black points (NMMB24) and blue points (NMMB48).

Nitrogen dioxide

The NO_x family plays an important role in O_3 production in the troposphere. It has a rather short lifetime; consequently, it is closely related to emission sources. As a result, NO_2 is more sensitive to errors in emissions than other pollutants, and an error in NO_x emissions can change NO_2 concentrations. Road transport and power plants are among the main sources of NO_x atmospheric emissions (Pouliot et al., 2012). Higher anthropogenic NO_x concentrations are found in Belgium, the Netherlands, Rhine-Ruhr (western Germany), Po Valley (northern Italy), and around several important European cities such as London, Milan, Paris, Madrid, Barcelona, etc.

Looking at the annual time series (Figure 5.2 second row, left panel), the model is able to successfully reproduce the seasonal cycle of NO_2, especially during the winter months when the emissions of NO_2 are higher (MNBE = 80.3 $\mu g\ m^{-3}$). However, there is a systematic positive bias throughout the year (MB = 2 (yhv)/1.94 (yda) $\mu g\ m^{-3}$ and r= 0.49 (yhv) /0.61 (yda)). Daily profiles (Figure 5.2 right panel) show that this positive bias is mainly due to higher values during the night. This result may be due to the lack of the heterogeneous formation of HNO_3 through N_2O_5 hydrolysis, an important sink of NO_2 at night. Moreover, the current model does not consider secondary aerosol formation for the present exercise. This may result in an atmosphere that is too oxidized (overestimation of OH radicals), and the nocturnal chemistry may lead to an accumulation of NO_2 in the surface layers. However, a slight underestimation is observed between 6-16 UTC. The model's ability to reproduce the daily maximum diminishes, showing significant errors and positive bias (r=0.48, MB = 3.3 $\mu g\ m^{-3}$ and RMSE = 18.8 $\mu g\ m^{-3}$). This is probably because the model's peak value (approximately 30 $\mu g\ m^{-3}$) occurs at around 20 UTC instead of at both 7 UTC and 20 UTC, as shown by the measurements (approximately 18 $\mu g\ m^{-3}$) (see Figure 5.2 and Table 5.3). High normalized errors are reduced when a threshold is applied to MNGE= 66.4% and MNGE =102.2%; thus the model performance improves when values lower than 1.5 $\mu g\ m^{-3}$ are eliminated. The best performance of NO_2 is produced over

central EU (r= 0.6 to 0.8 and RMSE = 6 to 12 $\mu g\ m^{-3}$), and lower values are obtained over the Mediterranean regions and most of the Spanish stations (r= 0.1 to 0.4 and RMSE $> 18\ \mu g\ m^{-3}$). An underestimation in central France and around the Alps and Pyrenees regions (MB= -2 to -10 $\mu g\ m^{-3}$) is identified (see Figure 5.4, second row). Higher errors (RMSE $> 18\ \mu g\ m^{-3}$) with positive bias (MB= 2 to 8 $\mu g\ m^{-3}$) are located in areas where anthropogenic NO_x emissions are greater.

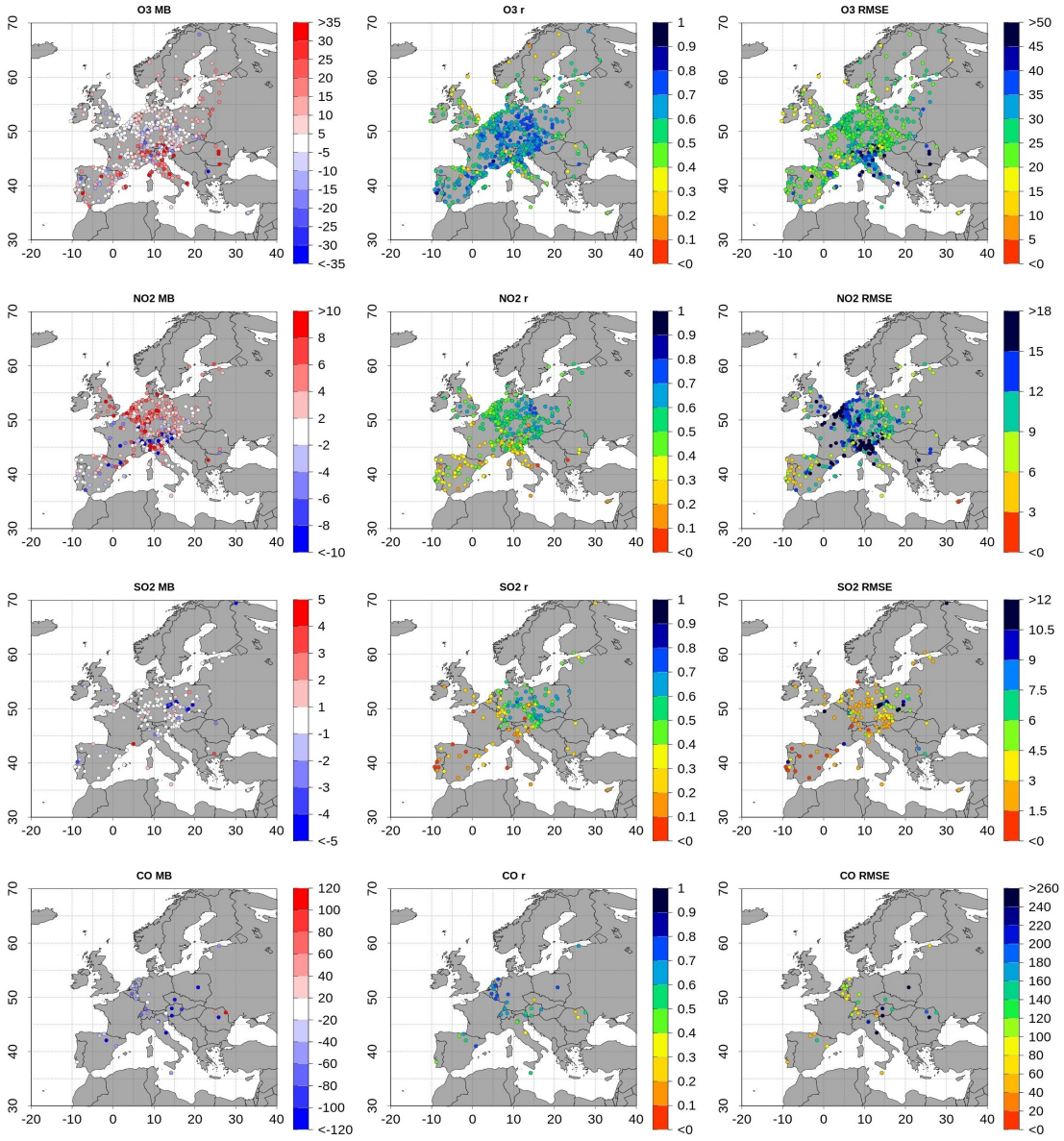

Figure 5.4: Spatial distribution of mean bias (MB, %) (left panel) , correlation (r) (middle panel) and root mean square error (RMSE,$\mu g\ m^{-3}$) (right panel) at all rural stations used for (from top) O_3 NO_2, SO_2, CO.

Sulphur dioxide

Like NO_2, SO_2 concentrations are highly influenced by anthropogenic emissions. Uncertainties in emission inventories for SO_2 have been shown to be generally large (de Meij et al., 2006).

SO_2 seasonal pattern is well captured by the model; it especially captures temporal variability and the maximum values during winter, with r =0.58 (see Figure 5.2 third row, left panel). Although, SO_2 levels are slightly underestimated in general (MB = -0.49 (yhv)/ -0.4 (yda) $\mu g\ m^{-3}$, RMSE= 6.22 (yhv) /4.3 (yda) $\mu g\ m^{-3}$), especially during the early morning, the model shows a good performance variability of the daily cycle in comparison with the measurement variability (see right panel in Figure 5.2). Daily peaks for SO_2 are poorly captured by the model (r= 0.37, RMSE= 14.2 $\mu g\ m^{-3}$) and underestimated (MB= -2.8 $\mu g\ m^{-3}$, see Table 5.3). Even though the maximum SO_2 ground level concentrations for both model and measurements occurs around 10 UTC, the decrease observed in the measurements after the maximum is not reproduced by the model.

Large normalized errors are reduced to almost half (MNGE= 63.5% and MNGE =110.6%) when applying concentrations above a threshold level of 0.2 $\mu g\ m^{-3}$. Correlation values improve when our calculations use daily mean data (r= 0.41 (yhv) /0.55 (yda)). This improvement is due to the poor quality of the hourly data for measurements from the Iberian Peninsula, Italy, France and the UK. We decided to keep these stations for calculating errors, bias, maximums and averages; however correlations from these countries using hourly data may have a limited representativeness (see Figure 5.4 second column, third row). EU statistics are shown in Figure 5.4 (third row). The model agrees better with observations in central EU, where most of the stations have MB ranging from -0.3 to 0.3 $\mu g\ m^{-3}$, RMSE from 1.5 to 3 $\mu g\ m^{-3}$ and r from 0.6 to 0.7. Only a few stations have MB $<$ -5 $\mu g\ m^{-3}$ and RMSE $>$ 10 $\mu g\ m^{-3}$, mostly located in Czech Republic.

Carbon monoxide

The number of available rural stations for CO is small for this evaluation exercise. However, CO is rather long-lived and correspondingly more uniformly distributed gas compared with other species. Thus, a low number of measurement sites is still sufficient to characterize the CO model performance.

The model's abilities are lower for CO (r= 0.39 (yhv) / 0.44 (yda)) in comparison with other species (see Figure 5.5 and Table 5.3), with high underestimation of concentrations and lower variability of data (MB = -66.98 (yhv) / -66.7 (yda) $\mu g\ m^{-3}$), especially in the winter months, when concentrations are higher (MB= -144.46 $\mu g\ m^{-3}$, r=0.28). Nevertheless, seasonal and daily patterns are well reproduced by the model (see Figure 5.2, last row). This underestimation is also seen in daily peaks, which have a low correlation factor (r=0.4), a negative bias of -117 $\mu g\ m^{-3}$, and RMSE = 285.4 $\mu g\ m^{-3}$. Part of this CO underestimation during the summer is due to severe European fire emissions that are not included in this simulation (more spatial evaluation in Section 5.4.3). When we focus on concentrations that exceed the threshold (11.45

$\mu g\ m^{-3}$), MNBE is reduced to more than half, 5.5%. Figure5.4 (last row) also presents the spatial distributions for CO. Correlation in central EU is between 0.5 - 0.7; however, some stations in Italy, Czech Republic, Romania and Spain drop to 0.3-0.4. Bias is negative in all Europe (MB= 40-80 $\mu g\ m^{-3}$), except in some stations from Romania.

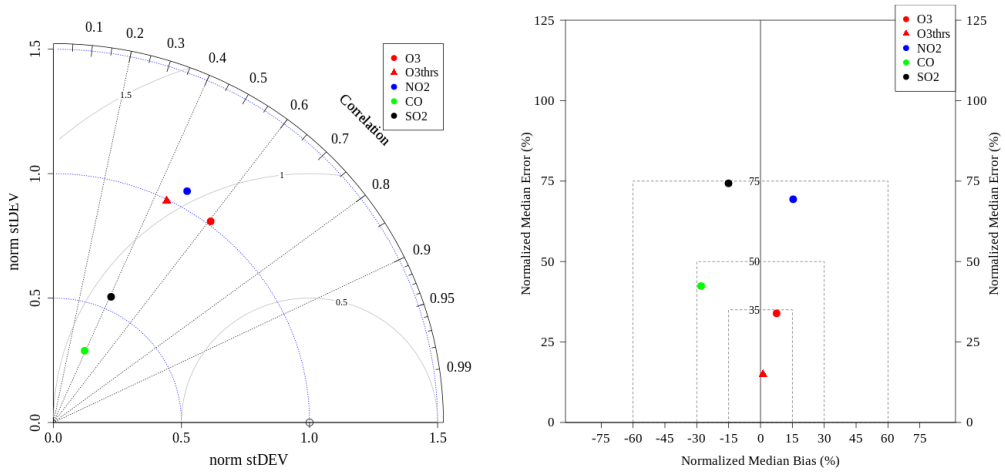

Figure 5.5: Taylor diagram (left panel) and Soccer-goal plot (right panel) of all the rural stations used for O_3 (red point), O_3 with threshold of 80 $\mu g\ m^{-3}$ (red triangle), NO_2 (blue point), CO (green point), SO_2 (black point).

5.4.2 Vertical profiles of ozone

The monthly average vertical profiles of ozone for both the model and observations are compared in Figure 5.6. Only results from May to November are discussed due to the limitation in the ozone boundary conditions described in Section 5.4.1. The comparison is made only when ozonesonde observations are available; thus, the same data from the model (NMMB24) and the observations is used. Measurements are represented by the solid red line, the NMMB24 simulation by the solid black line, and the NMMB48 by the dashed blue line. To know the variability of data, standard deviation is plotted in each vertical layer for both model (blue) and observations (red). The number of observations is given on the top of each plot.

Modelled values in the upper troposphere are mainly influenced by the BC, while the lower troposphere is basically characterized by an active photochemistry and well-mixed dynamics. The NMMB24 model simulation is in good agreement with observations during the period of study. There is a slight underestimation in the middle troposphere, which is more significant during July. In the upper troposphere, a negative bias is observed during August-October. Below 1000 m height, an overestimation ($<$ 2 ppb) is seen during summer and autumn. Variability of data is well-captured by the model, increasing from lower to higher tropospheric layers, although the modelled standard deviation is found to be lower in the upper troposphere when compared with the ozonesondes during the whole year.

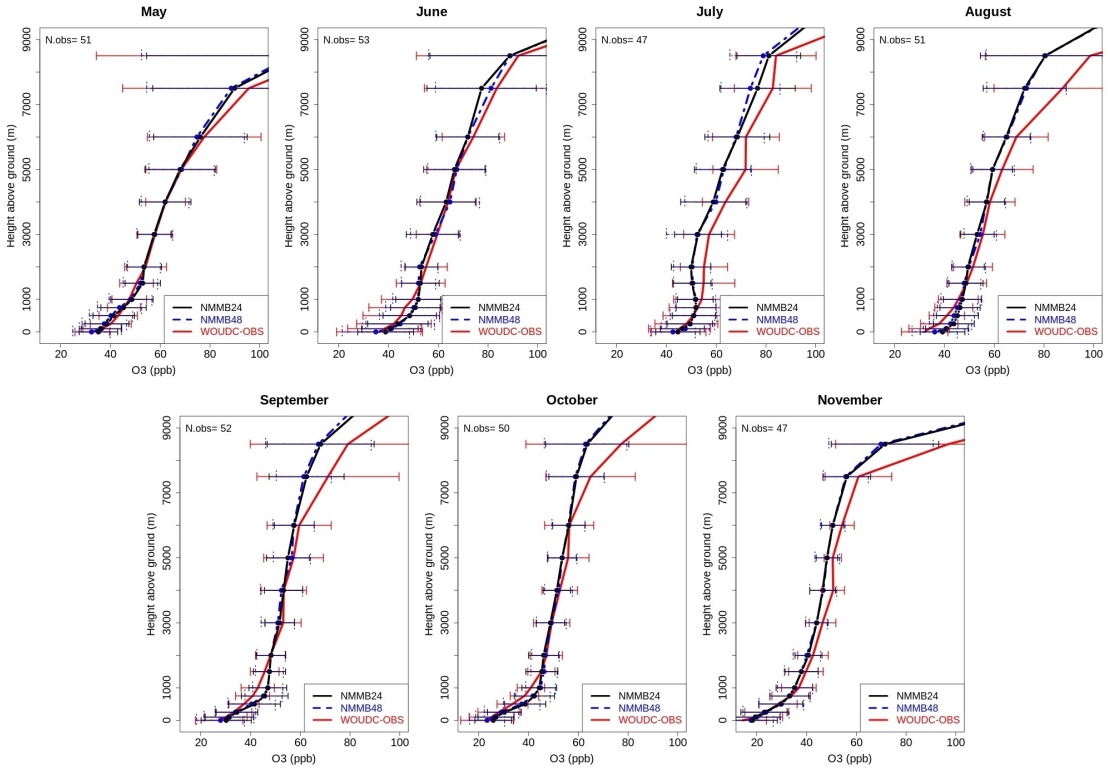

Figure 5.6: Comparison of the mean vertical profiles of ozone mixing ratio (ppb) retrieved by 7 available ozonesondes (WOUDC) and simulated by NMMB/BSC-CTM during (from left to right) winter (DJF), spring (MAM), summer (JJA) and autumn (SON) for the whole year 2010. Observations are a solid red line and model data are a solid black line (NMMB24) and dashed blue line (NMMB48).

5.4.3 Comparison with satellite data: NO_2 Tropospheric columns and CO surface-layer

Seasonally modelled VTC of NO_2 and CO mixing ratio at the surface-level are calculated here and compared with OMI and MOPITT satellite data, respectively, in Figures 5.7 and 5.8. Averaging kernels are taken into account to compute NO_2 VTC (Eskes and Boersma, 2003) and CO surface mixing ratio (Deeter, 2009). In the case of NO_2, the height of the troposphere was assumed to be fixed at 10km for all modelled data. Using the exact tropopause layer has little influence on the NO_2 VTCs, since the NO_2 concentration in the upper tropospheric layers is low. Normalized Mean bias (NMB) over land points are reported in the third column of Figure 5.7 and 5.8, where model simulation minus satellite data is displayed.

The model is in good agreement with the observations, capturing higher NO_2 and CO over the most polluted regions, such as the Netherlands, southern UK, Po Valley and big cities such as Paris and London. During the whole year, the model tends to overestimate NO_2 VTCs in big cities, especially during the colder months (NMB = 6.3 (land),%), and underestimate them in

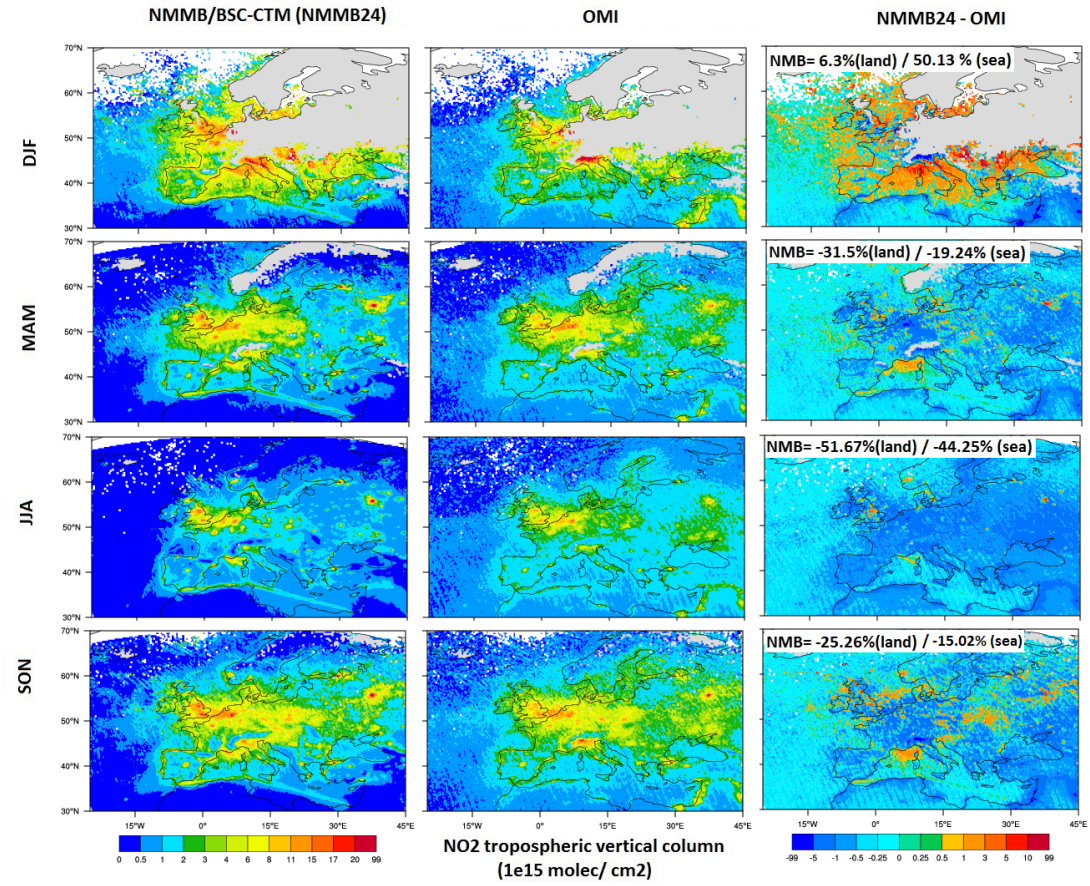

Figure 5.7: Comparison of modelled (NMMB24) NO_2 vertical tropospheric columns against satellite data (OMI) for (from top) winter (DJF), spring (MAM), summer (JJA) and autumn (SON) for the whole year 2010 in $1e^{15} molec/cm^2$. NMMB24 data is displayed in the left panel, OMI data in the middle panel and NMMB24 minus OMI data in the right panel where the NMB (%) over land is added.

rural regions. Significant differences are also seen in the Mediterranean and North sea during the cold months (DJF) (NMB = 50.13 (sea)%), probably because of overestimating shipping emissions or the lack of ship plume effects on the model (Vinken et al., 2011). During warm months, NO_2 VTCs are lower and the model tends to underestimate over all the EU land and sea (NMB= -51.67 (land)/ -44.25 (sea) %). These results are consistent with the underestimation seen in surface NO_2 during the daytime (Section5.4.1). Note that NO_2 concentrations due to NO_x lightning emissions are not included in this simulation. Satellite evaluation reaffirms that there is a general trend to underestimate CO in the surface layer (seen in Section5.4.1) with an NMB between -5.02 to -8.20 (land) % during the whole year. However, during periods of higher emissions, which take place in cold months (DJF and SON), the pattern of emissions in central EU is well-captured by the model, with only slight overestimation for big cities. Larger underestimations are observed over Eastern Europe. Biomass burning emissions are not included

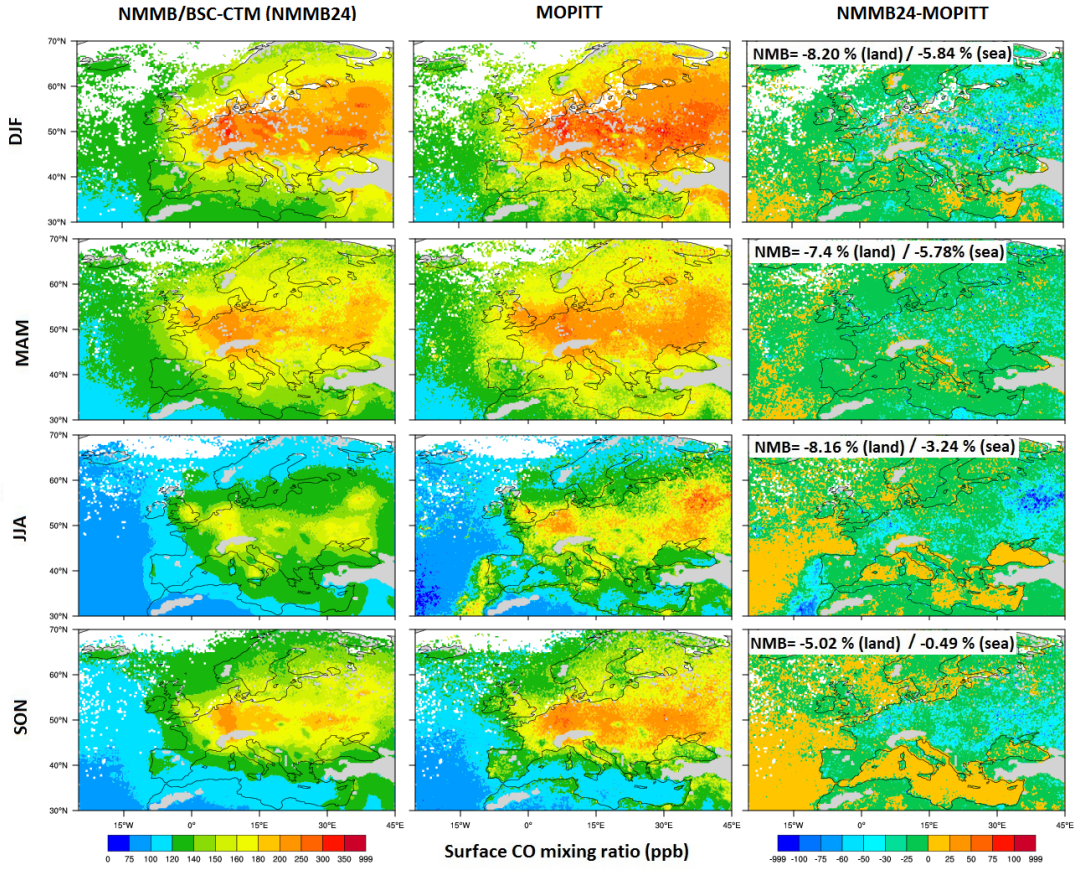

Figure 5.8: Comparison of modelled (NMMB24) CO mixing ratio against satellite data (MOPITT) for (from top) winter (DJF), spring (MAM), summer (JJA) and autumn (SON) for the whole year 2010 in ppb. NMMB24 data is displayed in the left panel, MOPITT data in the middle panel and NMMB24 minus MOPITT data in the right panel where the NMB (%) over land is added.

in this simulation, for that reason, a significant underestimation is observed mainly across Russia and Portugal during the summer, were several large wildfires took place. Other, less relevant forest fires also occurred in Spain, France, Italy, and Greece (Schmuck et al., 2011). North African countries, like Algeria, were affected in terms of wildfire; however, no emissions from Northern Africa are included in this simulation.

5.4.4 Effects of vertical resolution in chemical concentrations

Vertical resolution has a direct impact on the vertical distribution of emissions, on PBL height, and on the transport of air masses from the higher levels to the surface. All of these processes may have an effect on chemical concentrations.

Regarding the daily profiles in Figure 5.2 (right panel), one can observe lower concentrations of

O_3 (MB=-2.17 $\mu g\ m^{-3}$) and SO_2 (MB=-0.62 $\mu g\ m^{-3}$) during the whole day, and higher concentrations of NO_2 (MB=3.89 $\mu g\ m^{-3}$) and CO (MB=-59.52 $\mu g\ m^{-3}$) when the NMMB48 simulation is used. These differences in concentrations of NO_2, SO_2 and O_3 are seen mainly during the night time. They become more intense in summer for O_3, NO_2 and CO, and in winter for SO_2.

These differences in concentrations of primary pollutants are partly due to vertical distribution of emissions. The main sources of SO_2 emissions (90%) are from combustion in energy and transformation industries, non-industrial combustion plants, and combustion in the manufacturing industry (Pouliot et al., 2012). For that reason, a higher resolution shows that SO_2 emissions are better distributed within the vertical layers, becoming less concentrated at the surface layer. On the other hand, 52% of NO_x and 43% of CO emissions are from road transport and other mobile sources (Pouliot et al., 2012) emitted at the surface layer; thus, higher resolution produces less artificial redistribution of the emissions leading to larger concentrations over this surface layer (Wild and Prather, 2000).

Model vertical resolution is also critical for representing PBL height. Higher resolutions allow the model to calculate PBL height more precisely. PBL is lower using simulation with 48 layers (not show here); consequently, this has an influence on surface concentrations. This could explain higher concentrations of NO_2 and CO using higher resolution.

Secondary pollutants are influenced by primary pollutants. Thus, higher NO_2 concentrations in NMMB48 have a direct effect on O_3 destruction due to nocturnal NO_x titration.
Generally speaking, vertical structure in Figure5.6 does not show significant differences between the simulation with 24 vertical layers (NMMB24) and 48 vertical layers (NMMB48). However, in specific cases the differences may be significant.

5.4.5 NMMB/BSC-CTM in comparison with other regional air quality models over Europe

In this section, the NMMB/BSC-CTM model evaluation is compared with several evaluation studies of regional AQMs implemented over Europe. Details of these AQMs and their statistical results are found in Tables 5.4 and 5.5, respectively.

The O_3 daily mean/max performance in our model (r=0.68/0.75, RMSE= 21.2/22$\mu g\ m^{-3}$) for May-Nov are in the same range of results from other modelling systems. In the model intercomparison study van Loon et al. (2007), correlations are between 0.64 to 0.80 /0.75 to 0.84. Our model also presents results that are similar to the models LOTOS-EUROSv4 (Schaap et al., 2008) and CALIOPE-EU04 (Pay et al., 2010), with correlations of 0.65/0.75 and 0.66/0.69, and RMSE=25.22/20.39 and 20.6/21.8$\mu g\ m^{-3}$, respectively. Good results for daily mean O_3 (r=0.77 and RMSE= 19.2$\mu g\ m^{-3}$) are found in the evaluation of the CHIMERE model run for the year 2009 (Bessagnet et al., 2012). A validation of the online meteorological and chemical transport WRF/Chem model for 2007 is reported in Tuccella et al. (2012), with a good representation of O_3 daily max (r=0.71 and MNBE= -4.4$\mu g\ m^{-3}$). Hogrefe et al. (2013) present an

evaluation of O_3 concentrations over North America and Europe using the database generated from AQMEII-Phase1. Eleven offline regional AQMs from May-Sept 2006 over EU are utilized in this study. The statistical indices obtained here using both observations and model show that daily maximum 8-hr average concentrations are comparable to those reported in Hogrefe et al. (2013). Average correlation coefficient (0.69, with min=0.55 and max=0.8) is lower than the one obtained in this study for the NMMB/BSC-CTM model (0.76 from May-Nov). Errors are very similar for both studies. However, the horizontal resolution (0.2°) might be too coarse to identify relevant differences between offline and online models. Daily NO_2 statistics for NMMB/BSC-CTM (r=0.61, RMSE=9.72μg m^{-3}) show a very satisfactory performance in comparison to the other models, such as, LOTOS-EUROSv4 model (r= 0.4 and RMSE=11.44μg m^{-3}), CHIMERE model (r=0.61, RMSE=15.8μg m^{-3}) and WRF/CHEM (r=0.57). CALIOPE-EU04 presents higher performance for daily NO_2 (r=0.67 and RMSE=10.1μg m^{-3}). Similar to NO_2, the NMMB/BSC-CTM's abilities to reproduce daily mean SO_2 concentrations are comparable to other models (r= 0.55, RMSE= 4.3μg m^{-3}), such as the LOTOS-EUROSv3 model (r= 0.41 and RMSE=3.2μg m^{-3}), the WRF/CHEM model (r=0.47, MNBE=165.5μg m^{-3}) and CALIOPE-EU04 (r=0.6 and RMSE=2.2μg m^{-3}).

Knote et al. (2011) compare European NO_2 VTC estimations of the COSMO-ART model to OMI satellite data for each season of different years, with a resolution of 0.17 x 0.17° and 40 vertical layers. The NMMB/BSC-CTM model's performance for NO_2 VTC is in the same range as the COSMO-ART model. During the winter season, both models show the highest and positive bias: COSMO-ART with NMB= 59 (all)/ 40 (sea)% for winter 2006, and NMB= 19 (all)/ 6 (sea)% for NMMB/BSC-CTM during winter 2010. The main difference between the models corresponds to autumn and summer, where COSMO-ART presents positive NMB= 38 (land) / 108 (sea)% and -11 (land)/ 28 (sea)%, and NMMB/BSC-CTM presents negative NMB= -25 (land) / -15 (sea) % and -51 (land) /-44 (sea)%, respectively.

Table 5.4: List of published European model evaluation studies and their main characteristics used in the intercomparison exercise (Table 5.5)

Model	Reference	Year	Resolution
NMMB/BSC-CTM	This study	2010	0.2x 0.2°/24
AQMEII-Ph1	Hogrefe et al. (2013)	2006	15-50km
CALIOPE-EU04	Pay et al. (2010)	2004	12 x 12km/5
LOTOS-EUROSz3	Schaap et al. (2008)	1999	0.5 x 0.25°/3
LOTOS-EUROSz4	Schaap et al. (2008)	1999	0.5 x 0.25°/4
CHIMERE	Bessagnet et al. (2012)	2009	7 x 7km/9
WRF/CHEM	Tuccella et al. (2012)	2007	30x30 km/ 28
EMEP5	van Loon et al. (2007)	2001	50 x 50 km/20
LOTOS-EUROS	van Loon et al. (2007)	2001	0.5 x 0.25°/4
MATCH	van Loon et al. (2007)	2001	0.4 x 0.4°/14
CHIMERE	van Loon et al. (2007)	2001	0.5 x 0.5°/8
RCG5	van Loon et al. (2007)	2001	0.5 x 0.25°/5
DEHM	van Loon et al. (2007)	2001	50 x 50km/20

Table 5.5: Intercomparison of the statistical evaluation with other works. Results between NMMB/BSC-CTM model (NMMB24) and other European models for the gas phase (O_3, NO_2, SO_2 daily mean (dmean), O_3 daily max (dmax) and O_3 daily maximum 8-hr average). Statistics shown here are for the period of May-Nov concerning O_3, and for the whole year for the other pollutants (Mean Normalized Bias Error (MNBE, %), correlation (r), and Root Mean Squared Error (RMSE,μg m^{-3})).

Model	**O_3 dmean**			**O_3 max 8-hr**		**O_3 dmax**			**NO_2 dmean**			**SO_2 dmean**		
	MNBE	**r**	**RMSE**	**r**	**RMSE**	**MNBE**	**r**	**RMSE**	**MNBE**	**r**	**RMSE**	**MNBE**	**r**	**RMSE**
NMMB/BSC-CTM	**17**	**0.68**	**21.2**	**0.76**	**21.3**	**10.1**	**0.75**	**22.0**	**65.4**	**0.61**	**9.7**	**162**	**0.55**	**4.3**
AQMEII-Ph1				0.69	22.2									
CALIOPE-EU04	6	0.66	20.6			-3	0.69	21.8	-17	0.67	10.1	83	0.60	2.2
LOTOS-EUROSz3		0.65	24.5				0.75	19.9		0.37	12.4		0.41	3.2
LOTOS-EUROSz4		0.65	25.2				0.75	20.4		0.40	11.4		0.40	3.4
CHIMERE		0.77	19.2							0.61	15.8			
WRF/CHEM				0.70		-4	0.71		14.9	0.57		165	0.47	
EMEP5	10	0.72				1	0.75							
LOTOS-EUROS	2	0.70				7	0.76							
MATCH	6	0.80				2	0.81							
CHIMERE	29	0.76				10	0.84							
RCG5	3	0.71				7	0.76							
DEHM	18	0.64				-1	0.75							

5.5 Conclusions

In the framework of the AQMEII-Phase2 intercomparison exercise, the present work describes an annual evaluation of the online air quality model NMMB/BSC-CTM for the year 2010 over a European domain. The pollutants evaluated are ozone (O_3), nitrogen dioxide (NO_2), sulphur dioxide (SO_2) and carbon monoxide (CO). The evaluation dataset includes observational surface data compiled by AQMEII-Phase2 taken form the ENSEMBLE system (Bianconi et al., 2004; Galmarini et al., 2012), vertical O_3 measurements from the WOUDC database, retrievals of NO_2 tropospheric columns from the OMI satellite instrument, and surface CO mixing ratios retrievals from the MOPITT satellite instrument.

The surface O_3 results show a good agreement with the observations during May-November, especially in central EU (r=0.6-0.8). A general trend to overestimate the O_3 concentrations is identified mainly in summer and early autumn months (MB= 8.84 $\mu g\ m^{-3}$) where photochemical production of O_3 is more important. The model statistics indicate a poorer performance for NO_2 (r= 0.61) and SO_2 (r=0.55) in comparison with O_3, especially during night. For these two pollutants, large biases, positive for NO_2 (MB= 2.6 $\mu g\ m^{-3}$) and negative for SO_2 (MB= -0.6 $\mu g\ m^{-3}$), are found during the cold months where the emissions are higher. The weakest performance of the NMMB/BSC-CTM is found for surface CO concentrations, where the model exhibits a systematic underestimation trend, especially in winter months (MB= -144.5 $\mu g\ m^{-3}$). The lack of some important CO emission sources (i.e., biomass burning) may explain such behaviour. However, the spatial distribution of CO is well-captured by the model. Large polluted regions are well identified when the model is compared with the MOPITT satellite data. Furthermore, the vertical structure of O_3 is evaluated with ozonesondes. The model presents a cold bias above the PBL and through the troposphere for the whole year. This bias is reduced towards summer and autumn due to an improvement on the ozone boundary conditions applied. Good agreement with the observations is produced in the PBL, where the model slightly overestimates the ozone in these layers. Finally, the NO_2 VTC is compared with OMI observations. Overall, the model reproduces reasonably well the observations. Over land, the results show a trend to overestimate NO_2 VTC in large urban areas, especially during winter and autumn. On the other hand, underestimation is seen in rural areas and over the sea for the whole year.

The sensitivity of the model results to the vertical resolution of the model shows an improvement when the number of vertical layers is increased, from 24 to 48. A reduction of the error is found in O_3 and SO_2 concentrations and increase on NO_2 and CO concentration using 48 vertical layer simulation (NMMB48). In this sense, the NMMB48 configuration nicely reduces the bias on the surface ozone concentrations from June to October.

Overall, the NMMB/BSC-CTM statistics are in the same range as other regional modelling systems applied over Europe. And particularly, the NMMB/BSC-CTM model results are comparable with those described from the AQMEII-Phase1 intercomparison project.

Chapter 6

Conclusions and future research

In the present Ph.D. thesis a complete overview of the scientific context and the objectives were presented in the introductory Chapter 1, followed by Chapter 2 in which a full description of the NMMB/BSC-CTM model (for both the atmospheric driver NMMB and the gas-phase chemistry module) was given. Chapter 3 compared two simplified chemical approaches for the stratospheric ozone handling as an upper boundary condition to model the troospheric ozone STE in the global scale. Chapters 4, and 5 presented the model evaluation for the Global and Regional (European domain) runs over an annual cycle. A detailed discussion and conclusions of each of the results were included in Chapters 3, 4 and 5, respectively. The most relevant aspects of those conclusions are presented as a chapter summary in this section. A last sub-section is devoted to the future work related to the development and evaluation of the online NMMB/BSC-CTM for further research applications.

6.1 Synthesis of the results

The research conducted in this Ph.D. thesis has involved around the implementation and evaluation experience of the online NMMB/BSC-CTM model. The main conclusions drawn from this work are:

1. **The NMMB/BSC-CTM represents a very powerful tool which studies air quality and atmospheric chemistry and can be used in research applications at both global and regional scales with a unified dynamic-physics-chemistry framework.**

2. **The model's abilities to reproduce the relevant pollutants in the atmosphere are comparable to current state-of-the art models at global and regional scale.**

3. **A unified framework to model the atmospheric chemistry is reliable with the unified multiscale NMMB/BSC-CTM model.**

4. **The gas-phase chemistry evaluation shows that the NMMB/BSC-CTM model provides a suitable framework to further study the life cycle of aerosols (of both primary and secondary origin).**

More specific conclusions of the work are presented in the following sections.

6.1.1 Evaluation of the handling of stratospheric ozone

In Chapter 3, two different parametrizations for the treatment of the stratospheric ozone were implemented within the online global chemical transport model NMMB/BSC-CTM to handle the stratospheric ozone in a dynamic but computationally inexpensive approach. These approaches are linear schemes and depend only on the air temperature and the ozone amount in their formulation (see Section 2.2.5). The main difference between them is the way in which the heterogeneous ozone chemistry is treated. The first approach is based on the last version of the Cariolle linear stratospheric ozone scheme, Cariolle v2a (CAR; Cariolle and Teyssèdre, 2007), and includes a heterogeneous term in its parametrization. The second approach is based on the linear ozone scheme COPCAT (COP; Monge-Sanz et al., 2011) and incorporates the heterogeneous chemistry in their coefficients implicitly, thus, no extra term is added in this parametrization. A sensitivity analysis is presented with attention to the simulation of the stratospheric ozone with both linear schemes.

The two model simulations are evaluated with the total ozone columns from SCIAMACHY satellite retrievals, and with vertical profiles from ozonesondes data and HALOE satellite retrievals.

This study suggests several relevant points:

1. Both simulations well-performed the total ozone columns in comparison with the SCIAMACHY satellite data, capturing the main seasonal cycle features: higher values during spring in the NH extratropics, lower ozone concentrations in the tropics, and lowest values of the Antarctic ozone hole in the south pole during September-October.

2. CAR has systematic higher stratospheric ozone concentrations than COP.

3. The main limitation of CAR is the positive bias of the ozone columns in the NH during summer and autumn and also, in the south pole during the spring season. On the other hand, the main limitation of COP is its tendency to overestimate ozone values over the south polar region from December to May.

4. Higher ozone column values over the northern latitudes are underestimated by both simulations during the first half of the year.

5. Even though, both simulations perform a shorter duration of the ozone hole in comparison with the satellite data, the treatment in the heterogeneous chemistry adopted by COP provides a more realistic ozone hole performance during September-October over the Antarctic (for both spatial extension and magnitude intensity).

6. 6. Regarding the vertical structure of O_3 in the stratosphere and upper troposphere, major features are well-captured by both simulations: reproducibility of the maximum stratospheric ozone peak around 6-10hPa, higher ozone values in the tropics (20N-20S) and

lower in the mid-high latitudes (90N-50N and 50S-90S), and the strong ozone gradient in the tropopause layer.

7. Vertical profiles show that CAR has a tendency to simulate higher ozone concentrations, including the maximum stratospheric ozone peak, during the whole year. Vertical profiles are better-captured by COP with a slightly underestimation of the ozone in the upper stratosphere.

8. CAR and COP simulations exhibit an hemispheric asymmetry in STE of ozone where most of the stratospheric influx of ozone occurs in the NH. Over the tropics the STE balance is positive. Higher stratospheric inflow is seen in the COP simulation than in CAR and both simulation results are in good agreement with previous studies, although they exhibit a lower range value of the model estimates of STE.

The main conclusion drawn from the inter-comparison work is that these simple ozone stratospheric schemes can capture the main characteristics of the stratospheric ozone dynamics. Therefore, they are good alternatives to be implemented in the tropospheric CTMs or global meteorological models to provide a realistic ozone upper boundary condition with a very low computational cost.

6.1.2 Global run evaluation

A comprehensive benchmark evaluation of the tropospheric oxidant gas-phase chemistry of the NMMB/BSC-CTM on a global scale for the year 2004, is presented in Chapter 4. This is the first time that the model has been evaluated on a global scale over a whole annual cycle. Sections 4.1 and 4.2 provide an introduction and presents the modelling system experiment, respectively. The observational dataset used in the model evaluation is described in Section 4.3. The main results of this work are discussed in Section 4.5.

The model results for several important reactive gases (OH, CO, HCHO, NO_x, NO_2, PAN, HNO_3, and O_3) are compared with a variety of ground-base monitoring stations (EMEP, WDCGG and CASTNET), as well as ozonosondes (WOUDC, CMD and SHADOZ), aeroplane measurements (MOZAIC and several flight campaigns) and satellite measurements (SCIAMACHY and MOPITT) available .

The key findings of this model evaluation are as follows:

1. The evaluation of OH against a previous studies indicates that the oxidizing capacity is well represented at a global scale by the model. However, the overestimation in the model peak concentrations of OH could be explained by the lack of anthropogenic aerosols and secondary aerosol formation, leading to an atmosphere with excessive oxidizing capacity, especially, below the aerosol layers.

2. The global annual mean burden of CO is in good agreement with other studies with a positive bias over the tropics. The model well-performed the vertical profiles of CO during

the DJF and MAM, with positive biases during the warm months for most of the stations. The phase and amplitude of the seasonal cycles of the modelled CO at 800 and 500 hPa are in good agreement with the MOPITT measurements. However, CO distribution in the tropical area is overestimated, mainly located in West-Central Africa during winter, and underestimated in the high Northern latitudes. This bias could be related to emission errors.

3. Overall, the model accurately represents the latitudinal distribution of HCHO (formaldehyde), capturing the spatial and seasonal variation in HCHO tropospheric columns in comparison with the satellite measurements. Positive model biases are seen over Central Africa, Australia and Southeast Asia during the cold months, and over the Amazon region and the eastern United States during the warm months. This finding may indicate an overestimation of the HCHO biogenic emissions.

4. Nitrogen species are well-performed by the model capturing the surface-level concentrations and vertical structure. A negative bias of NO_x from March to August is observed over Asia. The model has a tendency to over-predict PAN and HNO_3 vertical profiles concentrations. HNO_3 wet deposition are well-performed by the model with higher correlations over USA and EU.

5. Ozone annual burden is in good agreement with the current state-of-the-art global atmospheric chemistry models. The model well-modelled ozone concentrations in the surface level, with significant positive bias from May to October over USA and China (the treatment of anthropogenic NO_x emissions as constant fluxes throughout the year may be one of the reasons for this bias). Ozone in the troposphere is simulated reasonably well, capturing the spatial and seasonal variation in observed background tropospheric O_3 profiles, with a positive bias of $\sim$ 5-20ppb along the troposphere. The significant overestimation of CO especially in the free troposphere could be the reason for this positive ozone bias.

Some pollutants (NO_x, CO, NMVOCS, and O_3) are sensitive to errors in emissions. Relevant conclusions about the emissions inventories implemented in the current version of the model are:

1. Part of these pollutant biases may be related to the uncertainties in the anthropogenic and biomass burning inventories, where the magnitude or the location of emission is not correctly modelled.

2. Land-based anthropogenic emissions have no seasonal cycle variation; this limitation is also observed in the results.

3. O_3 concentrations in the PBL are very sensitive to the emissions; consequently, the variability of ozone concentrations can potentially be enhanced by improving the spatio-temporal distribution of the ozone precursor emissions. In the ACCMIP emissions used for this study, the anthropogenic emissions were assumed as a constant flux for the whole year.

6.1.3 Regional run evaluation

During the Ph.D. development, we had the opportunity to participate in the AQMEII Phase-2. The AQMEII Phase2 aims to intercompare online coupled regional-scale models over North America and Europe. The NMMB/BSC-CTM was applied to Europe for the year 2010 in the framework of the AQMEII-Phase2 intercomparison exercise. The work described in Chapter 5 presents a spatial, temporal and vertical evaluation of the model results. This is the first time that the model has been evaluated on a regional scale over a whole annual cycle.

Section 5.1 gives an introduction about this work, Section 5.2 presents the modelling experiment, the observational dataset and the statistical metrics used to evaluate the model are described in Section 5.3, the results are discussed in Section 5.4 and are compared to other modelling studies in Section 5.4.5, finally the main conclusions of the work are presented in Section 5.5. Here we summarise the main outcomes.

The gas-phase model results were compared with available ground-based monitoring stations for relevant reactive gases, ozonesondes, NO_2 VTC from OMI satellite retrievals and surface CO from MOPITT satellite retrievals.

Relevant conclusions of this work are listed as follows:

1. The model reproduces reasonably well the seasonal cycle during the period of study for the surface O_3 results. Good agreement with the observations is observed during May-November, especially in central EU. There is a general trend to overestimate the O_3 concentrations during summer as a result of the increasing importance of the photochemical production of O_3.

2. The strong impact of the BC in background ozone concentrations with the troposphere is a critical point. Significant O_3 underestimation of the model was found for most of the stations during winter, when the photochemical activity of O_3 and precursors are lower and the concentrations are strongly driven by the boundary conditions. Due to this limitation in the O_3 BC, we decided to evaluate O_3 only from May to November.

3. The O_3 daily profiles and daily variability are well-captured by the model.

4. In the upper troposphere the model concentrations are mainly influenced by the BC, while in the lower troposphere they are basically characterized by an active photochemistry and well-mixed dynamics. Above the PBL and through the troposphere, the model presents a negative bias of O_3 that is reduced towards summer and autumn due to an improvement on the ozone BC applied. In the PBL, a good agreement with the observations is observed, with a slight overestimation.

5. The model statistics and qualitative comparisons with observations indicate a poorer performance for surface NO_2, especially during nighttime. This result may be due to the lack of the heterogeneous formation of HNO_3 through N_2O_5 hydrolysis, an important sink of NO_2 at night.

6. Large biases, positive for NO_2 and negative for SO_2, are found during the cold months where the emissions are higher. Uncertainties in the emission inventory and also in the spatial and temporal distribution of the sources may explain such behaviour.

7. Overall, the model reproduces reasonably well when compared with the NO_2 VTC from the OMI observations. Overestimation is seen over land in large polluted areas, especially during cold seasons. On the other hand, underestimation is seen in rural areas and over the sea for the whole year.

8. The weakest performance of the NMMB/BSC-CTM is found for surface CO concentrations, where the model exhibits a systematic underestimation trend, especially in winter months. Such results may arise in the lack of some important CO emission sources (i.e., biomass burning). When the model is compared with the MOPITT satellite data, the spatial distribution of CO is well-captured and identifies large polluted regions.

The influence of the vertical resolution on chemical concentrations was also studied. Changes on the vertical resolution have an impact on chemical concentrations due to changes on the vertical distribution of emissions, on the PBL height accuracy, and on the transport of air masses. Main conclusions concerning the sensitivity of the model results due to the vertical resolution of the model are:

1. A general improvement on the annual cycle is seen when the number of vertical layers is increased, from 24 to 48.

2. Lower concentrations of O_3 and SO_2 during the whole day, and higher concentrations of NO_2 and CO are seen in the daily profiles, when the 48 vertical-layer simulation is used. These changes in concentrations of primary pollutants might be attributed to vertical distribution of emissions.

3. A higher resolution shows that SO_2 emissions are better distributed within the vertical layers, becoming less concentrated at the surface layer. Moreover, higher resolution produces less artificial redistribution of the emissions leading to larger concentrations over this surface layer for NO_2 and CO.

4. Higher NO_2 concentrations in the 48 vertical-layer simulation have a direct effect on O_3 destruction due to nocturnal NO_x titration. In this sense, the higher resolution configuration nicely reduces the bias on the surface ozone concentrations from June to October.

5. Vertical structure does not show significant differences between the two simulations with different vertical resolution.

Gas-phase model results were compared with other regional AQMs currently applied in Europe. Main conclusions are summarised as follows:

1. The O_3 daily mean/max performance in our model for May-Nov are in the same range of results as for other modelling systems.

2. The model's abilities to reproduce daily NO_2 and SO_2 statistics are comparable to other models.

3. Overall, NMMB/BSC-CTM performs within the range of current air quality modelling systems at regional scale.

6.2 Future areas of research and perspectives

6.2.1 Implement and evaluate the fully coupled meteorology-chemistry model

This work is focused in the proper representation of the gaseous species, which is fundamental for the formation of secondary aerosols. NMMB/BSC-CTM is, however, a much larger project than this thesis alone. In this sense, this Ph.D. thesis is part of an ongoing effort (Pérez et al., 2011; Jorba et al., 2012; Spada et al., 2013; Badia and Jorba, 2014) on the development of a unified fully coupled chemical weather prediction system able to solve gas-aerosol-meteorology interactions within a wide range of scales which can be used in both operational and research applications.

Atmospheric aerosols can change climate and meteorology via direct, semi-direct, and indirect effects. Through aerosol direct effects, aerosol particles can either cool (directly scattering) or warm (absorbing the solar and thermal radiation) the atmosphere. Changes in surface temperature, wind speed, relative humidity and clouds that are caused by changes in radiation are examples of the semi-direct effect. The aerosol semi-direct effect also influences photolytic rate for major gaseous species such as O_3, NO_2, NO_3, HNO_2 and N_2O_5. The first indirect effect has an influence in the cloud drop size, number, reflectivity, and optical depth. The second aerosol indirect effect influences cloud liquid water content, lifetime, and precipitation (Jacobson et al., 2007; Zhang, 2008; Baklanov et al., 2014).

An aerosol module for the relevant global aerosols is under development within the NMMB/BSC-CTM. Extensive description and evaluation of the dust implementation is presented in Pérez et al. (2011) and Haustein et al. (2012). The sea-salt aerosol module is described and evaluated on a global scale in Spada et al. (2013); black carbon, organic carbon and sulphate are currently under development. Future versions of the model will include a complete secondary aerosol module, and, therefore, aerosol feedbacks (direct, semi-direct, first indirect and second indirect) on meteorology and trace gases will be considered.

The fully coupled chemical weather prediction system will need further evaluation to quantify these model improvements. Thus, the main objective will be to analyse the chemical and meteorological results to estimate the relative importance of aerosol direct and indirect effects in model predictions. During this Ph.D. thesis, I have been performing an extensive evaluation of the gas-phase chemistry of the model. Hence, from my experience, general recommendations in the future model evaluation are: (1) use a wide-range of different observational data-sets that provide complete spatial, temporal and vertical information of the relevant pollutants, (2) observations are not perfect, therefore, the errors and uncertainties of the measurements need to be

taken into account when they are used, (3) review other model evaluation studies to compare if the model is in good agreement with the other modelling systems currently used, and (4) improve the emissions of gas-species with proper temporal disaggregation and with detailed online coupling with the meteorology and relevant feedback effects.

Here, as a initial step on the model development we decided to focus the efforts in analysing only one year. However, several of the tropospheric species evaluated in this dissertation show large inter annual variations (see Voulgarakis et al. (2010)). Thus, in future works we also recommend to study the inter-annual variations where further analysis of the global quantities related to hydroxyl radical and methane lifetime will be performed.

6.2.2 Increase the vertical and horizontal resolution

Generally speaking, the higher the resolution of the model simulation, the better the representation of atmospheric processes. Hence, higher resolution improves the topographical details (e.g. land-use, boundary layer height and the total cloud), flow characteristics and associated vertical and horizontal dynamic processes. In addition, lower resolution can introduce artificial dilution caused by averaging point source emissions into coarse grids. Although higher resolution will not automatically reduce the systematic errors, there are indications that some individual processes are better captured at higher horizontal resolution.

The resolution of the models depends on the area coverage. CTMs are usually applied to wide domains at coarse resolution or at high resolution over small regions. Higher resolution on the model provides much more detailed information, but increases the computing time. However, the dramatic increase in computational power during the last years will enables us to run our model experiments at higher resolution for global and regional applications.

An updated version of the nested-grid GEOS-Chem model is presented in Chen et al. (2009). In this study, a comparison of the nested-grid (0.5°x 0.667°) with global models indicates that the fine-resolution nested-grid model is capable of resolving individual cities with high associated emission intensities. In Dore et al. (2012) the Fine Resolution Atmospheric Multi-pollutant Exchange model (FRAME) was applied to model the spatial distribution of reactive nitrogen deposition and air concentration over the United Kingdom at horizontal resolutions of 1 km, 5 km and 50 km. The modelled concentrations of NO_2 were validated by comparison with measurements and the results shown better agreement with the high model resolution.

In Section 5.4.4 the effects of vertical resolution in chemical concentrations were presented. The main conclusion about this specific study is that the model shows an improvement when the number of vertical layers is increased. Therefore, this future study will attempt to analyse the sensitivity of relevant air pollutants to different model resolutions for regional and global domains.

6.2.3 Simplified stratospheric scheme

In applications focused on the troposphere, such as AQMs, the stratospheric chemistry needs to be solve using a simplified approach avoiding detailed full stratospheric chemistry schemes. Section 2.2.5 and Chapter 3 describe and present two simplified approaches used to solve the stratospheric ozone in the NMMB/BSC-CTM. Then, in the current version of the model, stratospheric ozone is calculated using a linear ozone stratospheric scheme: Cariolle v2a (Cariolle and Teyssèdre, 2007) or COPCAT (Monge-Sanz et al., 2011). In addition, mixing ratios of other species (NO, NO_2, N_2O_5, HNO_3 and CO) are initialised each day from a global chemical model MOZART-4 (Emmons et al., 2010).

Thus, future challenges on the development of the global model would be to implement simplified stratospheric chemistry for other species, such as CO. Claeyman et al. (2010) present a new linear scheme, named LINCO, for the computation of the CO chemical tendencies which is based on a similar methodology to the Cariolle v2a for the stratospheric ozone. An evaluation of this linear parametrization is also presented in Claeyman et al. (2010) which uses satellite data from MOPITT observations and the aircraft measurements from MOZAIC.

6.2.4 Emission sensitivity

Model results have shown the need to improve the spatio-temporal distribution of the emissions, specially for the global scale. The land-based anthropogenic emissions inventory implemented in the global model evaluation does not have any seasonal variation, consequently, relevant gases that are sensitive to emission rates exhibit a significant bias.

Biogenic emissions are computed online with the MEGAN2.04 depending on several factors that include: landcover, meteorological conditions. Ashworth et al. (2010) evaluates the effect of varying the temporal resolution of the weather input data on isoprene emission estimates generated by the MEGAN. This study suggests that, by using daily or monthly data instead of hourly data a reduction of 3% and 7% of the isoprene emissions is obtained. Moreover, the impact on a local scale can be more significant with reductions of up to 55% at some locations when using monthly average data compared to using hourly data. Another study, Marais et al. (2014), performs several sensitivity model runs to study the impact of different model input and model settings on isoprene estimates and resulted in differences of up to $\pm$ 17% of the reference isoprene total. Land cover, emission factors, and meteorological parameters are important driving variables of MEGAN, and the uncertainties of estimated biogenic volatile organic compounds (BVOCs) emissions and their impact on surface ozone are hence associated with uncertainties in these inputs. In this sense, Situ et al. (2013) present a sensitivity of surface ozone to BVOC emissions model driving variables over China. It is shown that the impact of BVOC emissions on the surface ozone peak is $\sim$ 3 ppb on average with a maximum of 24.8 ppb, while the impact is $\sim$ 10 ppb on average.

Thus, immediate future research in emission modelling should focus on: (1) introducing a sea-

sonal land-based anthropogenic emissions variation on the global scale, (2) implementing the NOx emissions from lightning (which can have a strong impact on the modelled OH concentrations (Labrador et al., 2004), (3) implementing the biomass burning emissions on the regional scale (which can reduce part of the CO underestimation observed in the regional evaluation), (4) making several sensitivity tests to study the impact of different driving variables in order to find the most suitable configuration for the biogenic emissions, and (5) implementing the feedback aerosol-radiation that affects indirectly the calculation of the online biogenic emissions.

6.2.5 Chemical boundary conditions tests

The importance of chemical BC in regional AQMs is well-known in the atmospheric community. In the current version of the model, the regional configuration uses the chemical BC from the MACC re-analysis data. However, future versions of the model will address a nesting approach for coupling the regional NMMB/BSC-CTM model with the global NMMB/BSC-CTM model. Then, the main idea is to evaluate and compare the regional results when the global NMMB/BSC-CTM model outputs are used as the chemical BCs for the regional model, instead of other global model outputs. From the regional run evaluation, the BC for ozone has appeared as a critical issue for the overall model performance. In this sense, the treatment of chemical BC demands further attention. This approach will assure consistency of the whole physics and chemistry processes across the scales of study.

In addition, we had the opportunity to participate in the AQMEII Phase-2 (see Chapter 5). Currently, AQMEII Phase-3 is starting in collaboration with The Task Force on Hemispheric Transport of Air Pollution (TF HTAP; `http://www.htap.org/`). TF HTAP is an international scientific cooperative effort focused on improving the understanding of the intercontinental transport of air pollutants in the Northern Hemisphere.

The main objectives for AQMEII Phase-3 are:

1. Perform model evaluation analyses on global models coordinated with the analyses of regional models under AQMEII
2. Perform regional model simulations with BCs derived from global simulations with perturbed emissions

This initiative focuses on the following questions:

1. How well do regional and global models simulate air quality at various space and time scales over North America (NA) and Europe (EU) ?
2. How sensitive are regional model predictions to the BCs chosen?
3. How sensitive are estimates of the impacts of upwind emission perturbations to grid resolution?

All participating groups will perform simulations for a whole year 2010 over the NA and/or EU domains. Our group plans to participate in this initiative in the EU and NA domains with the regional NMMB/BSC-CTM model.

Bibliography

H. Akimoto. Global air quality and pollution. *Science*, (302):1716–1719, 2003.

A. Altshuller. Production of aldehydes as primary emissions and from secondary atmospheric reactions of alkenes and alkanes during the night and early morning hours . *Atmospheric Environment. Part A. General Topics*, 27(1):21 – 32, 1993. ISSN 0960-1686. doi: http://dx.doi.org/10.1016/0960-1686(93)90067-9. URL http://www.sciencedirect.com/science/article/pii/0960168693900679.

L. G. Anderson, J. A. Lanning, R. Barrell, J. Miyagishima, R. H. Jones, and P. Wolfe. Sources and sinks of formaldehyde and acetaldehyde: An analysis of denver's ambient concentration data. *Atmospheric Environment*, 30(12):2113 – 2123, 1996. ISSN 1352-2310. doi: http://dx.doi.org/10.1016/1352-2310(95)00175-1. URL http://www.sciencedirect.com/science/article/pii/1352231095001751. A WMA International Specialty Conference on Regional Photochemical Measurements and Modeling.

E. Andersson, A. Beljaars, J. Bidlot, M. Miller, A. Simmons, and J. Thepaut. A major new cycle of the IFS: cycle 25R4, ECMWF Newsletter 97, ECMWF, Shinfield Park. *Reading, Berkshire RG2, 9AX, UK*, 2003.

A. Arakawa. Computational design for long-term numerical integration of the equations of fluid motion: Two-dimensional incompressible flow. Part I . *Journal of Computational Physics*, 1(1):119 – 143, 1966. ISSN 0021-9991. doi: http://dx.doi.org/10.1016/0021-9991(66)90015-5. URL http://www.sciencedirect.com/science/article/pii/0021999166900155.

A. Arakawa, V. Lamb, and L. A. California Univ. Computational design of the basic dynamical processes of the UCLA general circulation model. *General circulation models of the atmosphere.(A 78-10662 01-47) New York, Academic Press, Inc.*, 1977.

A. Arakawa, J.-H. Jung, and C.-M. Wu. Toward unification of the multiscale modeling of the atmosphere. *Atmospheric Chemistry and Physics*, 11(8):3731–3742, 2011. doi: 10.5194/acp-11-3731-2011. URL http://www.atmos-chem-phys.net/11/3731/2011/.

D. Arlander, D. Brüning, U. Schmidt, and D. Ehhalt. The tropospheric distribution of formaldehyde during TROPOZ II. *Journal of Atmospheric Chemistry*, 22(3):251–269, 1995. ISSN 0167-7764. doi: 10.1007/BF00696637. URL http://dx.doi.org/10.1007/BF00696637.

K. Ashworth, O. Wild, and C. N. Hewitt. Sensitivity of isoprene emissions estimated using MEGAN to the time resolution of input climate data. *Atmospheric Chemistry and Physics*, 10(3):1193–1201, 2010. doi: 10.5194/acp-10-1193-2010. URL http://www.atmos-chem-phys.net/10/1193/2010/.

R. Atkinson. Atmospheric chemistry of VOCs and NO_x. *Atmos. Environ.*, 34:2063–2101, 2000.

R. Atkinson, D. L. Baulch, R. A. Cox, J. N. Crowley, R. F. Hampson, R. G. Hynes, M. E. Jenkin, M. J. Rossi, and J. Troe. Evaluated kinetic and photochemical data for atmospheric chemistry: Volume I - gas phase reactions of O_x, HO_x, NO_x and SO_x species. *Atmospheric Chemistry and Physics*, 4(6):1461–1738, 2004. doi: 10.5194/acp-4-1461-2004. URL http://www.atmos-chem-phys.net/4/1461/2004/.

E. L. Atlas, B. A. Ridley, and C. A. Cantrell. The Tropospheric Ozone Production about the Spring Equinox (TOPSE) Experiment: Introduction. *Journal of Geophysical Research: Atmospheres*, 108(D4), 2003. ISSN 2156-2202. doi: 10.1029/2002JD003172. URL http://dx.doi.org/10.1029/2002JD003172.

A. Badia and O. Jorba. Gas-phase evaluation of the online NMMB/BSC-CTM model over Europe for 2010 in the framework of the AQMEII-Phase2 project. *Atmospheric Environment*, (0), 2014. ISSN 1352-2310. doi: http://dx.doi.org/10.1016/j.atmosenv.2014.05.055. URL http://www.sciencedirect.com/science/article/pii/S1352231014004026.

A. Baklanov. Numerical Modelling in Mine Aerology, Apatity: USSR Academy of Science, 200 pp. *Russian*, 1988.

A. Baklanov and U. Korsholm. On-line integrated meteorological and chemical transport modelling: advantages and prospectives. *Air Pollution Modeling and Its Application XIX*, pages 3–17, 2007.

A. Baklanov and J. Sørensen. Parameterisation of radionuclide deposition in atmospheric long-range transport modelling. *Physics and Chemistry of the Earth, Part B: Hydrology, Oceans and Atmosphere*, 26(10):787–799, 2001.

A. Baklanov, U. Korsholm, A. Mahura, C. Petersen, and A. Gross. ENVIRO-HIRLAM: on-line coupled modelling of urban meteorology and air pollution. *Advances in Science and Research*, 2:41–46, 2008. doi: 10.5194/asr-2-41-2008. URL http://www.adv-sci-res.net/2/41/2008/.

A. Baklanov, K. Schlünzen, P. Suppan, J. Baldasano, D. Brunner, S. Aksoyoglu, G. Carmichael, J. Douros, J. Flemming, R. Forkel, S. Galmarini, M. Gauss, G. Grell, M. Hirtl, S. Joffre, O. Jorba, E. Kaas, M. Kaasik, G. Kallos, X. Kong, U. Korsholm, A. Kurganskiy, J. Kushta, U. Lohmann, A. Mahura, A. Manders-Groot, A. Maurizi, N. Moussiopoulos, S. T. Rao, N. Savage, C. Seigneur, R. S. Sokhi, E. Solazzo, S. Solomos, B. Sørensen, G. Tsegas, E. Vignati, B. Vogel, and Y. Zhang. Online coupled regional meteorology chemistry models in Europe: current status and prospects. *Atmospheric Chemistry and Physics*, 14(1):317–398,

2014. doi: 10.5194/acp-14-317-2014. URL http://www.atmos-chem-phys.net/14/317/2014/.

D. D. Baldocchi, B. B. Hicks, and P. Camara. A canopy stomatal resistance model for gaseous deposition to vegetated surfaces. *Atmospheric Environment*, 21(1):91–101, 1987.

J. Barnard, E. Chapman, J. Fast, J. Schmelzer, J. Slusser, and R. Shetter. An evaluation of the FAST-J photolysis algorithm for predicting nitrogen dioxide photolysis rates under clear and cloudy sky conditions. *Atmospheric Environment*, 38(21):3393–3403, 2004.

R. Benoit, M. Desgagne, P. Pellerin, S. Pellerin, and S. Desjardins. The Canadian MC2: A Semi-Lagrangian, Semi-Implicit Wideband Atmospheric Model Suited for Finescale Process Studies and Simulation. *Monthly Weather Review*, 125:2382–2415. doi: doi: 10.1175/1520-0493(1997)125<2382:TCMASL>2.0.CO;2. URL http://dx.doi.org/10.1175/1520-0493(1997)125<2382:TCMASL>2.0.CO;2.

P. Bergamaschi, R. Hein, M. Heimann, and P. J. Crutzen. Inverse modeling of the global CO cycle: 1. Inversion of CO mixing ratios. *Journal of Geophysical Research: Atmospheres*, 105(D2):1909–1927, 2000. ISSN 2156-2202. doi: 10.1029/1999JD900818. URL http://dx.doi.org/10.1029/1999JD900818.

E. Berge, H.-C. Huang, J. Chang, and T.-H. Liu. A study of the importance of initial conditions for photochemical oxidant modeling. *Journal of Geophysical Research: Atmospheres*, 106 (D1):1347–1363, 2001. ISSN 2156-2202. doi: 10.1029/2000JD900227. URL http://dx.doi.org/10.1029/2000JD900227.

B. Bessagnet, E. Terrenoire, F. Tognet, L. Rouïl, A. Colette, L. Letinois, and L. Malherbe. EC4MACS Modelling Methodology: the CHIMERE Atmospheric Model, 2012. URL http://www.ec4macs.eu/content/report/EC4MACS_Publications/MR_Final%20in%20pdf/Chimere_Methodologies_Final.pdf.

A. K. Betts. A new convective adjustment scheme. Part I: Observational and theoretical basis. *Quarterly Journal of the Royal Meteorological Society*, 112(473):677–691, 1986. ISSN 1477-870X. doi: 10.1002/qj.49711247307. URL http://dx.doi.org/10.1002/qj.49711247307.

A. K. Betts and M. J. Miller. A new convective adjustment scheme. Part II: Single column tests using GATE wave, BOMEX, ATEX and arctic air-mass data sets. *Quarterly Journal of the Royal Meteorological Society*, 112(473):693–709, 1986. ISSN 1477-870X. doi: 10.1002/qj.49711247308. URL http://dx.doi.org/10.1002/qj.49711247308.

I. Bey, D. Jacob, R. Yantosca, J. Logan, B. Field, A. Fiore, Q. Li, H. Liu, L. Mickley, and M. Schultz. Global modeling of tropospheric chemistry with assimilated meteorology- Model description and evaluation. *Journal of Geophysical Research*, 106(23):073–23, 2001a.

I. Bey, D. J. Jacob, R. M. Yantosca, J. A. Logan, B. D. Field, A. M. Fiore, Q. Li, H. Y. Liu, L. J. Mickley, and M. G. Schultz. Global modeling of tropospheric chemistry with assimilated

meteorology: Model description and evaluation. *Journal of Geophysical Research: Atmospheres*, 106(D19):23073–23095, 2001b. ISSN 2156-2202. doi: 10.1029/2001JD000807. URL http://dx.doi.org/10.1029/2001JD000807.

P. Bhatt, E. Remsberg, L. Gordley, M. McInerney, V. Brackett, and J. Russell III. An evaluation of the quality of Halogen Occultation Experiment ozone profiles in the lower stratosphere. *Journal of geophysical research*, 104(D8):9261–9275, 1999.

R. Bianconi, S. Galmarini, and R. Bellasio. Web-based system for decision support in case of emergency: ensemble modelling of long-range atmospheric dispersion of radionuclides. *Environmental Modelling and Software*, 19(4):401–411, 2004.

F. Binkowski and U. Shankar. The regional particulate matter model 1. Model description and preliminary results. *Journal of Geophysical Research*, 100(D12):26191, 1995.

K. Boersma, D. Jacob, E. Bucsela, A. Perring, R. Dirksen, R. van der A, R. Yantosca, R. Park, M. Wenig, T. Bertram, and R. Cohen. Validation of OMI tropospheric NO_2 observations during INTEX-B and application to constrain emissions over the eastern United States and Mexico . *Atmospheric Environment*, 42(19):4480 – 4497, 2008. ISSN 1352-2310. doi: http://dx.doi.org/10.1016/j.atmosenv.2008.02.004. URL http://www.sciencedirect.com/science/article/pii/S1352231008001258.

K. F. Boersma, H. J. Eskes, and E. J. Brinksma. Error analysis for tropospheric NO2 retrieval from space. *Journal of Geophysical Research: Atmospheres*, 109(D4), 2004. ISSN 2156-2202. doi: 10.1029/2003JD003962. URL http://dx.doi.org/10.1029/2003JD003962.

K. F. Boersma, D. J. Jacob, M. Trainic, Y. Rudich, I. DeSmedt, R. Dirksen, and H. J. Eskes. Validation of urban NO_2 concentrations and their diurnal and seasonal variations observed from the SCIAMACHY and OMI sensors using in situ surface measurements in Israeli cities. *Atmospheric Chemistry and Physics*, 9(12):3867–3879, 2009. doi: 10.5194/acp-9-3867-2009. URL http://www.atmos-chem-phys.net/9/3867/2009/.

K. F. Boersma, H. J. Eskes, R. J. Dirksen, R. J. van der A, J. P. Veefkind, P. Stammes, V. Huijnen, Q. L. Kleipool, M. Sneep, J. Claas, J. Leitão, A. Richter, Y. Zhou, and D. Brunner. An improved tropospheric NO_2 column retrieval algorithm for the Ozone Monitoring Instrument. *Atmospheric Measurement Techniques*, 4(9):1905–1928, 2011. doi: 10.5194/amt-4-1905-2011. URL http://www.atmos-meas-tech.net/4/1905/2011/.

F. Borchi and J.-P. Pommereau. Evaluation of ozonesondes, HALOE, SAGE II and III, Odin-OSIRIS and -SMR, and ENVISAT-GOMOS, -SCIAMACHY and -MIPAS ozone profiles in the tropics from SAOZ long duration balloon measurements in 2003 and 2004. *Atmospheric Chemistry and Physics*, 7(10):2671–2690, 2007. doi: 10.5194/acp-7-2671-2007. URL http://www.atmos-chem-phys.net/7/2671/2007/.

G. Brasseur, S. Walters, P. Rasch, X. Tie, and D. Hauglustaine. MOZART, a global chemical transport model for ozone and related chemical tracers. I- Model description. *Journal of Geophysical Research*, 103:28265–28289, 1998.

A. W. Brewer. Evidence for a world circulation provided by the measurements of helium and water vapour distribution in the stratosphere. *Quarterly Journal of the Royal Meteorological Society*, 75(326):351–363, 1949. ISSN 1477-870X. doi: 10.1002/qj.49707532603. URL http://dx.doi.org/10.1002/qj.49707532603.

E. J. Brinksma, G. Pinardi, H. Volten, R. Braak, A. Richter, A. Schönhardt, M. van Roozendael, C. Fayt, C. Hermans, R. J. Dirksen, T. Vlemmix, A. J. C. Berkhout, D. P. J. Swart, H. Oetjen, F. Wittrock, T. Wagner, O. W. Ibrahim, G. de Leeuw, M. Moerman, R. L. Curier, E. A. Celarier, A. Cede, W. H. Knap, J. P. Veefkind, H. J. Eskes, M. Allaart, R. Rothe, A. J. M. Piters, and P. F. Levelt. The 2005 and 2006 DANDELIONS NO_2 and aerosol intercomparison campaigns. *Journal of Geophysical Research: Atmospheres*, 113(D16), 2008. ISSN 2156-2202. doi: 10.1029/2007JD008808. URL http://dx.doi.org/10.1029/2007JD008808.

C. Brühl, S. Drayson, J. Russell III, P. Crutzen, J. McInerney, P. Purcell, H. Claude, H. Gernandt, T. McGee, I. McDermid, et al. Halogen Occultation Experiment ozone channel validation. *Journal of geophysical research*, 101(D6):10217–10, 1996.

R. Bubnová, G. Hello, P. Bénard, and J. Geleyn. Integration of the fully elastic equations cast in the hydrostatic pressure terrain-following coordinate in the framework of the ARPEGE/Aladin NWP system. *Monthly weather review*, 123(2):515–535, 1995.

A. Buzzi, M. Fantini, P. Malguzzi, and F. Nerozzi. Validation of a limited area model in cases of mediterranean cyclogenesis: Surface fields and precipitation scores. *Meteorology and Atmospheric Physics*, 53(3-4):137–153, 1994. ISSN 0177-7971. doi: 10.1007/BF01029609. URL http://dx.doi.org/10.1007/BF01029609.

D. Byun. Fundamentals of one-atmosphere dynamics for multiscale Air Quality Modeling. Technical report, EPA/600/R-99/030, 1990. URL http://www.epa.gov/AMD/CMAQ/ch05.pdf.

D. Byun and J. Ching. Science algorithms of the EPA Models-3 community multiscale air quality (CMAQ) modeling system. *Rep. EPA/600/R-99*, 30, 1999.

D. Byun, J. Pleim, R. Tang, and A. Bourgeois. Meteorology-Chemistry Interface Processor (MCIP) for Models-3 Community Multiscale Air Quality (CMAQ) Modeling System Chapter 12. Technical report, EPA/600/R-99/030, 1990. URL http://www.epa.gov/AMD/CMAQ/ch12.pdf.

J.-P. Cammas, J. Brioude, J.-P. Chaboureau, J. Duron, C. Mari, P. Mascart, P. Nédélec, H. Smit, H.-W. Pätz, A. Volz-Thomas, A. Stohl, and M. Fromm. Injection in the lower stratosphere of biomass fire emissions followed by long-range transport: a MOZAIC case study. *Atmospheric Chemistry and Physics*, 9(15):5829–5846, 2009. doi: 10.5194/acp-9-5829-2009. URL http://www.atmos-chem-phys.net/9/5829/2009/.

D. Cariolle and M. Déqué. Southern hemisphere medium-scale waves and total ozone disturbances in a spectral general circulation model. *Journal of Geophysical Research: Atmospheres*, 91(D10):10825–10846, 1986. ISSN 2156-2202. doi: 10.1029/JD091iD10p10825. URL http://dx.doi.org/10.1029/JD091iD10p10825.

D. Cariolle and H. Teyssèdre. A revised linear ozone photochemistry parameterization for use in transport and general circulation models: multi-annual simulations, journal = Atmospheric Chemistry and Physics. 7(9):2183–2196, 2007. doi: 10.5194/acp-7-2183-2007. URL http://www.atmos-chem-phys.net/7/2183/2007/.

P. Carlier, H. Hannachi, and G. Mouvier. The chemistry of carbonyl compounds in the atmosphere-A review . *Atmospheric Environment (1967)*, 20(11):2079 – 2099, 1986. ISSN 0004-6981. doi: http://dx.doi.org/10.1016/0004-6981(86)90304-5. URL http://www.sciencedirect.com/science/article/pii/0004698186903045.

W. Carter. A detailed mechanism for the gas-phase atmospheric reactions of organic compounds. *Atmospheric Environment. Part A. General Topics*, 24(3):481–518, 1990.

W. Carter. Documentation of the SAPRC-99 chemical mechanism for VOC reactivity assessment volume 1 of 2 documentation text, 2000. URL http://www.cert.ucr.edu/~carter/pubs/s99txt.pdf.

W. Carter. Programs and Files Implementing the SAPRC-99 Mechanism and its Associated Emissions Processing Procedures for Models-3 and Other Regional Models., January, 2000. URL http://pah.cert.ucr.edu/~carter/SAPRC99.htm.

K. Chance, P. I. Palmer, R. J. D. Spurr, R. V. Martin, T. P. Kurosu, and D. J. Jacob. Satellite observations of formaldehyde over North America from GOME. *Geophysical Research Letters*, 27(21):3461–3464, 2000. ISSN 1944-8007. doi: 10.1029/2000GL011857. URL http://dx.doi.org/10.1029/2000GL011857.

S. Chandrasekhar. *Radiative transfer*. Dover Pubns, 1960.

J. S. Chang, R. A. Brost, I. S. A. Isaksen, S. Madronich, P. Middleton, W. R. Stockwell, and C. J. Walcek. A three-dimensional Eulerian acid deposition model: Physical concepts and formulation. *Journal of Geophysical Research: Atmospheres*, 92(D12):14681–14700, 1987. ISSN 2156-2202. doi: 10.1029/JD092iD12p14681. URL http://dx.doi.org/10.1029/JD092iD12p14681.

D. Chen, Y. Wang, M. B. McElroy, K. He, R. M. Yantosca, and P. Le Sager. Regional co pollution and export in china simulated by the high-resolution nested-grid geos-chem model. *Atmospheric Chemistry and Physics*, 9(11):3825–3839, 2009. doi: 10.5194/acp-9-3825-2009. URL http://www.atmos-chem-phys.net/9/3825/2009/.

M. Chipperfield. New version of the TOMCAT/SLIMCAT off-line chemical transport model: Intercomparison of stratospheric tracer experiments. *Quarterly Journal of the Royal Meteorological Society*, 132(617):1179–1203, 2006.

M. Claeyman, J.-L. Attié, L. El Amraoui, D. Cariolle, V.-H. Peuch, H. Teyssèdre, B. Josse, P. Ricaud, S. Massart, A. Piacentini, J.-P. Cammas, N. J. Livesey, H. C. Pumphrey, and D. P. Edwards. A linear CO chemistry parameterization in a chemistry-transport model: evaluation and application to data assimilation. *Atmospheric Chemistry and Physics*, 10(13):6097–6115,

2010. doi: 10.5194/acp-10-6097-2010. URL http://www.atmos-chem-phys.net/10/6097/2010/.

J. Côté, S. Gravel, A. Méthot, A. Patoine, and S. A. Roch, M. The Operational CMC-MRB Global Environmental Multiscale (GEM) Model. Part I: Design Considerations and Formulation. *Monthly Weather Review*, 126(6):1373–1395, 1998.

W. M. Cox and J. A. Tikvart. A statistical procedure for determining the best performing air quality simulation model . *Atmospheric Environment. Part A. General Topics*, 24(9):2387 – 2395, 1990. ISSN 0960-1686. doi: http://dx.doi.org/10.1016/0960-1686(90)90331-G. URL http://www.sciencedirect.com/science/article/pii/096016869090331G.

P. J. Crutzen. Photochemical reactions initiated by and influencing ozone in unpolluted tropospheric air. *Tellus*, 26(1-2):47–57, 1974. ISSN 2153-3490. doi: 10.1111/j.2153-3490.1974.tb01951.x. URL http://dx.doi.org/10.1111/j.2153-3490.1974.tb01951.x.

A. de Meij, M. Krol, F. Dentener, E. Vignati, C. Cuvelier, and P. Thunis. The sensitivity of aerosol in Europe to two different emission inventories and temporal distribution of emissions. *Atmospheric Chemistry and Physics*, 6(12):4287–4309, 2006. doi: 10.5194/acp-6-4287-2006. URL http://www.atmos-chem-phys.net/6/4287/2006/.

I. De Smedt, J.-F. Müller, T. Stavrakou, R. van der A, H. Eskes, and M. Van Roozendael. Twelve years of global observations of formaldehyde in the troposphere using GOME and SCIAMACHY sensors. *Atmospheric Chemistry and Physics*, 8(16):4947–4963, 2008. doi: 10.5194/acp-8-4947-2008. URL http://www.atmos-chem-phys.net/8/4947/2008/.

M. N. Deeter. *MOPITT (Measurements of Pollution in the Troposphere) Validated Version 4 Product User's Guide*, 2009. URL http://www.acd.ucar.edu/mopitt/v4_users_guide_val.pdf.

M. N. Deeter, D. P. Edwards, J. C. Gille, L. K. Emmons, G. Francis, S.-P. Ho, D. Mao, D. Masters, H. Worden, J. R. Drummond, and P. C. Novelli. The MOPITT version 4 CO product: Algorithm enhancements, validation, and long-term stability. *Journal of Geophysical Research: Atmospheres*, 115(D7):n/a–n/a, 2010. ISSN 2156-2202. doi: 10.1029/2009JD013005. URL http://dx.doi.org/10.1029/2009JD013005.

M. N. Deeter, S. Martínez-Alonso, D. P. Edwards, L. K. Emmons, J. C. Gille, H. M. Worden, J. V. Pittman, B. C. Daube, and S. C. Wofsy. Validation of MOPITT Version 5 thermal-infrared, near-infrared, and multispectral carbon monoxide profile retrievals for 2000-2011. *Journal of Geophysical Research: Atmospheres*, 118(12):6710–6725, 2013. ISSN 2169-8996. doi: 10.1002/jgrd.50272. URL http://dx.doi.org/10.1002/jgrd.50272.

W. DeMore, S. Sander, D. Golden, R. Hampson, M. Kurylo, C. Howard, A. Ravishankara, C. Kolb, M. Molina, and P. Jet Propulsion Lab., California Inst. of Tech. Chemical kinetics and photochemical data for use in stratospheric modeling Evaluation Number 11. Technical report, Citeseer, 1985.

W. DeMore, S. Sander, D. Golden, R. Hampson, M. Kurylo, C. Howard, A. Ravishankara, C. Kolb, and M. Molina. Chemical kinetics and photochemical data for use in stratospheric modeling. *JPL Publication 97-4*, pages 1–266, 2000.

R. Derwent, M. Jenkin, and S. Saunders. Photochemical ozone creation potentials for a large number of reactive hydrocarbons under European conditions. *Atmospheric Environment*, 30(2):181 – 199, 1996. ISSN 1352–2310. doi: http://dx.doi.org/10.1016/1352-2310(95)00303-G. URL http://www.sciencedirect.com/science/article/pii/135223109500303G.

G. M. Dobson. Origin and distribution of the polyatomic molecules in the atmosphere. *Proc. Roy. Soc. Lond. A*, 236:187–193, 1956.

A. J. Dore, M. Kryza, J. R. Hall, S. Hallsworth, V. J. D. Keller, M. Vieno, and M. A. Sutton. The influence of model grid resolution on estimation of national scale nitrogen deposition and exceedance of critical loads. *Biogeosciences*, 9(5):1597–1609, 2012. doi: 10.5194/bg-9-1597-2012. URL http://www.biogeosciences.net/9/1597/2012/.

G. Dufour, F. Wittrock, M. Camredon, M. Beekmann, A. Richter, B. Aumont, and J. P. Burrows. SCIAMACHY formaldehyde observations: constraint for isoprene emission estimates over Europe. *Atmospheric Chemistry and Physics*, 9(5):1647–1664, 2009. doi: 10.5194/acp-9-1647-2009. URL http://www.atmos-chem-phys.net/9/1647/2009/.

R. Easter, S. Ghan, Y. Zhang, R. Saylor, E. Chapman, N. Laulainen, H. Abdul-Razzak, L. Leung, X. Bian, and R. Zaveri. MIRAGE: Model description and evaluation of aerosols and trace gases. *J. Geophys. Res*, 109:D20210, 2004.

EEA. EMEP/CORINAIR Atmospheric Emission Inventory Guidebook. Technical report, Technical report 16/2007, 2007. URL http://www.emep.int.

EEA. Air quality in Europe - 2011 report. EEA Technical report No 12/2011. Technical report, 2011. URL http://www.eea.europa.eu/publications/air-quality-in-europe-2011.

EEA. EMEP/EEA Air Pollutant Emission Inventory Guidebook. Technical report, 2013. URL http://www.eea.europa.eu/publications/emep-eea-guidebook-2013.

M. B. Ek, K. E. Mitchell, Y. Lin, E. Rogers, P. Grunmann, V. Koren, G. Gayno, and J. D. Tarpley. Implementation of Noah land surface model advances in the National Centers for Environmental Prediction operational mesoscale Eta model. *Journal of Geophysical Research: Atmospheres*, 108(D22):n/a–n/a, 2003. ISSN 2156-2202. doi: 10.1029/2002JD003296. URL http://dx.doi.org/10.1029/2002JD003296.

N. Elguindi, H. Clark, C. Ordóñez, V. Thouret, J. Flemming, O. Stein, V. Huijnen, P. Moinat, A. Inness, V.-H. Peuch, A. Stohl, S. Turquety, G. Athier, J.-P. Cammas, and M. Schultz. Current status of the ability of the GEMS/MACC models to reproduce the tropospheric CO

vertical distribution as measured by MOZAIC. *Geoscientific Model Development*, 3(2):501–518, 2010. doi: 10.5194/gmd-3-501-2010. URL http://www.geosci-model-dev.net/3/501/2010/gmd-3-501-2010.html.

EMEP. Report- Part 1, Wet Deposition , 2003. URL http://www.emep.int/UniDoc/node12.html.

L. K. Emmons, D. A. Hauglustaine, J.-F. Müller, M. A. Carroll, G. P. Brasseur, D. Brunner, J. Staehelin, V. Thouret, and A. Marenco. Data composites of airborne observations of tropospheric ozone and its precursors. *Journal of Geophysical Research: Atmospheres*, 105(D16):20497–20538, 2000. ISSN 2156-2202. doi: 10.1029/2000JD900232. URL http://dx.doi.org/10.1029/2000JD900232.

L. K. Emmons, P. Hess, A. Klonecki, X. Tie, L. Horowitz, J.-F. Lamarque, D. Kinnison, G. Brasseur, E. Atlas, E. Browell, C. Cantrell, F. Eisele, R. L. Mauldin, J. Merrill, B. Ridley, and R. Shetter. Budget of tropospheric ozone during TOPSE from two chemical transport models. *Journal of Geophysical Research: Atmospheres*, 108(D8):n/a–n/a, 2003. ISSN 2156-2202. doi: 10.1029/2002JD002665. URL http://dx.doi.org/10.1029/2002JD002665.

L. K. Emmons, S. Walters, P. G. Hess, J.-F. Lamarque, G. G. Pfister, D. Fillmore, C. Granier, A. Guenther, D. Kinnison, T. Laepple, J. Orlando, X. Tie, G. Tyndall, C. Wiedinmyer, S. L. Baughcum, and S. Kloster. Description and evaluation of the Model for Ozone and Related chemical Tracers, version 4 (MOZART-4). *Geoscientific Model Development*, 3(1):43–67, 2010. doi: 10.5194/gmd-3-43-2010. URL http://www.geosci-model-dev.net/3/43/2010/.

EPA. Air Quality Management Online Portal , 2011. URL http://www.epa.gov/air/aqmportal/management/modeling/index.htm.

J. W. Erisman, A. V. Pul, and P. Wyers. Parametrization of surface resistance for the quantification of atmospheric deposition of acidifying pollutants and ozone. *Atmospheric Environment*, 28(16):2595 – 2607, 1994. ISSN 1352-2310. doi: http://dx.doi.org/10.1016/1352-2310(94)90433-2. URL http://www.sciencedirect.com/science/article/pii/1352231094904332.

H. J. Eskes and K. F. Boersma. Averaging kernels for DOAS total-column satellite retrievals. *Atmospheric Chemistry and Physics*, 3(5):1285–1291, 2003. doi: 10.5194/acp-3-1285-2003. URL http://www.atmos-chem-phys.net/3/1285/2003/.

V. Eyring, N. Butchart, D. Waugh, H. Akiyoshi, J. Austin, S. Bekki, G. Bodeker, B. Boville, C. Brühl, M. Chipperfield, et al. Assessment of temperature, trace species, and ozone in chemistry-climate model simulations of the recent past. *J. Geophys. Res*, 111(10.1029), 2006.

K. Fahey and S. Pandis. Optimizing model performance: variable size resolution in cloud chemistry modeling. *Atmospheric Environment*, 35(26):4471–4478, 2001.

J. D. Fast, W. I. Gustafson, R. C. Easter, R. A. Zaveri, J. C. Barnard, E. G. Chapman, G. A. Grell, and S. E. Peckham. Evolution of ozone, particulates, and aerosol direct radiative forcing in the vicinity of Houston using a fully coupled meteorology-chemistry-aerosol model. *Journal of Geophysical Research: Atmospheres*, 111(D21):n/a–n/a, 2006. ISSN 2156-2202. doi: 10.1029/2005JD006721. URL http://dx.doi.org/10.1029/2005JD006721.

S. B. Fels and M. D. Schwarzkopf. The Simplified Exchange Approximation: A New Method for Radiative Transfer Calculations. *J. Atmos. Sci.*, 32:1475–1488, 1975. doi: 10.1175/1520-0469(1975)032<1475:TSEAAN>2.0.CO;2. URL http://dx.doi.org/10.1175/1520-0469(1975)032<1475:TSEAAN>2.0.CO;2.

B. S. Ferrier, J. Y., L. Y., B. T., R. E., and D. G. Implementation of a new grid-scale cloud and precipitation scheme in the NCEP Eta model. paper presented at 15th Conference on Numerical Weather Prediction, Am. Meteorol. Soc., San Antonio, Tex., 2002.

B. J. Finlayson-Pitts and J. N. Pitts. Academic Press, San Diego, 2000. URL http://www.sciencedirect.com/science/book/9780122570605.

E. V. Fischer, D. J. Jacob, R. M. Yantosca, M. P. Sulprizio, D. B. Millet, J. Mao, F. Paulot, H. B. Singh, A. Roiger, L. Ries, R. Talbot, K. Dzepina, and S. Pandey Deolal. Atmospheric peroxyacetyl nitrate (PAN): a global budget and source attribution. *Atmospheric Chemistry and Physics*, 14(5):2679–2698, 2014. doi: 10.5194/acp-14-2679-2014. URL http://www.atmos-chem-phys.net/14/2679/2014/.

A. Flossmann, W. Hall, and H. Pruppacher. A theoretical study of the wet removal of atmospheric pollutants: Part I. The redistribution of aerosol particles captured through nucleation and impaction scavenging by growing cloud drops. *J. Atmos. Sci.*, 42:582–606, 1985. doi: http://dx.doi.org/10.1175/1520-0469(1985)042<0583:ATSOTW>2.0.CO;2.

G. A. Folberth, D. A. Hauglustaine, J. Lathière, and F. Brocheton. Interactive chemistry in the Laboratoire de Météorologie Dynamique general circulation model: model description and impact analysis of biogenic hydrocarbons on tropospheric chemistry. *Atmospheric Chemistry and Physics*, 6(8):2273–2319, 2006. doi: 10.5194/acp-6-2273-2006. URL http://www.atmos-chem-phys.net/6/2273/2006/.

K. M. Foley, S. J. Roselle, K. W. Appel, P. V. Bhave, J. E. Pleim, T. L. Otte, R. Mathur, G. Sarwar, J. O. Young, R. C. Gilliam, C. G. Nolte, J. T. Kelly, A. B. Gilliland, and J. O. Bash. Incremental testing of the Community Multiscale Air Quality (CMAQ) modeling system version 4.7. *Geoscientific Model Development*, 3(1):205–226, 2010. doi: 10.5194/gmd-3-205-2010. URL http://www.geosci-model-dev.net/3/205/2010/.

P. Forster, V. Ramaswamy, P. Artaxo, T. Berntsen, R. Betts, D. W. Fahey, J. Haywood, J. Lean, D. W. Lowe, G. Myhre, J. Nganga, R. Prinn, G. Raga, M. Schulz, , and van Dorland. R. Changes in atmospheric constituents and in radiative forcing. Technical report, 2007.

S. Galmarini, R. Bianconi, W. Appel, E. Solazzo, S. Mosca, P. Grossi, M. Moran, S. K., and S. Rao. ENSEMBLE and AMET: two systems and approaches to a harmonised, simplified

and efficient assistance to air quality model developments and evaluation. *Atmospheric Environment*, 53:51– 59, 2012.

L. Ganzeveld, J. Lelieveld, and G. Roelofs. A dry deposition parameterization for sulfur oxides in a chemistry and general circulation model. *Journal of Geophysical Research*, 103(D5): 5679–5694, 1998.

J. A. Garland. The dry deposition of sulphur dioxide to land and water surfaces. *Proc. R. Sot. Land.*, 12:245–268, 1977.

GEIA/ACCENT. GEIA-ACCENT database, an international cooperative activity of AIMES/IGBP. Technical report, ACCENT EU Network of Excellence, 2005. URL `http://www.geiacenter.organdhttp://www.accent-network.org`.

C. D. Geron, A. B. Guenther, and T. E. Pierce. An improved model for estimating emissions of volatile organic compounds from forests in the eastern United States. *Journal of Geophysical Research: Atmospheres*, 99(D6):12773–12791, 1994. ISSN 2156-2202. doi: 10.1029/94JD00246. URL `http://dx.doi.org/10.1029/94JD00246`.

M. Gery, G. Whitten, and J. Killus. Development and testing of the CBM-IV for urban and regional modeling. Technical report, Environmental Protection Agency, Research Triangle Park, North Carolina by Systems Applications International, San Rafael, California (SYSAPP-88/002)., 1988.

M. Gery, G. Whitten, J. Lillus, and M. Dodge. A photochemical kinetics mechanism for urban and regional scale computer modelling. *J. Geophys. Res.*, 94:12925–12956, 1989.

L. Giordano, J. Brunner, Flemming, D., U. Im, C. Hogrefe, B. Bianconi, A. Badia, A. Balzarini, R. Baró, C. Chemel, G. Curci, R. Forkel, P. Jiménez-Guerrero, M. Hirtl, A. Hodzic, L. Honzak, O. Jorba, C. Knote, J. Kuenen, P. Makar, A. Manders-Groot, L. Neal, J. Pérez, G. Pirovano, R. Pouliot, G. San Jose, N. Savage, W. Schroder, R. Sokhi, D. Syrakov, A. Torian, R. Tuccella, J. Werhahn, R. Wolke, K. Yahya, R. Zabkar, Y. Zhang, and S. Galmarini. Assessment of the MACC/IFS-MOZART model and its influence as chemical boundary conditions in AQMEII phase 2. *Atmospheric Environment (submitted)*, 2014.

F. Giorgi and W. L. Chameides. Rainout lifetimes of highly soluble aerosols and gases as inferred from simulations with a general circulation model. *J. Geophys R. es.*, 91:14,367–14,376, 1986.

S. L. Gong, D. Lavoué, T. L. Zhao, P. Huang, and J. W. Kaminski. GEM-AQ/EC, an online global multi-scale chemical weather modelling system: model development and evaluation of global aerosol climatology. *Atmospheric Chemistry and Physics*, 12(17):8237–8256, 2012. doi: 10.5194/acp-12-8237-2012. URL `http://www.atmos-chem-phys.net/12/8237/2012/`.

C. Granier, J. Lamarque, A. Mieville, J. Muller, J. Olivier, J. Orlando, J. Peters, G. Petron, G. Tyndall, and S. Wallens. POET, a database of surface emissions of ozone precursors. *http://www. aero. jussieu. fr/projet/ACCENT/POET. php*, 6988(6989):30, 2005.

G. Grell, J. Dudhia, and D. Stauffer. A description of the ïňĄfth-generation Penn State/NCAR mesoscale model (MM5). Technical report, National Center for Atmospheric Research, Boulder, Colorado, 1994.

G. Grell, S. Peckham, R. Schmitz, S. McKeen, G. Frost, W. Skamarock, and B. Eder. Fully coupled online chemistry within the WRF model. *Atmospheric Environment*, 39(37):6957–6975, 2005.

W. Guelle, Y. Balkanski, J. Dibb, M. Schulz, and F. Dulac. Wet deposition in a global size-dependent aerosol transport model 2. Influence of the scavenging scheme on 210Pb vertical profiles, surface concentrations, and depositoin. *Journal of Geophysical Research*, 103(D22): 28875, 1998.

A. Guenther, T. Karl, P. Harley, C. Wiedinmyer, P. I. Palmer, and C. Geron. Estimates of global terrestrial isoprene emissions using MEGAN (Model of Emissions of Gases and Aerosols from Nature). *Atmospheric Chemistry and Physics*, 6(11):3181–3210, 2006. doi: 10.5194/acp-6-3181-2006. URL http://www.atmos-chem-phys.net/6/3181/2006/.

M. Guevara, F. Martínez, G. Arévalo, S. Gassó, and J. M. Baldasano. An improved system for modelling Spanish emissions: HERMESv2.0 . *Atmospheric Environment*, 81(0):209 – 221, 2013. ISSN 1352-2310. doi: http://dx.doi.org/10.1016/j.atmosenv.2013.08.053. URL http://www.sciencedirect.com/science/article/pii/S1352231013006730.

P. Hadjinicolaou, J. A. Pyle, and N. R. P. Harris. The recent turnaround in stratospheric ozone over northern middle latitudes: A dynamical modeling perspective. *Geophys. Res. Lett*, 32 (12):L12821, 2005.

T. Halenka, K. Eben, J. Brechler, J. Bednar, P. Jurus, M. Belda, and E. Pelikan. On the Comparison of Nesting of Lagrangian Air-Pollution Model Smog to Numerical Weather Prediction Model ETA and Eulerian CTM CAMX to NWP Model MM5: Ozone Episode Simulation. In C. Borrego and A.-L. Norman, editors, *Air Pollution Modeling and Its Application XVII*, pages 711–713. Springer US, 2007. ISBN 978-0-387-28255-8. doi: 10.1007/978-0-387-68854-1_85. URL http://dx.doi.org/10.1007/978-0-387-68854-1_85.

J. Harries, J. Russell III, A. Tuck, L. Gordley, P. Purcell, K. Stone, R. Bevilacqua, M. Gunson, G. Nedoluha, and W. Traub. Validation of measurements of water vapor from the Halogen Occultation Experiment (HALOE). *Journal of geophysical research*, 101(D6):10205–10, 1996.

H. Hass. Description of the EURAD chemistry transport module (CTM) version 2. *Report*, 83, 1991.

H. Hass, A. Ebel, H. Feldmann, H. Jakobs, and M. Memmesheimer. Evaluation studies with a regional chemical transport model (EURAD) using air quality data from the EMEP monitoring network. *Atmospheric Environment. Part A. General Topics*, 27(6):867–887, 1993.

D. A. Hauglustaine, G. P. Brasseur, S. Walters, P. J. Rasch, J.-F. Müller, L. K. Emmons, and M. A. Carroll. MOZART, a global chemical transport model for ozone and related chemical

tracers: 2. Model results and evaluation. *Journal of Geophysical Research: Atmospheres*, 103(D21):28291–28335, 1998. ISSN 2156-2202. doi: 10.1029/98JD02398. URL http://dx.doi.org/10.1029/98JD02398.

K. Haustein, C. Pérez, J. M. Baldasano, O. Jorba, B. S., R. Miller, Z. Janjic, T. Black, S. Nickovic, M. Todd, and R. Washington. Atmospheric dust modeling from meso to global scales with the online NMMB/BSC-Dust model - Part 2: Experimental campaigns in Northern Africa. *Atmos. Chem. Phys.*, 12:2933–2958, 2012. doi: 10.5194/acp-12-2933-2012.

O. Hertel, R. Berkowicz, J. Christensen, and ÃŸystein Hov. Test of two numerical schemes for use in atmospheric transport-chemistry models . *Atmospheric Environment. Part A. General Topics*, 27(16):2591 – 2611, 1993. ISSN 0960-1686. doi: http://dx.doi.org/10.1016/0960-1686(93)90032-T. URL http://www.sciencedirect.com/science/article/pii/096016869390032T.

K.-P. Heue, A. Richter, M. Bruns, J. P. Burrows, C. v. Friedeburg, U. Platt, I. Pundt, P. Wang, and T. Wagner. Validation of SCIAMACHY tropospheric NO_2-columns with AMAXDOAS measurements. *Atmospheric Chemistry and Physics*, 5(4):1039–1051, 2005. doi: 10.5194/acp-5-1039-2005. URL http://www.atmos-chem-phys.net/5/1039/2005/.

B. Hicks, D. Baldocchi, T. Meyers, R. Hosker, and D. Matt. A preliminary multiple resistance routine for deriving dry deposition velocities from measured quantities. *Water, Air, & Soil Pollution*, 36(3):311–330, 1987.

A. Hilboll, A. Richter, A. Rozanov, O. Hodnebrog, A. Heckel, S. Solberg, F. Stordal, and J. P. Burrows. Improvements to the retrieval of tropospheric NO_2 from satellite-stratospheric correction using SCIAMACHY limb/nadir matching and comparison to Oslo CTM2 simulations. *Atmospheric Measurement Techniques*, 6(3):565–584, 2013. doi: 10.5194/amt-6-565-2013. URL http://www.atmos-meas-tech.net/6/565/2013/.

C. Hogrefe, S. Roselle, R. Mathur, S. Rao, and S. Galmarini. Space-Time Analysis of AQMEII Phase 1 Air Quality Simulations. *Journal of the Air & Waste Management Association*, 2013. doi: 10.1080/10962247.2013.811127. URL http://www.tandfonline.com/doi/abs/10.1080/10962247.2013.811127.

J. Holton, P. Haynes, M. McIntyre, A. Douglas, R. Rood, and L. Pfister. Stratosphere-troposphere exchange. *Reviews of Geophysics*, 33(4):403–440, 1995.

L. Horowitz, J. Liang, G. Gardner, and D. Jacob. Export of reactive nitrogen from North America during summertime: Sensitivity to hydrocarbon chemistry. *Journal of Geophysical Research*, 103(D11):13451–76, 1998.

L. W. Horowitz, S. Walters, D. L. Mauzerall, L. K. Emmons, P. J. Rasch, C. Granier, X. Tie, J.-F. Lamarque, M. G. Schultz, G. S. Tyndall, J. J. Orlando, and G. P. Brasseur. A global simulation of tropospheric ozone and related tracers: Description and evaluation of MOZART, version 2. *Journal of Geophysical Research: Atmospheres*, 108(D24), 2003. ISSN 2156-2202. doi: 10.1029/2002JD002853. URL http://dx.doi.org/10.1029/2002JD002853.

S. Houweling, F. Dentener, and J. Lelieveld. The impact of nonmethane hydrocarbon compounds on tropospheric photochemistry. *Journal of Geophysical Research*, 103(10):673–10, 1998.

J. Hsu and M. J. Prather. Stratospheric variability and tropospheric ozone. *Journal of Geophysical Research: Atmospheres*, 114(D6), 2009. ISSN 2156-2202. doi: 10.1029/2008JD010942. URL http://dx.doi.org/10.1029/2008JD010942.

V. Huijnen, J. Williams, M. van Weele, T. van Noije, M. Krol, F. Dentener, A. Segers, S. Houweling, W. Peters, J. de Laat, F. Boersma, P. Bergamaschi, P. van Velthoven, P. Le Sager, H. Eskes, F. Alkemade, R. Scheele, P. Nédélec, and H. Pätz. The global chemistry transport model TM5: description and evaluation of the tropospheric chemistry version 3.0. *Geoscientific Model Development*, 3(2):445–473, 2010. doi: 10.5194/gmd-3-445-2010. URL http://www.geosci-model-dev.net/3/445/2010/.

U. Im, B. Bianconi, E. Solazzo, I. Kioutsioukis, A. Badia, A. Balzarini, R. Baró, R. Bellasio, D. Brunner, C. Chemel, G. Curci, J. Flemming, R. Forkel, L. Giordano, P. Jiménez-Guerrero, M. Hirtl, A. Hodzic, L. Honzak, O. Jorba, C. Knote, J. Kuenen, P. Makar, A. Manders-Groot, L. Neal, J. Pérez, G. Pirovano, R. Pouliot, G. San Jose, N. Savage, W. Schroder, R. Sokhi, D. Syrakov, A. Torian, R. Tuccella, J. Werhahn, R. Wolke, K. Yahya, R. Zabkar, Y. Zhang, J. Zhang, C. Hogrefe, and S. Galmarini. Evaluation of operational online-coupled regional air quality models over Europe and North America in the context of AQMEII phase 2. Part I: Ozone. *Atmospheric Environment*, (0):–, 2014a. ISSN 1352-2310. doi: http://dx.doi.org/10.1016/j.atmosenv.2014.09.042. URL http://www.sciencedirect.com/science/article/pii/S1352231014007353.

U. Im, B. Bianconi, E. Solazzo, I. Kioutsioukis, A. Badia, A. Balzarini, R. Baró, R. Bellasio, D. Brunner, C. Chemel, G. Curci, J. Flemming, R. Forkel, L. Giordano, P. Jiménez-Guerrero, M. Hirtl, A. Hodzic, L. Honzak, O. Jorba, C. Knote, J. Kuenen, P. Makar, A. Manders-Groot, L. Neal, J. Pérez, G. Pirovano, R. Pouliot, G. San Jose, N. Savage, W. Schroder, R. Sokhi, D. Syrakov, A. Torian, R. Tuccella, J. Werhahn, R. Wolke, K. Yahya, R. Zabkar, Y. Zhang, J. Zhang, C. Hogrefe, and S. Galmarini. Evaluation of operational online-coupled regional air quality models over Europe and North America in the context of AQMEII phase 2. Part II: Particulate Matter . *Atmospheric Environment*, (0):–, 2014b. ISSN 1352-2310. doi: http://dx.doi.org/10.1016/j.atmosenv.2014.08.072. URL http://www.sciencedirect.com/science/article/pii/S1352231014006839.

A. Inness, F. Baier, A. Benedetti, I. Bouarar, S. Chabrillat, H. Clark, C. Clerbaux, P. Coheur, R. J. Engelen, Q. Errera, J. Flemming, M. George, C. Granier, J. Hadji-Lazaro, V. Huijnen, D. Hurtmans, L. Jones, J. W. Kaiser, J. Kapsomenakis, K. Lefever, J. Leitão, M. Razinger, A. Richter, M. G. Schultz, A. J. Simmons, M. Suttie, O. Stein, J.-N. Thépaut, V. Thouret, M. Vrekoussis, C. Zerefos, and the MACC team. The MACC reanalysis: an 8 yr data set of atmospheric composition. *Atmospheric Chemistry and Physics*, 13(8):4073–4109, 2013. doi: 10.5194/acp-13-4073-2013. URL http://www.atmos-chem-phys.net/13/4073/2013/.

IPCC. IPCC Guidelines for National Greenhouse Gas Inventorie. Technical report, Intergovernmental Panel on Climate Change, Japan, 2013.

D. J. Jacob. Heterogeneous chemistry and tropospheric ozone . *Atmospheric Environment*, 34(12-14):2131 – 2159, 2000. ISSN 1352-2310. doi: http://dx.doi.org/10.1016/S1352-2310(99)00462-8. URL http://www.sciencedirect.com/science/article/pii/S1352231099004628.

D. J. Jacob, J. H. Crawford, M. M. Kleb, V. S. Connors, R. J. Bendura, J. L. Raper, G. W. Sachse, J. C. Gille, L. Emmons, and C. L. Heald. Transport and Chemical Evolution over the Pacific (TRACE-P) aircraft mission: Design, execution, and first results. *Journal of Geophysical Research: Atmospheres*, 108(D20):n/a–n/a, 2003. ISSN 2156-2202. doi: 10.1029/2002JD003276. URL http://dx.doi.org/10.1029/2002JD003276.

M. Z. Jacobson. *Developing, Coupling, and Applying a Gas, Aerosol, Transport, and Radiation Model to Study Urban and Regional Air Pollution. PhD. Dissertation*. PhD thesis, Department of Atmospheric Sciences, UCLA, 1994.

M. Z. Jacobson. Development and application of a new air pollution modeling system - Part II. Aerosol module structure and design . *Atmospheric Environment*, 31(2):131 – 144, 1997a. ISSN 1352-2310. doi: http://dx.doi.org/10.1016/1352-2310(96)00202-6. URL http://www.sciencedirect.com/science/article/pii/1352231096002026.

M. Z. Jacobson. Development and application of a new air pollution modeling system - Part III. Aerosol-phase simulations. *Atmospheric Environment*, 31(4):587 – 608, 1997b. ISSN 1352-2310. doi: http://dx.doi.org/10.1016/S1352-2310(96)00201-4. URL http://www.sciencedirect.com/science/article/pii/S1352231096002014.

M. Z. Jacobson. Numerical techniques to solve condensational and dissolutional growth equations when growth is coupled to reversible reactions. *Aerosol Science and Technology*, 27(4): 491–498, 1997c.

M. Z. Jacobson. *Fundamentals of Atmospheric Modeling*. Cambridge University Press, 1999.

M. Z. Jacobson. GATOR-GCMM: A global- through urban-scale air pollution and weather forecast model: 1. Model design and treatment of subgrid soil, vegetation, roads, rooftops, water, sea ice, and snow. *Journal of Geophysical Research: Atmospheres*, 106(D6):5385–5401, 2001a. ISSN 2156-2202. doi: 10.1029/2000JD900560. URL http://dx.doi.org/10.1029/2000JD900560.

M. Z. Jacobson. GATOR-GCMM: A global- through urban-scale air pollution and weather forecast model: 1. Model design and treatment of subgrid soil, vegetation, roads, rooftops, water, sea ice, and snow. *Journal of Geophysical Research: Atmospheres*, 106(D6):5385–5401, 2001b. ISSN 2156-2202. doi: 10.1029/2000JD900560. URL http://dx.doi.org/10.1029/2000JD900560.

M. Z. Jacobson. GATOR-GCMM 2. A study of daytime and nighttime ozone layers aloft, ozone in national parks, and weather during the SARMAP field campaign. *Journal of geophysical research*, 106(D6):5403–5420, 2001c.

M. Z. Jacobson, R. Lu, R. P. Turco, and O. B. Toon. Development and application of a new air pollution modeling system - Part I: Gas-phase simulations . *Atmospheric Environment*, 30(12):1939 – 1963, 1996. ISSN 1352-2310. doi: http://dx.doi.org/10.1016/1352-2310(95)00139-5. URL http://www.sciencedirect.com/science/article/pii/1352231095001395. A WMA International Specialty Conference on Regional Photochemical Measurements and Modeling.

M. Z. Jacobson, Y. J. Kaufman, and Y. Rudich. Examining feedbacks of aerosols to urban climate with a model that treats 3-D clouds with aerosol inclusions. *Journal of Geophysical Research: Atmospheres*, 112(D24):n/a–n/a, 2007. ISSN 2156-2202. doi: 10.1029/2007JD008922. URL http://dx.doi.org/10.1029/2007JD008922.

Z. Janjic. Pressure gradient force and advection scheme used for forecasting with steep and small scale topography. Contrib. Atmos. Phys., 50, 186–199., 1977.

Z. Janjic. Forward-backward scheme modified to prevent two-grid-interval noise and its application in sigma coordinate models. Contrib. Atmos. Phys., 52, 69–84, 1979.

Z. Janjic. Nonlinear Advection Schemes and Energy Cascade on Semi-Staggered Grids. 112: 1234–1245, 1984. doi: doi:10.1175/1520-0493(1984)112<1234:NASAEC>2.0.CO;2. URL http://dx.doi.org/10.1175/1520-0493(1984)112<1234:NASAEC>2.0.CO;2.

Z. Janjic. The step-mountain coordinates: physical package. *Monthly Weather Review*, 118:1429–1443, 1990. doi: 10.1175/1520-0493(1990)118<1429:TSMCPP>2.0.CO;2. URL http://dx.doi.org/10.1175/1520-0493(1990)118<1429:TSMCPP>2.0.CO;2.

Z. Janjic. The step-mountain eta coordinate model: further developments of the convection, viscous sublayer and turbulence closure schemes. *Mon. Wea. Rev*, 122:927–945, 1994.

Z. Janjic. Comments on Development and Evaluation of a Convection Scheme for Use in Climate Models. *Journal of the Atmospheric Sciences*, 57:3686–3686, 2000.

Z. Janjic. A nonhydrostatic model based on a new approach. *Meteorology and Atmospheric Physics*, 82(1):271–285, 2003.

Z. Janjic. The WRF NMM Core: Overview of Basic Principles. 2007.

Z. Janjic. Further development of a model for a broad range of spatial and temporal scales. Proc 23rd Conference on Weather Analysis and Forecasting/19th Conference on Numerical Weather Prediction. Technical report, 2009.

Z. Janjic and T. Black. A unified model approach from meso to global scales. 7(05582): 24–29, 2005. URL http://meetings.copernicus.org/www.cosis.net/abstracts/EGU05/05582/EGU05-J-05582.pdf.

Z. Janjic and B. Ferrier. The WRF NMM Overview of PBL, Surface Layer, Moist Convection and Microphysics. 2006.

Z. Janjic and I. Gall. Scientific documentation of the NCEP nonhydrostatic multiscale model on the B grid (NMMB). Part 1 Dynamics. Technical report, Tech. rep., NCAR/TN-489+STR, 2012. URL http://nldr.library.ucar.edu/repository/collections/TECH-NOTE-000-000-000-857.

Z. Janjic, J. Gerrity Jr., and S. Nickovic. An alternative approach to nonhydrostatic modeling. *Monthly Weather Review*, 129:1164–1178, 2001. URL http://journals.ametsoc.org/doi/pdf/10.1175/1520-0493(2001)129%3C1164%3AAAATNM%3E2.0.CO%3B2.

Z. Janjic, H. Huang, and S. Lu. A unified atmospheric model suitable for studying transport of mineral aerosols from meso to global scales. In *IOP Conference Series: Earth and Environmental Science*, volume 7, page 012011. IOP Publishing, 2009.

Janusz Cofala and Markus Amann and Zbigniew Klimont and Kaarle Kupiainen and Lena Höglund-Isaksson. Scenarios of global anthropogenic emissions of air pollutants and methane until 2030 . *Atmospheric Environment*, 41(38):8486–8499, 2007. ISSN 1352–2310. doi: http://dx.doi.org/10.1016/j.atmosenv.2007.07.010. URL http://www.sciencedirect.com/science/article/pii/S135223100700622X.

P. Jiménez, R. Parra, and J. M. Baldasano. Influence of initial and boundary conditions for ozone modeling in very complex terrains: A case study in the northeastern Iberian Peninsula. *Environmental Modelling & Software*, 22(9):1294 – 1306, 2007. ISSN 1364-8152. doi: http://dx.doi.org/10.1016/j.envsoft.2006.08.004. URL http://www.sciencedirect.com/science/article/pii/S1364815206002015.

P. Jöckel, R. Sander, A. Kerkweg, H. Tost, and J. Lelieveld. Technical note: the modular earth submodel system (MESSy)–a new approach towards earth system modeling. *Atmos. Chem. Phys*, 5:433–444, 2005.

P. Jöckel, H. Tost, A. Pozzer, C. Brühl, J. Buchholz, L. Ganzeveld, P. Hoor, A. Kerkweg, M. Lawrence, R. Sander, et al. The atmospheric chemistry general circulation model ECHAM5/MESSy1: consistent simulation of ozone from the surface to the mesosphere. *Atmospheric Chemistry & Physics*, 6:5067–5104, 2006.

J. Jonson, J. Bartnicki, K. Olendrzynski, H. A. Jakobsenb, and E. Bergea. EMEP Eulerian model for atmospheric transport and deposition of nitrogen species over Europe . *Environmental Pollution*, 102(1):289–298, 1998.

O. Jorba, D. Dabdub, C. Blaszczak-Boxe, C. Pérez, Z. Janjic, J. M. Baldasano, M. Spada, A. Badia, and M. GonÃğalves. Potential significance of photoexcited NO_2 on global air quality with the NMMB/BSC chemical transport model. *Journal of Geophysical Research: Atmospheres*, 117(D13), 2012. ISSN 2156-2202. doi: 10.1029/2012JD017730. URL http://dx.doi.org/10.1029/2012JD017730.

J. Joseph, W. Wiscombe, and J. Weinman. The delta-Eddington approximation for radiative flux transfer. *Journal of the Atmospheric Sciences*, 33(12):2452–2459, 1976.

B. Josse, P. Simon, and V. Peuch. Radon global simulations with the multiscale chemistry and transport model MOCAGE. *Tellus B*, 56(4):339–356, 2004.

H.-J. Jost, K. Drdla, A. Stohl, L. Pfister, M. Loewenstein, J. P. Lopez, P. K. Hudson, D. M. Murphy, D. J. Cziczo, M. Fromm, T. P. Bui, J. Dean-Day, C. Gerbig, M. J. Mahoney, E. C. Richard, N. Spichtinger, J. V. Pittman, E. M. Weinstock, J. C. Wilson, and I. Xueref. In-situ observations of mid-latitude forest fire plumes deep in the stratosphere. *Geophysical Research Letters*, 31(11):n/a–n/a, 2004. ISSN 1944-8007. doi: 10.1029/2003GL019253. URL http://dx.doi.org/10.1029/2003GL019253.

J. Kaminski, L. Neary, J. Struzewska, J. McConnell, A. Lupu, J. Jarosz, K. Toyota, S. Gong, J. Côté, X. Liu, et al. GEM-AQ, an on-line global multiscale chemical weather system: model description and evaluation of gas phase chemistry processes. *Atmospheric Chemistry and Physics Discussions*, 7(5):14895–14937, 2007.

A. Kerkweg, J. Buchholz, L. Ganzeveld, A. Pozzer, H. Tost, and P. Jöckel. Technical Note: an implementation of the dry removal processes dry deposition and sedimentation in the Modular Earth Submodel System (MESSy). *Atmospheric Chemistry and Physics*, 6(12):4617–4632, 2006.

Z. Klimont and D. G. Streets. Emissions inventories and projections for assessing hemispheric or intercontinental transport, in: Hemispheric transport of air pollution 2007, 2007.

C. Knote, D. Brunner, H. Vogel, J. Allan, A. Asmi, M. Äijälä, S. Carbone, H. D. van der Gon, J. L. Jiménez, A. Kiendler-Scharr, C. Mohr, L. Poulain, A. S. H. Prévôt, E. Swietlicki, and B. Vogel. Towards an online-coupled chemistry-climate model: evaluation of trace gases and aerosols in COSMO-ART. *Geoscientific Model Development*, 4(4):1077–1102, 2011. doi: 10.5194/gmd-4-1077-2011. URL http://www.geosci-model-dev.net/4/1077/2011/.

U. Korsholm, A. Baklanov, A. Gross, A. S. B. Mahura, and K. E. Online coupled chemical weather forecasting based on HIRLAM - overview and prospective of Enviro-HIRLAM.

M. Krol, S. Houweling, B. Bregman, M. Van Den Broek, A. Segers, P. Van Velthoven, W. Peters, F. Dentener, and P. Bergamaschi. The two-way nested global chemistry-transport zoom model TM5: algorithm and applications. *Atmos. Chem. Phys*, 5:417–432, 2005.

J. Kuenen, D. van der Gon, A. Visschedijk, and van der Brugh H. High resolution European emission inventory for the years 2002-2007. Technical report, Utrecht,TNO report TNO-060-UT-2011-00588, 2011.

J. Kuenen, A. Visschedijk, M. Jozwicka, and H. Denier van der Gon. TNO-MACC II emission inventory: a multi-year (2003-2009) consistent high-resolution European emission inventory for air quality modelling. *Atmospheric Chemistry and Physics Discussions*, 14(5):5837–5869, 2014. doi: 10.5194/acpd-14-5837-2014. URL http://www.atmos-chem-phys-discuss.net/14/5837/2014/.

J. Kukkonen, T. Olsson, D. M. Schultz, A. Baklanov, T. Klein, A. I. Miranda, A. Monteiro, M. Hirtl, V. Tarvainen, M. Boy, V.-H. Peuch, A. Poupkou, I. Kioutsioukis, S. Finardi, M. Sofiev, R. Sokhi, K. E. J. Lehtinen, K. Karatzas, R. San José, M. Astitha, G. Kallos, M. Schaap, E. Reimer, H. Jakobs, and K. Eben. A review of operational, regional-scale, chemical weather forecasting models in Europe. *Atmospheric Chemistry and Physics*, 12(1): 1–87, 2012. doi: 10.5194/acp-12-1-2012. URL http://www.atmos-chem-phys.net/12/1/2012/.

A. Kylling, A. Bais, M. Blumthaler, J. Schreder, C. Zerefos, and E. Kosmidis. Effect of aerosols on solar UV irradiances during the Photochemical Activity and Solar Ultraviolet Radiation campaign. *Journal of Geophysical Research*, 103(D20):26051–26060, 1998.

L. J. Labrador, R. von Kuhlmann, and M. G. Lawrence. Strong sensitivity of the global mean oh concentration and the tropospheric oxidizing efficiency to the source of no_x from lightning. *Geophysical Research Letters*, 31(6), 2004. ISSN 1944–8007. doi: 10.1029/2003GL019229. URL http://dx.doi.org/10.1029/2003GL019229.

J.-F. Lamarque, T. C. Bond, V. Eyring, C. Granier, A. Heil, Z. Klimont, D. Lee, C. Liousse, A. Mieville, B. Owen, M. G. Schultz, D. Shindell, S. J. Smith, E. Stehfest, J. Van Aardenne, O. R. Cooper, M. Kainuma, N. Mahowald, J. R. McConnell, V. Naik, K. Riahi, and D. P. van Vuuren. Historical (1850-2000) gridded anthropogenic and biomass burning emissions of reactive gases and aerosols: methodology and application. *Atmospheric Chemistry and Physics*, 10(15):7017–7039, 2010. doi: 10.5194/acp-10-7017-2010. URL http://www.atmos-chem-phys.net/10/7017/2010/.

J.-F. Lamarque, D. T. Shindell, B. Josse, P. J. Young, I. Cionni, V. Eyring, D. Bergmann, P. Cameron-Smith, W. J. Collins, R. Doherty, S. Dalsoren, G. Faluvegi, G. Folberth, S. J. Ghan, L. W. Horowitz, Y. H. Lee, I. A. MacKenzie, T. Nagashima, V. Naik, D. Plummer, M. Righi, S. T. Rumbold, M. Schulz, R. B. Skeie, D. S. Stevenson, S. Strode, K. Sudo, S. Szopa, A. Voulgarakis, and G. Zeng. The Atmospheric Chemistry and Climate Model Intercomparison Project (ACCMIP): overview and description of models, simulations and climate diagnostics. *Geoscientific Model Development*, 6(1):179–206, 2013. doi: 10.5194/gmd-6-179-2013. URL http://www.geosci-model-dev.net/6/179/2013/.

J. Landgraf and P. Crutzen. An efficient method for online calculations of photolysis and heating rates. *Journal of the Atmospheric Sciences*, 55(5):863–878, 1998.

R. Laprise. The Euler equations of motion with hydrostatic pressure as an independent variable. *Monthly Weather Review*, 120(1):197–207, 1992.

M. Lattuati. Contribution a l'etude du bilan de l'ozone tropospherique a l'interface de l'Europe et de lâĂŹAtlantique Nord: modelisation lagrangienne et mesures en altitude. 1997.

F. Lefevre, G. Brasseur, I. Folkins, A. Smith, and P. Simon. Chemistry of the 1991-1992 stratospheric winter: Three-dimensional model simulations. *Journal of Geophysical Research. D. Atmospheres*, 99(4):8183–8195, 1994.

J. Lelieveld, W. Peters, F. J. Dentener, and M. C. Krol. Stability of tropospheric hydroxyl chemistry. *Journal of Geophysical Research: Atmospheres*, 107(D23):ACH 17–1–ACH 17–11, 2002. ISSN 2156-2202. doi: 10.1029/2002JD002272. URL http://dx.doi.org/10.1029/2002JD002272.

C. Lerot, M. Van Roozendael, R. Spurr, D. Loyola, M. Coldewey-Egbers, S. Kochenova, J. van Gent, M. Koukouli, D. Balis, J.-C. Lambert, J. Granville, and C. Zehner. Homogenized total ozone data records from the European sensors GOME/ERS-2, SCIAMACHY/Envisat, and GOME-2/MetOp-A. *Journal of Geophysical Research: Atmospheres*, 119(3):1639–1662, 2014. ISSN 2169-8996. doi: 10.1002/2013JD020831. URL http://dx.doi.org/10.1002/2013JD020831.

V. Lindfors, S. Joffre, and J. Damski. Meteorological variability of the wet and dry deposition of sulphur and nitrogen compounds over the Baltic Sea. *Water, Air, & Soil Pollution*, 66(1): 1–28, 1993.

H. Liu, D. Jacob, I. Bey, and R. Yantosca. Constraints from 210Pb and 7Be on wet deposition and transport in a global three-dimensional chemical tracer model driven by assimilated meteorological fields. *J. Geophys. Res*, 106:12–109, 2001a.

T.-H. Liu, F.-T. Jeng, H.-C. Huang, E. Berge, and J. S. Chang. Influences of initial conditions and boundary conditions on regional and urban scale Eulerian air quality transport model simulations . *Chemosphere - Global Change Science*, 3(2):175 – 183, 2001b. ISSN 1465-9972. doi: http://dx.doi.org/10.1016/S1465-9972(00)00048-9. URL http://www.sciencedirect.com/science/article/pii/S1465997200000489.

J. Logan, M. Prather, S. Wofsy, and M. McElroy. Tropospheric chemistry: A global perspective. *Journal of Geophysical Research*, 86(72):10–7254, 1981.

G. Loosmore and R. Cederwall. Precipitation scavenging of atmospheric aerosols for emergency response applications: testing an updated model with new real-time data. *Atmospheric Environment*, 38(7):993–1003, 2004.

R. Lu and R. P. Turco. Air pollutant transport in a coastal environmentâĂŤII. Three-dimensional simulations over Los Angeles basin . *Atmospheric Environment*, 29(13):1499 – 1518, 1995. ISSN 1352-2310. doi: http://dx.doi.org/10.1016/1352-2310(95)00015-Q. URL http://www.sciencedirect.com/science/article/pii/135223109500015Q.

F. W. Lurmann, A. C. Lloyd, and R. Atkinson. A chemical mechanism for use in long-range transport/acid deposition computer modeling. *Journal of Geophysical Research: Atmospheres*, 91(D10):10905–10936, 1986. ISSN 2156-2202. doi: 10.1029/JD091iD10p10905. URL http://dx.doi.org/10.1029/JD091iD10p10905.

S. Madronich. Photodissociation in the atmosphere. I- Actinic flux and the effects of ground reflections and clouds. *Journal of Geophysical Research*, 92(D8):9740–9752, 1987.

S. Madronich and S. Flocke. The Role of Solar Radiation in Atmospheric Chemistry. *Environmental photochemistry*, 2(Part I):1, 1999.

E. A. Marais, D. J. Jacob, A. Guenther, K. Chance, T. P. Kurosu, J. G. Murphy, C. E. Reeves, and H. O. T. Pye. Improved model of isoprene emissions in Africa using Ozone Monitoring Instrument (OMI) satellite observations of formaldehyde: implications for oxidants and particulate matter. *Atmospheric Chemistry and Physics*, 14(15):7693–7703, 2014. doi: 10.5194/acp-14-7693-2014. URL http://www.atmos-chem-phys.net/14/7693/2014/.

G. Marchuk. *Mathematical models in environmental problems*. North Holland, 1986.

R. Mathur, J. E. Pleim, D. C. Wong, T. L. Otte, R. C. Gilliam, S. J. Roselle, J. O. Young, F. S. Binkowski, and X. A. *Air Pollution Modeling and its Applications XX*. Springer Netherlands, C(2.9):155-159, 2010.

P. Maul. Atmospheric transport of sulfur compound pollutants. Central Electricity Generating Bureau MID. Technical report, SSD/80/0026/R. Nottingham, England, 1980.

J. McCormack, S. Eckermann, L. Coy, D. Allen, Y. Kim, T. Hogan, B. Lawrence, A. Stephens, E. Browell, J. Burris, et al. NOGAPS-ALPHA model simulations of stratospheric ozone during the SOLVE2 campaign. *Atmospheric Chemistry & Physics*, 4:2401–2423, 2004.

J. McCormack, S. Eckermann, D. Siskind, and T. McGee. A new linearized gas-phase ozone photochemistry parameterization for high-altitude NWP and climate models. *Atmospheric Chemistry & Physics Discussions*, 6:4943–4972, 2006. URL http://www.atmos-chem-phys.net/6/4943/2006/.

C. McLinden, S. Olsen, B. Hannegan, O. Wild, M. Prather, and J. Sundet. Stratospheric ozone in 3-D models: A simple chemistry and the cross-tropopause ux. *J. Geophys. Res*, 105(14,653): 14–665, 2000.

G. J. McRae, W. R. Goodin, and J. H. Seinfeld. Development of a second-generation mathematical model for Urban air pollution – I. Model formulation . *Atmospheric Environment (1967)*, 16(4):679 – 696, 1982. ISSN 0004-6981. doi: http://dx.doi.org/10.1016/0004-6981(82)90386-9. URL http://www.sciencedirect.com/science/article/pii/0004698182903869.

M. Mircea, M. DâĂŹIsidoro, A. Maurizi, L. Vitali, F. Monforti, G. Zanini, and F. Tampieri. A comprehensive performance evaluation of the air quality model BOLCHEM to reproduce the ozone concentrations over Italy . *Atmospheric Environment*, 42(6):1169 – 1185, 2008. ISSN 1352-2310. doi: http://dx.doi.org/10.1016/j.atmosenv.2007.10.043. URL http://www.sciencedirect.com/science/article/pii/S1352231007009636.

K. Miyazaki, H. J. Eskes, and K. Sudo. Global no_x emission estimates derived from an assimilation of omi tropospheric no_2 columns. *Atmospheric Chemistry and Physics*, 12(5): 2263–2288, 2012. doi: 10.5194/acp-12-2263-2012. URL http://www.atmos-chem-phys.net/12/2263/2012/.

E. J. Mlawer, S. J. Taubman, P. D. Brown, M. J. Iacono, and S. A. Clough. Radiative transfer for inhomogeneous atmospheres: Rrtm, a validated correlated-k model for the longwave. *Journal*

of Geophysical Research: Atmospheres, 102(D14):16663–16682, 1997. ISSN 2156-2202. doi: 10.1029/97JD00237. URL http://dx.doi.org/10.1029/97JD00237.

B. M. Monge-Sanz, M. P. Chipperfield, D. Cariolle, and W. Feng. Results from a new linear O_3 scheme with embedded heterogeneous chemistry compared with the parent full-chemistry 3-D CTM. *Atmospheric Chemistry and Physics*, 11(3):1227–1242, 2011. doi: 10.5194/acp-11-1227-2011. URL http://www.atmos-chem-phys.net/11/1227/2011/.

A. S. Monin and A. M. Obukhov. Osnovnye zakonomernosti turbulentnogo peremesivanija v prizemnom sloe atmosfery. *Trudy geofiz. inst. AN SSSR*, 24 (151):163–187, 1954.

V. Naik, A. Voulgarakis, A. M. Fiore, L. W. Horowitz, J.-F. Lamarque, M. Lin, M. J. Prather, P. J. Young, D. Bergmann, P. J. Cameron-Smith, I. Cionni, W. J. Collins, S. B. Dalsøren, R. Doherty, V. Eyring, G. Faluvegi, G. A. Folberth, B. Josse, Y. H. Lee, I. A. MacKenzie, T. Nagashima, T. P. C. van Noije, D. A. Plummer, M. Righi, S. T. Rumbold, R. Skeie, D. T. Shindell, D. S. Stevenson, S. Strode, K. Sudo, S. Szopa, and G. Zeng. Preindustrial to present-day changes in tropospheric hydroxyl radical and methane lifetime from the Atmospheric Chemistry and Climate Model Intercomparison Project (ACCMIP). *Atmospheric Chemistry and Physics*, 13(10):5277–5298, 2013. doi: 10.5194/acp-13-5277-2013. URL http://www.atmos-chem-phys.net/13/5277/2013/.

P. A. Newman, S. R. Kawa, and E. R. Nash. On the size of the antarctic ozone hole. *Geophysical Research Letters*, 31(21):n/a–n/a, 2004. ISSN 1944-8007. doi: 10.1029/2004GL020596. URL http://dx.doi.org/10.1029/2004GL020596.

J. Noilhan and S. Planton. A simple parameterization of land surface processes for meteorological models. *Monthly Weather Review*, 117(3):536–549, 1989.

U. Nopmongcol, B. Koo, E. Tai, J. Jung, P. Piyachaturawat, C. Emery, G. Yarwood, G. Pirovano, C. Mitsakou, and G. Kallos. Modeling Europe with CAMx for the Air Quality Model Evaluation International Initiative (AQMEII) . *Atmospheric Environment*, 53(0):177 – 185, 2012. ISSN 1352-2310. doi: http://dx.doi.org/10.1016/j.atmosenv.2011.11.023. URL http://www.sciencedirect.com/science/article/pii/S1352231011012064.

T. Ohara, H. Akimoto, J. Kurokawa, N. Horii, K. Yamaji, X. Yan, and T. Hayasaka. An Asian emission inventory of anthropogenic emission sources for the period 1980-2020. *Atmospheric Chemistry and Physics*, 7(16):4419–4444, 2007. doi: 10.5194/acp-7-4419-2007. URL http://www.atmos-chem-phys.net/7/4419/2007/.

J. Olivier, A. Bouwman, J. Berdowski, C. Veldt, J. Bloos, A. Visschedijk, P. Zandveld, and J. Haverlag. Description of EDGAR Version 2.0: A set of global emission inventories of greenhouse gases and ozone-depleting substances for all anthropogenic and most natural sources on a per country basis and on 1 ° x 1 ° grid. 1996.

J. Olivier, A. Bouwman, J. Berdowski, C. Veldt, J. Bloos, A. Visschedijk, C. van der Maas, and P. Zandveld. Sectoral emission inventories of greenhouse gases for 1990 on a per country basis as well as on 1ÂřÃů1Âř . *Environmental Science and Policy*, 2(3):241 – 263, 1999.

ISSN 1462-9011. doi: http://dx.doi.org/10.1016/S1462-9011(99)00027-1. URL http://www.sciencedirect.com/science/article/pii/S1462901199000271.

J. Park, J. Russell III, L. Gordley, S. Drayson, D. Benner, J. McInerney, M. Gunson, G. Toon, B. Sen, J. Blavier, et al. Validation of Halogen Occultation Experiment CH4 measurements from the UARS. *Journal of geophysical research*, 101(D6):10183–10, 1996.

R. J. Park, K. E. Pickering, D. J. Allen, G. L. Stenchikov, and M. S. Fox-Rabinovitz. Global simulation of tropospheric ozone using the University of Maryland Chemical Transport Model (UMD-CTM): 1. Model description and evaluation. *Journal of Geophysical Research: Atmospheres*, 109(D9):n/a–n/a, 2004. ISSN 2156-2202. doi: 10.1029/2003JD004266. URL http://dx.doi.org/10.1029/2003JD004266.

M. Pay, M. Piot, O. Jorba, S. Gassó, M. Gonçalves, S. Basart, D. Dabdub, P. Jiménez-Guerrero, and J. Baldasano. A full year evaluation of the CALIOPE-EU air quality modeling system over Europe for 2004. *Atmospheric Environment*, 44(9):3322–3342, 2010. ISSN 1352-2310. doi: http://dx.doi.org/10.1016/j.atmosenv.2010.05.040. URL http://www.sciencedirect.com/science/article/pii/S1352231010004231.

V. Penenko and A. Aloyan. Models and methods for environmental protection problems. *Science, Novosibirsk*, 1985.

C. Pérez, K. Haustein, Z. Janjic, O. Jorba, N. Huneeus, J. M. Baldasano, T. Black, S. Basart, S. Nickovic, R. L. Miller, J. P. Perlwitz, M. Schulz, and M. Thomson. Atmospheric dust modeling from meso to global scales with the online NMMB/BSC-Dust model Part 1: Model description, annual simulations and evaluation. *Atmospheric Chemistry and Physics*, 11(24):13001–13027, 2011. doi: 10.5194/acp-11-13001-2011. URL http://www.atmos-chem-phys.net/11/13001/2011/.

L. K. Peters, C. M. Berkowitz, G. R. Carmichael, R. C. Easter, G. Fairweather, S. J. Ghan, J. M. Hales, L. R. Leung, W. R. Pennell, F. A. Potra, R. D. Saylor, and T. T. Tsang. The current state and future direction of Eulerian models in simulating the tropospheric chemistry and transport of trace species: a review . *Atmospheric Environment*, 29(2):189 – 222, 1995. ISSN 1352-2310. doi: http://dx.doi.org/10.1016/1352-2310(94)00235-D. URL http://www.sciencedirect.com/science/article/pii/135223109400235D.

A. Petritoli, P. Bonasoni, G. Giovanelli, F. Ravegnani, I. Kostadinov, D. Bortoli, A. Weiss, D. Schaub, A. Richter, and F. Fortezza. First comparison between ground-based and satellite-borne measurements of tropospheric nitrogen dioxide in the Po basin. *Journal of Geophysical Research: Atmospheres*, 109(D15):n/a–n/a, 2004. ISSN 2156-2202. doi: 10.1029/2004JD004547. URL http://dx.doi.org/10.1029/2004JD004547.

V. Peuch, M. Amodei, T. Barthet, M. Cathala, and B. Josse. MOCAGE: Modèle de Chimie Atmosphérique à Grande Echelle, 1999.

W. Pierson, A. Gertler, and R. Bradow. Comparison of the SCAQS tunnel study with other on-road vehicle emission data. *J. Air Waste Manage. Assoc*, 40(11):1495–1504, 1990.

G. Pirovano, A. Balzarini, B. Bessagnet, C. Emery, G. Kallos, F. Meleux, C. Mitsakou, U. Nopmongcol, G. Riva, and G. Yarwood. Investigating impacts of chemistry and transport model formulation on model performance at European scale . *Atmospheric Environment*, 53(0):93 – 109, 2012. ISSN 1352-2310. doi: http://dx.doi.org/10.1016/j.atmosenv.2011.12.052. URL http://www.sciencedirect.com/science/article/pii/S1352231011013422.

D. Plummer. *On-line chemistry in a mesoscale model: Assessment of the Toronto emission inventory and lake-breeze effects on air quality*. PhD thesis, York University,Toronto, Canada, 1999.

D. Plummer, J. McConnell, L. Neary, J. Kominski, R. Benoit, J. Drummond, J. Narayan, V. Young, and D. Hastie. Assessment of emissions data for the Toronto region using aircraft-based measurements and an air quality model. *Atmospheric Environment*, 35(36):6453–6463, 2001.

G. Pouliot, T. Pierce, H. Denier van der Gon, M. Schaap, and U. Nopmongcol. Comparing Emissions Inventories and Model-Ready Emissions Datasets between Europe and North America for the AQMEII Project. *Atmospheric Environment (AQMEII issue)*, 53, 2012.

M. Prather, D. Ehhalt, and F. Dentener. Atmospheric chemistry and greenhouse gases in Climate Change 2001. 2001.

R. Prinn, J. Huang, R. Weiss, D. Cunnold, P. Fraser, P. Simmonds, A. McCulloch, C. Harth, P. Salameh, S. O'Doherty, R. Wang, L. Porter, and B. Miller. Evidence for substantial variations of atmospheric hydroxyl radicals in the past two decades. *Science*, 292(5523):1882–1888, June 2001. URL http://www.sciencemag.org/content/292/5523/1882.

H. Pruppacher and J. Klett. *Microphysics of Clouds and Precipitation*. Kluwer Academic Publishers, Dordrecht., 1997.

D. A. Randell, R. A. Wood, S. Bony, R. Colman, T. Fichefet, J. Fyfe, V. Kattsov, A. Pitman, J. Shukla, J. Srinivasan, R. J. Stouffer, A. Sumi, , and K. E. Taylor. Climate Change 2007: The Physical Science Basis. Contribution of Working Group 1 to the Fourth Assesment Report of the Intergovernmental Panel on Climate Change, Chapter 8: Climate Models and Their Evaluation, Tech. rep., IPCC, 2007.

S. Rao, S. Galmarini, and K. Puckett. Air quality model evaluation international initiative(AQMEII) . *Bulletin of the American Meteorological Society*, 92:23–30, 2011. doi: 10.1175/2010BAMS3069.1.

E. Remsberg. On the response of Halogen Occultation Experiment (HALOE) stratospheric ozone and temperature to the 11-year solar cycle forcing. *Journal of Geophysical Research*, 113(D22):D22304, 2008.

A. Richter, J. P. Burrows, H. Nüß, C. Granier, and U. Niemeier. Increase in tropospheric nitrogen dioxide over China observed from space. *Nature*, 437(7055):129–132, 2005.

R. Rinke. *Parametrisierung des Auswaschens von Aerosolpartikeln durch Niederschlag*. PhD thesis, Inst. fur Meteorol. und Klimaforsch. der Univ. Karlsruhe (TH), Karlsruhe, Germany, 2008.

B. Ritter and J. GELEYN. A comprehensive radiation scheme for numerical weather prediction models with potential applications in climate simulations. *Monthly weather review*, 120(2): 303–325, 1992.

E. Roeckner, G. Bäuml, L. Bonaventura, R. Brokopf, M. Esch, M. Giorgetta, S. Hagemann, I. Kirchner, L. Kornblueh, E. Manzini, A. Rhodin, U. Schlese, U. Schulzweida, and A. Tompkins. The atmospheric general circulation model ECHAM 5. PART I: Model description. Technical report, Max-Planck-Institut für Meteorologie, Retrieved January 2009. URL http://www.mpimet.mpg.de/fileadmin/models/echam/mpi_report_349.pdf.

G. Roelofs and J. Lelieveld. Distribution and budget of O3 in the troposphere calculated with a chemistry general circulation model. *J. Geophys. Res*, 100(20):20983–20998, 1995.

S. Roselle and F. Binkowski. Cloud dynamics and chemistry. *Science algorithms of the EPA Models-3 Community Multi-scale Air Quality (CMAQ) Modeling System. EPA/600/R-99/030,(Byun, DW and JKS Ching, Eds.)*, 1999.

A. Russell and R. Dennis. NARSTO critical review of photochemical models and modeling . *Atmospheric Environment*, 34(12-14):2283 – 2324, 2000. ISSN 1352-2310. doi: http://dx.doi.org/10.1016/S1352-2310(99)00468-9. URL http://www.sciencedirect.com/science/article/pii/S1352231099004689.

A. Russell, D. Winner, R. Harley, K. McCue, and G. Cass. Mathematical modeling and control of the dry deposition flux of nitrogen-containing air pollutants. *Environmental science & technology*, 27(13):2772–2782, 1993a.

J. M. Russell, L. L. Gordley, J. H. Park, S. R. Drayson, W. D. Hesketh, R. J. Cicerone, A. F. Tuck, J. E. Frederick, J. E. Harries, and P. J. Crutzen. The Halogen Occultation Experiment. *Journal of Geophysical Research: Atmospheres*, 98(D6):10777–10797, 1993b. ISSN 2156-2202. doi: 10.1029/93JD00799. URL http://dx.doi.org/10.1029/93JD00799.

J. Russell III, L. Deaver, M. Luo, R. Cicerone, J. Park, L. Gordley, G. Toon, M. Gunson, W. Traub, D. Johnson, et al. Validation of hydrogen fluoride measurements made by the Halogen Occultation Experiment from the UARS platform. *Journal of geophysical research*, 101(D6):10163–10, 1996.

R. Sander, A. Kerkweg, P. Jöckel, and J. Lelieveld. Technical note: The new comprehensive atmospheric chemistry module MECCA. *Atmospheric Chemistry and Physics*, 5(2):445–450, 2005. doi: 10.5194/acp-5-445-2005. URL http://www.atmos-chem-phys.net/5/445/2005/.

S. P. Sander, D. Golden, M. Kurylo, G. Moortgat, P. Wine, A. Ravishankara, C. Kolb, M. Molina, B. Finlayson-Pitts, R. Huie, et al. Chemical kinetics and photochemical data for use in atmospheric studies evaluation number 15. 2006.

B. Santer, M. Wehner, T. Wigley, R. Sausen, G. Meehl, K. Taylor, C. Ammann, J. Arblaster, W. Washington, J. Boyle, et al. Contributions of anthropogenic and natural forcing to recent tropopause height changes. *Science*, 301(5632):479, 2003.

M. Schaap, R. Timmermans, M. Roemer, G. Boersen, P. Builtjes, F. Sauter, G. Velders, and J. Beck. The LOTOS-EUROS model: description, validation and latest developments. *Int. J. Environ. Pollut.*, 32:270–290, 2008.

G. Schmuck, J. San-Miguel-Ayanz, A. Camia, T. H. Durrant, S. Santos de Oliveira, R. Boca, C. Whitmore, C. Giovando, G. Libertá, P. Corti, and E. Schulte. Forest Fires in Europe 2010. Technical Report 11, Joint Research Centre, Ispra, Italy, 2011. URL http://forest.jrc.ec.europa.eu/media/cms_page_media/9/forest-fires-in-europe-2010.pdf.

H.-R. Schneider. A numerical transport scheme which avoids negative mixing ratios. *Monthly Weather Review*, 112(6):1206–1217, 1984. doi: 10.1175/1520-0493(1984)112<1206:ANTSWA>2.0.CO;. URL http://dx.doi.org/10.1175/1520-0493(1984)112<1206:ANTSWA>2.0.CO;2.

M. Schultz and S. Rast. Emission datasets and methodologies for estimating emissions . Technical report, RETRO Report D1-6, 2007. URL http://retro.enes.org.

M. Schultz, L. Backman, Y. Balkanski, et al. REanalysis of the TROpospheric chemical composition over the past 40 years (RETRO): A long-term global modeling study of tropospheric chemistry, Jülich/Hamburg, Germany, 48. *2007 report on Earth System Science of the Max Planck Institute for Meteorology, Hamburg, h ttp://retro. enes. or g, ISSN*, pages 1614–1199, 2007.

J. Seinfeld and S. Pandis. *Atmospheric Chemistry and Physics*. Wiley-Interscience, New York., 1998.

D. T. Shindell, G. Faluvegi, D. S. Stevenson, M. C. Krol, L. K. Emmons, J.-F. Lamarque, G. Pétron, F. J. Dentener, K. Ellingsen, M. G. Schultz, O. Wild, M. Amann, C. S. Atherton, D. J. Bergmann, I. Bey, T. Butler, J. Cofala, W. J. Collins, R. G. Derwent, R. M. Doherty, J. Drevet, H. J. Eskes, A. M. Fiore, M. Gauss, D. A. Hauglustaine, L. W. Horowitz, I. S. A. Isaksen, M. G. Lawrence, V. Montanaro, J.-F. Müller, G. Pitari, M. J. Prather, J. A. Pyle, S. Rast, J. M. Rodriguez, M. G. Sanderson, N. H. Savage, S. E. Strahan, K. Sudo, S. Szopa, N. Unger, T. P. C. van Noije, and G. Zeng. Multimodel simulations of carbon monoxide: Comparison with observations and projected near-future changes. *Journal of Geophysical Research: Atmospheres*, 111(D19):n/a–n/a, 2006. ISSN 2156-2202. doi: 10.1029/2006JD007100. URL http://dx.doi.org/10.1029/2006JD007100.

K. L. Shrestha, A. Kondo, A. Kaga, and Y. Inoue. High-resolution modeling and evaluation of ozone air quality of Osaka using MM5-CMAQ system . *Journal of Environmental Sciences*, 21(6):782 – 789, 2009. ISSN 1001-0742. doi: http://dx.doi.org/10.1016/S1001-0742(08)62341-4. URL http://www.sciencedirect.com/science/article/pii/S1001074208623414.

C. Silibello and G. Calori. FARM (Flexible Air quality Regional Model) Model formulation. *Report Arianet*, 2003.

D. Simpson. Biogenic emissions in Europe: 2. Implications for ozone control strategies. *Journal of Geophysical Research: Atmospheres*, 100(D11):22891–22906, 1995. ISSN 2156-2202. doi: 10.1029/95JD01878. URL http://dx.doi.org/10.1029/95JD01878.

D. Simpson, Y. Andersson-Sköld, and M. E. Jenkin. Updating the chemical scheme for the EMEP MSC-W oxidant model; current status. Technical report, EMEP/MSC-W Note 2/93, 1993. URL http://www.emep.int/mscw/mscw_publications.html.

H. B. Singh and P. L. Hanst. Peroxyacetyl nitrate (PAN) in the unpolluted atmosphere: An important reservoir for nitrogen oxides. *Geophysical Research Letters*, 8(8):941–944, 1981. ISSN 1944-8007. doi: 10.1029/GL008i008p00941. URL http://dx.doi.org/10.1029/GL008i008p00941.

S. Situ, A. Guenther, X. Wang, X. Jiang, A. Turnipseed, Z. Wu, J. Bai, and X. Wang. Impacts of seasonal and regional variability in biogenic VOC emissions on surface ozone in the Pearl River delta region, China. *Atmospheric Chemistry and Physics*, 13(23):11803–11817, 2013. doi: 10.5194/acp-13-11803-2013. URL http://www.atmos-chem-phys.net/13/11803/2013/.

W. C. Skamarock, J. B. Klemp, J. Dudhia, D. O. Gill, D. M. Barker, M. G. Duda, X. Y. Huang, W. Wang, and J. G. Powers. A Description of the Advanced Research WRF Version 3. Technical report, NCAR/TN-475+STR, National Center for Atmospheric Research, Boulder, CO, USA, 2008.

S. J. Smith, J. van Aardenne, Z. Klimont, R. J. Andres, A. Volke, and S. Delgado Arias. Anthropogenic sulfur dioxide emissions: 1850-2005. *Atmospheric Chemistry and Physics*, 11(3):1101–1116, 2011. doi: 10.5194/acp-11-1101-2011. URL http://www.atmos-chem-phys.net/11/1101/2011/.

M. Sofiev. A model for the evaluation of long-term airborne pollution transport at regional and continental scales. *Atmospheric Environment*, 34(15):2481–2493, 2000.

M. Sofiev, P. Siljamo, I. Valkama, M. Ilvonen, and J. Kukkonen. A dispersion modelling system SILAM and its evaluation against ETEX data. *Atmospheric Environment*, 40(4):674–685, 2006.

E. Solazzo, R. Bianconi, R. Vautard, K. W. Appel, M. D. Moran, C. Hogrefe, B. Bessagnet, J. A. Brandt, J. H. Christensen, C. Chemel, I. Coll, H. D. van der Gon, J. Ferreira, R. Forkel, X. V. Francis, G. Grell, P. Grossi, A. B. Hansen, A. Jeričević, L. Kraljevic, A. I. Miranda, U. Nopmongcol, G. Pirovano, M. Prank, A. Riccio, K. N. Sartelet, M. Schaap, J. D. Silver, R. S. Sokhi, J. Vira, J. Werhahn, R. Wolke, G. Yarwood, J. Zhang, Rao, and S. Galmarini. Model evaluation and ensemble modelling of surface-level ozone in Europe and North America in the context of AQMEII. *Atmospheric Environment*, 53:60–74, 2012.

doi: 10.1016/j.atmosenv.2012.01.003. URL http://www.sciencedirect.com/science/article/pii/S1352231012000064.

M. Spada, O. Jorba, C. Pérez García-Pando, Z. Janjic, and J. M. Baldasano. Modeling and evaluation of the global sea-salt aerosol distribution: sensitivity to size-resolved and sea-surface temperature dependent emission schemes. *Atmospheric Chemistry and Physics*, 13(23):11735–11755, 2013. doi: 10.5194/acp-13-11735-2013. URL http://www.atmos-chem-phys.net/13/11735/2013/.

C. M. Spivakovsky, J. A. Logan, S. A. Montzka, Y. J. Balkanski, M. Foreman-Fowler, D. B. A. Jones, L. W. Horowitz, A. C. Fusco, C. A. M. Brenninkmeijer, M. J. Prather, S. C. Wofsy, and M. B. McElroy. Three-dimensional climatological distribution of tropospheric OH: Update and evaluation. *Journal of Geophysical Research: Atmospheres*, 105(D7):8931–8980, 2000. ISSN 2156-2202. doi: 10.1029/1999JD901006. URL http://dx.doi.org/10.1029/1999JD901006.

B. Steil, M. Dameris, C. Brühl, P. Crutzen, V. Grewe, M. Ponater, and R. Sausen. Development of a chemistry module for GCMs: first results of a multiannual integration. In *Annales Geophysicae*, volume 16, pages 205–228. Springer, 1998.

O. Stein, M. G. Schultz, I. Bouarar, H. Clark, V. Huijnen, A. Gaudel, M. George, and C. Clerbaux. On the wintertime low bias of northern hemisphere carbon monoxide found in global model simulations. *Atmospheric Chemistry and Physics*, 14(17):9295–9316, 2014. doi: 10.5194/acp-14-9295-2014. URL http://www.atmos-chem-phys.net/14/9295/2014/.

J. Steppeler, G. Doms, U. Schättler, H. W. Bitzer, A. Gassmann, U. Damrath, and G. Gregoric. Meso-gamma scale forecasts using the nonhydrostatic model LM. *Meteorology and Atmospheric Physics*, 82(1-4):75–96, 2003. ISSN 0177-7971. doi: 10.1007/s00703-001-0592-9. URL http://dx.doi.org/10.1007/s00703-001-0592-9.

D. S. Stevenson, F. J. Dentener, M. G. Schultz, K. Ellingsen, T. P. C. van Noije, O. Wild, G. Zeng, M. Amann, C. S. Atherton, N. Bell, D. J. Bergmann, I. Bey, T. Butler, J. Cofala, W. J. Collins, R. G. Derwent, R. M. Doherty, J. Drevet, H. J. Eskes, A. M. Fiore, M. Gauss, D. A. Hauglustaine, L. W. Horowitz, I. S. A. Isaksen, M. C. Krol, J.-F. Lamarque, M. G. Lawrence, V. Montanaro, J.-F. Müller, G. Pitari, M. J. Prather, J. A. Pyle, S. Rast, J. M. Rodriguez, M. G. Sanderson, N. H. Savage, D. T. Shindell, S. E. Strahan, K. Sudo, and S. Szopa. Multimodel ensemble simulations of present-day and near-future tropospheric ozone. *Journal of Geophysical Research: Atmospheres*, 111(D8), 2006. ISSN 2156-2202. doi: 10.1029/2005JD006338. URL http://dx.doi.org/10.1029/2005JD006338.

W. R. Stockwell, P. Middleton, J. S. Chang, and X. Tang. The second generation regional acid deposition model chemical mechanism for regional air quality modeling. *Journal of Geophysical Research: Atmospheres*, 95(D10):16343–16367, 1990. ISSN 2156-2202. doi: 10.1029/JD095iD10p16343. URL http://dx.doi.org/10.1029/JD095iD10p16343.

W. R. Stockwell, F. Kirchner, M. Kuhn, and S. Seefeld. A new mechanism for regional atmospheric chemistry modeling. *Journal of Geophysical Research: Atmospheres*, 102(D22):

25847–25879, 1997. ISSN 2156-2202. doi: 10.1029/97JD00849. URL http://dx.doi.org/10.1029/97JD00849.

A. Stohl, P. Bonasoni, P. Cristofanelli, W. Collins, J. Feichter, A. Frank, C. Forster, E. Gerasopoulos, H. Gäggeler, P. James, T. Kentarchos, H. Kromp-Kolb, B. Krüger, C. Land, J. Meloen, A. Papayannis, A. Priller, P. Seibert, M. Sprenger, G. J. Roelofs, H. E. Scheel, C. Schnabel, P. Siegmund, L. Tobler, T. Trickl, H. Wernli, V. Wirth, P. Zanis, and C. Zerefos. Stratosphere-troposphere exchange: A review, and what we have learned from STACCATO. *Journal of Geophysical Research: Atmospheres*, 108(D12):n/a–n/a, 2003. ISSN 2156-2202. doi: 10.1029/2002JD002490. URL http://dx.doi.org/10.1029/2002JD002490.

D. G. Streets, Q. Zhang, L. Wang, K. He, J. Hao, Y. Wu, Y. Tang, and G. R. Carmichael. Revisiting China's CO emissions after the Transport and Chemical Evolution over the Pacific (TRACE-P) mission: Synthesis of inventories, atmospheric modeling, and observations. *Journal of Geophysical Research: Atmospheres*, 111(D14):n/a–n/a, 2006. ISSN 2156-2202. doi: 10.1029/2006JD007118. URL http://dx.doi.org/10.1029/2006JD007118.

A. M. Thompson. The oxidizing capacity of the earthâĂŹs atmosphere: Probable past and future changes. *Science*, 256:1157–1168, 1992. doi: 10.1126/science.256.5060.1157. URL http://www.sciencemag.org/content/256/5060/1157.

A. M. Thompson, J. C. Witte, R. D. McPeters, S. J. Oltmans, F. J. Schmidlin, J. A. Logan, M. Fujiwara, V. W. J. H. Kirchhoff, F. Posny, G. J. R. Coetzee, B. Hoegger, S. Kawakami, T. Ogawa, B. J. Johnson, H. Vömel, and G. Labow. Southern Hemisphere Additional Ozonesondes (SHADOZ) 1998-2000 tropical ozone climatology 1. Comparison with Total Ozone Mapping Spectrometer (TOMS) and ground-based measurements. *Journal of Geophysical Research: Atmospheres*, 108(D2), 2003a. ISSN 2156-2202. doi: 10.1029/2001JD000967. URL http://dx.doi.org/10.1029/2001JD000967.

A. M. Thompson, J. C. Witte, S. J. Oltmans, F. J. Schmidlin, J. A. Logan, M. Fujiwara, V. W. J. H. Kirchhoff, F. Posny, G. J. R. Coetzee, B. Hoegger, S. Kawakami, T. Ogawa, J. P. F. Fortuin, and H. M. Kelder. Southern Hemisphere Additional Ozonesondes (SHADOZ) 1998-2000 tropical ozone climatology 2. Tropospheric variability and the zonal wave-one. *Journal of Geophysical Research: Atmospheres*, 108(D2):n/a–n/a, 2003b. ISSN 2156-2202. doi: 10.1029/2002JD002241. URL http://dx.doi.org/10.1029/2002JD002241.

X. Tie, S. Madronich, S. Walters, R. Zhang, P. Rasch, and W. Collins. Effect of clouds on photolysis and oxidants in the troposphere. *J. Geophys. Res*, 108(D20):4642, 2003.

S. Tilmes, J.-F. Lamarque, L. K. Emmons, A. Conley, M. G. Schultz, M. Saunois, V. Thouret, A. M. Thompson, S. J. Oltmans, B. Johnson, and D. Tarasick. Technical Note: Ozonesonde climatology between 1995 and 2011: description, evaluation and applications. *Atmospheric Chemistry and Physics*, 12(16):7475–7497, 2012. doi: 10.5194/acp-12-7475-2012. URL http://www.atmos-chem-phys.net/12/7475/2012/.

G. Tonnesen, J. Olaguer, M. Bergin, T. Russell, A. Hanna, P. Makar, D. Derwent, , and Z. Wang. Air Quality Models Draft as of 11/26/98. Technical report, 1998a.

G. Tonnesen, J. Olaguer, M. Bergin, T. Russell, A. Hanna, P. Makar, D. Derwent, , and Z. Wang. Air Quality Models Draft as of 11/26/98. Technical report, 1998b. URL http://ftp.narsto.org/sites/narsto-dev.ornl.gov/files/AssessModels.pdf.

P. Tuccella, G. Curci, G. Visconti, B. Bessagnet, L. Menut, and R. J. Park. Modeling of gas and aerosol with WRF/Chem over Europe: Evaluation and sensitivity study. *Journal of Geophysical Research: Atmospheres*, 117(D3), 2012. ISSN 2156-2202. doi: 10.1029/2011JD016302. URL http://dx.doi.org/10.1029/2011JD016302.

S. Turquety, C. Clerbaux, K. Law, P.-F. Coheur, A. Cozic, S. Szopa, D. A. Hauglustaine, J. Hadji-Lazaro, A. M. S. Gloudemans, H. Schrijver, C. D. Boone, P. F. Bernath, and D. P. Edwards. CO emission and export from Asia: an analysis combining complementary satellite measurements (MOPITT, SCIAMACHY and ACE-FTS) with global modeling. *Atmospheric Chemistry and Physics*, 8(17):5187–5204, 2008. doi: 10.5194/acp-8-5187-2008. URL http://www.atmos-chem-phys.net/8/5187/2008/.

P. Unden, L. Rontu, H. Järvinen, P. Lynch, J. Calvo, G. Cats, J. Cuxart, K. Eerola, C. Fortelius, J. A. Garcia-Moya, C. Jones, Geert, G. Lenderlink, A. Mcdonald, R. Mcgrath, B. Navascues, N. W. Nielsen, V. Degaard, E. Rodriguez, M. Rummukainen, K. Sattler, B. H. Sass, H. Savijarvi, B. W. Schreur, R. Sigg, and H. The. HIRLAM-5 Scientific Documentation, 2002.

U.S.EPA. Guideline for Regulatory Application of the Urban Airshed Model. Technical report, EPA-450/4-91-013. U.S. Environmental Protection Agency, Office of Air Quality Planning and Standards, Research Triangle Park, NC., 1991.

D. A. Vallero. Academic Press, Burlington, fourth edition edition, 2007. URL http://www.sciencedirect.com/science/book/9780123736154.

J. A. Van Aardenne, F. J. Dentener, J. G. J. Olivier, and J. A. H. W. Peters. The EDGAR 3.2 Fast Track 2000 dataset (32FT2000). Technical report, 2005. URL http://www.mnp.nl/edgar/model/v32ft2000edgar/docv32ft20.

M. van Loon, R. Vautard, M. Schaap, R. Bergström, B. Bessagnet, J. Brandt, P. Builtjes, J. Christensen, C. Cuvelier, A. Graff, J. Jonson, M. Krol, J. Langner, P. Roberts, L. Rouil, R. Stern, L. TarrasÃşn, P. Thunis, E. Vignati, L. White, and P. Wind. Evaluation of long-term ozone simulations from seven regional air quality models and their ensemble. *Atmospheric Environment*, 41(10):2083–2097, 2007. doi: http://dx.doi.org/10.1016/j.atmosenv.2006.10.073. URL http://www.sciencedirect.com/science/article/pii/S1352231006011046.

R. Vautard, D. Martin, M. Beekmann, P. Drobinski, R. Friedrich, A. Jaubertie, D. Kley, M. Lattuati, P. Moral, B. Neininger, et al. Paris emission inventory diagnostics from ESQUIF airborne measurements and a chemistry transport model. *Journal of Geophysical Research*, 108 (D17):8564, 2003.

V. Vestreng and E. Støren. Analysis of UNECE/EMEP emission data. *MSC-W status report*, 2000.

G. C. M. Vinken, K. F. Boersma, D. J. Jacob, and E. W. Meijer. Accounting for non-linear chemistry of ship plumes in the GEOS-Chem global chemistry transport model. *Atmospheric Chemistry and Physics*, 11(22):11707–11722, 2011. doi: 10.5194/acp-11-11707-2011. URL http://www.atmos-chem-phys.net/11/11707/2011/.

B. Vogel, H. Vogel, D. Bäumer, M. Bangert, K. Lundgren, R. Rinke, and T. Stanelle. The comprehensive model system COSMO-ART - Radiative impact of aerosol on the state of the atmosphere on the regional scale. *Atmospheric Chemistry and Physics*, 9(22):8661–8680, 2009. doi: 10.5194/acp-9-8661-2009. URL http://www.atmos-chem-phys.net/9/8661/2009/.

A. Voulgarakis, N. H. Savage, O. Wild, P. Braesicke, P. J. Young, G. D. Carver, and J. A. Pyle. Interannual variability of tropospheric composition: the influence of changes in emissions, meteorology and clouds. *Atmospheric Chemistry and Physics*, 10(5):2491–2506, 2010. doi: 10.5194/acp-10-2491-2010. URL http://www.atmos-chem-phys.net/10/2491/2010/.

A. Voulgarakis, V. Naik, J.-F. Lamarque, D. T. Shindell, P. J. Young, M. J. Prather, O. Wild, R. D. Field, D. Bergmann, P. Cameron-Smith, I. Cionni, W. J. Collins, S. B. Dalsøren, R. M. Doherty, V. Eyring, G. Faluvegi, G. A. Folberth, L. W. Horowitz, B. Josse, I. A. MacKenzie, T. Nagashima, D. A. Plummer, M. Righi, S. T. Rumbold, D. S. Stevenson, S. A. Strode, K. Sudo, S. Szopa, and G. Zeng. Analysis of present day and future oh and methane lifetime in the accmip simulations. *Atmospheric Chemistry and Physics*, 13(5):2563–2587, 2013. doi: 10.5194/acp-13-2563-2013. URL http://www.atmos-chem-phys.net/13/2563/2013/.

A. Vukovic, R. B., and J. Z. Land ice sea surface model: Short description and verification. , paper presented at 2010 International Congress on Environmental Modelling and Software Modelling for EnvironmentâĂŹs Sake, Int. Environ. Modell. and Software Soc., Ottaw, 2010.

C. Walcek, R. Brost, J. Chang, and M. L. Wesely. SO_2, sulfate and HNO_3 deposition velocities computed using regional landuse and meteorological data . *Atmos. Environ.*, 20(5):949–964, 1986.

J. Walmsley and M. L. Wesely. Modification of coded parametrizations of surface resistances to gaseous dry deposition . *Atmos. Environ.*, 30(7):1181–1188, 1996.

Y. Wang, D. Jacob, and J. Logan. Global simulation of tropospheric $O_3 - NO_x$-hydrocarbon chemistry, 1. Model formulation. *Journal of Geophysical Research*, 103(D9):10713–10726, 1998.

M. Weber, S. Dikty, J. P. Burrows, H. Garny, M. Dameris, A. Kubin, J. Abalichin, and U. Langematz. The brewer-dobson circulation and total ozone from seasonal to decadal time scales. *Atmospheric Chemistry and Physics*, 11(21):11221–11235, 2011. doi: 10.5194/acp-11-11221-2011. URL http://www.atmos-chem-phys.net/11/11221/2011/.

Weber, M. Algorithm Theoretical Basis Document Version/Issue 2 (ATBDv2), Ozone-cci. Technical report, IUP Bremen, 2014. URL http://www.esa-ozone-cci.org/?q=webfm_send/145.

M. Wesely. Parameterization of surface resistances to gaseous dry deposition in regional-scale numerical models . *Atmospheric Environment (1967)*, 23(6):1293 – 1304, 1989. ISSN 0004-6981. doi: http://dx.doi.org/10.1016/0004-6981(89)90153-4. URL http://www.sciencedirect.com/science/article/pii/0004698189901534.

M. Wesely and B. Hicks. A review of the current status of knowledge on dry deposition. *Atmospheric Environment*, 34(12âĂŞ14):2261 – 2282, 2000. ISSN 1352-2310. doi: http://dx.doi.org/10.1016/S1352-2310(99)00467-7. URL http://www.sciencedirect.com/science/article/pii/S1352231099004677.

M. L. Wesely and B. B. Hicks. Some factors that affect the deposition rates of sulfur dioxide and similar gases on vegetation. *J. Air Pollut. Control Ass.*, 27:1110–1116, 1997.

WHO. Ambient (outdoor) air quality and health, 2014. URL http://www.who.int/mediacentre/factsheets/fs313/en/.

O. Wild and M. J. Prather. Excitation of the primary tropospheric chemical mode in a global three-dimensional model. *Journal of Geophysical Research: Atmospheres*, 105(D20):24647–24660, 2000. ISSN 2156-2202. doi: 10.1029/2000JD900399. URL http://dx.doi.org/10.1029/2000JD900399.

O. Wild, X. Zhu, and M. J. Prather. Fast-J: Accurate Simulation of In- and Below-Cloud Photolysis in Tropospheric Chemical Models. *Journal of Atmospheric Chemistry*, 37(3):245–282, 2000. ISSN 0167-7764. doi: 10.1023/A:1006415919030. URL http://dx.doi.org/10.1023/A%3A1006415919030.

J. E. Williams, J. Landgraf, A. Bregman, and H. Walter. A modified band approach for the accurate calculation of on-line photolysis rates in stratospheric-tropospheric Chemical Transport Models. *Atmospheric Chemistry and Physics Discussions*, 6(3):3513–3570, 2006.

F. Winninghoff. On the Adjustment Toward a Geostrophic Balance in a Simple Primitive Equation Model with Application to the Problems of Initialization and Objective Analysis. 1968.

G. Wotawa, P. C. Novelli, M. Trainer, and C. Granier. Inter-annual variability of summertime CO concentrations in the Northern Hemisphere explained by boreal forest fires in North America and Russia. *Geophysical Research Letters*, 28(24):4575–4578, 2001. ISSN 1944-8007. doi: 10.1029/2001GL013686. URL http://dx.doi.org/10.1029/2001GL013686.

G. Yarwood, S. Rao, M. Yocke, and G. Whitten. Updates to the Carbon Bond Chemical Mechanism: CB05. Final Report to the US EPA, RT-0400675, 2005. URL http://www.camx.com/publ/pdfs/CB05_Final_Report_120805.pdf.

P. J. Young, A. T. Archibald, K. W. Bowman, J.-F. Lamarque, V. Naik, D. S. Stevenson, S. Tilmes, A. Voulgarakis, O. Wild, D. Bergmann, P. Cameron-Smith, I. Cionni, W. J. Collins, S. B. Dalsøren, R. M. Doherty, V. Eyring, G. Faluvegi, L. W. Horowitz, B. Josse, Y. H. Lee, I. A. MacKenzie, T. Nagashima, D. A. Plummer, M. Righi, S. T. Rumbold, R. B. Skeie, D. T.

Shindell, S. A. Strode, K. Sudo, S. Szopa, and G. Zeng. Pre-industrial to end 21st century projections of tropospheric ozone from the atmospheric chemistry and climate model intercomparison project (accmip). *Atmospheric Chemistry and Physics*, 13(4):2063–2090, 2013. doi: 10.5194/acp-13-2063-2013. URL http://www.atmos-chem-phys.net/13/2063/2013/.

R. A. Zaveri and L. K. Peters. A new lumped structure photochemical mechanism for large-scale applications. *Journal of Geophysical Research: Atmospheres*, 104(D23):30387–30415, 1999. ISSN 2156-2202. doi: 10.1029/1999JD900876. URL http://dx.doi.org/10.1029/1999JD900876.

Y. Zhang. Online-coupled meteorology and chemistry models: history, current status, and outlook. *Atmospheric Chemistry and Physics*, 8(11):2895–2932, 2008. doi: 10.5194/acp-8-2895-2008. URL http://www.atmos-chem-phys.net/8/2895/2008/.

Y. Zhang, M. Bocquet, V. Mallet, C. Seigneur, and A. Baklanov. Real-time air quality forecasting, part I: History, techniques, and current status . *Atmospheric Environment*, 60(0):632 – 655, 2012a. ISSN 1352-2310. doi: http://dx.doi.org/10.1016/j.atmosenv.2012.06.031. URL http://www.sciencedirect.com/science/article/pii/S1352231012005900.

Y. Zhang, M. Bocquet, V. Mallet, C. Seigneur, and A. Baklanov. Real-time air quality forecasting, part II: State of the science, current research needs, and future prospects . *Atmospheric Environment*, 60(0):656 – 676, 2012b. ISSN 1352-2310. doi: http://dx.doi.org/10.1016/j.atmosenv.2012.02.041. URL http://www.sciencedirect.com/science/article/pii/S1352231012001562.

Y. Zhao, C. P. Nielsen, Y. Lei, M. B. McElroy, and J. Hao. Quantifying the uncertainties of a bottom-up emission inventory of anthropogenic atmospheric pollutants in China. *Atmospheric Chemistry and Physics*, 11(5):2295–2308, 2011. doi: 10.5194/acp-11-2295-2011. URL http://www.atmos-chem-phys.net/11/2295/2011/.

S. Zilitinkevich. Bulk characteristics of turbulence in the atmospheric planetary boundary layer. *Tr. GGO*, 167:49–52, 1965.